Enzyme Kinetics

A MODERN APPROACH

A. G. Marangoni

ENZYME KINETICS

ENZYME KINETICS
A Modern Approach

ALEJANDRO G. MARANGONI

Department of Food Science
University of Guelph

To Dianne, Isaac, and Joshua

CONTENTS

PREFACE

We live in the age of biology—the human and many other organisms' genomes have been sequenced and we are starting to understand the function of the metabolic machinery responsible for life on our planet. Thousands of new genes have been discovered, many of these coding for enzymes of yet unknown function. Understanding the kinetic behavior of an enzyme provides clues to its possible physiological role. From a biotechnological point of view, knowledge of the catalytic properties of an enzyme is required for the design of immobilized enzyme-based industrial processes. Biotransformations are of key importance to the pharmaceutical and food industries, and knowledge of the catalytic properties of enzymes, essential. This book is about understanding the principles of enzyme kinetics and knowing how to use mathematical models to describe the catalytic function of an enzyme. Coverage of the material is by no means exhaustive. There exist many books on enzyme kinetics that offer thorough, in-depth treatises of the subject. This book stresses understanding and practicality, and is not meant to replace, but rather to complement, authoritative treatises on the subject such as Segel's *Enzyme Kinetics*.

This book starts with a review of the tools and techniques used in kinetic analysis, followed by a short chapter entitled "How Do Enzymes Work?", embodying the philosophy of the book. Characterization of enzyme activity; reversible and irreversible inhibition; pH effects on enzyme activity; multisubstrate, immobilized, interfacial, and allosteric enzyme kinetics; transient phases of enzymatic reactions; and enzyme

stability are covered in turn. In each chapter, models are developed from first principles, assumptions stated and discussed clearly, and applications shown.

The treatment of enzyme kinetics in this book is radically different from the traditional way in which this topic is usually covered. In this book, I have tried to stress the understanding of how models are arrived at, what their limitations are, and how they can be used in a practical fashion to analyze enzyme kinetic data. With the advent of computers, linear transformations of models have become unnecessary—this book does away with linear transformations of enzyme kinetic models, stressing the use of nonlinear regression techniques. Linear transformations are not required to carry out analysis of enzyme kinetic data. In this book, I develop new ways of analyzing kinetic data, particularly in the study of pH effects on catalytic activity and multisubstrate enzymes. Since a large proportion of traditional enzyme kinetics used to deal with linearization of data, removing these has both decreased the amount of information that must be acquired and allowed for the development of a deeper understanding of the models used. This, in turn, will increase the efficacy of their use.

The book is relatively short and concise, yet complete. Time is today's most precious commodity. This book was written with this fact in mind; thus, the coverage strives to be both complete and thorough, yet concise and to the point.

<div align="right">

ALEJANDRO MARANGONI

</div>

Guelph, September, 2001

ENZYME KINETICS

CHAPTER 1

TOOLS AND TECHNIQUES OF KINETIC ANALYSIS

1.1 GENERALITIES

Chemists are concerned with the laws of chemical interactions. The theories that have been expounded to explain such interactions are based largely on experimental results. Two main approaches have been used to explain chemical reactivity: *thermodynamic* and *kinetic*. In thermodynamics, conclusions are reached on the basis of changes in energy and entropy that accompany a particular chemical change in a system. From the magnitude and sign of the free-energy change of a reaction, it is possible to predict the direction in which a chemical change will take place. Thermodynamic quantities do not, however, provide any information on the rate or mechanism of a chemical reaction. Theoretical analysis of the kinetics, or time course, of processes can provide valuable information concerning the underlying mechanisms responsible for these processes. For this purpose it is necessary to construct a mathematical model that embodies the hypothesized mechanisms. Whether or not the solutions of the resulting equations are consistent with the experimental data will either prove or disprove the hypothesis.

Consider the simple reaction $A + B \rightleftharpoons C$. The *law of mass action* states that the rate at which the reactant A is converted to product C is proportional to the number of molecules of A available to participate in the chemical reaction. Doubling the concentration of either A or B will double the number of collisions between molecules that lead to product formation.

1

The *stoichiometry* of a reaction is the simplest ratio of the number of reactant molecules to the number of product molecules. It should not be mistaken for the mechanism of the reaction. For example, three molecules of hydrogen react with one molecule of nitrogen to form ammonia: $N_2 + 3H_2 \rightleftharpoons 2NH_3$.

The *molecularity* of a reaction is the number of reactant molecules participating in a simple reaction consisting of a single elementary step. Reactions can be unimolecular, bimolecular, and trimolecular. *Unimolecular reactions* can include isomerizations ($A \rightarrow B$) and decompositions ($A \rightarrow B + C$). *Bimolecular reactions* include association ($A + B \rightarrow AB$; $2A \rightarrow A_2$) and exchange reactions ($A + B \rightarrow C + D$ or $2A \rightarrow C + D$). The less common *termolecular reactions* can also take place ($A + B + C \rightarrow P$).

The task of a kineticist is to predict the rate of any reaction under a given set of experimental conditions. At best, a mechanism is proposed that is in qualitative and quantitative agreement with the known experimental kinetic measurements. The criteria used to propose a mechanism are (1) consistency with experimental results, (2) energetic feasibility, (3) microscopic reversibility, and (4) consistency with analogous reactions. For example, an exothermic, or least endothermic, step is most likely to be an important step in the reaction. *Microscopic reversibility* refers to the fact that for an elementary reaction, the reverse reaction must proceed in the opposite direction by exactly the same route. Consequently, it is not possible to include in a reaction mechanism any step that could not take place if the reaction were reversed.

1.2 ELEMENTARY RATE LAWS

1.2.1 Rate Equation

The *rate equation* is a quantitative expression of the change in concentration of reactant or product molecules in time. For example, consider the reaction $A + 3B \rightarrow 2C$. The rate of this reaction could be expressed as the disappearance of reactant, or the formation of product:

$$\text{rate} = -\frac{d[A]}{dt} = -\frac{1}{3}\frac{d[B]}{dt} = \frac{1}{2}\frac{d[C]}{dt} \tag{1.1}$$

Experimentally, one also finds that the rate of a reaction is proportional to the amount of reactant present, raised to an exponent n:

$$\text{rate} \propto [A]^n \tag{1.2}$$

where n is the order of the reaction. Thus, the rate equation for this reaction can be expressed as

$$-\frac{d[A]}{dt} = k_r[A]^n \qquad (1.3)$$

where k_r is the rate constant of the reaction.

As stated implicitly above, the rate of a reaction can be obtained from the slope of the *concentration–time curve* for disappearance of reactant(s) or appearance of product(s). Typical reactant concentration–time curves for zero-, first-, second-, and third-order reactions are shown in Fig. 1.1(*a*). The dependence of the rates of these reactions on reactant concentration is shown in Fig. 1.1(*b*).
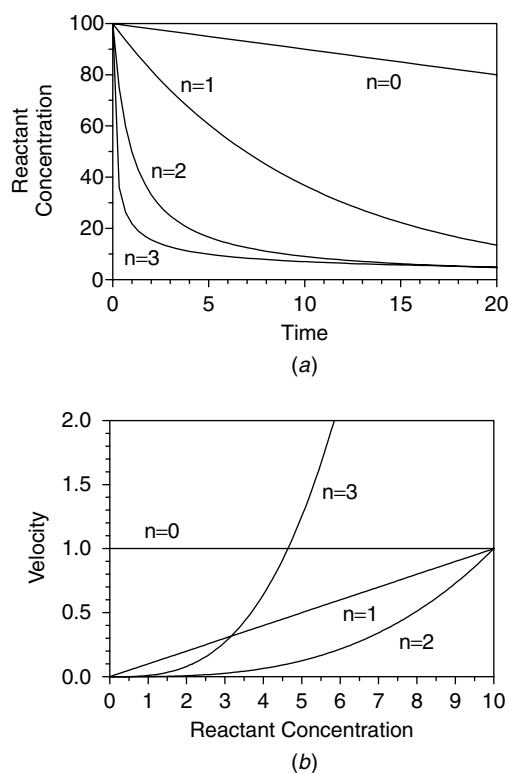
Figure 1.1. (*a*) Changes in reactant concentration as a function of time for zero-, first-, second-, and third-order reactions. (*b*) Changes in reaction velocity as a function of reactant concentration for zero-, first-, second-, and third-order reactions.

1.2.2   Order of a Reaction

If the rate of a reaction is *independent* of a particular reactant concentration, the reaction is considered to be zero order with respect to the concentration of that reactant ($n = 0$). If the rate of a reaction is *directly proportional* to a particular reactant concentration, the reaction is considered to be *first-order* with respect to the concentration of that reactant ($n = 1$). If the rate of a reaction is proportional to the square of a particular reactant concentration, the reaction is considered to be *second-order* with respect to the concentration of that reactant ($n = 2$). In general, for any reaction $A + B + C + \cdots \rightarrow P$, the rate equation can be generalized as

$$\text{rate} = k_r[A]^a[B]^b[C]^c \cdots \tag{1.4}$$

where the exponents a, b, c correspond, respectively, to the order of the reaction with respect to reactants A, B, and C.

1.2.3   Rate Constant

The *rate constant* (k_r) of a reaction is a concentration-independent measure of the velocity of a reaction. For a first-order reaction, k_r has units of $(\text{time})^{-1}$; for a second-order reaction, k_r has units of $(\text{concentration})^{-1}(\text{time})^{-1}$. In general, the rate constant of an nth-order reaction has units of $(\text{concentration})^{-(n-1)}(\text{time})^{-1}$.

1.2.4   Integrated Rate Equations

By integration of the rate equations, it is possible to obtain expressions that describe changes in the concentration of reactants or products as a function of time. As described below, integrated rate equations are extremely useful in the experimental determination of rate constants and reaction order.

1.2.4.1   Zero-Order Integrated Rate Equation

The reactant concentration–time curve for a typical zero-order reaction, $A \rightarrow$ products, is shown in Fig. 1.1(a). The rate equation for a zero-order reaction can be expressed as

$$\frac{d[A]}{dt} = -k_r[A]^0 \tag{1.5}$$

Since $[A]^0 = 1$, integration of Eq. (1.5) for the boundary conditions $A = A_0$ at $t = 0$ and $A = A_t$ at time t,

$$\int_{A_0}^{A_t} d[A] = -k_r \int_0^t dt \tag{1.6}$$

Figure 1.2. Changes in reactant concentration as a function of time for a zero-order reaction used in the determination of the reaction rate constant (k_r).

yields the integrated rate equation for a zero-order reaction:

$$[A_t] = [A_0] - k_r t \tag{1.7}$$

where $[A_t]$ is the concentration of reactant A at time t and $[A_0]$ is the initial concentration of reactant A at $t = 0$. For a zero-order reaction, a plot of $[A_t]$ versus time yields a straight line with negative slope $-k_r$ (Fig. 1.2).

1.2.4.2 First-Order Integrated Rate Equation

The reactant concentration–time curve for a typical first-order reaction, A → products, is shown in Fig. 1.1(a). The rate equation for a first-order reaction can be expressed as

$$\frac{d[A]}{dt} = -k_r[A] \tag{1.8}$$

Integration of Eq. (1.8) for the boundary conditions A = A$_0$ at $t = 0$ and A = A$_t$ at time t,

$$\int_{A_0}^{A_t} \frac{d[A]}{[A]} = -k_r \int_0^t dt \tag{1.9}$$

yields the integrated rate equation for a first-order reaction:

$$\ln \frac{[A_t]}{[A_0]} = -k_r t \tag{1.10}$$

or

$$[A_t] = [A_0] \, e^{-k_r t} \tag{1.11}$$

For a first-order reaction, a plot of $\ln([A_t]/[A_0])$ versus time yields a straight line with negative slope $-k_r$ (Fig. 1.3).

A special application of the first-order integrated rate equation is in the determination of *decimal reduction times*, or D values, the time required for a one-$\log_{10}$ reduction in the concentration of reacting species (i.e., a 90% reduction in the concentration of reactant). Decimal reduction times are determined from the slope of $\log_{10}([A_t]/[A_0])$ versus time plots (Fig. 1.4). The modified integrated first-order integrated rate equation can be expressed as

$$\log_{10} \frac{[A_t]}{[A_0]} = -\frac{t}{D} \tag{1.12}$$

or

$$[A_t] = [A_0] \cdot 10^{-(t/D)} \tag{1.13}$$
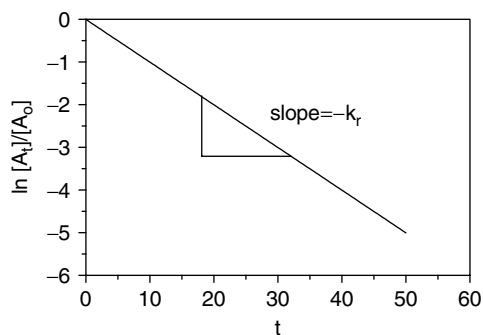
Figure 1.3. Semilogarithmic plot of changes in reactant concentration as a function of time for a first-order reaction used in determination of the reaction rate constant (k_r).
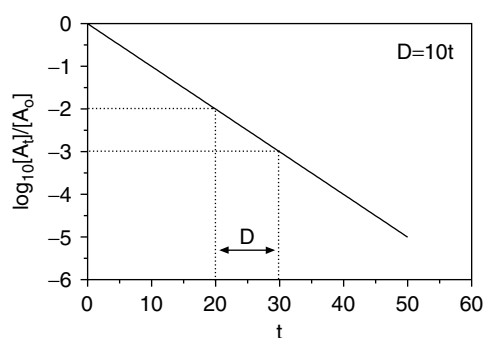
Figure 1.4. Semilogarithmic plot of changes in reactant concentration as a function of time for a first-order reaction used in determination of the decimal reduction time (D value).

The decimal reduction time (D) is related to the first-order rate constant (k_r) in a straightforward fashion:

$$D = \frac{2.303}{k_r} \tag{1.14}$$

1.2.4.3 Second-Order Integrated Rate Equation

The concentration–time curve for a typical second-order reaction, $2A \rightarrow$ products, is shown in Fig. 1.1(a). The rate equation for a second-order reaction can be expressed as

$$\frac{d[A]}{dt} = -k_r[A]^2 \tag{1.15}$$

Integration of Eq. (1.15) for the boundary conditions $A = A_0$ at $t = 0$ and $A = A_t$ at time t,

$$\int_{A_0}^{A_t} \frac{d[A]}{[A]^2} = -k_r \int_0^t dt \tag{1.16}$$

yields the integrated rate equation for a second-order reaction:

$$\frac{1}{[A_t]} = \frac{1}{[A_0]} + k_r t \tag{1.17}$$

or

$$[A_t] = \frac{[A_0]}{1 + [A_0]k_r t} \tag{1.18}$$

For a second-order reaction, a plot of $1/A_t$ against time yields a straight line with positive slope k_r (Fig. 1.5).

For a second-order reaction of the type $A + B \rightarrow$ products, it is possible to express the rate of the reaction in terms of the amount of reactant that is converted to product (P) in time:

$$\frac{d[P]}{dt} = k_r[A_0 - P][B_0 - P] \tag{1.19}$$

Integration of Eq. (1.19) using the method of partial fractions for the boundary conditions $A = A_0$ and $B = B_0$ at $t = 0$, and $A = A_t$ and $B = B_t$ at time t,

$$\frac{1}{[A_0] - [B_0]} \int_0^{P_t} \left(\frac{dP}{[B_0 - P]} - \frac{dP}{[A_0 - P]} \right) = -k_r \int_0^t dt \tag{1.20}$$
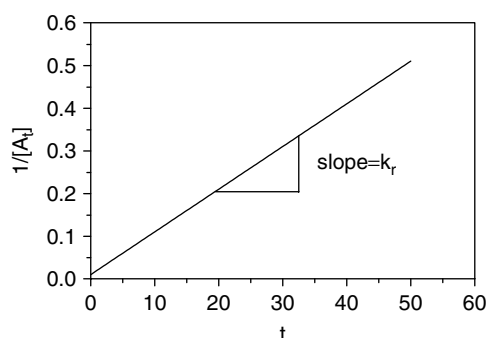
Figure 1.5. Linear plot of changes in reactant concentration as a function of time for a second-order reaction used in determination of the reaction rate constant (k_r).

yields the integrated rate equation for a second-order reaction in which two different reactants participate:

$$\frac{1}{[A_0 - B_0]} \ln \frac{[B_0][A_t]}{[A_0][B_t]} = k_r t \qquad (1.21)$$

where $[A_t] = [A_0 - P_t]$ and $[B_t] = [B_0 - P_t]$. For this type of second-order reaction, a plot of $(1/[A_0 - B_0]) \ln([B_0][A_t]/[A_0][B_t])$ versus time yields a straight line with positive slope k_r.

1.2.4.4 *Third-Order Integrated Rate Equation*

The reactant concentration–time curve for a typical second-order reaction, $3A \rightarrow$ products, is shown in Fig. 1.1(a). The rate equation for a third-order reaction can be expressed as

$$\frac{d[A]}{dt} = -k_r[A]^3 \qquad (1.22)$$

Integration of Eq. (1.22) for the boundary conditions $A = A_0$ at $t = 0$ and $A = A_t$ at time t,

$$\int_{A_0}^{A_t} \frac{d[A]}{[A]^3} = -k_r \int_0^t dt \qquad (1.23)$$

yields the integrated rate equation for a third-order reaction:

$$\frac{1}{2[A_t]^2} = \frac{1}{2[A_0]^2} + k_r t \qquad (1.24)$$

or

$$[A_t] = \frac{[A_0]}{\sqrt{1 + 2[A_0]^2 k_r t}} \tag{1.25}$$

For a third-order reaction, a plot of $1/(2[A_t]^2)$ versus time yields a straight line with positive slope k_r (Fig. 1.6).

1.2.4.5 Higher-Order Reactions

For any reaction of the type $nA \rightarrow$ products, where $n > 1$, the integrated rate equation has the general form

$$\frac{1}{(n-1)[A_t]^{n-1}} = \frac{1}{(n-1)[A_0]^{n-1}} + k_r t \tag{1.26}$$

or

$$[A_t] = \frac{[A_0]}{\sqrt[n-1]{1 + (n-1)[A_0]^{n-1} k_r t}} \tag{1.27}$$

For an nth-order reaction, a plot of $1/[(n-1)[A_t]^{n-1}]$ versus time yields a straight line with positive slope k_r.

1.2.4.6 Opposing Reactions

For the simplest case of an opposing reaction $A \rightleftharpoons B$,

$$\frac{d[A]}{dt} = -k_1[A] + k_{-1}[B] \tag{1.28}$$

where k_1 and k_{-1} represent, respectively, the rate constants for the forward $(A \rightarrow B)$ and reverse $(B \rightarrow A)$ reactions. It is possible to express the rate
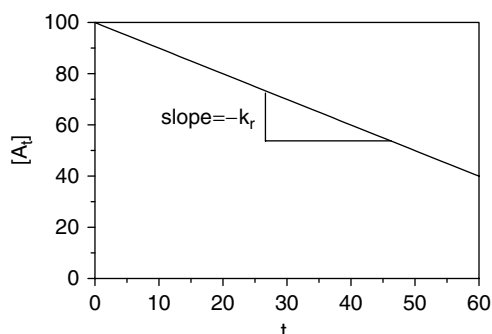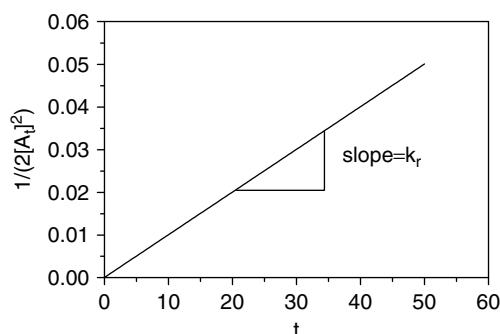

Figure 1.6. Linear plot of changes in reactant concentration as a function of time for a third-order reaction used in determination of the reaction rate constant (k_r).

of the reaction in terms of the amount of reactant that is converted to product (B) in time (Fig. 1.7*a*):

$$\frac{d[B]}{dt} = k_1[A_0 - B] - k_{-1}[B] \qquad (1.29)$$

At equilibrium, $d[B]/dt = 0$ and $[B] = [B_e]$, and it is therefore possible to obtain expressions for k_{-1} and $k_1[A_0]$:

$$k_{-1} = \frac{k_1[A_0 - B_e]}{[B_e]} \quad \text{and} \quad k_1[A_0] = (k_{-1} + k_1)[B_e] \qquad (1.30)$$

Substituting the $k_1[A_0 - B_e]/[B_e]$ for k_{-1} into the rate equation, we obtain

$$\frac{d[B]}{dt} = k_1[A_0 - B] - \frac{k_1[A_0 - B_e][B]}{B_e} \qquad (1.31)$$
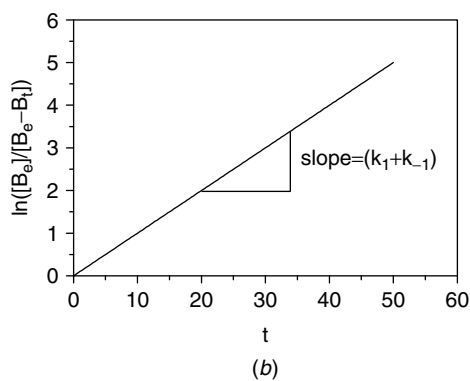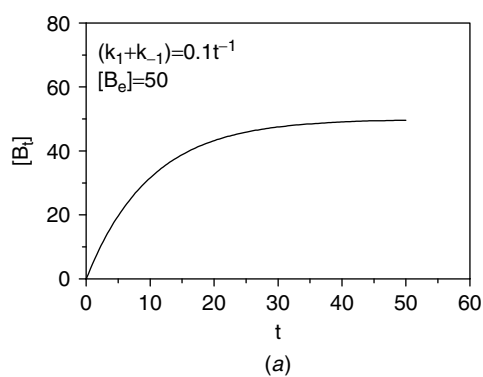
Figure 1.7. (*a*) Changes in product concentration as a function of time for a reversible reaction of the form $A \rightleftharpoons B$. (*b*) Linear plot of changes in product concentration as a function of time used in the determination of forward (k_1) and reverse (k_{-1}) reaction rate constants.

Summing together the terms on the right-hand side of the equation, substituting $(k_{-1} + k_1)[B_e]$ for $k_1[A_0]$, and integrating for the boundary conditions $B = 0$ at $t = 0$ and $B = B_t$ at time t,

$$\int_0^{B_t} \frac{dB}{[B_e - B]/[B_e]} = (k_1 + k_{-1}) \int_0^t dt \tag{1.32}$$

yields the integrated rate equation for the opposing reaction $A \rightleftharpoons B$:

$$\ln \frac{[B_e]}{[B_e - B_t]} = (k_1 + k_{-1})t \tag{1.33}$$

or

$$[B_t] = [B_e] - [B_e] e^{-(k_1 + k_{-1})t} \tag{1.34}$$

A plot of $\ln([B_e]/[B_e - B])$ versus time results in a straight line with positive slope $(k_1 + k_{-1})$ (Fig. 1.7b).

The rate equation for a more complex case of an opposing reaction, $A + B \rightleftharpoons P$, assuming that $[A_0] = [B_0]$, and $[P] = 0$ at $t = 0$, is

$$\frac{[P_e]}{[A_0]^2 - [P_e]^2} \ln \frac{[P_e][A_0^2 - P_e]}{[A_0]^2[P_e - P_t]} = k_1 t \tag{1.35}$$

The rate equation for an even more complex case of an opposing reaction, $A + B \rightleftharpoons P + Q$, assuming that $[A_0] = [B_0]$, $[P] = [Q]$, and $[P] = 0$ at $t = 0$, is

$$\frac{[P_e]}{2[A_0][A_0 - P_e]} \ln \frac{[P_t][A_0 - 2P_e] + [A_0][P_e]}{[A_0][P_e - P_t]} = k_1 t \tag{1.36}$$

1.2.4.7 *Reaction Half-Life*

The half-life is another useful measure of the rate of a reaction. A reaction half-life is the time required for the initial reactant(s) concentration to decrease by $\frac{1}{2}$. Useful relationships between the rate constant and the half-life can be derived using the integrated rate equations by substituting $\frac{1}{2}A_0$ for A_t.

The resulting expressions for the half-life of reactions of different orders (n) are as follows:

$$n = 0 \cdots t_{1/2} = \frac{0.5[A_0]}{k_r} \tag{1.37}$$

$$n = 1 \cdots t_{1/2} = \frac{\ln 2}{k_r} \tag{1.38}$$

$$n = 2 \cdots t_{1/2} = \frac{1}{k_r[A_0]} \tag{1.39}$$

$$n = 3 \cdots t_{1/2} = \frac{3}{2k_r[A_0]^2} \tag{1.40}$$

The half-life of an nth-order reaction, where $n > 1$, can be calculated from the expression

$$t_{1/2} = \frac{1 - (0.5)^{n-1}}{(n-1)k_r[A_0]^{n-1}} \tag{1.41}$$

1.2.5 Experimental Determination of Reaction Order and Rate Constants

1.2.5.1 Differential Method (Initial Rate Method)

Knowledge of the value of the rate of the reaction at different reactant concentrations would allow for determination of the rate and order of a chemical reaction. For the reaction $A \rightarrow B$, for example, reactant or product concentration–time curves are determined at different initial reactant concentrations. The absolute value of slope of the curve at $t = 0$, $|d[A]/dt)_0|$ or $|d[B]/dt)_0|$, corresponds to the initial rate or initial velocity of the reaction (Fig. 1.8).

As shown before, the reaction velocity (v_A) is related to reactant concentration,

$$v_A = \left| \frac{d[A]}{dt} \right| = k_r[A]^n \tag{1.42}$$

Taking logarithms on both sides of Eq. (1.42) results in the expression

$$\log v_A = \log k_r + n \log [A] \tag{1.43}$$
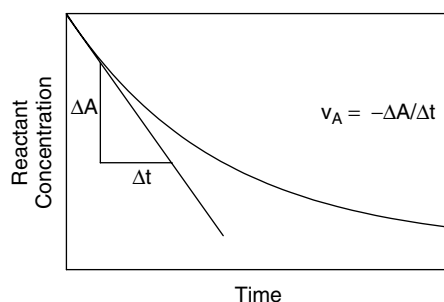
Figure 1.8. Determination of the initial velocity of a reaction as the instantaneous slope of the substrate depletion curve in the vicinity of $t = 0$.
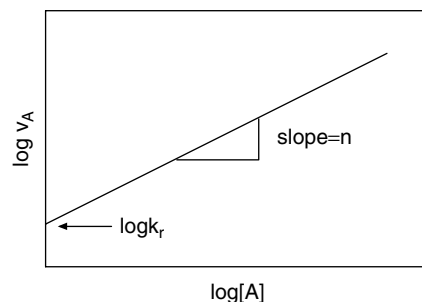
Figure 1.9. Log-log plot of initial velocity versus initial substrate concentration used in determination of the reaction rate constant (k_r) and the order of the reaction.

A plot of the logarithm of the initial rate against the logarithm of the initial reactant concentration yields a straight line with a y-intercept corresponding to log k_r and a slope corresponding to n (Fig. 1.9). For more accurate determinations of the initial rate, changes in reactant concentration are measured over a small time period, where less than 1% conversion of reactant to product has taken place.

1.2.5.2 Integral Method

In the integral method, the rate constant and order of a reaction are determined from least-squares fits of the integrated rate equations to reactant depletion or product accumulation concentration–time data. At this point, knowledge of the reaction order is required. If the order of the reaction is not known, one is assumed or guessed at: for example, $n = 1$. If necessary, data are transformed accordingly [e.g., $\ln([A_t]/[A_0])$] if a linear first-order model is to be used. The model is then fitted to the data using standard least-squares error minimization protocols (i.e., linear or nonlinear regression). From this exercise, a best-fit slope, y-intercept, their corresponding standard errors, as well as a coefficient of determination (CD) for the fit, are determined. The r-squared statistic is sometimes used instead of the CD; however, the CD statistic is the true measure of the fraction of the total variance accounted for by the model. The closer the values of $|r^2|$ or $|CD|$ to 1, the better the fit of the model to the data.

This procedure is repeated assuming a different reaction order (e.g., $n = 2$). The order of the reaction would thus be determined by comparing the coefficients of determination for the different fits of the kinetic models to the transformed data. The model that fits the data best defines the order of that reaction. The rate constant for the reaction, and its corresponding standard error, is then determined using the appropriate model. If coefficients of determination are similar, further experimentation may

be required to determine the order of the reaction. The advantage of the differential method over the integral method is that no reaction order needs to be assumed. The reaction order is determined directly from the data analysis. On the other hand, determination of initial rates can be rather inaccurate.

To use integrated rate equations, knowledge of reactant or product concentrations is not an absolute requirement. Any parameter *proportional* to reactant or product concentration can be used in the integrated rate equations (e.g., absorbance or transmittance, turbidity, conductivity, pressure, volume, among many others). However, certain modifications may have to be introduced into the rate equations, since reactant concentration, or related parameters, may not decrease to zero—a minimum, nonzero value (A_{min}) might be reached. For product concentration and related parameters, a maximum value (P_{max}) may be reached, which does not correspond to 100% conversion of reactant to product. A certain amount of product may even be present at $t = 0$ (P_0). The modifications introduced into the rate equations are straightforward. For reactant (A) concentration,

$$[A_t] \Longrightarrow [A_t - A_{min}] \quad \text{and} \quad [A_0] \Longrightarrow [A_0 - A_{min}] \qquad (1.44)$$

For product (P) concentration,

$$[P_t] \Longrightarrow [P_t - P_0] \quad \text{and} \quad [P_0] \Longrightarrow [P_{max} - P_0] \qquad (1.45)$$

These modified rate equations are discussed extensively in Chapter 12, and the reader is directed there if a more-in-depth discussion of this topic is required at this stage.

1.3   DEPENDENCE OF REACTION RATES ON TEMPERATURE

1.3.1   Theoretical Considerations

The rates of chemical reactions are highly dependent on temperature. Temperature affects the rate constant of a reaction but not the order of the reaction. Classic thermodynamic arguments are used to derive an expression for the relationship between the reaction rate and temperature.

The molar standard-state free-energy change of a reaction (ΔG°) is a function of the equilibrium constant (K) and is related to changes in the molar standard-state enthalpy (ΔH°) and entropy (ΔS°), as described by the Gibbs–Helmholtz equation:

$$\Delta G^\circ = -RT \ln K = \Delta H^\circ - T \Delta S^\circ \qquad (1.46)$$

Rearrangement of Eq. (1.46) yields the well-known van't Hoff equation:

$$\ln K = -\frac{\Delta H^\circ}{RT} + \frac{\Delta S^\circ}{R} \tag{1.47}$$

The change in ΔS° due to a temperature change from T_1 to T_2 is given by

$$\Delta S^\circ_{T_2} = \Delta S^\circ_{T_1} + \Delta C_p \ln \frac{T_2}{T_1} \tag{1.48}$$

and the change in ΔH° due to a temperature change from T_1 to T_2 is given by

$$\Delta H^\circ_{T_2} = \Delta H^\circ_{T_1} + \Delta C_p (T_2 - T_1) \tag{1.49}$$

If the heat capacities of reactants and products are the same (i.e., $\Delta C_p = 0$) ΔS° and ΔH° are independent of temperature. Subject to the condition that the difference in the heat capacities between reactants and products is zero, differentiation of Eq. (1.47) with respect to temperature yields a more familiar form of the van't Hoff equation:

$$\frac{d \ln K}{dT} = \frac{\Delta H^\circ}{RT^2} \tag{1.50}$$

For an endothermic reaction, ΔH° is positive, whereas for an exothermic reaction, ΔH° is negative. The van't Hoff equation predicts that the ΔH° of a reaction defines the effect of temperature on the equilibrium constant. For an endothermic reaction, K increases as T increases; for an exothermic reaction, K decreases as T increases. These predictions are in agreement with Le Chatelier's principle, which states that increasing the temperature of an equilibrium reaction mixture causes the reaction to proceed in the direction that absorbs heat. The van't Hoff equation is used for the determination of the ΔH° of a reaction by plotting $\ln K$ against $1/T$. The slope of the resulting line corresponds to $-\Delta H^\circ / R$ (Fig. 1.10). It is also possible to determine the ΔS° of the reaction from the y-intercept, which corresponds to $\Delta S^\circ / R$. It is important to reiterate that this treatment applies only for cases where the heat capacities of the reactants and products are equal and temperature independent.

Enthalpy changes are related to changes in internal energy:

$$\Delta H^\circ = \Delta E^\circ + \Delta(PV) = \Delta E^\circ + P_1 V_1 - P_2 V_2 \tag{1.51}$$

Hence, ΔH° and ΔE° differ only by the difference in the PV products of the final and initial states. For a chemical reaction at constant pressure
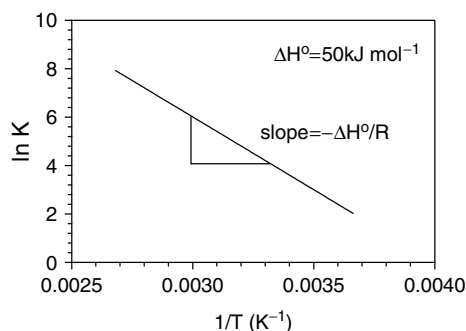
Figure 1.10. van't Hoff plot used in the determination of the standard-state enthalpy ΔH° of a reaction.

in which only solids and liquids are involved, $\Delta(PV) \approx 0$, and therefore ΔH° and ΔE° are nearly equal. For gas-phase reactions, $\Delta(PV) \neq 0$, unless the number of moles of reactants and products remains the same. For ideal gases it can easily be shown that $\Delta(PV) = (\Delta n)RT$. Thus, for gas-phase reactions, if $\Delta n = 0$, $\Delta H^\circ = \Delta E^\circ$.

At equilibrium, the rate of the forward reaction (v_1) is equal to the rate of the reverse reaction (v_{-1}), $v_1 = v_{-1}$. Therefore, for the reaction $A \rightleftharpoons B$ at equilibrium,

$$k_1[A_e] = k_{-1}[B_e] \tag{1.52}$$

and therefore

$$K = \frac{[\text{products}]}{[\text{reactants}]} = \frac{[B_e]}{[A_e]} = \frac{k_1}{k_{-1}} \tag{1.53}$$

Considering the above, the van't Hoff Eq. (1.50) can therefore be rewritten as

$$\frac{d \ln k_1}{dT} - \frac{d \ln k_{-1}}{dT} = \frac{\Delta E^\circ}{RT^2} \tag{1.54}$$

The change in the standard-state internal energy of a system undergoing a chemical reaction from reactants to products (ΔE°) is equal to the energy required for reactants to be converted to products minus the energy required for products to be converted to reactants (Fig. 1.11). Moreover, the energy required for reactants to be converted to products is equal to the difference in energy between the ground and transition states of the reactants ($\Delta E_1^\ddagger$), while the energy required for products to be converted to reactants is equal to the difference in energy between the ground and
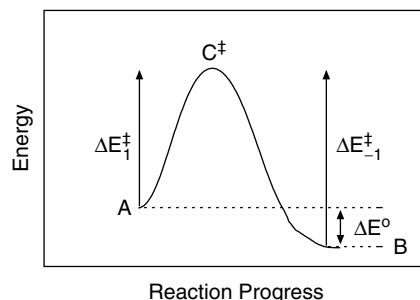
Figure 1.11. Changes in the internal energy of a system undergoing a chemical reaction from substrate A to product B. $\Delta E^{\ddagger}$ corresponds to the energy barrier (energy of activation) for the forward (1) and reverse (-1) reactions, $C^{\ddagger}$ corresponds to the putative transition state structure, and ΔE° corresponds to the standard-state difference in the internal energy between products and reactants.

transition states of the products ($\Delta E^{\ddagger}_{-1}$). Therefore, the change in the internal energy of a system undergoing a chemical reaction from reactants to products can be expressed as

$$\Delta E^{\circ} = E_{\text{products}} - E_{\text{reactants}} = \Delta E^{\ddagger}_{1} - \Delta E^{\ddagger}_{-1} \qquad (1.55)$$

Equation (1.54) can therefore be expressed as two separate differential equations corresponding to the forward and reverse reactions:

$$\frac{d \ln k_1}{dT} = \frac{\Delta E^{\ddagger}_{1}}{RT^2} + C \quad \text{and} \quad \frac{d \ln k_{-1}}{dT} = \frac{\Delta E^{\ddagger}_{-1}}{RT^2} + C \qquad (1.56)$$

Arrhenius determined that for many reactions, $C = 0$, and thus stated his law as:

$$\frac{d \ln k_r}{dT} = \frac{\Delta E^{\ddagger}}{RT^2} \qquad (1.57)$$

The Arrhenius law can also be expressed in the more familiar integrated form:

$$\ln k_r = \ln A - \frac{\Delta E^{\ddagger}}{RT} \quad \text{or} \quad k_r = Ae^{-(\Delta E^{\ddagger}/RT)} \qquad (1.58)$$

$\Delta E^{\ddagger}$, or E_a as Arrhenius defined this term, is the energy of activation for a chemical reaction, and A is the *frequency factor*. The frequency factor has the same dimensions as the rate constant and is related to the frequency of collisions between reactant molecules.

1.3.2   Energy of Activation

Figure 1.11 depicts a potential energy reaction coordinate for a hypothetical reaction $A \rightleftharpoons B$. For A molecules to be converted to B (forward reaction), or for B molecules to be converted to A (reverse reaction), they must acquire energy to form an activated complex $C^{\ddagger}$. This potential energy barrier is therefore called the *energy of activation* of the reaction. For the reaction to take place, this energy of activation is the minimum energy that must be acquired by the system's molecules. Only a small fraction of the molecules may possess sufficient energy to react. The rate of the forward reaction depends on $\Delta E_1^{\ddagger}$, while the rate of the reverse reaction depends on $\Delta E_{-1}^{\ddagger}$ (Fig. 1.11). As will be shown later, the rate constant is inversely proportional to the energy of activation.

To determine the energy of activation of a reaction, it is necessary to measure the rate constant of a particular reaction at different temperatures. A plot of $\ln k_r$ versus $1/T$ yields a straight line with slope $-\Delta E^{\ddagger}/R$ (Fig. 1.12). Alternatively, integration of Eq. (1.58) as a definite integral with appropriate boundary conditions,

$$\int_{k_1}^{k_2} d \ln k_r = \int_{T_1}^{T_2} \frac{dT}{T^2} \tag{1.59}$$

yields the following expression:

$$\ln \frac{k_2}{k_1} = \frac{\Delta E^{\ddagger}}{R} \frac{T_2 - T_1}{T_2 T_1} \tag{1.60}$$
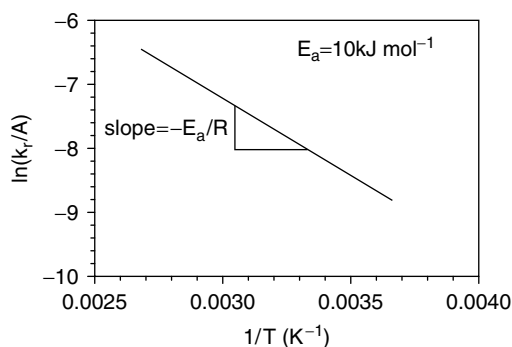
Figure 1.12. Arrhenius plot used in determination of the energy of activation (E_a) of a reaction.

This equation can be used to obtain the energy of activation, or predict the value of the rate constant at T_2 from knowledge of the value of the rate constant at T_1, and of $\Delta E^\ddagger$.

A parameter closely related to the energy of activation is the *Z value*, the temperature dependence of the decimal reduction time, or *D value*. The *Z* value is the temperature increase required for a one-$\log_{10}$ reduction (90% decrease) in the *D* value, expressed as

$$\log_{10} D = \log_{10} C - \frac{T}{Z} \qquad (1.61)$$

or

$$D = C \cdot 10^{-T/Z} \qquad (1.62)$$

where *C* is a constant related to the frequency factor A in the Arrhenius equation.

The *Z* value can be determined from a plot of $\log_{10} D$ versus temperature (Fig. 1.13). Alternatively, if *D* values are known only at two temperatures, the *Z* value can be determined using the equation

$$\log_{10} \frac{D_2}{D_1} = -\frac{T_2 - T_1}{Z} \qquad (1.63)$$

It can easily be shown that the *Z* value is inversely related to the energy of activation:

$$Z = \frac{2.303 R T_1 T_2}{\Delta E^\ddagger} \qquad (1.64)$$

where T_1 and T_2 are the two temperatures used in the determination of $\Delta E^\ddagger$.
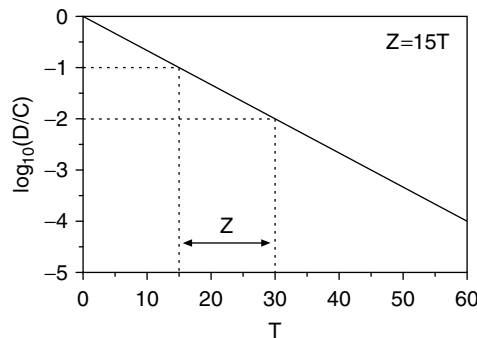
Figure 1.13. Semilogarithmic plot of the decimal reduction time (*D*) as a function of temperature used in the determination of the *Z* value.

1.4   ACID–BASE CHEMICAL CATALYSIS

Many homogeneous reactions in solution are catalyzed by acids and bases. A Brönsted acid is a proton donor,

$$HA + H_2O \longleftrightarrow H_3O^+ + A^- \qquad (1.65)$$
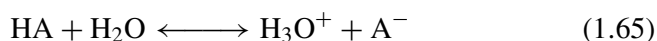
while a Brönsted base is a proton acceptor,

$$A^- + H_2O \longleftrightarrow HA + OH^- \qquad (1.66)$$
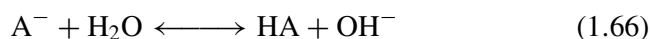
The equilibrium ionization constants for the weak acid (K_{HA}) and its conjugate base (K_{A^-}) are, respectively,

$$K_{HA} = \frac{[H_3O^+][A^-]}{[HA][H_2O]} \qquad (1.67)$$

and

$$K_{A^-} = \frac{[HA][OH^-]}{[A^-][H_2O]} \qquad (1.68)$$

The concentration of water can be considered to remain constant (~ 55.3 M) in dilute solutions and can thus be incorporated into K_{HA} and K_{A^-}. In this fashion, expressions for the acidity constant (K_a), and the basicity, or hydrolysis, constant (K_b) are obtained:

$$K_a = K_{HA}[H_2O] = \frac{[H_3O^+][A^-]}{[HA]} \qquad (1.69)$$

$$K_b = K_{A^-}[H_2O] = \frac{[HA][OH^-]}{[A^-]} \qquad (1.70)$$

These two constants are related by the self-ionization or autoprotolysis constant of water. Consider the ionization of water:

$$2H_2O \longleftrightarrow H_3O^+ + OH^- \qquad (1.71)$$

where

$$K_{H_2O} = \frac{[H_3O^+][OH^-]}{[H_2O]^2} \qquad (1.72)$$

The concentration of water can be considered to remain constant (~ 55.3 M) in dilute solutions and can thus be incorporated into K_{H_2O}.

Equation (1.72) can then be expressed as

$$K_w = K_{H_2O}[H_2O]^2 = [H_3O^+][OH^-] \qquad (1.73)$$

where K_w is the self-ionization or autoprotolysis constant of water. The product of K_a and K_b corresponds to this self-ionization constant:

$$K_w = K_a K_b = \frac{[H_3O^+][A^-]}{[HA]} \cdot \frac{[HA][OH^-]}{[A^-]} = [H_3O^+][OH^-] \qquad (1.74)$$

Consider a substrate S that undergoes an elementary reaction with an undissociated weak acid (HA), its conjugate conjugate base (A^-), hydronium ions (H_3O^+), and hydroxyl ions (OH^-). The reactions that take place in solution include

$$S \xrightarrow{k_0} P$$

$$S + H_3O^+ \xrightarrow{k_{H^+}} P + H_3O^+$$

$$S + OH^- \xrightarrow{k_{OH^-}} P + OH^- \qquad (1.75)$$

$$S + HA \xrightarrow{k_{HA}} P + HA$$

$$S + A^- \xrightarrow{k_{A^-}} P + A^-$$
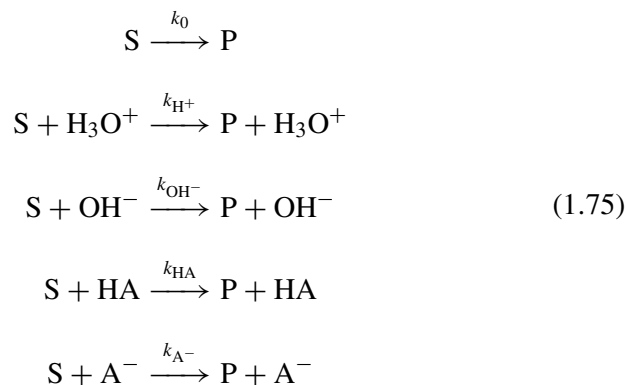
The rate of each of the reactions above can be written as

$$v_0 = k_0[S]$$
$$v_{H^+} = k_{H^+}[H_3O^+][S]$$
$$v_{OH^-} = k_{OH^-}[OH^-][S] \qquad (1.76)$$
$$v_{HA} = k_{HA}[HA][S]$$
$$v_{A^-} = k_{A^-}[A^-][S]$$

where k_0 is the rate constant for the uncatalyzed reaction, k_{H^+} is the rate constant for the hydronium ion–catalyzed reaction, k_{OH^-} is the rate constant for the hydroxyl ion–catalyzed reaction, k_{HA} is the rate constant for the undissociated acid-catalyzed reaction, and k_{A^-} is the rate constant for the conjugate base–catalyzed reaction.

The overall rate of this acid/base-catalyzed reaction (v) corresponds to the summation of each of these individual reactions:

$$
\begin{aligned}
v &= v_0 + v_{H^+} + v_{OH^-} + v_{HA} + v_{A^-} \\
&= k_0[S] + k_{H^+}[H_3O^+][S] + k_{OH^-}[OH^-][S] \\
&\quad + k_{HA}[HA][S] + k_{A^-}[A^-][S] \\
&= (k_0 + k_{H^+}[H_3O^+] + k_{OH^-}[OH^-] + k_{HA}[HA] + k_{A^-}[A^-])[S] \\
&= k_c[S]
\end{aligned}
\tag{1.77}
$$

where k_c is the catalytic rate coefficient:

$$
k_c = k_0 + k_{H^+}[H_3O^+] + k_{OH^-}[OH^-] + k_{HA}[HA] + k_{A^-}[A^-] \tag{1.78}
$$

Two types of acid–base catalysis have been observed: general and specific. *General acid–base catalysis* refers to the case where a solution is buffered, so that the rate of a chemical reaction is not affected by the concentration of hydronium or hydroxyl ions. For these types of reactions, k_{H^+} and k_{OH^-} are negligible, and therefore

$$
k_{HA}, \ k_{A^-} \ggg k_{H^+}, \ k_{OH^-} \tag{1.79}
$$

For general acid–base catalysis, assuming a negligible contribution from the uncatalyzed reaction ($k_0 \lll k_{HA}, \ k_{A^-}$), the catalytic rate coefficient is mainly dependent on the concentration of undissociated acid HA and conjugate base A^- at constant ionic strength. Thus, k_c reduces to

$$
k_c = k_{HA}[HA] + k_{A^-}[A^-] \tag{1.80}
$$

which can be expressed as

$$
k_c = k_{HA}[HA] + k_{A^-}\frac{K_a[HA]}{[H^+]} = \left(k_{HA} + k_{A^-}\frac{K_a}{[H^+]}\right)[HA] \tag{1.81}
$$

Thus, a plot of k_c versus HA concentration at constant pH yields a straight line with

$$
\text{slope} = k_{HA} + k_{A^-}\frac{K_a}{[H^+]} \tag{1.82}
$$

Since the value of K_a is known and the pH of the reaction mixture is fixed, carrying out this experiment at two values of pH allows for the determination of k_{HA} and k_{A^-}.

Of greater relevance to our discussion is *specific acid–base catalysis*, which refers to the case where the rate of a chemical reaction is proportional only to the concentration of hydrogen and hydroxyl ions present. For these type of reactions, k_{HA} and k_{A^-} are negligible, and therefore

$$k_{H^+}, \, k_{OH^-} \ggg k_{HA}, \, k_{A^-} \tag{1.83}$$

Thus, k_c reduces to

$$k_c = k_0 + k_{H^+}[H^+] + k_{OH^-}[OH^-] \tag{1.84}$$

The catalytic rate coefficient can be determined by measuring the rate of the reaction at different pH values, at constant ionic strength, using appropriate buffers.

Furthermore, for acid-catalyzed reactions at high acid concentrations where $k_0, k_{OH^-} \lll k_{H^+}$,

$$k_c = k_{H^+}[H^+] \tag{1.85}$$

For base-catalyzed reactions at high alkali concentrations where $k_0, k_{H^+} \lll k_{OH^-}$,

$$k_c = k_{OH^-}[OH^-] = k_{OH^-}\frac{K_w}{[H^+]} \tag{1.86}$$

Taking base 10 logarithms on both sides of Eqs. (1.85) and (1.86) results, respectively, in the expressions

$$\log_{10} k_c = \log_{10} k_{H^+} + \log_{10}[H^+] = \log_{10} k_{H^+} - pH \tag{1.87}$$

for acid-catalyzed reactions and

$$\log_{10} k_c = \log_{10}(K_w k_{OH^-}) - \log_{10}[H^+] = \log_{10}(K_w k_{OH^-}) + pH \tag{1.88}$$

for base-catalyzed reactions.

Thus, a plot of $\log_{10} k_c$ versus pH is linear in both cases. For an acid-catalyzed reaction at low pH, the slope equals -1, and for a base-catalyzed reaction at high pH, the slope equals $+1$ (Fig. 1.14). In regions of intermediate pH, $\log_{10} k_c$ becomes independent of pH and therefore of hydroxyl and hydrogen ion concentrations. In this pH range, k_c depends solely on k_0.

1.5 THEORY OF REACTION RATES

Absolute reaction rate theory is discussed briefly in this section. Collision theory will not be developed explicitly since it is less applicable to
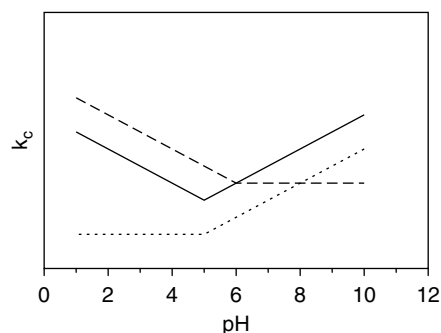
Figure 1.14. Changes in the reaction rate constant for an acid/base-catalyzed reaction as a function of pH. A negative sloping line (slope $= -1$) as a function of increasing pH is indicative of an acid-catalyzed reaction; a positive sloping line (slope $= +1$) is indicative of a base-catalyzed reaction. A slope of zero is indicative of pH independence of the reaction rate.

the complex systems studied. Absolute reaction rate theory is a collision theory which assumes that chemical activation occurs through collisions between molecules. The central postulate of this theory is that the rate of a chemical reaction is given by the rate of passage of the activated complex through the transition state.

This theory is based on two assumptions, a dynamical bottleneck assumption and an equilibrium assumption. The first asserts that the rate of a reaction is controlled by the decomposition of an activated transition-state complex, and the second asserts that an equilibrium exists between reactants (A and B) and the transition-state complex, $C^{\ddagger}$:

$$A + B \rightleftharpoons C^{\ddagger} \longrightarrow C + D \tag{1.89}$$
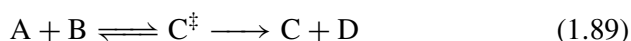
It is therefore possible to define an equilibrium constant for the conversion of reactants in the ground state into an activated complex in the transition state. For the reaction above,

$$K^{\ddagger} = \frac{[C^{\ddagger}]}{[A][B]} \tag{1.90}$$

As discussed previously, $\Delta G^{\circ} = -RT \ln K$ and $\ln K = \ln k_1 - \ln k_{-1}$. Thus, in an analogous treatment to the derivation of the Arrhenius equation (see above), it would be straightforward to show that

$$k_r = ce^{-(\Delta G^{\ddagger}/RT)} = cK^{\ddagger} \tag{1.91}$$

where $\Delta G^{\ddagger}$ is the free energy of activation for the conversion of reactants into activated complex. By using statistical thermodynamic arguments, it is possible to show that the constant c equals

$$c = \kappa \nu \qquad (1.92)$$

where κ is the transmission coefficient and ν is the frequency of the normal-mode oscillation of the transition-state complex along the reaction coordinate—more rigorously, the average frequency of barrier crossing. The transmission coefficient, which can differ dramatically from unity, includes many correction factors, including tunneling, barrier recrossing correction, and solvent frictional effects. The rate of a chemical reaction depends on the equilibrium constant for the conversion of reactants into activated complex.

Since $\Delta G = \Delta H - T\Delta S$, it is possible to rewrite Eq. (1.91) as

$$k_r = \kappa \nu e^{\Delta S^{\ddagger}/R} e^{-(\Delta H^{\ddagger}/RT)} \qquad (1.93)$$

Consider $\Delta H = \Delta E + (\Delta n)RT$, where Δn equals the difference between the number of moles of activated complex (n_{ac}) and the moles of reactants (n_r). The term n_r also corresponds to the molecularity of the reaction (e.g., unimolecular, bimolecular). At any particular time, $n_r \ggg n_{ac}$ and therefore $\Delta H \approx \Delta E - n_r RT$. Substituting this expression for the enthalpy change into Eq. (1.93) and rearranging, we obtain

$$k_r = \kappa \nu \, e^{(n_r + \Delta S^{\ddagger})/R} e^{-(\Delta E^{\ddagger}/RT)} \qquad (1.94)$$

Comparison of this equation with the Arrhenius equation sheds light on the nature of the frequency factor:

$$A = \kappa \nu \, e^{(n_r + \Delta S^{\ddagger})/R} \qquad (1.95)$$

The concept of entropy of activation ($\Delta S^{\ddagger}$) is of utmost importance for an understanding of reactivity. Two reactions with similar $\Delta E^{\ddagger}$ values at the same temperature can proceed at appreciably different rates. This effect is due to differences in their entropies of activation. The entropy of activation corresponds to the difference in entropy between the ground and transition states of the reactants. Recalling that entropy is a measure of the randomness of a system, a positive $\Delta S^{\ddagger}$ suggests that the transition state is more disordered (more degrees of freedom) than the ground state. Alternatively, a negative $\Delta S^{\ddagger}$ value suggests that the transition state is

more ordered (less degrees of freedom) than the ground state. Freely diffusing, noninteracting molecules have many translational, vibrational and rotational degrees of freedom. When two molecules interact at the onset of a chemical reaction and pass into a more structured transition state, some of these degrees of freedom will be lost. For this reason, most entropies of activation for chemical reactions are negative. When the change in entropy for the formation of the activated complex is small ($\Delta S^{\ddagger} \approx 0$), the rate of the reaction is controlled solely by the energy of activation ($\Delta E^{\ddagger}$).

It is interesting to use the concept of entropy of activation to explain the failure of collision theory to explain reactivity. Consider that for a bimolecular reaction $A + B \rightarrow$ products, the frequency factor (A) equals the number of collisions per unit volume between reactant molecules (Z) times a steric, or probability factor (P):

$$A = PZ = \kappa \nu \, e^{2 + \Delta S^{\ddagger}/R} \qquad (1.96)$$

If only a fraction of the collisions result in conversion of reactants into products, then $P < 1$, implying a negative $\Delta S^{\ddagger}$. For this case, the rate of the reaction will be slower than predicted by collision theory. If a greater number of reactant molecules than predicted from the number of collisions are converted into products, $P > 1$, implying a positive $\Delta S^{\ddagger}$. For this case, the rate of the reaction will be faster than predicted by collision theory. On the other hand, when $P = 1$ and $\Delta S^{\ddagger} = 0$, predictions from collision theory and absolute rate theory agree.

1.6   COMPLEX REACTION PATHWAYS

In this section we discuss briefly strategies for tackling more complex reaction mechanisms. The first step in any kinetic modeling exercise is to write down the differential equations and mass balance that describe the process. Consider the reaction

$$A \xrightarrow{k_1} B \xrightarrow{k_2} C \qquad (1.97)$$

Typical concentration–time patterns for A, B, and C are shown in Fig. 1.15. The differential equations and mass balance that describe this reaction are
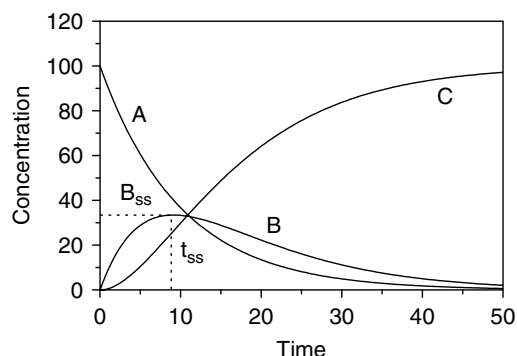
Figure 1.15. Changes in reactant, intermediate, and product concentrations as a function of time for a reaction of the form A → B → C. B_{ss} denotes the steady-state concentration in intermediate B at time t_{ss}.

$$\frac{dA}{dt} = -k_1[A] \tag{1.98}$$

$$\frac{d[B]}{dt} = k_1[A] - k_2[B] \tag{1.99}$$

$$\frac{d[C]}{dt} = k_2[B] \tag{1.100}$$

$$[A_0] + [B_0] + [C_0] = [A_t] + [B_t] + [C_t] \tag{1.101}$$

Once the differential equations and mass balance have been written down, three approaches can be followed in order to model complex reaction schemes. These are (1) numerical integration of differential equations, (2) steady-state approximations to solve differential equations analytically, and (3) exact analytical solutions of the differential equations without using approximations.

It is important to remember that in this day and age of powerful computers, it is no longer necessary to find analytical solutions to differential equations. Many commercially available software packages will carry out numerical integration of differential equations followed by nonlinear regression to fit the model, in the form of differential equations, to the data. Estimates of the rate constants and their variability, as well as measures of the goodness of fit of the model to the data, can be obtained in this fashion. Eventually, all modeling exercises are carried out in this fashion since it is difficult, and sometimes impossible, to obtain analytical solutions for complex reaction schemes.

1.6.1   Numerical Integration and Regression

1.6.1.1   Numerical Integration

Finding the numerical solution of a system of first-order ordinary differential equations,

$$\frac{dY}{dx} = F(x, Y(x)) \qquad Y(x_0) = Y_0 \qquad (1.102)$$

entails finding the numerical approximations of the solution $Y(x)$ at discrete points $x_0, x_1, x_2 < \cdots < x_n < x_{n+1} < \cdots$ by $Y_0, Y_1, Y_2, \ldots, Y_n,$ $Y_{n+1}, \ldots$. The distance between two consecutive points, $h_n = x_n - x_{n+1}$, is called the *step size*. Step sizes do not necessarily have to be constant between all grid points x_n. All numerical methods have one property in common: finding approximations of the solution $Y(x)$ at grid points one by one. Thus, if a formula can be given to calculate Y_{n+1} based on the information provided by the known values of $Y_n, Y_{n-1}, \cdots, Y_0$, the problem is solved. Many numerical methods have been developed to find solutions for ordinary differential equations, the simplest one being the Euler method. Even though the Euler method is seldom used in practice due to lack of accuracy, it serves as the basis for analysis in more accurate methods, such as the Runge–Kutta method, among many others.

For a small change in the dependent variable (Y) in time (x), the following approximation is used:

$$\frac{dY}{dx} \sim \frac{\Delta Y}{\Delta x} \qquad (1.103)$$

Therefore, we can write

$$\frac{Y_{n+1} - Y_n}{x_{n+1} - x_n} = F(x_n, Y_n) \qquad (1.104)$$

By rearranging Eq. (1.104), Euler obtained an expression for Y_{n+1} in terms of Y_n:

$$Y_{n+1} = Y_n + (x_{n+1} - x_n)F(x_n, Y_n) \quad \text{or} \quad Y_{n+1} = Y_n + hF(x_n, Y_n) \qquad (1.105)$$

Consider the reaction $A \rightarrow B \rightarrow C$. As discussed before, the analytical solution for the differential equation that describes the first-order decay in [A] is $[A_t] = [A_0] e^{-kt}$. Hence, the differential equation that describes changes in [B] in time can be written as

$$\frac{d[B]}{dt} = k_1[A_0] e^{-k_1 t} - k_2[B] \qquad (1.106)$$

A numerical solution for the differential equation (1.106) is found using *the initial value* $[B_0]$ at $t = 0$, and from knowledge of the values of k_1, k_2, and $[A_0]$. Values for $[B_t]$ are then calculated as follows:

$$[B_1] = [B_0] + h(k_1[A_0] - k_2[B_0])$$

$$[B_2] = [B_1] + h(k_1[A_0] e^{-k_1 t_1} - k_2[B_1])$$

$$\vdots \tag{1.107}$$

$$[B_{n+1}] = [B_n] + h(k_1[A_0] e^{-k_1 t_n} - k_2[B_n])$$

It is therefore possible to generate a numerical solution (i.e., a set of numbers predicted by the differential equation) of the ordinary differential equation (1.106). Values obtained from the numerical integration (i.e., predicted data) can now be compared to experimental data values.

1.6.1.2 Least-Squares Minimization (Regression Analysis)

The most common way in which models are fitted to data is by using least-squares minimization procedures (regression analysis). All these procedures, linear or nonlinear, seek to find estimates of the equation parameters $(\alpha, \beta, \gamma, \ldots)$ by determining parameter values for which the sum of squared residuals is at a minimum, and therefore

$$\left[\frac{\partial \sum_1^n (y_i - \hat{y}_i)^2}{\partial \alpha} \right]_{\beta, \gamma, \delta, \ldots} = 0 \tag{1.108}$$

where y_i and $\hat{y}_i$ correspond, respectively, to the ith experimental and predicted points at x_i. If the variance (s_i^2) of each data point is known from experimental replication, a weighted least-squares minimization can be carried out, where the weights (w_i) correspond to $1/s_i^2$. In this fashion, data points that have greater error contribute less to the analysis. Estimates of equation parameters are found by determining parameter values for which the chi-squared (χ^2) value is at a minimum, and therefore

$$\left[\frac{\partial \sum_1^n w_i (y_i - \hat{y}_i)^2}{\partial \alpha} \right]_{\beta, \gamma, \delta, \ldots} = 0 \tag{1.109}$$

At this point it is necessary to discuss differences between uniresponse and multiresponse modeling. Take, for example, the reaction $A \rightarrow B \rightarrow C$. Usually, equations in differential or algebraic form are fitted to individual data sets, A, B, and C and a set of parameter estimates obtained.

However, if changes in the concentrations of A, B, and C as a function of time are determined, it is possible to use the entire data set (A, B, C) simultaneously to obtain parameter estimates. This procedure entails fitting the functions that describe changes in the concentration of A, B, and C to the experimental data *simultaneously*, thus obtaining one global estimate of the rate constants. This *multivariate response modeling* helps increase the precision of the parameter estimates by using all available information from the various responses.

A determinant criterion is used to obtain least-squares estimates of model parameters. This entails minimizing the determinant of the matrix of cross products of the various residuals. The maximum likelihood estimates of the model parameters are thus obtained without knowledge of the variance–covariance matrix. The residuals ϵ_{iu}, ϵ_{ju}, and ϵ_{ku} correspond to the difference between predicted and actual values of the dependent variables at the different values of the uth independent variable ($u = t_0$ to $u = t_n$), for the ith, jth, and kth experiments (A, B, and C), respectively. It is possible to construct an error covariance matrix with elements v_{ij}:

$$v_{ij} = \sum_{u=1}^{n} \epsilon_{iu}\epsilon_{ju} \qquad (1.110)$$

The determinant of this matrix needs to be minimized with respect to the parameters. The diagonal of this matrix corresponds to the sums of squares for each response (v_{ii}, v_{jj}, v_{kk}).

Regression analysis involves several important assumptions about the function chosen and the error structure of the data:

1. The correct equation is used.
2. Only dependent variables are subject to error; while independent variables are known exactly.
3. Errors are normally distributed with zero mean, are the same for all responses (homoskedastic errors), and are uncorrelated (zero covariance).
4. The correct weighting is used.

For linear functions, single or multiple, it is possible to find analytical solutions of the error minimization partial differential. Therefore, exact mathematical expressions exist for the calculation of slopes and intercepts. It should be noted at this point that a linear function of parameters does not imply a straight line. A model is *linear* if the first partial derivative

of the function with respect to the parameter(s) is independent of such parameter(s), therefore, higher-order derivatives would be zero.

For example, equations used to calculate the best-fit slope and y-intercept for a data set that fits the linear function $y = mx + b$ can easily be obtained by considering that the minimum sum-of-squared residuals (SS) corresponds to parameter values for which the partial differential of the function with respect to each parameter equals zero. The squared residuals to be minimized are

$$(\text{residual})^2 = (y_i - \hat{y}_i)^2 = [y_i - (mx_i + b)]^2 \tag{1.111}$$

The partial differential of the slope (m) for a constant y-intercept is therefore

$$\left(\frac{\partial \text{SS}}{\partial m}\right)_b = -2\sum_1^n x_i y_i + 2b\sum_1^n x_i + 2m\sum_1^n x_i^2 = 0 \tag{1.112}$$

and therefore

$$m = \frac{\sum_1^n x_i y_i - b\sum_1^n x_i}{\sum_1^n x_i^2} \tag{1.113}$$

The partial differential of the y-intercept for a constant slope is

$$\left(\frac{\partial \text{SS}}{\partial b}\right)_m = m\sum_1^n x_i - \sum_1^n y_i + nb = 0 \tag{1.114}$$

and therefore

$$b = \frac{\sum_1^n y_i - m\sum_1^n x_i}{n} = \overline{y} - m\overline{x} \tag{1.115}$$

where x and y correspond to the overall averages of all x and y data, respectively. Substituting b into m and rearranging, we obtain an equation for direct calculation of the best-fit slope of the line:

$$m = \frac{\sum_{i=1}^n x_i y_i - \left(\sum_{i=1}^n x_i \sum_{i=1}^n y_i / n\right)}{\sum_{i=1}^n x_i^2 - \left(\sum_{i=1}^n x_i\right)^2 / n} = \frac{\sum_{i=1}^n (x_i - \overline{x})(y_i - \overline{y})}{\sum_{i=1}^n (x_i - \overline{x})^2} \tag{1.116}$$

The best-fit y-intercept of the line is given by

$$b = \overline{y} - \frac{\sum_{i=1}^{n}(x_i - \overline{x})(y_i - \overline{y})}{\sum_{i=1}^{n}(x_i - \overline{x})^2}\overline{x} \qquad (1.117)$$

These equations could have also been derived by considering the orthogonality of residuals using $\sum(y_i - \hat{y}_i)(x_i) = 0$.

Goodness-of-Fit Statistics

At this point it would be useful to mention goodness-of-fit statistics. A useful parameter for judging the goodness of fit of a model to experimental data is the reduced χ^2 value:

$$\chi_v^2 = \frac{\sum_{1}^{n}w_i(y_i - \hat{y}_i)^2}{v} \qquad (1.118)$$

where w_i is the weight of the ith data point and v corresponds to the degrees of freedom, defined as $v = (n - p - 1)$, where n is the total number of data values and p is the number of parameters that are estimated. The reduced χ^2 value should be roughly equal to the number of degrees of freedom if the model is correct (i.e., $\chi_v^2 \approx 1$). Another statistic most appropriately applied to linear regression, as an indication of how closely the dependent and independent variables approximate a linear relationship to each other is the *correlation coefficient* (CC):

$$CC = \frac{\sum_{i=1}^{n}w_i(x_i - \overline{x})(y_i - \overline{y})}{\left[\sum_{i=1}^{n}w_i(x_i - \overline{x})^2\right]^{1/2}\left[\sum_{i=1}^{n}w_i(y_i - \overline{y})^2\right]^{1/2}} \qquad (1.119)$$

Values for the correlation coefficient can range from -1 to $+1$. A CC value close to ± 1 is indicative of a strong correlation. The *coefficient of determination* (CD) is the fraction ($0 < CD \leq 1$) of the total variability accounted for by the model. This is a more appropriate measure of the goodness of fit of a model to data than the R-squared statistic. The CD has the general form

$$CD = \frac{\sum_{i=1}^{n}w_i(y_i - \overline{y})^2 - \sum_{i=1}^{n}w_i(y_i - \hat{y}_i)^2}{\sum_{i=1}^{n}w_i(y_i - \overline{y})^2} \qquad (1.120)$$

Finally, the r^2 statistic is similar to the CD. This statistic is often used erroneously when, strictly speaking, the CD should be used. The root of

the r^2 statistic is sometimes erroneously reported to correspond to the CD. An r^2 value close to ± 1 is indicative that the model accounts for most of the variability in the data. The r^2 statistic has the general form

$$r^2 = \frac{\sum_{i=1}^{n} w_i y_i{}^2 - \sum_{i=1}^{n} w_i (y_i - \hat{y}_i)^2}{\sum_{i=1}^{n} w_i y_i{}^2} \qquad (1.121)$$

Nonlinear Regression: Techniques and Philosophy

For nonlinear functions, however, the situation is more complex. Iterative methods are used instead, in which parameter values are changed simultaneously, or one at a time, in a prescribed fashion until a global minimum is found. The algorithms used include the Levenberg–Marquardt method, the Powell method, the Gauss–Newton method, the steepest-descent method, simplex minimization, and combinations thereof. It is beyond our scope in this chapter to discuss the intricacies of procedures used in nonlinear regression analysis. Suffice to say, most modern graphical software packages include nonlinear regression as a tool for curve fitting.

Having said this, however, some comments on curve fitting and nonlinear regression are required. There is no general method that guarantees obtaining the best global solution to a nonlinear least-squares minimization problem. Even for a single-parameter model, several minima may exist! A minimization algorithm will eventually succeed in find *a minimum*; however, there is no assurance that this corresponds to the *global minimum*. It is theoretically possible for one, and maybe two, parameter functions to search all parameter initial values exhaustively and find the global minimum. However, this approach is usually not practical even beyond a single parameter function.

There are, however, some guidelines that can be followed to increase the likelihood of finding the best fit to nonlinear models. All nonlinear regression algorithms require *initial estimates* of parameter values. These initial estimates should be as close as possible to their best-fit value so that the program can actually succeed in finding the global minimum. The development of good initial estimates comes primarily from the scientists' physical knowledge of the problem at hand as well as from intuition and experience. Curve fitting can sometimes be somewhat of an artform.

Generally, it is useful to carry out simulations varying initial estimates of parameter values in order to develop a feeling for how changes in initial estimate values will affect the nonlinear regression results obtained. Some programs offer simplex minimization algorithms that do not require the input of initial estimates. These secondary minimization procedures

may provide values of initial estimates for the primary minimization pro-
cedures. Once a minimum is found, there is no assurance, however, that it
corresponds to the global minimum. A standard procedure to test whether
the global minimum has been reached is called *sensitivity analysis*. Sen-
sitivity analysis refers to the variability in results (parameter estimates)
obtained from nonlinear regression analysis due to changes in the values
of initial estimates. In sensitivity analysis, least-squares minimizations are
carried out for different starting values of initial parameter estimates to
determine whether the convergence to the same solution is attained. If
the same minimum is found for different values of initial estimates, the
scientist can be fairly confident that the minimum proposed is the best
answer. Another approach is to fit the model to the data using different
weighting schemes, since it is possible that the largest or smallest val-
ues in the data set may have an undue influence on the final result. Very
important as well is the visual inspection of the data and plotted curve(s),
since a graph can provide clues that may aid in finding a better solution
to the problem.

Strategies exist for systematically finding minima and hence finding the
best minimum. In a multiparameter model, it is sometimes useful to vary
one or two parameters at a time. This entails carrying out the least-squares
minimization procedure floating one parameter at a time while fixing the
value of the other parameters as constants and/or analyzing a subset of the
data. This simplifies calculations enormously, since the greater the number
of parameters to be estimated simultaneously, the more difficult it will be
for the program to find the global minimum. For example, for the reaction
$A \rightarrow B \rightarrow C$, k_1 can easily be estimated from the first-order decay of
[A] in time. The parameter k_1 can therefore be fixed as a constant, and
only k_2 and k_3 floated. After preliminary parameter estimates are obtained
in this fashion, these parameters should be fixed as constants and the
remaining parameters estimated. Only after estimates are obtained for all
the parameters should the entire parameter set be fitted simultaneously.
It is also possible to assign physical limits, or constraints, to the values
of the parameters. The program will find a minimum that corresponds to
parameter values within the permissible range.

Care should be exercised at the data-gathering stage as well. A common
mistake is to gather all the experimental data without giving much thought
as to how the data will be analyzed. It is extremely useful to use the model
to simulate data sets and then try to fit the model to the simulated data.
This exercise will promptly point out where more data would be useful
to the model-building process. It is a good investment of time to simulate
the experiment and data analysis to identify where problems may lie and
identify regions of data that may be most important in determining the

properties of the model. The data gathered must be amenable to analysis in such a way as to shed light on the model.

For difficult problems, the determination of best-fit parameters is a procedure that benefits greatly from experience, intuition, perseverance, skepticism, and scientific reasoning. A good answer requires good initial estimates. Start the minimization procedure with the best possible initial estimates for parameters, and if the parameters have physical limits, specify constraints on their value. For complicated models, begin model fitting by floating a single parameter and using a subset of the data that may be most sensitive to changes in the value of the particular parameter. Subsequently, add parameters and data until it is possible to fit the full model to the complete data set. After the minimization is accomplished, test the answers by carrying out sensitivity analysis. Perhaps run a simplex minimization procedure to determine if there are other minima nearby and whether or not the minimization wanders off in another direction. Finally, plot the data and calculated values and check visually for goodness of fit—the human eye is a powerful tool. Above all, care should be exercised; if curve fitting is approached blindly without understanding its inherent limitations and nuances, erroneous results will be obtained.

The F-test is the most common statistical tool used to judge whether a model fits the data better than another. The models to be compared are fitted to data and reduced χ^2 values (χ_ν^2) obtained. The ratio of the χ_ν^2 values obtained is the F-statistic:

$$F_{\mathrm{df}_n,\mathrm{df}_d} = \frac{\chi_\nu^2(a)}{\chi_\nu^2(b)} \tag{1.122}$$

where df stands for *degrees of freedom*, which are determined from

$$\mathrm{df} = n - p - 1 \tag{1.123}$$

where n and p correspond, respectively, to the total number of data points and the number of parameters in the model. Using standard statistical tables, it is possible to determine if the fits of the models to the data are significantly different from each other at a certain level of statistical significance.

The analysis of residuals ($\hat{y}_i - y_i$), in the form of the *serial correlation coefficient* (SCC), provides a useful measure of how much the model deviates from the experimental data. Serial correlation is an indication of whether residuals tend to run in groups of positive or negative values or tend to be scattered randomly about zero. A large positive value of the SCC is indicative of a systematic deviation of the model from the data.

The SCC has the general form

$$\text{SCC} = \sqrt{n-1} \frac{\sum_{i=1}^{n} \sqrt{w_i}(\hat{y}_i - y_i)\sqrt{w_{i-1}}(\hat{y}_{i-1} - y_{i-1})}{\sum_{i=1}^{n} [w_i(\hat{y}_i - y_i)]^2} \qquad (1.124)$$

Weighting Scheme for Regression Analysis

As stated above, in regression analysis, a model is fitted to experimental data by minimizing the sum of the squared differences between experimental and predicted data, also known as the *chi-square* (χ^2) *statistic*:

$$\chi^2 = \sum_{i=1}^{n} \frac{(y_i - \hat{y}_i)^2}{s_i^2} = \sum_{i=1}^{n} w_i(y_i - \hat{y}_i)^2 \qquad (1.125)$$

Consider a typical experiment where the value of a dependent variable is measured several times at a particular value of the independent variable. From these repeated determinations, a mean and variance of a sample of population values can be calculated. If the experiment itself is then replicated several times, a set of sample means ($\overline{y}_i$) and variances of *sample means* (s_i^2) can be obtained. This variance is a measure of the experimental variability (i.e., the experimental error, associated with $\overline{y}_i$). The central limit theorem clearly states that it is the means of population values, and not individual population values, that are distributed in a Gaussian fashion. This is an essential condition if parametric statistical analysis is to be carried out on the data set. The variance is defined as

$$s_i^2 = \frac{\sum_{i=1}^{n_i} (y_i - \overline{y}_i)^2}{n_i - 1} \qquad (1.126)$$

A weight w_i is merely the inverse of this variance:

$$w_i = \frac{1}{s_i^2} \qquad (1.127)$$

The two most basic assumptions made in regression analysis are that experimental errors are normally distributed with mean zero and that errors are the same for all data points (error homoskedasticity). Systematic trends in the experimental errors or the presence of outliers would invalidate these assumptions. Hence, the purpose of weighting residuals is to eliminate systematic error heteroskedasticity and excessively noisy data. The next challenge is to determine which error structure is present in the experimental data—not a trivial task by any means.

Ideally, each experiment would be replicated sufficiently so that individual data weights could be calculated directly from experimentally determined variances. However, replicating experiments to the extent that would be required to obtain accurate estimates of the errors is expensive, time consuming, and impractical. It is important to note that if insufficient data points are used to estimate individual errors of data points, incorrect estimates of weights will be obtained. The use of incorrect weights in regression analysis will make matters worse—if in doubt, do not weigh the data.

A useful technique for the determination of weights is described below. The relationship between the variance of a data point and the value of the point can be explored using the relationship

$$s_i^2 = K y_i^\alpha \tag{1.128}$$

A plot of $\ln s_i^2$ against $\ln y_i$ yields a straight line with slope $= \alpha$ and y-intercept $= \ln K$ (Fig. 1.16). The weight for the ith data point can then be calculated as

$$w_i = \frac{1}{s_i^2} \sim \frac{K}{s_i^2} = y_i^{-\alpha} \tag{1.129}$$

K is merely a constant that is not included in the calculations, since interest lies in the determination of the *relative* weighting scheme for a particular data set, not in the absolute values of the weights.

If $\alpha = 0$, s_i^2 is not dependent on the magnitude of the y values, and $w = 1/K$ for all data points. This is the case for an error that is constant throughout the data (homogeneous or constant error). Thus, if the error structure is homogeneous, weighting of the data is not required. A value
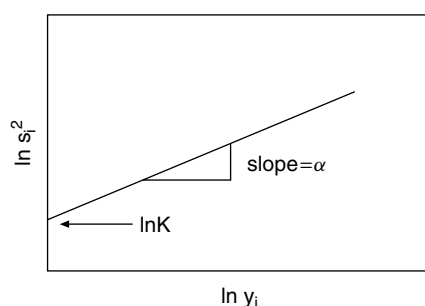
Figure 1.16. Log-log plot of changes in the variance (s_i^2) of the ith sample mean as a function of the value of the ith sample mean (y_i). This plot is used in determination of the type of error present in the experimental data set for the establishment of a weighting scheme to be used in regression analysis of the data.

of $\alpha > 0$ is indicative of a dependence of s_i^2 on the magnitude of the y value. This is referred to as *heterogeneous* or *relative error structure*. Classic heterogeneous error structure analysis usually places $\alpha = 2$ and therefore $w_i \sim 1/Ky_i^2$. However, all values between 0 and 2 and even greater than 2 are possible. The nature of the error structure in the data (homogeneous or heterogeneous) can be visualized in a plot of residual errors $(y_i - \overline{y}_i)$ (Figs. 1.17 and 1.18).

To determine an expression for the weights to be used, the following equation can be used:

$$w_i = y_i^{-\alpha} \tag{1.130}$$

The form of y_i will vary depending on the function used. It could correspond to the velocity of the reaction (v) or the reciprocal of the velocity of the reaction $(1/v$ or $[S]/v)$. For example, for a classic heterogeneous
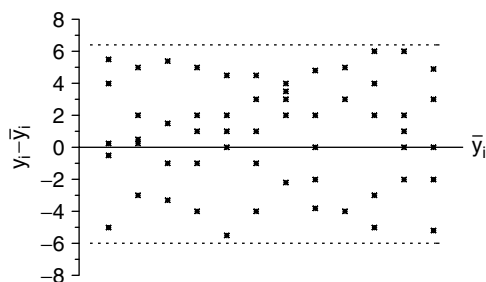
Figure 1.17. Mean residual pattern characteristic of a homogeneous, or constant, error structure in the experimental data.
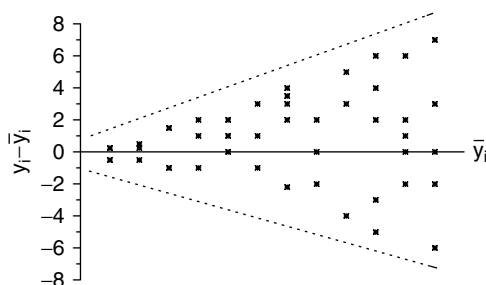
Figure 1.18. Mean residual pattern characteristic of a heterogeneous, or relative, error structure in the experimental data.

error with $\alpha = 2$, the weights for different functions would be

$$w_i(v_i) = \frac{1}{v_i^2} \qquad w_i\left(\frac{1}{v_1}\right) = v_i^2 \qquad w_i\left(\frac{[S_i]}{v_i}\right) = \frac{v_i^2}{[S_i]^2} \qquad (1.131)$$

It is a straightforward matter to obtain expressions for the slope and y-intercept of a weighted least-squares fit to a straight line by solving the partial differential of the χ^2 value. The resulting expression for the slope (m) is

$$m = \frac{\sum_{i=1}^{n} w_i x_i y_i - \left(\sum_{i=1}^{n} w_i x_i \sum_{i=1}^{n} w_i y_i \middle/ \sum_{i=1}^{n} w_i\right)}{\sum_{i=1}^{n} w_i x_i^2 - \left(\sum_{i=1}^{n} w_i x_i\right)^2 \middle/ \sum_{i=1}^{n} w_i}$$

$$= \frac{\sum_{i=1}^{n} w_i(x_i - \overline{x})(y_i - \overline{y})}{\sum_{i=1}^{n} w_i(x_i - \overline{x})^2} \qquad (1.132)$$

and the corresponding expression for the y-intercept (b) is

$$b = \frac{\sum_{i=1}^{n} w_i y_i}{\sum_{i=1}^{n} w_i} - \frac{\sum_{i=1}^{n} w_i(x_i - \overline{x})(y_i - \overline{y})}{\sum_{i=1}^{n} w_i(x_i - \overline{x})^2} \frac{\sum_{i=1}^{n} w_i y_i}{\sum_{i=1}^{n} w_i} \qquad (1.133)$$

1.6.2 Exact Analytical Solution (Non-Steady-State Approximation)

Exact analytical solutions for the reaction $A \rightarrow B \rightarrow C$ can be obtained by solving the differential equations using standard mathematical procedures. Exact solutions to the differential equations for the boundary conditions $[B_0] = [C_0] = 0$ at $t = 0$, and therefore $[A_0] = [A_t] + [B_t] + [C_t]$, are

$$[A_t] = [A_0]e^{-k_1 t} \qquad (1.134)$$

$$[B_t] = k_1[A_0]\frac{e^{-k_1 t} - e^{-k_2 t}}{k_2 - k_1} \qquad (1.135)$$

$$[C_t] = [A_0]\left[1 + \frac{1}{k_1 - k_2}(k_2 e^{-k_1 t} - k_1 e^{-k_2 t})\right] \qquad (1.136)$$

Figure 1.15 shows the simulation of concentration changes in the system $A \rightarrow B \rightarrow C$. The models (equations) are fitted to the experimental data

using nonlinear regression, as described previously, to obtain estimates of k_1 and k_2.

1.6.3 Exact Analytical Solution (Steady-State Approximation)

Steady-state approximations are useful and thus are used extensively in the development of mathematical models of kinetic processes. Take, for example, the reaction $A \rightarrow B \rightarrow C$ (Fig. 1.15). If the rate at which A is converted to B equals the rate at which B is converted to C, the concentration of B remains constant, or in a steady state. It is important to remember that molecules of B are constantly being created and destroyed, but since these processes are occurring at the same rate, the net effect is that the concentration of B remains unchanged ($d[B]/dt = 0$), thus:

$$\frac{d[B]}{dt} = 0 = k_1[A] - k_2[B] \tag{1.137}$$

Decreases in [A] as a function of time are modeled as a first-order decay process:

$$[A_t] = [A_0]\,e^{-k_1 t} \tag{1.138}$$

The value of k_1 can be determined as discussed previously.

From Eqs. (1.137) and (1.138) we can deduce that

$$[B] = \frac{k_1}{k_2}[A] = \frac{k_1}{k_2}[A_0]\,e^{-k_1 t} \tag{1.139}$$

If the steady state concentration of B [B_{ss}], the value of k_1, and the time at which that steady state was reached (t_{ss}) are known, k_2 can be determined from

$$k_2 = \frac{k_1}{[B_{ss}]}[A_0]\,e^{-k_1 t_{ss}} \tag{1.140}$$

The steady state of B in the reaction $A \rightarrow B \rightarrow C$ is short lived (see Fig. 1.15). However, for many reactions, such as enzyme-catalyzed reactions, the concentrations of important reaction intermediates are in a steady state. This allows for the use of steady-state approximations to obtain analytical solutions for the differential equations and thus enables estimation of the values of the rate constants.

CHAPTER 2

HOW DO ENZYMES WORK?

An *enzyme* is a protein with catalytic properties. As a catalyst, an enzyme lowers the energy of activation of a reaction (E_a), thereby increasing the rate of that reaction without affecting the position of equilibrium—forward and reverse reactions are affected to the same extent (Fig. 2.1). Since the rate of a chemical reaction is proportional to the concentration of the transition-state complex ($S^{\ddagger}$), lowering the activation energy effectively leads to an increase in the reaction rate. An enzyme increases the rate of a reaction mostly by specifically binding to, and thus stabilizing, the transition-state structure.

Based on Linus Pauling's views, Joseph Kraut eloquently pointed out that "an enzyme can be considered a flexible molecular template, designed by evolution to be precisely complementary to the reactants in their activated transition-state geometry, as distinct from their ground-state geometry. Thus an enzyme *strongly binds the transition state*, greatly increasing its concentration, and accelerating the reaction proportionately. This description of enzyme catalysis is now usually referred to as transition-state stabilization."

Consider the thermodynamic cycle that relates substrate binding to transition-state binding:
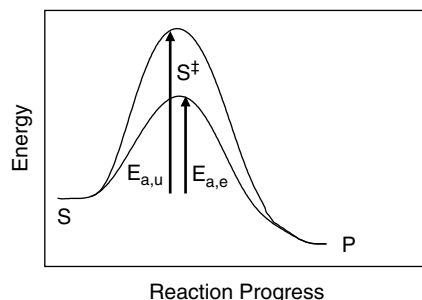
Figure 2.1. Changes in the internal energy of a system undergoing a chemical reaction from substrate S to product P. E_a corresponds to the energy of activation for the forward reaction of enzyme-catalyzed (e) and uncatalyzed (u) reactions. $S^{\ddagger}$ corresponds to the putative transition-state structure.

$$
\begin{array}{ccc}
E + S & \xrightleftharpoons{K_u^{\ddagger}} & E + S^{\ddagger} \xrightarrow{k_u} E + P \\
\Big\updownarrow K_s & & \Big\updownarrow K_t \\
ES \underset{K_e^{\ddagger}}{\rightleftharpoons} & & ES^{\ddagger} \xrightarrow{k_e} E + P
\end{array}
\tag{2.1}
$$
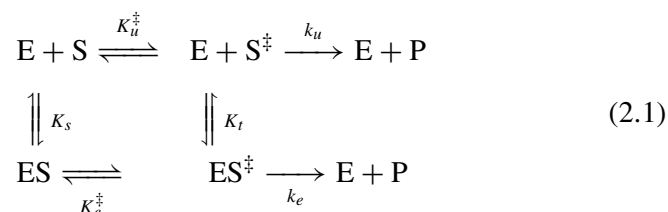
The upper pathway represents the uncatalyzed reaction; the lower pathway represents the enzyme-catalyzed reaction. Four equilibrium constants can be written for the scheme (2.1):

$$
K_s = \frac{[E][S]}{[ES]} \qquad K_t = \frac{[E][S^{\ddagger}]}{[ES^{\ddagger}]}
$$
$$
K_e^{\ddagger} = \frac{[ES^{\ddagger}]}{[ES]} \qquad K_u^{\ddagger} = \frac{[E][S^{\ddagger}]}{[E][S]}
\tag{2.2}
$$

The ratio of the equilibrium constants for conversion of substrate from the ground state to the transition state in the presence and absence of enzyme is related to the ratio of the dissociation constants for ES and $ES^{\ddagger}$ complexes:

$$
\frac{K_e^{\ddagger}}{K_u^{\ddagger}} = \frac{[ES^{\ddagger}]/[ES]}{[E][S^{\ddagger}]/[E][S]} = \frac{[E][S]/[ES]}{[E][S^{\ddagger}]/[ES^{\ddagger}]} = \frac{K_s}{K_t}
\tag{2.3}
$$

As discussed in Chapter 1, absolute reaction rate theory predicts that the rate constant of a reaction (k_r) is directly proportional to the equilibrium

constant for formation of the transition-state complex from reactants in the ground state ($K^{\ddagger}$):

$$k_r = \kappa \nu K^{\ddagger} \tag{2.4}$$

Relative changes in reaction rates due to enzyme catalysis are given by the ratio of reaction rates for the conversion of substrate to product in the presence (k_e) and absence (k_u) of enzyme:

$$\frac{k_e}{k_u} = \frac{\kappa_e \nu_e K_e^{\ddagger}}{\kappa_u \nu_u K_u^{\ddagger}} = \frac{\kappa_e \nu_e K_s}{\kappa_u \nu_u K_t} \tag{2.5}$$

The magnitudes of the enzymatic rate acceleration, k_e/k_n, can be extremely large, in the range 10^{10} to 10^{14}. Considering that it is unlikely that the ratio $\kappa_e \nu_e / \kappa_n \nu_n$ differs from unity by orders of magnitude (even though no data exist to support this assumption), we can rewrite Eq. (2.5) as

$$\frac{k_e}{k_u} \approx \frac{K_s}{K_t} \tag{2.6}$$

The ratio K_s/K_t must therefore also be in the range 10^{10} to 10^{14}.

This important result suggests that substrate in the transition state must necessarily bind to the enzyme much more strongly than substrate in the ground state, by a factor roughly equal to that of the enzymatic rate acceleration. Equation (2.6) provides a conceptual framework for understanding enzyme action. For example, one can address the question of how good an enzyme can be. Identifying k_e with k_{cat}, Eq. (2.5) can be rewritten as

$$\frac{k_{\text{cat}}}{K_s} = k_u \frac{\kappa_e \nu_e}{\kappa_u \nu_u} \frac{1}{K_t} \tag{2.7}$$

The ratio k_{cat}/K_s (M^{-1} s^{-1}) is the second-order rate constant for the reaction of free enzyme with substrate. The magnitude of this rate constant cannot be greater than the diffusion coefficient of the reactants. Thus, a perfectly evolved enzyme will have increased strength of transition-state binding (i.e., decreased K_t) until such a diffusion limit is reached for the thermodynamically favored direction of the reaction.

CHAPTER 3

CHARACTERIZATION OF ENZYME ACTIVITY

3.1 PROGRESS CURVE AND DETERMINATION OF REACTION VELOCITY

To determine reaction velocities, it is necessary to generate a progress curve. For the conversion of substrate (S) to product (P), the general shape of the progress curve is that of a first-order exponential decrease in substrate concentration (Fig. 3.1):

$$[S - S_{min}] = [S_0 - S_{min}]e^{-kt} \tag{3.1}$$

or that of a first-order exponential increase in product concentration (Fig. 3.1):

$$[P - P_0] = [P_{max} - P_0](1 - e^{-kt}) \tag{3.2}$$

where $[S_0]$, $[S_{min}]$, and $[S]$ correspond, respectively, to initial substrate concentration ($t = 0$), minimum substrate concentration ($t \to \infty$), and substrate concentration at time t, while $[P_0]$, $[P_{max}]$, and $[P]$ correspond, respectively, to initial product concentration ($t = 0$), maximum product concentration ($t \to \infty$), and product concentrations at time t (Fig. 3.1).

The rate of the reaction, or reaction velocity (v), corresponds to the instantaneous slope of either of the progress curves:

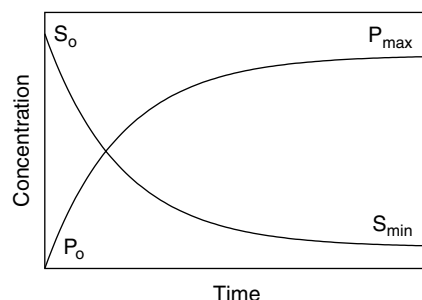$$v = -\frac{dS}{dt} = \frac{dP}{dt} \tag{3.3}$$

Figure 3.1. Changes in substrate (S) and product (P) concentration as a function of time, from initial values (S_0 and P_0) to final values (P_{max} and S_{min}).

However, as can be appreciated in Fig. 3.1, reaction velocity (i.e., the slope of the curve) decreases in time. Some causes for the drop include:

1. The enzyme becomes unstable during the course of the reaction.
2. The degree of saturation of the enzyme by substrate decreases as substrate is depleted.
3. The reverse reaction becomes more predominant as product accumulates.
4. The products of the reaction inhibit the enzyme.
5. Any combination of the factors above cause the drop.

It is for these reasons that progress curves for enzyme-catalyzed reactions do not fit standard models for homogeneous chemical reactions, and a different approach is therefore required. Enzymologists use *initial velocities* as a measure of reaction rates instead. During the early stages of an enzyme-catalyzed reaction, conversion of substrate to product is small and can thus be considered to remain constant and effectively equal to initial substrate concentration ($[S_t] \approx [S_0]$). By the same token, very little product has accumulated ($[P_t] \approx 0$); thus, the reverse reaction can be considered to be negligible, and any possible inhibitory effects of product on enzyme activity, not significant. More important, the enzyme can be considered to remain stable during the early stages of the reaction. To obtain initial velocities, a tangent to the progress curve is drawn as close as possible to its origin (Fig. 3.2). The slope of this tangent (i.e., the initial velocity, is obtained using linear regression). Progress curves are usually linear below 20% conversion of substrate to product.

Progress curves will vary depending on medium pH, temperature, ionic strength, polarity, substrate type, and enzyme and coenzyme concentration, among many others. Too often, researchers use one-point measurements to
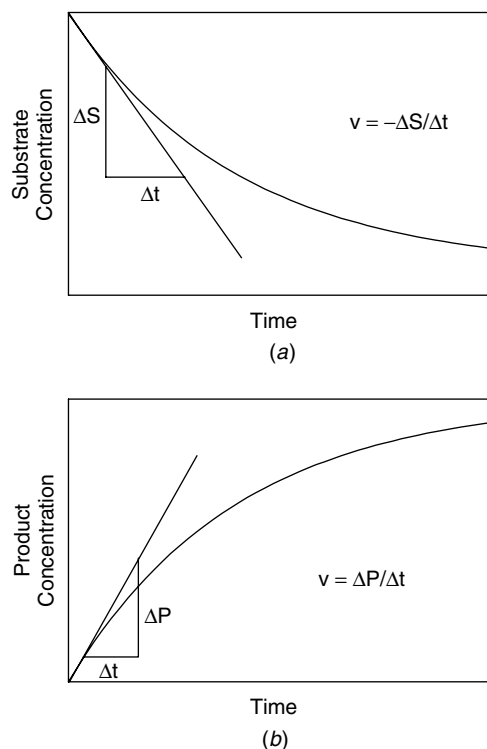
Figure 3.2. Determination of the initial velocity of an enzyme-catalyzed reaction from the instantaneous slope at $t = 0$ of substrate depletion (*a*) or product accumulation (*b*) progress curves.

determine reaction velocities. The time at which a one-time measurement takes place is usually determined from very few progress curves and for a limited set of experimental conditions. A one-point measurement may not be valid for all reaction conditions and treatments studied. For proper enzyme kinetic analysis, it is essential to obtain reaction velocities strictly from the initial region of the progress curve. By using the wrong time for the derivation of rates (not necessarily initial velocities), a linear relationship between enzyme concentration and velocity will not be obtained, this being a basic requirement for enzyme kinetic analysis. For the reaction to be kinetically controlled by the enzyme, the reaction velocity must be directly proportional to enzyme concentration (Fig. 3.3).

To reiterate, for valid kinetic data to be collected:

1. The enzyme must be stable during the time course of the measurements used in the calculation of the initial velocities.

Figure 3.3. Dependence of reaction initial velocity on enzyme concentration in the reaction mixture.

2. Initial rates are used as reaction velocities.
3. The reaction velocity must be proportional to the enzyme concentration.

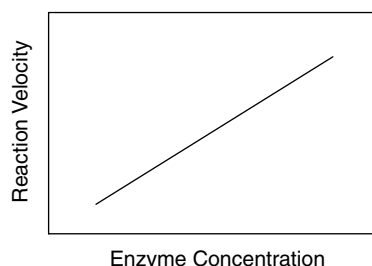Sometimes the shape of progress curves is not that of a first-order exponential increase or decrease, shown in Fig. 3.1. If this is the case, the best strategy is to determine the cause for the abnormal behavior and modify testing conditions accordingly, to eliminate the abnormality. Continuous and discontinuous methods used to monitor the progress of an enzymatic reaction may not always agree. This can be the case particularly for two-stage reactions, in which an intermediate between product and substrate accumulates. In this case, disappearance of substrate may be a more reliable indicator of activity than product accumulation. For discontinuous methods, at least three points are required, one at the beginning of the reaction ($t = 0$), one at a convenient time 1, and one at time 2, which should correspond to twice the length of time 1. This provides a check of the linearity of the progress curve.

The *enzyme unit* (e.u.) is the most commonly used standard unit of enzyme activity. One enzyme unit is defined as that amount of enzyme that causes the disappearance of 1 μmol (or μEq) of substrate, or appearance of 1 μmol (or μEq) of product, per minute:

$$1 \text{ e.u.} = \frac{1 \text{ } \mu\text{mol}}{\text{min}} \tag{3.4}$$

Specific activity is defined as the number of enzyme units per unit mass. This mass could correspond to the mass of the pure enzyme, the amount of protein in a particular isolate, or the total mass of the tissue from where the enzyme was derived. Regardless of which case it is, this must be stated clearly. *Molecular activity (turnover number)*, on the other hand,

corresponds to the number of substrate molecules converted to product per molecule (or active center) of enzyme per unit time.

3.2 CATALYSIS MODELS: EQUILIBRIUM AND STEADY STATE

An enzymatic reaction is usually modeled as a two-step process: substrate (S) binding by enzyme (E) and formation of an enzyme–substrate (ES) complex, followed by an irreversible breakdown of the enzyme–substrate complex to free enzyme and product (P):

$$\text{E} + \text{S} \underset{k_1}{\overset{k_{-1}}{\rightleftharpoons}} \text{ES} \overset{k_{\text{cat}}}{\longrightarrow} \text{E} + \text{P} \tag{3.5}$$
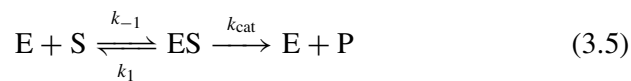
3.2.1 Equilibrium Model

In the equilibrium model of Michaelis and Menten, the substrate-binding step is assumed to be fast relative to the rate of breakdown of the ES complex. Therefore, the substrate binding reaction is assumed to be at equilibrium. The equilibrium dissociation constant for the ES complex (K_s) is a measure of the affinity of enzyme for substrate and corresponds to substrate concentration at $\frac{1}{2}V_{\text{max}}$:

$$K_s = \frac{[\text{E}][\text{S}]}{[\text{ES}]} \tag{3.6}$$

Thus, the lower the value of K_s, the higher the affinity of enzyme for substrate.

The velocity of the enzyme-catalyzed reaction is limited by the rate of breakdown of the ES complex and can therefore be expressed as

$$v = k_{\text{cat}}[\text{ES}] \tag{3.7}$$

where k_{cat} corresponds to the effective first-order rate constant for the breakdown of ES complex to free product and free enzyme. The rate equation is usually normalized by total enzyme concentration ($[\text{E}_T] = [\text{E}] + [\text{ES}]$):

$$\frac{v}{[\text{E}_T]} = \frac{k_{\text{cat}}[\text{ES}]}{[\text{E}] + [\text{ES}]} \tag{3.8}$$

where [E] and [ES] correspond, respectively, to the concentrations of free enzyme and enzyme–substrate complex. Substituting $[\text{E}][\text{S}]/K_s$ for [ES] yields

$$\frac{v}{[E_T]} = \frac{k_{\text{cat}}([E][S]/K_s)}{[E] + [E][S]/K_s} \tag{3.9}$$

Dividing both the numerator and denominator by [E], multiplying the numerator and denominator by K_s, and rearranging yields the familiar expression for the velocity of an enzyme-catalyzed reaction:

$$v = \frac{k_{\text{cat}}[E_T][S]}{K_s + [S]} \tag{3.10}$$

By defining V_{max} as the maximum reaction velocity, $V_{\text{max}} = k_{\text{cat}}[E_T]$, Eq. (3.10) can be expressed as

$$v = \frac{V_{\text{max}}[S]}{K_s + [S]} \tag{3.11}$$

The assumptions of the Michaelis–Menten model are:

1. The substrate-binding step and formation of the ES complex are fast relative to the breakdown rate. This leads to the approximation that the substrate binding reaction is at equilibrium.
2. The concentration of substrate remains essentially constant during the time course of the reaction ($[S_0] \approx [S_t]$). This is due partly to the fact that initial velocities are used and that $[S_0] \ggg [E_T]$.
3. The conversion of product back to substrate is negligible, since very little product has had time to accumulate during the time course of the reaction.

These assumptions are based on the following conditions:

1. The enzyme is stable during the time course of the measurements used to determine the reaction velocities.
2. Initial rates are used as reaction velocities.
3. The reaction velocity is directly proportional to the total enzyme concentration.

Rapid equilibrium conditions need not be assumed for the derivation of an enzyme catalysis model. A steady-state approximation can also be used to obtain the rate equation for an enzyme-catalyzed reaction.

3.2.2 Steady-State Model

The main assumption made in the steady-state approximation is that the concentration of enzyme–substrate complex remains constant in time (i.e.,

$d[\text{ES}]/dt = 0$). Thus, the differential equation that describes changes in the concentration of the ES complex in time equals zero:

$$\frac{d[\text{ES}]}{dt} = k_1[\text{E}][\text{S}] - k_{-1}[\text{ES}] - k_2[\text{ES}] = 0 \qquad (3.12)$$

Rearrangement yields an expression for the Michaelis constant, K_m:

$$K_m = \frac{[\text{E}][\text{S}]}{[\text{ES}]} = \frac{k_{-1} + k_2}{k_{-1}} \qquad (3.13)$$

This K_m will be equivalent to the dissociation constant of the ES complex (K_s) only for the case where $k_{-1} \gg k_2$, and therefore $K_m = k_{-1}/k_1$. The Michaelis constant K_m corresponds to substrate concentration at $\frac{1}{2}V_{\max}$.

As stated before, the rate-limiting step of an enzyme-catalyzed reaction is the breakdown of the ES complex. The velocity of an enzyme-catalyzed reaction can thus be expressed as

$$v = k_{\text{cat}}[\text{ES}] \qquad (3.14)$$

As for the case of the equilibrium model, substitution of the [ES] term for $[\text{E}][\text{S}]/K_m$ and normalization of the rate equation by total enzyme concentration, $[\text{E}_T] = [\text{E} + \text{ES}]$ yields

$$\frac{v}{[\text{E}_T]} = \frac{k_{\text{cat}}([\text{E}][\text{S}]/K_m)}{[\text{E}] + [\text{E}][\text{S}]/K_m} \qquad (3.15)$$

Dividing both the numerator and denominator by [E], multiplying the numerator and denominator by K_m, substituting $V_{\max}$ for $k_{\text{cat}}[\text{E}_T]$, and rearranging yields the familiar expression for the velocity of an enzyme-catalyzed reaction:

$$v = \frac{V_{\max}[\text{S}]}{K_m + [\text{S}]} \qquad (3.16)$$

For the steady-state case, K_s has been replaced by K_m. In most cases, though, substrate binding occurs faster than the breakdown of the ES complex, and thus $K_s \approx K_m$. This makes the models equivalent.

3.2.3 Plot of *v* versus [S]

The general shape of a velocity versus substrate concentration curve is that of a rectangular hyperbola (Fig. 3.4). At low substrate concentrations, the rate of the reaction is proportional to substrate concentration. In

this region, the enzymatic reaction is first order with respect to substrate concentration (Fig. 3.4). For the case where $[S] \ll K_m$, Eq. (3.16) will reduce to

$$v = \frac{k_{cat}}{K_m}[E_T][S] = \frac{V_{max}}{K_m}[S] \qquad (3.17)$$

where k_{cat}/K_m ($M^{-1}\,s^{-1}$) is the second-order rate constant for the reaction, while V_{max}/K_m (s^{-1}) is the first-order rate constant for the reaction. Knowledge of enzyme concentration allows for the calculation of k_{cat}/K_m from V_{max}/K_m. There are some physical limits to this ratio. The ultimate limit on the value of k_{cat}/K_m is dictated by k_1. This step is controlled solely by the rate of diffusion of substrate to the active site of the enzyme. This, in turn, is related to the solvent viscosity. This limits the value of k_1 to 10^8 to 10^9 M^{-1} s^{-1}. The ratio k_{cat}/K_m for many enzymes is in this range. This suggests that the catalytic activity of many enzymes depends solely on the rate of diffusion of the substrate to the active site! However, specific spatial arrangements of enzymes can lead to the removal of this maximum rate limitation imposed by diffusion. For example, the product of one enzymatic reaction can be channeled into the active site of a second enzyme, for further conversion.

At higher concentrations, the velocity of the reaction remains approximately constant and effectively insensitive to changes in substrate concentration. In this region the order of the enzymatic reactions is zero order with respect to substrate (Fig. 3.4). For the case where $[S] \gg K_m$, Eq. (3.17) will reduce to

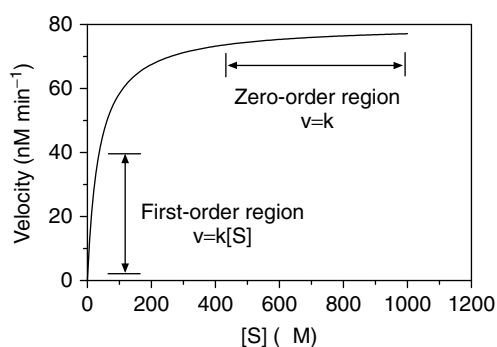$$v = k_{cat}[E_T] = V_{max} \qquad (3.18)$$

Figure 3.4. Initial velocity versus substrate concentration plot for an enzyme-catalyzed reaction. Notice the first- and zero-order regions of the curve, where the reaction velocity is, respectively, linearly dependent and independent of substrate concentration.
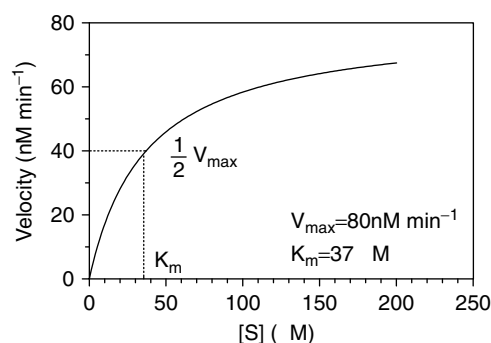
Figure 3.5. Initial velocity versus substrate concentration plot for an enzyme with $V_{max} = 80$ nM min^{-1} and $K_m = 37$ μM.

The value of K_m varies widely, for most enzymes; however, it generally lies between 10^{-1} and 10^{-7} M. The value of K_m depends on the type of substrate and on environmental conditions such as pH, temperature, ionic strength, and polarity. K_m and K_s correspond to the concentration of substrate at half-maximum velocity (Fig. 3.5). This fact can readily be shown by substitution of [S] by $\frac{1}{2}K_m$ in Eq. (3.16). It is important to remember that K_m equals K_s only when the breakdown of the ES complex takes place much more slowly than the binding of substrate to the enzyme (i.e., when $k_{-1} \ggg k_2$) and thus

$$K_m = \frac{k_{-1}}{k_1} = K_s \qquad (3.19)$$

Under these conditions, K_m is also a measure of the strength of the ES complex or the affinity of enzyme for substrate. The k_{cat}, molecular activity, or turnover number of an enzyme is the number of substrate molecules converted to product by an enzyme molecule *per* unit time when the enzyme is fully saturated with substrate.

3.3   GENERAL STRATEGY FOR DETERMINATION OF THE CATALYTIC CONSTANTS K_m AND V_{max}

The first step in the determination of the catalytic constants of an enzyme-catalyzed reaction is validation of the Michaelis–Menten assumptions, in particular the fact that the enzyme should be stable during the time course of the reaction. Selwyn's test can be used to test for enzyme stability. Briefly, plots of the extent of the reaction (%) as a function of the product
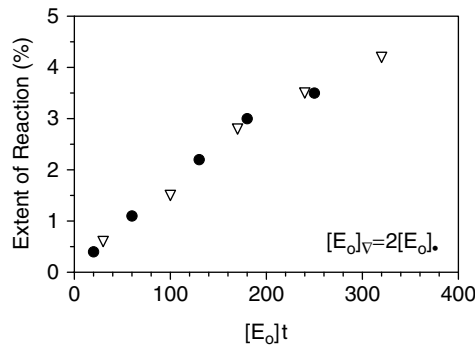
Figure 3.6. Selwyn plot for an enzyme.

of initial enzyme concentration by time ($[E_0]t$) for different initial enzyme concentrations ($[E_0]$) should be superimposable (Fig. 3.6). If the enzyme is becoming inactivated during the course of the reaction, the rate of the reaction will not be proportional to initial enzyme concentration ($[E_0]$), and the plots will not be superimposable.

Reaction velocity should also be linearly proportional to enzyme concentration (Fig. 3.3). The latter condition also constitutes an implicit check of the assumption that combination of enzyme with substrate does not significantly deplete substrate concentration. Reaction velocities at substrate concentrations in the range 0.5 to $10K_m$ should be used if possible. These should be spaced more closely at low substrate concentrations, with at least one high concentration approaching V_{max}. Concentrations of $\frac{1}{3}$, $\frac{1}{2}$, 1, 2, 4, and $8K_m$ are appropriate, with at least three replicate determinations per substrate concentration. The Michaelis–Menten model can then be fitted to velocity versus concentration data using standard nonlinear regression techniques to obtain estimates of K_m and V_{max}.

3.4 PRACTICAL EXAMPLE

In what follows, we describe a typical analysis of velocity versus substrate concentration data set. Five replicates of reaction velocities were determined at each substrate concentration, and the data are shown in Table 3.1. It is good practice to start by constructing a residual plot (Fig. 3.7). In this case, residuals refer to the difference between the mean of a set of data points ($\overline{y}_i$) and each individual data point j at a particular substrate concentration i:

$$\text{mean residual} = y_{ij} - \overline{y}_i \qquad (3.20)$$

TABLE 3.1   Velocity as a Function of Substrate Concentration for a Putative Enzyme

Substrate Concentration (mM)	Velocity (nmol L^{-1} min^{-1})				
	a	b	c	d	e
0	0	0	0	0	0
8.33	13.8	11.5	10	12.6	15
10	16	14.5	17	10	21
12.5	19	16	21	13	23
16.7	23.6	21.4	26	19.5	27
20	26.7	22	28	20	29
25	40	38.6	42.5	39	41
33.3	36.3	41	35	37	40
40	40	39	42	37.6	43
50	44.4	38.6	47	36	50
60	48	47	49	45	51.2
80	50	48.4	52.6	46.3	54.6
100	70	65	75	62.5	76
150	60	59.5	63.8	57.3	65.8
200	66.7	62.5	70	61	72
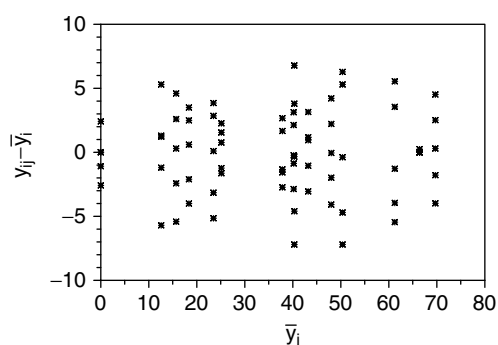
Figure 3.7. Mean residual analysis for the experimental data set. The patterns obtained suggest a homogeneous, or constant, error structure in the data.

These residuals will be referred to as *mean residuals*. It is important to realize that the criterion used to judge whether a weighted regression analysis should be carried out is the error structure of the experimental data, *not* the error structure of the fit of the model to the data. The mean-residuals plot depicted in Fig. 3.7 suggests that the error structure of the data is homogeneous, or constant. This being the case, weighting is not necessary. A more quantitative analysis of the error structure of

**TABLE 3.2   Average and Standard Deviation of the
Five Replicates of Velocity Determinations**

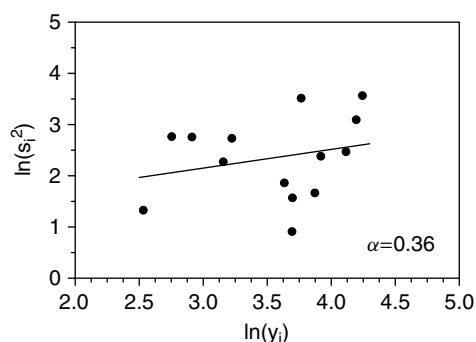| Substrate Concentration (mM)	v (nmol L^{-1} min^{-1})	SD x	n
0	0	0	5
8.3	12.6	1.94	5
10	15.7	3.99	5
12.5	18.4	3.97	5
16.7	23.5	3.11	5
20	25.1	3.93	5
25	40.2	1.57	5
33.3	37.9	2.53	5
40	40.3	2.19	5
50	43.2	5.81	5
60	48.0	2.30	5
80	50.4	3.29	5
100	69.7	5.95	5
150	61.3	3.44	5
200	66.4	4.71	5

Figure 3.8. Log-log plot of changes in the variance (s_i^2) of the ith sample mean as a function of the value of the ith sample mean (y_i). This plot is used in determination of the type of error present in the experimental data set for the establishment of a weighting scheme to be used in regression analysis of the data. The value of the slope of the line (α) suggests a homogeneous, or constant, error in the experimental data.

the data can also be carried out as described in Chapter 1. A log-log plot of the variance of the mean ($\overline{y}_i$) of the five replicates at each substrate concentration (Table 3.2) versus that particular mean is shown in Fig. 3.8. The slope of the line is 0.36 ($r^2 = 0.063$, $p = 0.39$) and is not significantly

different from zero ($p > 0.05$). We can therefore safely conclude that it is not necessary to carry out weighted regression analysis.

Nonlinear regression (no weighting) of the Michaelis–Menten model to the experimental data allowed for rapid and accurate determination of the catalytic parameters of this enzyme-catalyzed reaction. The estimates of V_{max} and K_m, their standard error, 95% confidence intervals, and the goodness of the fit of the model to the data are shown in Table 3.3. The fit of the model to data was excellent ($r^2 = 0.93$), as can be appreciated in Fig. 3.9. This particular software package also provides a *runs test*. The runs test determines whether the curve deviates systematically from the data. A *run* is a series of consecutive points that are either all above or all below the regression curve. Another way of saying this is that a run is a consecutive series of points whose residuals are either all positive or all negative. If the data points are randomly distributed above and below the regression curve, it is possible to calculate the expected number of runs. If fewer runs than expected are observed, it may be a coincidence

TABLE 3.3 Results for the Nonlinear Least-Squares Fit of Experimental Data to the Michaelis–Menten Model

|	
Best-fit values	
$\quad V$	81.1
$\quad K$	38.62
Std. error	
$\quad V$	2.727
$\quad K$	3.315
95% Confidence intervals	
$\quad V$	75.66–86.54
$\quad K$	32.00–45.23
Goodness of fit	
$\quad$ Degrees of freedom	73
$\quad r^2$	0.934
$\quad$ Absolute sum of squares	2022
$\quad$ SD x	5.263
Runs test	
$\quad$ Points above curve	29
$\quad$ Points below curve	41
$\quad$ Number of runs	40
$\quad p$ Value (runs test)	0.915
$\quad$ Deviation from model	Not significant
Data	
$\quad$ Number of x values	15
$\quad$ Number of y replicates	5
$\quad$ Total number of values	75
$\quad$ Number of missing values	0
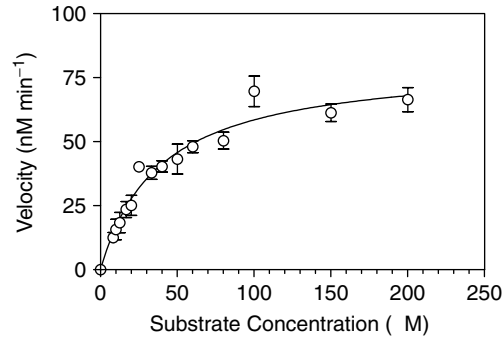
Figure 3.9. Velocity versus substrate concentration plot for the experimental data set.

or it may mean that an inappropriate regression model was chosen and the curve deviates systematically from the experimental data. The p value provides a measure of statistical certainty to the test. The p values are always one-tailed, asking about the probability of observing as few runs (or fewer) than observed. If more runs than expected are observed, the p value will be higher than 0.50. If the runs test reports a low p value, it may be concluded that the data do not follow the selected model adequately. Another check for the adequacy of the model in describing the trends observed in the data is a residuals plot. This time, however, a residual refers to the difference between the value predicted by the model ($\hat{y}_i$) and the individual experimental points:
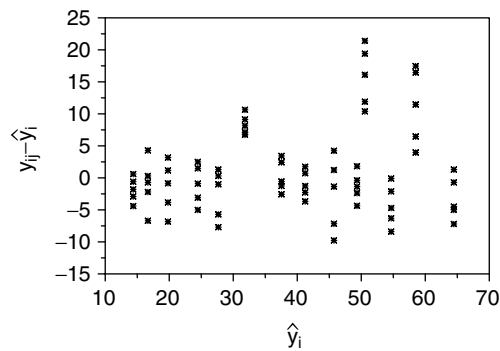
$$\text{fit residual} = y_{ij} - \hat{y}_i \tag{3.21}$$

These residuals will be referred to as *fit residuals*. The values of the velocities predicted, at each substrate concentration, used in the calculation of these fit residuals are shown in Table 3.4. Finally, the random distribution of fit residuals shown in Fig. 3.10 suggests that the model fits the data adequately. A systematic trend in the fit residuals would suggest a systematic error in the fit and possibly a failure of the model to describe the behavior of the system. It is important to remember that these fit residuals should not be used in determination of the error structure of the data or to make judgments on possible weighting strategies. This would be the case only if $\hat{y}_i = \overline{y}_i$.

The fit of the model to the data should be carried out using the entire set of experimental values rather than the means of the replicate determinations at each substrate concentration. This will increase the precision, and possibly the accuracy, of the estimates obtained.

TABLE 3.4 Velocities Predicted at Various Substrate Concentrations

Substrate Concentration (mM)	Predicted Velocity (nmol L^{-1} min^{-1})
8.3	14.3
10	16.6
12.5	19.8
16.7	24.4
20	27.6
25	31.8
33.3	37.5
40	41.2
50	45.7
60	49.3
80	54.6
100	58.5
150	64.4
199	50.5

Figure 3.10. Fit residual analysis for the experimental data set. The patterns obtained suggest that the model fits the data well.

3.5   DETERMINATION OF ENZYME CATALYTIC PARAMETERS FROM THE PROGRESS CURVE

It is theoretically possible to derive V_{max} and K_m values for an enzyme from a single progress curve (Fig. 3.11). This is certainly an attractive proposition since measuring initial velocity as a function of several substrate concentrations can be a lengthy and tedious task. The velocity of an enzyme-catalyzed reaction can be determined from the disappearance
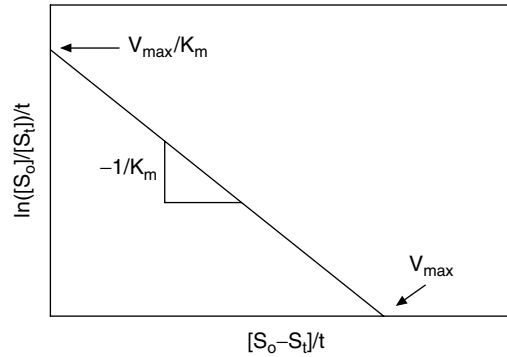
Figure 3.11. Linear plot used in the determination of catalytic parameters V_{max} and K_m from a single progress curve.

of substrate $(-d[S]/dt)$ or appearance of product $(d[P]/dt)$ as a function of time. In terms of disappearance of substrate, the Michaelis–Menten model can be expressed as

$$-\frac{d[S]}{dt} = \frac{V_{max}[S]}{K_s + [S]} \tag{3.22}$$

Multiplication of the numerator and denominator on both sides by $(K_m + [S])$, division of both sides by $[S]$, and integration for the boundary conditions $[S] = [S_0]$ at $t = 0$ and $[S] = [S_t]$ at time t,

$$-K_m \int_{S_0}^{S} \frac{d[S]}{[S]} - \int_{S_0}^{S} d[S] = V_{max} \int_{0}^{t} dt \tag{3.23}$$

yields the integrated form of the Michaelis–Menten model:

$$K_m \ln \frac{[S_0]}{[S_t]} + [S_0 - S_t] = V_{max}t \tag{3.24}$$

In this model, $[S_t]$ is not an explicit function of time. This can represent a problem since most commercially available curve-fitting programs cannot fit implicit functions to experimental data. Thus, to be able to use this implicit function in the determination of k_{cat} and K_m, it is necessary to modify its form and transform the experimental data accordingly. Dividing both sides by t and K_m and rearranging results in the expression

$$\frac{1}{t} \ln \frac{[S_0]}{[S_t]} = -\frac{[S_0 - S_t]}{K_m t} + \frac{V_{max}}{K_m} \tag{3.25}$$

A plot of $t^{-1}\ln([S_0]/[S_t])$ versus $[S_0 - S_t]/t$ yields a straight line with slope $= -1/K_m$, x-intercept $= V_{\max}$, and y-intercept $= V_{\max}/K_m$ (Fig. 3.11). The values of the slope and intercept can readily be obtained using linear regression. Thus, from a single progress curve (i.e., a single $[S_t]-t$ data set) it is possible to obtain estimates of K_m and k_{cat}.

If this procedure sounds too good to be true, it probably is. The major problem with this procedure is that the following conditions must be met:

1. The enzyme must be stable during the time course of the measurements used in the determination of reaction velocity.
2. The reverse reaction (product to substrate) must be negligible.
3. The product must not be inhibitory to enzyme activity.

If these conditions are not met, particularly the first one, this procedure is not valid. Enzyme destabilization, reaction reversibility, and product inhibition considerations can be incorporated into the kinetic model; however, this procedure is complex, and the validity of the results obtained can be questionable.
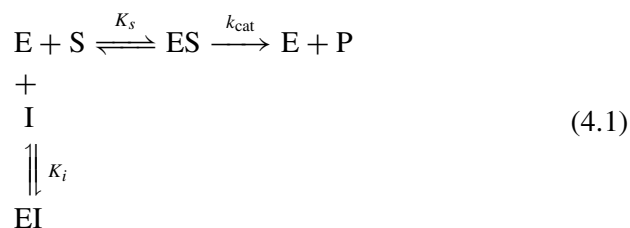
CHAPTER 4

REVERSIBLE ENZYME INHIBITION

An inhibitor is a compound that decreases the rate of an enzyme-catalyzed reaction. Moreover, this inhibition can be reversible or irreversible. Reversible enzyme inhibition can be competitive, uncompetitive, or linear mixed type, each affecting K_s and V_{max} in a specific fashion. In this chapter, each type of reversible inhibition is discussed in turn. This is followed by two examples of strategies used to determine the nature of the inhibition as well as to obtain estimates of the enzyme–inhibitor dissociation constant (K_i).

4.1   COMPETITIVE INHIBITION

In this type of reversible inhibition, a compound competes with an enzyme's substrate for binding to the active site,

$$
\begin{array}{l}
\mathrm{E} + \mathrm{S} \underset{}{\overset{K_s}{\rightleftharpoons}} \mathrm{ES} \xrightarrow{k_{cat}} \mathrm{E} + \mathrm{P} \\[4pt]
+ \\
\mathrm{I} \\[4pt]
\big\Updownarrow K_i \\[2pt]
\mathrm{EI}
\end{array}
\qquad (4.1)
$$

This results in an apparent increase in the enzyme–substrate dissociation constant (K_s) (i.e., an apparent decrease in the affinity of enzyme for

61

substrate) without affecting the enzyme's maximum velocity (V_{max}). The rate equation for the formation of product, the dissociation constants for enzyme–substrate (ES) and enzyme–inhibitor (EI) complexes, and the enzyme mass balance are, respectively:

$$v = k_{cat} \, [ES]$$

$$K_s = \frac{[E][S]}{[ES]} \qquad K_i = \frac{[E][I]}{[EI]} \tag{4.2}$$

$$[E_T] = [E] + [ES] + [EI] = [E] + \frac{[E][S]}{K_s} + \frac{[E][I]}{K_i}$$

Normalization of the rate equation by total enzyme concentration ($v/[E_T]$) and rearrangement results in the following expression for the velocity of an enzymatic reaction in the presence of a competitive inhibitor:

$$v = \frac{V_{max}[S]}{K_s^* + [S]} = \frac{V_{max}[S]}{\alpha K_s + [S]} \tag{4.3}$$

where K_s^* corresponds to the apparent enzyme–substrate dissociation constant in the presence of an inhibitor. In the case of competitive inhibition, $K_s^* = \alpha K_s$, where

$$\alpha = 1 + \frac{[I]}{K_i} \tag{4.4}$$

4.2 UNCOMPETITIVE INHIBITION

In this type of reversible inhibition, a compound interacts with the enzyme–substrate complex at a site other than the active site,

$$
\begin{array}{c}
E + S \; \underset{}{\overset{K_s}{\rightleftharpoons}} \; ES \; \xrightarrow{k_{cat}} \; E + P \\[4pt]
+ \\
I \\
\Big\Updownarrow {\scriptstyle K_i} \\
ESI
\end{array}
\tag{4.5}
$$

This results in an apparent decrease in both V_{max} and K_s. The apparent increase in affinity of enzyme for substrate (i.e., a decrease in K_s) is due to unproductive substrate binding, resulting in a decrease in free enzyme

concentration. Half-maximum velocity, or half-maximal saturation, will therefore be attained at a relatively lower substrate concentration. The rate equation for the formation of product, the dissociation constants for enzyme–substrate (ES) and ES–inhibitor (ESI) complexes and the enzyme mass balance are, respectively,

$$v = k_{cat}[ES]$$

$$K_s = \frac{[E][S]}{[ES]} \qquad K_i = \frac{[ES][I]}{[ESI]} \tag{4.6}$$

$$[E_T] = [E] + [ES] + [ESI] = [E] + \frac{[E][S]}{K_s} + \frac{[E][S][I]}{K_s K_i}$$

Normalization of the rate equation by total enzyme concentration ($v/[E_T]$) and rearrangement results in the following expression for the velocity of an enzymatic reaction in the presence of an uncompetitive inhibitor:

$$v = \frac{V_{max}^*(S)}{K_s^* + (S)} = \frac{(V_{max}/\alpha)[S]}{(K_s/\alpha) + [S]} \tag{4.7}$$

where V_{max}^* and K_s^* correspond, respectively, to the apparent enzyme maximum velocity and apparent enzyme–substrate dissociation constant in the presence of an inhibitor. In the case of uncompetitive inhibition, $V_{max}^* = V_{max}/\alpha$ and $K_s^* = K_s/\alpha$, where

$$\alpha = 1 + \frac{[I]}{K_i} \tag{4.8}$$

4.3   LINEAR MIXED INHIBITION

In this type of reversible inhibition, a compound can interact with both the free enzyme and the enzyme–substrate complex at a site other than the active site:

$$
\begin{array}{ccc}
\text{E} + \text{S} \xrightleftharpoons{K_s} & \text{ES} \xrightarrow{k_{cat}} \text{E} + \text{P} & \\
+ & + & \\
\text{I} & \text{I} & \\
\Big\Vert K_i & \Big\Vert \delta K_i & \tag{4.9} \\
\text{EI} + \text{S} \underset{\delta K_s}{\rightleftharpoons} & \text{ESI} &
\end{array}
$$
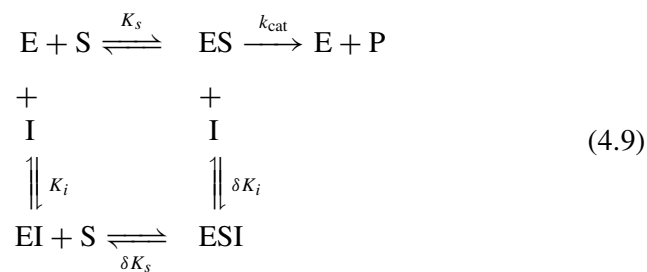
This results in an apparent decrease in $V_{\max}$ and an apparent increase in K_s. The rate equation for the formation of product, the dissociation constants for enzyme–substrate (ES and ESI) and enzyme–inhibitor (EI and ESI) complexes, and the enzyme mass balance are, respectively,

$$v = k_{\text{cat}}[\text{ES}]$$

$$K_s = \frac{[\text{E}][\text{S}]}{[\text{ES}]} \quad \delta K_s = \frac{[\text{EI}][\text{S}]}{[\text{ESI}]} \quad K_i = \frac{[\text{E}][\text{I}]}{[\text{EI}]} \quad \delta K_i = \frac{[\text{ES}][\text{I}]}{[\text{ESI}]}$$

$$[\text{E}_T] = [\text{E}] + [\text{ES}] + [\text{EI}] + [\text{ESI}] = [\text{E}] + \frac{[\text{E}][\text{S}]}{K_s} + \frac{[\text{E}][\text{I}]}{K_i} + \frac{[\text{E}][\text{S}][\text{I}]}{K_s \delta K_i}$$

$$(4.10)$$

Normalization of the rate equation by total enzyme concentration ($v/[\text{E}_T]$) and rearrangement results in the following expression for the velocity of an enzymatic reaction in the presence of a linear mixed type inhibitor:

$$v = \frac{V_{\max}^*(\text{S})}{K_s^* + (\text{S})} = \frac{(V_{\max}/\beta)[\text{S}]}{(\alpha/\beta)K_s + [\text{S}]} \tag{4.11}$$

where $V_{\max}^*$ and K_s^* correspond, respectively, to the apparent enzyme maximum velocity and apparent enzyme–substrate dissociation constant in the presence of an inhibitor. In the case of linear mixed inhibition, $V_{\max}^* = V_{\max}/\beta$ and $K_s^* = (\alpha/\beta)K_s$, where

$$\alpha = 1 + \frac{[\text{I}]}{K_i} \tag{4.12}$$

and

$$\beta = 1 + \frac{[\text{I}]}{\delta K_i} \tag{4.13}$$

4.4   NONCOMPETITIVE INHIBITION

Noncompetitive inhibition is a special case of linear mixed inhibition where $\delta = 1$ and $\alpha = \beta$. Thus, the expression for the velocity of an enzymatic reaction in the presence of a noncompetitive inhibitor becomes

$$v = \frac{V_{\max}^*(\text{S})}{K_s + (\text{S})} = \frac{(V_{\max}/\alpha)[\text{S}]}{K_s + [\text{S}]} \tag{4.14}$$

TABLE 4.1   Summary of the Effects of Reversible Inhibitors on Apparent Enzyme Catalytic Parameters $V^*_{\max}$ and K^*_s

	Competitive	Uncompetitive	Linear Mixed	Noncompetitive
$V^*_{\max}$	No effect ($-$)	Decrease ($\downarrow$)	Decrease ($\downarrow$)	Decrease ($\downarrow$)
	$V_{\max}$	$V_{\max}/\alpha$	$V_{\max}/\beta$	$V_{\max}/\alpha$
K^*_s	Increase ($\uparrow$)	Decrease ($\downarrow$)	Increase ($\uparrow$)	No effect ($-$)
	αK_s	K_s/α	$(\alpha/\beta)K_s$	K_s

where $V^*_{\max}$ corresponds to the apparent enzyme maximum velocity in the presence of an inhibitor. In the case of noncompetitive inhibition, $V^*_{\max} = V_{\max}/\alpha$, where

$$\alpha = 1 + \frac{[I]}{K_i} \tag{4.15}$$

Thus, for noncompetitive inhibition, an apparent decrease in $V_{\max}$ is observed while K_s remains unaffected. A summary of the effects of reversible inhibitors on the catalytic parameters K_s and $V_{\max}$ is presented in Table 4.1.

4.5   APPLICATIONS

A typical enzyme inhibition experiment will be designed to determine the nature of the inhibition process as well estimate the magnitude of K_i. For this purpose, initial velocities should be determined at substrate concentrations in the range 0.5 to $2-5K_s$, in the absence of an inhibitor, as well as at inhibitor concentrations in the range 0.5 to $2-5K_i$. Collecting data in this range of substrate and inhibitor concentrations will allow for the accurate and unambiguous determination of both the nature of the inhibition process and the magnitude of K_i. In the examples below, only four substrate concentrations and one inhibitor concentration are used. This can only be done if the single inhibitor concentration is *close to* the K_i and substrate concentrations are in the range 0.5 to $2-5K_s$. Otherwise, catalytic parameters cannot be estimated accurately using regression techniques—or any technique, for that matter.

4.5.1   Inhibition of Fumarase by Succinate

The enzyme fumarase catalyzes the hydration of fumarate to malate. This enzyme is known to be reversibly inhibited by succinate. Reaction velocities were determined in triplicate at different substrate concentrations, in

the presence and absence of succinate, and the results are summarized in Table 4.2.

The Michaelis–Menten model was fitted to the experimental data using standard nonlinear regression techniques to obtain estimates of V_{max}^* and K_s^* (Fig. 4.1). Best-fit values of V_{max}^* and K_s^* of corresponding standard errors of the estimates plus the number of values used in the calculation of the standard error, and of the goodness-of-fit statistic r^2 are reported in Table 4.3. These results suggest that succinate is a competitive inhibitor of fumarase. This prediction is based on the observed apparent increase in K_s in the absence of changes in V_{max} (see Table 4.1). At this point, however, the experimenter cannot state with any certainty whether the observed apparent increase in K_s is a true effect of the inhibitor or merely an act of chance. A proper statistical analysis has to be carried out. For the comparison of two values, a two-tailed t-test is appropriate. When more than two values are compared, a one-way analysis of variance (ANOVA),

TABLE 4.2   Rate of Hydration of Fumarate to Malate by Fumarase at various Substrate Concentrations[a]

Substrate Concentration (M)	Velocity (a.u.)					
	Without Inhibitor			With Inhibitor		
5.0×10^{-5}	0.91	0.95	0.99	0.57	0.53	0.61
1.0×10^{-4}	1.43	1.47	1.39	0.95	0.91	0.99
2.0×10^{-4}	2.00	2.04	1.96	1.40	1.36	1.44
5.0×10^{-4}	2.50	2.54	2.46	2.13	2.09	2.17

[a] In the presence and absence of 0.05 M succinate.
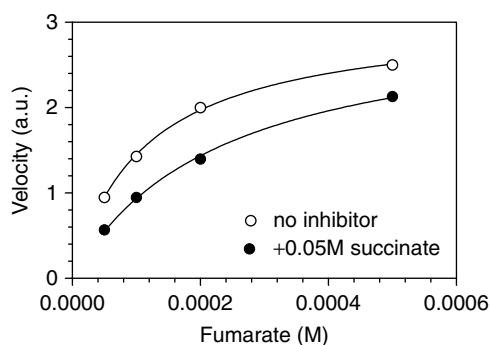
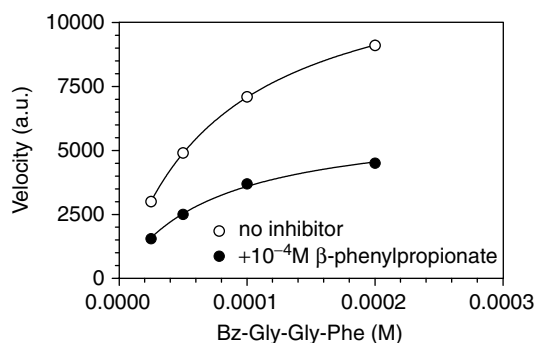**Figure 4.1.** Initial velocity versus substrate concentration plot for fumarase in the absence and presence of the reversible inhibitor succinate.

TABLE 4.3   Estimates of the Catalytic Parameters for the Fumarase-Catalyzed hydration of Fumarate to Malate[a]

	V_{max}^* (a.u.)	Std. Error[b] (M)	K_s^* (M)	Std. Error[b] (M)	r^2
Without inhibitor	3.07	4.54×10^{-2} (12)	112×10^{-6}	4.57×10^{-6} (12)	0.9959
With inhibitor	3.10	8.34×10^{-2} (12)	232×10^{-6}	1.34×10^{-5} (12)	0.9953

[a]In the presence and absence of succinate.
[b]Number in parentheses.

followed by a post-test to determine the statistical significance of differences between individual values, has to be carried out. Two-tailed t-tests revealed significant differences between K_s values in the presence and absence of succinate ($p < 0.001$), whereas no significant differences were detected between V_{max} values ($p > 0.05$).

Having established that succinate acts as a competitive inhibitor, it is possible to determine the value of α:

$$\alpha = \frac{K_s^*}{K_s} = \frac{0.232}{0.112} = 2.07 \tag{4.16}$$

The magnitude of the enzyme–inhibitor dissociation constant can be obtained from knowledge of [I] and α using Eq. 4.4,

$$K_i = \frac{[I]}{\alpha - 1} = \frac{5.00 \times 10^{-2} \ M}{2.07 - 1} = 0.0465 \ M \tag{4.17}$$

4.5.2   Inhibition of Pancreatic Carboxypeptidase A by β-Phenylpropionate

The enzyme carboxypeptidase catalyzes the hydrolysis of the synthetic peptide substrate benzoylglycylglycyl-L-phenylalanine (Bz-Gly-Gly-Phe). This enzyme is known to be reversibly inhibited by β-phenylpropionate. Reaction velocities were determined in triplicate at different substrate concentrations, in the presence and absence of β-phenylpropionate, and results summarized in Table 4.4.

The Michaelis–Menten model was fitted to the experimental data using standard nonlinear regression techniques to obtain estimates of V_{max}^* and K_s^* (Fig. 4.2). Best-fit values of V_{max}^* and K_s^*, corresponding standard errors of the estimates plus the number of values used in the calculation of the standard error, and goodness-of-fit statistic r^2 are reported in Table 4.5.

A statistically significant decrease in V_{max} ($p < 0.0001$) and increase in K_s ($p = 0.0407$) were observed upon addition of the inhibitor. This

TABLE 4.4 Rate of Hydrolysis of the Synthetic Substrate Benzoylglycylglycyl-L-Phenylalanine by Pancreatic Carboxypeptidase A as a Function of Substrate Concentration[a]

Substrate	Velocity (a.u.)					
Concentration (M)	Without Inhibitor			With Inhibitor		
2.5×10^{-5}	3000	2950	3050	1550	1500	1600
5.0×10^{-5}	4900	4950	4850	2500	2550	2450
1.0×10^{-4}	7100	7050	7150	3700	3750	3650
2.0×10^{-4}	9100	9150	9050	4500	4550	4450

[a] In the presence and absence of 1×10^{-4} M of the reversible inhibitor β-phenylpropionate.

Figure 4.2. Initial velocity versus substrate concentration plot for pancreatic carboxypeptidase A in the absence and presence of the reversible inhibitor β-phenylpropionate.

TABLE 4.5 Estimates of the Catalytic Parameters for the Carboxypeptidase-Catalyzed Hydrolysis of Bz-Gly-Gly-Phe[a]

	V_{max}^* (a.u.)	Std. Error[b] (M)	K_s^* (M)	Std. Error[b] (M)	r^2
No inhibitor	1.28×10^4	84.0 (12)	8.07×10^{-5}	1.22×10^{-6} (12)	0.9996
Plus inhibitor	6.20×10^3	130 (12)	7.24×10^{-5}	3.64×10^{-6} (12)	0.9955

[a] In the presence and absence of β-phenylpropionate.
[b] Number in parentheses.

suggested that β-phenylpropionate acts as a linear mixed-type inhibitor of carboxypeptidase A. Having established that β-phenylpropionate acts as a linear mixed-type competitive inhibitor of carboxypeptidase A, it is

possible to determine the values of α and α/β,

$$\beta = \frac{V_{\max}}{V_{\max}^*} = \frac{12{,}790}{6196} = 2.06 \qquad (4.18)$$

$$\frac{\alpha}{\beta} = \frac{K_s^*}{K_s} = \frac{8.07e-5}{7.24e-5} = 1.12 \qquad (4.19)$$

Using this information, α was estimated to have a value of 2.30. The magnitude of the enzyme–inhibitor dissociation constant (K_i) could then be estimated from knowledge of α using Eq. 4.12:

$$K_i = \frac{[I]}{\alpha - 1} = \frac{1 \times 10^{-4}\ M}{(2.30 - 1)} = 7.68 \times 10^{-5}\ M \qquad (4.20)$$

Finally, an estimate of the magnitude of δ can be obtained from knowledge of [I], K_i, and β using Eq. 4.13:

$$\delta = \frac{[I]}{(\beta - 1)K_i} = \frac{1 \times 10^{-4}\ M}{(2.06 - 1)(7.68 \times 10^{-5}\ M)} = 1.22 \qquad (4.21)$$

Using this value, δK_i was estimated to be $9.40 \times 10^{-5}\ M$.

4.5.3 Alternative Strategies

It is also theoretically possible to determine the nature of the inhibition process by comparing the goodness of fit for each of the inhibition models to experimental data. An F-test could then be carried out to determine if a particular model fits the data significantly better than another. In principle, the model that best fits the data should help define the nature of the inhibition process. In the author's opinion, however, this strategy is not very fruitful. Usually, differences in the goodness of fit between inhibition models, and even between inhibition and the non inhibition model, are not statistically significant. Even though this procedure could be automated, it is cumbersome and time consuming.

CHAPTER 5

IRREVERSIBLE ENZYME INHIBITION

In many circumstances, inhibitors affect enzyme activity in an irreversible fashion. It is sometimes difficult to distinguish between the effects of a reversible and irreversible inhibitors since irreversible inhibition could be interpreted as noncompetitive reversible inhibition. However, the apparent enzyme–inhibitor equilibrium dissociation constant (K_i) derived for an irreversible inhibitor is dependent on enzyme concentration, preincubation time, and substrate concentration. A true equilibrium K_i would be independent of all these factors. Not a conclusive proof, time dependence of the inhibitory effects may be indicative of irreversibility.

We present some simple models that can be used to analyze irreversible inhibition data. In all of these treatments, the concentration of inhibitor will be considered to be in excess of that of enzyme (i.e., $[I] \ggg [E]$). Under these conditions, inhibitor concentration is assumed to remain constant during the course of the reaction. Thus, inhibitor concentration will remain unchanged from its initial value $[I_0]$, (i.e., $[I] \approx [I_0]$). This condition, which is relevant to an experimental situation, will simplify the mathematical treatment considerably.

Under conditions where $[I] \ggg [E]$, all irreversible inhibition patterns can be modeled using a first-order association kinetic model of the form

$$[EI^*] = [E_T](1 - \exp^{-k't}) \tag{5.1}$$

where $[EI^*]$ corresponds to the concentration of irreversible enzyme–inhibitor complex and $[E_T]$ corresponds to total enzyme concentration

70
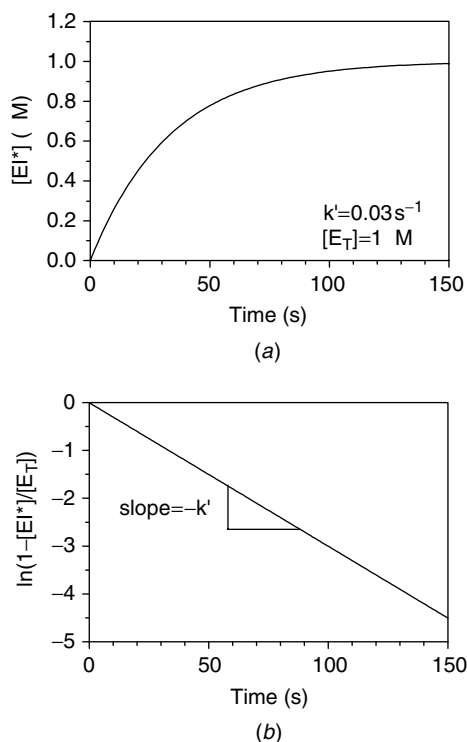
Figure 5.1. (*a*) Increases in the concentration of inhibited enzyme as a function of time for simple irreversible enzyme inhibition. (*b*) Semilogarithmic plot used in determination of the inhibition rate constant for the case of simple irreversible inhibition.

(Fig. 5.1*a*). The first-order association rate constant can therefore be determined by fitting this model to [EI*] versus time data using nonlinear regression procedures. Alternatively, the model can be linearized to

$$\ln \left(1 - \frac{[\text{EI}^*]}{[\text{E}_T]} \right) = -k't \qquad (5.2)$$

Thus, a plot of the natural logarithm of $1 - [\text{EI}^*]/[\text{E}_T]$ as a function of time should yield a straight line (Fig. 5.1*b*). The slope of the line, which corresponds to $-k'$, can be determined using standard linear regression procedures.

The pseudo-first-order inhibition constant, k' (s^{-1}), will have different meanings, depending on the exact inhibition mechanism (see below). Four different phenomenological irreversible inhibition mechanisms are discussed in turn.

5.1   SIMPLE IRREVERSIBLE INHIBITION

The interaction of an enzyme (E) with an irreversible inhibitor (I), which results in the formation of an irreversible enzyme–inhibitor complex (EI*), can be modeled as a second-order reaction between two dissimilar substrates:

$$\text{E} + \text{I} \xrightarrow{k_i} \text{EI}^* \tag{5.3}$$

where k_i is the second-order rate constant of inhibition ($M^{-1}\ \text{s}^{-1}$). The differential equation that describes the formation of irreversible enzyme–inhibitor complex, and the mass balance for the enzyme are, respectively,

$$\frac{d[\text{EI}^*]}{dt} = k_i[\text{I}][\text{E}] \tag{5.4}$$

and

$$[\text{E}_T] = [\text{E}] + [\text{EI}^*] \tag{5.5}$$

where $[\text{E}_T]$, $[\text{E}]$, $[\text{EI}^*]$, and $[\text{I}]$ correspond, respectively, to total enzyme concentration, irreversible enzyme–inhibitor complex, free enzyme, and inhibitor concentrations. Substitution of [E] for $[\text{E}_T] - [\text{EI}^*]$, and $[\text{I}_0]$ for [I] into Eq. (5.4) results in a first-order ordinary differential equation of the form

$$\frac{d[\text{EI}^*]}{dt} = k_i[\text{I}_0][\text{E}_T - \text{EI}^*] = k'[\text{E}_T - \text{EI}^*] \tag{5.6}$$

where

$$k' = k_i[\text{I}_0] \tag{5.7}$$

Integration of Eq. (5.5) after variable separation,

$$\int_0^{\text{EI}^*} \frac{d[\text{EI}^*]}{[\text{E}_T - \text{EI}^*]} = k' \int_0^t dt \tag{5.8}$$

yields a first-order association kinetic model that describes the changes in concentration of the reversible enzyme–inhibitor complex (EI*) in time:

$$[\text{EI}^*] = [\text{E}_T](1 - \exp^{-k't}) \tag{5.9}$$

Since the initial inhibitor concentration is known, the experimentally determined peudo-first-order inhibition rate constant, k' (s^{-1}), can be used to

obtain estimates of the second-order inhibition rate constant k_i (M^{-1} s^{-1}):

$$k_i = \frac{k'}{[I_0]} \tag{5.10}$$

Substrate may protect the enzyme from the effects of irreversible inhibitors, and the model has to be modified to take this fact into consideration.

5.2 SIMPLE IRREVERSIBLE INHIBITION IN THE PRESENCE OF SUBSTRATE

Consider the interactions of free enzyme with inhibitor and substrate:

$$E + I \xrightarrow{k_i} EI^*$$

$$E + S \underset{}{\overset{K_s}{\rightleftharpoons}} ES \tag{5.11}$$
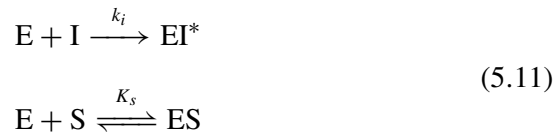
The differential equation that describes the formation of irreversible enzyme–inhibitor complex, the dissociation constant for the ES complex, and the mass balance for the enzyme are, respectively,

$$\frac{d[EI^*]}{dt} = k_i[E][I] \tag{5.12}$$

$$K_s = \frac{[E][S]}{[ES]} \tag{5.13}$$

$$[E_T] = [E] + [EI^*] + [ES] \tag{5.14}$$

where $[E_T]$, $[E]$, $[EI^*]$ and $[ES]$ correspond, respectively, to total enzyme concentration, and the concentrations of free enzyme, irreversible enzyme–inhibitor complex, and enzyme–substrate complex. The concentration of free enzyme is given by

$$[E] = \frac{[ES] \cdot K_s}{[S]} \tag{5.15}$$

Substitution of $[E_T] - [E] - [EI^*]$ for $[ES]$, and rearrangement, results in the following expression for the concentration of free enzyme:

$$[E] = \frac{[E_T - EI^*] \cdot K_s}{K_s + [S]} \tag{5.16}$$

Substitution of Eq. (5.16) for [E], and $[I_0]$ for [I] into Eq. (5.12), results in a first-order ordinary differential equation of the form

$$\frac{d[EI^*]}{dt} = k_i[I_0]\frac{[E_T - EI^*] \cdot K_s}{K_s + [S]} = k'[E_T - EI^*] \qquad (5.17)$$

where

$$k' = \frac{k_i K_s}{K_s + [S]}[I_0] \qquad (5.18)$$

Integration of Eq. (5.17) after variable separation,

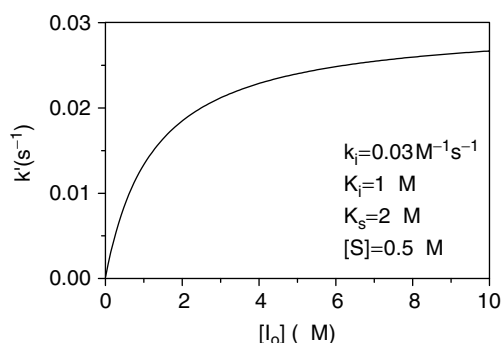$$\int_0^{EI^*} \frac{d[EI^*]}{[E_T - EI^*]} = k'\int_0^t dt \qquad (5.19)$$

yields a first-order association kinetic model that describes the time-dependent changes in concentration of an irreversible enzyme–inhibitor complex (EI*) in the presence of substrate:

$$[EI^*] = [E_T](1 - \exp^{-k't}) \qquad (5.20)$$

To obtain an estimate of k_i, a k' versus $[I_0]$ data set has to be created at a fixed substrate concentration. A plot of this k' versus $[I_0]$ data would yield a straight line (Fig. 5.2). With the aid of standard linear regression procedures, the value of the slope of this line can be obtained. This slope corresponds to

$$\text{slope} = \frac{k_i K_s}{K_s + [S]} \qquad (5.21)$$
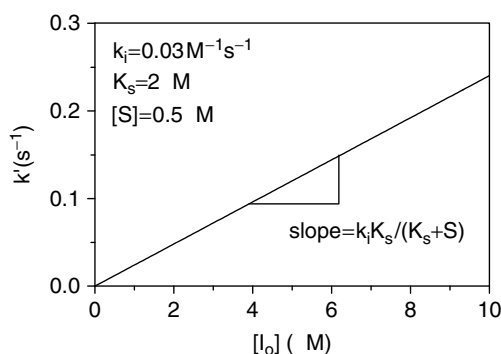
Figure 5.2. Initial inhibitor concentration dependence of the inhibition rate constant for simple irreversible enzyme inhibition in the presence of substrate.

Since accurate estimates of K_s can be obtained independently, it is therefore possible simply to solve for k_i.

5.3 TIME-DEPENDENT SIMPLE IRREVERSIBLE INHIBITION

Consider the time-dependent interaction of inhibitor with free enzyme:

$$E + I \xrightleftharpoons{K_i} EI \xrightarrow{k_i} EI^* \tag{5.22}$$

A rapid reversible interaction between enzyme (E) and inhibitor (I) is followed by a slower, irreversible reaction, which transforms the reversible enzyme–inhibitor complex (EI) into an irreversible enzyme–inhibitor complex (EI*). The differential equation that describes the formation of enzyme–inhibitor complex, the dissociation constant for the EI complex, and the mass balance for the enzyme are, respectively,

$$\frac{d[EI^*]}{dt} = k_i[EI] \tag{5.23}$$

$$K_i = \frac{[E][I]}{[EI]} \tag{5.24}$$

$$[E_T] = [E] + [EI] + [EI^*] \tag{5.25}$$

Substitution of $[E_T] - [EI] - [EI^*]$ for [E] in Eq. (5.24) and rearrangement yields

$$[EI] = \frac{[E_T - EI^*]}{1 + K_i/[I_0]} \tag{5.26}$$

Substitution of Eq. (5.26) into Eq. (5.23) results in a first-order ordinary differential equation of the form

$$\frac{d[EI^*]}{dt} = k_i \frac{[E_T - EI^*]}{1 + K_i/[I_0]} = k'[E_T - EI^*] \tag{5.27}$$

where

$$k' = \frac{k_i}{1 + K_i/[I_0]} = \frac{k_i[I_0]}{K_i + [I_0]} \tag{5.28}$$

Integration of Eq. (5.27) after variable separation,

$$\int_0^{EI^*} \frac{d[EI^*]}{[E_T - EI^*]} = k' \int_0^t dt \tag{5.29}$$
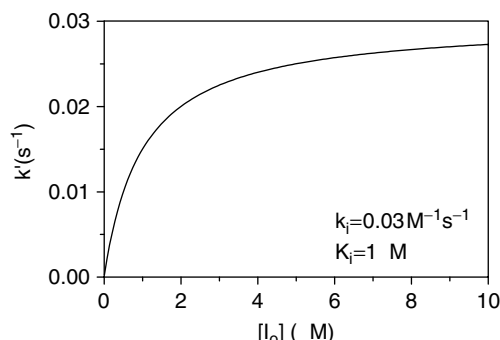
Figure 5.3. Initial inhibitor concentration dependence of the inhibition rate constant for time-dependent irreversible enzyme inhibition.

yields a first-order association kinetic model that describes the time dependence of changes in concentration of the irreversible enzyme–inhibitor complex (EI*):

$$[EI^*] = [E_T](1 - \exp^{-k't}) \tag{5.30}$$

To obtain estimates of K_i and k_i, a k' versus $[I_0]$ data set has to be created. A plot of these k' versus $[I_0]$ data would yield a rectangular hyperbola (Fig. 5.3). With the aid of standard nonlinear regression procedures, the values of K_i and k_i can be obtained.

5.4 TIME-DEPENDENT SIMPLE IRREVERSIBLE INHIBITION IN THE PRESENCE OF SUBSTRATE

Consider the interactions of free enzyme with inhibitor and substrate:

$$E + I \underset{}{\overset{K_i}{\rightleftharpoons}} EI \xrightarrow{k_i} EI^*$$

$$E + S \underset{}{\overset{K_s}{\rightleftharpoons}} ES \tag{5.31}$$
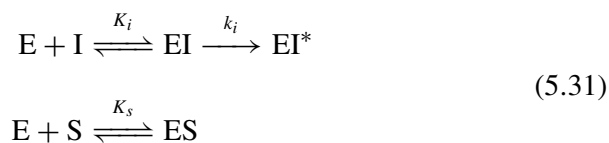
The differential equation that describes the formation of the irreversible enzyme–inhibitor complex, the equilibrium dissociation constants for the reversible enzyme–inhibitor (K_i) and enzyme–substrate (K_s) complexes, and the mass balance for the enzyme are, respectively,

$$\frac{d[EI^*]}{dt} = k_i[EI] \tag{5.32}$$

$$K_i = \frac{[E][I]}{[EI]} \qquad K_s = \frac{[E][S]}{[ES]} \qquad (5.33)$$

$$[E_T] = [E] + [EI] + [EI^*] + [ES] \qquad (5.34)$$

An expression for the concentration of the EI complex can be obtained from the enzyme mass balance and dissociation constants:

$$[EI] = \frac{[E][I]}{K_i} = \frac{[E_T - EI - EI^* - ES][I]}{K_i} = \frac{[E_T - EI^* - ES]}{1 + K_i/[I_0]} \qquad (5.35)$$

A relationship between [ES] and [EI] can be obtained from the dissociation constants for enzyme–substrate and enzyme–inhibitor complexes:

$$[E] = [ES]\frac{K_s}{[S]} = [EI]\frac{K_i}{[I]} \qquad (5.36)$$

The concentration of the ES complex can therefore be expressed as

$$[ES] = [EI]\frac{K_i[S]}{K_s[I]} \qquad (5.37)$$

Substitution of Eq. (5.37) into Eq. (5.35) and rearrangement yields

$$[EI] = \frac{[E_T - EI^*]}{1 + K_i/[I_0](1 + [S]/K_S)} \qquad (5.38)$$

Substitution of Eq. (5.38) into Eq. (5.32) yields a first-order ordinary differential equation of the form

$$\frac{d[EI^*]}{dt} = k_i[EI] = \frac{k_i}{1 + K_i/[I_0](1 + [S]/K_S)}[E_T - EI^*] = k'[E_T - EI^*] \qquad (5.39)$$

where

$$k' = \frac{k_i}{1 + K_i/[I_0](1 + [S]/K_S)} = \frac{k_i[I_0]}{K_i(1 + [S]/K_S) + [I_0]} \qquad (5.40)$$

Integration of Eq. (5.39) after variable separation,

$$\int_0^{EI^*} \frac{d[EI^*]}{[E_T - EI^*]} = k' \int_0^t dt \qquad (5.41)$$

Figure 5.4. Initial inhibitor concentration dependence of the inhibition rate constant for time-dependent irreversible enzyme inhibition in the presence of substrate.

yields a first-order association kinetic model which describes the time dependence of changes in concentration of the irreversible enzyme–inhibitor complex (EI*) in the presence of substrate:

$$[\text{EI}^*] = [\text{E}_T](1 - \exp^{-k't}) \qquad (5.42)$$

To obtain estimates of K_i and k_i, a k' versus $[I_0]$ data set at a fixed substrate concentration has to be created. A plot of these k' versus $[I_0]$ data would yield a rectangular hyperbola (Fig. 5.4). Estimates of K_i and k_i can be obtained by fitting Eq. (5.40) to the k' versus $[I_0]$ data using standard nonlinear regression procedures. Since accurate estimates of K_s can be obtained independently, it is fixed as a constant.

5.5   DIFFERENTIATION BETWEEN TIME-DEPENDENT AND TIME-INDEPENDENT INHIBITION

In principle, it is possible to distinguish between time-dependent and time-independent irreversible inhibition from k' versus $[I_0]$ plots. A straight line suggests time-independent irreversible inhibition (Fig. 5.2), whereas a rectangular hyperbola is suggestive of time-dependent irreversible inhibition (Fig. 5.4).

CHAPTER 6

pH DEPENDENCE OF ENZYME-CATALYZED REACTIONS

The activity of an enzyme is profoundly affected by pH. Usually, enzymes display a bell-shaped activity versus pH profile (Fig. 6.1). The decrease in activity on either side of the pH optimum can be due to two general causes. First, pH may affect the stability of the enzyme, causing it to become irreversibly inactivated. Second, pH may affect the kinetic parameters of the enzymatic reaction: It may affect the stability of the ES complex, the velocity of the rate-limiting step, or both. The second case is relevant to the discussion in this chapter. Interestingly, the pH dependence of enzyme-catalyzed reactions is similar to that of acid- and base-catalyzed chemical reactions. Thus, it is possible, at least in principle, to determine the pK and state of ionization of the functional groups directly involved in catalysis, and possibly their chemical nature.

6.1   THE MODEL

To understand the effects of pH on enzyme-catalyzed reactions, a model must be built that can account for both the pH dependence of the catalytically active functional groups in the enzyme, and any ionizable groups in the substrate. We consider the case where the substrate does not ionize, while ionizable groups are present in the free enzyme and enzyme–substrate (ES) complex. The reactive form of the enzyme and the ES complex is the monoionized (EH or EHS) form of a diacidic (EH_2)

79
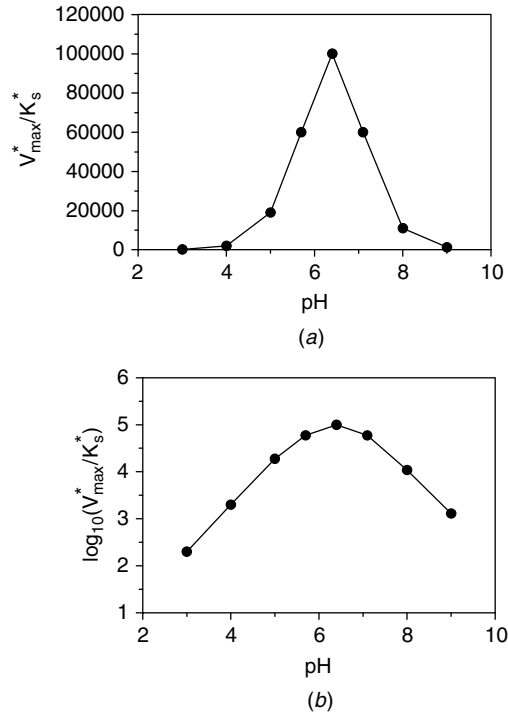
Figure 6.1. pH dependence of the first-order rate constant (V_{max}/K_s) of an enzyme in (*a*) linear and (*b*) semilogarithmic scales.

species. Thus, the catalytic process, taking into consideration the state of ionization of the enzyme, can be modeled as

$$
\begin{array}{ccc}
\text{E} & & \text{ES} \\
\Big\updownarrow K_{e2} & & \Big\updownarrow K_{es2} \\
\text{S} + \text{EH} \underset{}{\overset{K_s}{\rightleftharpoons}} & \text{EHS} \xrightarrow{k_{cat}} & \text{EH} + \text{P} \\
\Big\updownarrow K_{e1} & & \Big\updownarrow K_{es1} \\
\text{EH}_2 & & \text{EH}_2\text{S}
\end{array}
\tag{6.1}
$$
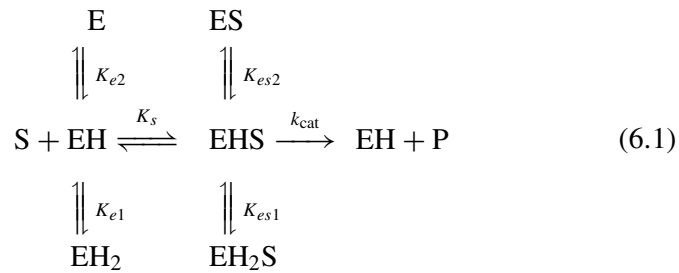
The velocity of the reaction, equilibrium dissociation, and ionization constants for the different enzyme species, and enzyme mass balance are

$$
v = k_{cat}\,[\text{EHS}]
\tag{6.2}
$$

$$
K_s = \frac{[\text{EH}][\text{S}]}{[\text{EHS}]}
\tag{6.3}
$$

$$K_{e1} = \frac{[EH][H]}{[EH_2]} \qquad K_{e2} = \frac{[E][H]}{[EH]}$$

$$K_{es1} = \frac{[EHS][H]}{[EH_2S]} \qquad K_{es2} = \frac{[ES][H]}{[EHS]} \tag{6.4}$$

$$[E_T] = [E] + [EH] + [EH_2] + [ES] + [EHS] + [EH_2S] \tag{6.5}$$

Normalization of the velocity term by total enzyme concentration ($v/[E_T]$) and rearrangement results in the following expression:

$$v = \frac{V_{max}^*[S]}{K_s^* + [S]} = \frac{(V_{max}/\alpha)[S]}{(\beta/\alpha)K_s + [S]} \tag{6.6}$$

where V_{max}^* and K_s^* correspond, respectively, to apparent enzyme maximum velocity and apparent enzyme–substrate dissociation constant at a particular pH. For the model above, $V_{max}^* = V_{max}/\alpha$ and $K_s^* = (\beta/\alpha)K_s$, where

$$\alpha = 1 + \frac{[H^+]}{K_{es1}} + \frac{K_{es2}}{[H^+]} \tag{6.7}$$

and

$$\beta = 1 + \frac{[H^+]}{K_{e1}} + \frac{K_{e2}}{[H^+]} \tag{6.8}$$

Explicit expressions for the relationship between apparent and true enzyme catalytic parameters are shown below.

$$V_{max}^* = V_{max}\left(1 + \frac{[H^+]}{K_{es1}} + \frac{K_{es2}}{[H^+]}\right)^{-1} \tag{6.9}$$

$$K_s^* = K_s\frac{1 + [H^+]/K_{e1} + K_{e2}/[H^+]}{1 + [H^+]/K_{es1} + K_{es2}/[H^+]} \tag{6.10}$$

$$\frac{V_{max}^*}{K_s^*} = \frac{V_{max}}{K_s}\left(1 + \frac{[H^+]}{K_{e1}} + \frac{K_{e2}}{[H^+]}\right)^{-1} \tag{6.11}$$

Since $V_{max} = k_{cat}[E_T]$, Eq. (6.11) can be expressed in terms of k_{cat}/K_s if so required:

$$\frac{k_{cat}^*}{K_s^*} = \frac{k_{cat}}{K_s}\left(1 + \frac{[H^+]}{K_{e1}} + \frac{K_{e2}}{[H^+]}\right)^{-1} \tag{6.12}$$

These expressions are particularly useful in helping determine the pK and chemical nature of the catalytically active functional groups in the
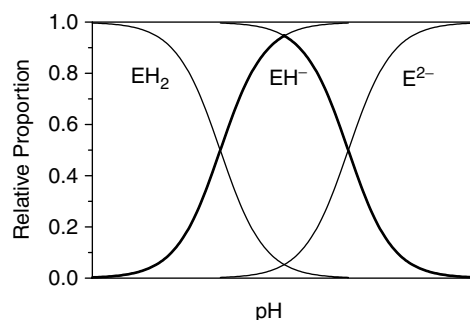
Figure 6.2. Relative proportions of a diprotic enzyme as a function of pH.

enzyme. In general, if V_{max}^*, K_s^*, V_{max}^*/K_s^*, or k_{cat}^*/K_s^* are plotted versus pH, the patterns obtained will reflect the chemical nature and acid–base properties (pK values) of the functional groups present.

The treatment above is essentially equivalent to the treatment of the pH dependence of a polyprotic acid (see Chapter 1). In our case, the enzyme is considered to be a diprotic acid. Increases and decreases in activity as a function of pH simply mirror the increases and decreases in the concentration of the catalytically active species EH (Fig. 6.2). Notice how the bell-shaped pattern for activity as a function of pH (darker lines) corresponds to the net increase and decrease in EH concentration.

6.2   pH DEPENDENCE OF THE CATALYTIC PARAMETERS

For our model, the patterns obtained for the pH dependence of $\log_{10} V_{max}^*$, $\log_{10}(V_{max}^*/K_s^*)$, and $-\log_{10} K_s^*$ are shown in Fig. 6.3. The $\log_{10} V_{max}^*$ and $\log_{10}(V_{max}^*/K_s^*)$ versus pH graphs may be broken down into linear segments having slopes of -1, 0, and $+1$. As discussed in the review of specific acid–base catalysis of chemical reactions, a change in the slope of a $\log_{10}(V_{max}^*/K_s^*)$, or $\log_{10} V_{max}^*$, versus pH plot from $+1$ to 0 as a function of increasing pH suggests the necessity of a basic group in the catalytic step, while a change of slope from 0 to -1 suggests the necessity of an acidic group in the catalytic step. The pH at which these linear segments intersect corresponds to the kinetically apparent pK value of the enzyme's amino acid side-chain functional groups involved in catalysis (Fig. 6.3). These pK values are usually shifted significantly from their corresponding pK values in a free amino acid. This effect is due to both shielding of the groups from the aqueous environment by the substrate and by the protein itself. Active sites of enzymes have unique chemical characteristics, which
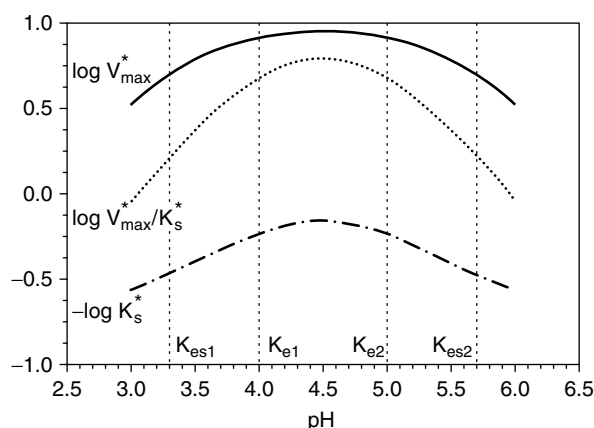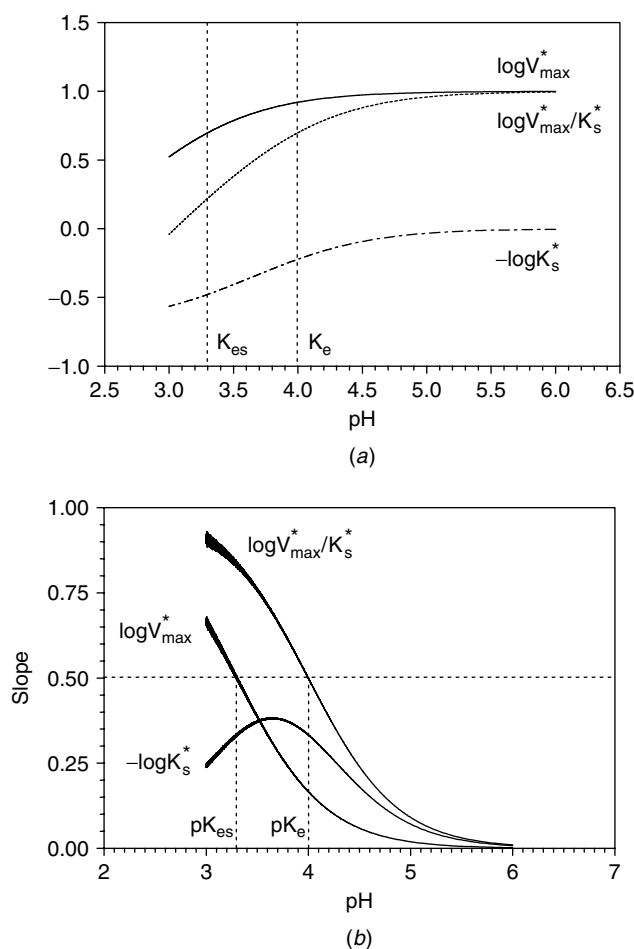
Figure 6.3. Simulation of the pH dependence of the logarithm of the catalytic parameters V_{max}, V_{max}/K_s, and K_s for a diprotic enzyme.

TABLE 6.1   pK and Enthalpy of Ionization Values for Amino Acid Side Groups

Group	pK_a (298 K)	ΔH° (kcal mol^{-1})
α-Carboxyl (terminal)	3.0–3.2	0 ± 1.5
β-Carboxyl (aspartic)	3.0–4.7	0 ± 1.5
γ-Carboxyl (glutamic)	4.4	0 ± 1.5
Imidazolium (histidine)	5.6–7.0	$+6.9$–7.5
α-Amino (terminal)	7.6–8.4	$+10$–13
Sulfhydryl (cysteine)	8–9	$+6.5$–7.0
ϵ-Amino (lysine)	9.4–10.6	$+10$–12
Phenolic hydroxyl (tyrosine)	9.8–10.4	$+6.0$
Guanidinium (arginine)	11.6–12.6	$+12$–13

can lead to the promotion, or inhibition, of ionization of groups located within. Nevertheless, comparison of the experimentally determined pK values to tabulated pK values for side-chain functional groups of amino acids (Table 6.1) can help identify the chemical nature of such groups within the enzyme.

Another parameter that can prove helpful in identification of the chemical nature of the charged groups involved in the reaction is the enthalpy of ionization (ΔH°). This enthalpy of ionization is determined from the temperature dependence of the equilibrium ionization constant K_a, as described in the chemical kinetics section. The identity of amino acids present in the active site of an enzyme could be potentially identified from their characteristic pK and ΔH° (Table 6.1).

6.3   NEW METHOD OF DETERMINING p*K* VALUES OF CATALYTICALLY RELEVANT FUNCTIONAL GROUPS

The usual way in which the putative pK values of catalytic groups were determined in the past was by considering the $\log_{10}(V^*_{max}/K^*_s)$ and $\log_{10} V^*_{max}$ versus pH curves in Fig. 6.3 to be composed of three straight lines with slopes $+1$, 0, and -1. The pH at which these lines intercept corresponds roughly to the pK values of the catalytic groups. However, a more efficient way of determining the points of inflection of these curves is to determine the pH at which the slope of the $\log_{10}(V^*_{max}/K^*_s)$ and $\log_{10} V^*_{max}$ versus pH curves equals 0.5 and -0.5. For the $\log_{10}(V^*_{max}/K^*_s)$ versus pH curve, the pH where the slope equals 0.5 corresponds to the pK_{e1} value, while the pH where the slope equals -0.5 corresponds to the pK_{e2} value. For the $\log_{10} V^*_{max}$ versus pH curve, the pH where the slope equals 0.5 corresponds to pK_{es1}, while the pH where the slope equals -0.5 corresponds to pK_{es2} (Fig. 6.4).

Consider the expression for the hydrogen ion dependence of V_{max} or V_{max}/K_s of an enzyme-catalyzed reaction:

$$Y^* = Y \left(1 + \frac{[H^+]}{K_1} + \frac{K_2}{[H^+]}\right)^{-1} = Y \frac{K_1[H^+]}{[H^+]^2 + K_1[H^+] + K_1 K_2} \quad (6.13)$$

where Y^* represents V^*_{max} or V^*_{max}/K^*_s, Y represents V_{max} or V_{max}/K_s, K_1 represents K_{es1} or K_{e1}, and K_2 represents K_{es2} or K_{e2}. A logarithmic transformation of Eq. (6.13), results in the expression

$$\log Y^* = \log (Y K_1) + \log [H^+] - \log ([H^+]^2 + K_1[H^+] + K_1 K_2) \tag{6.14}$$

The first derivative of Eq. (6.14) as a function of $-\log [H^+]$ (i.e., pH) is

$$\frac{d(\log Y^*)}{d(\text{pH})} = \frac{2[H^+]^2 - K_1[H^+]}{[H^+]^2 + K_1[H^+] + K_1 K_2} - 1 \quad (6.15)$$

For the case where $[H^+] = K_1$ and $K_1^2 \ggg K_1 K_2$,

$$\frac{d(\log Y^*)}{d(\text{pH})} = 0.5 \quad (6.16)$$

For the case where $[H^+] = K_2$ and $K_1^2 \ggg K_1 K_2$,

$$\frac{d(\log Y^*)}{d(\text{pH})} = -0.5 \quad (6.17)$$
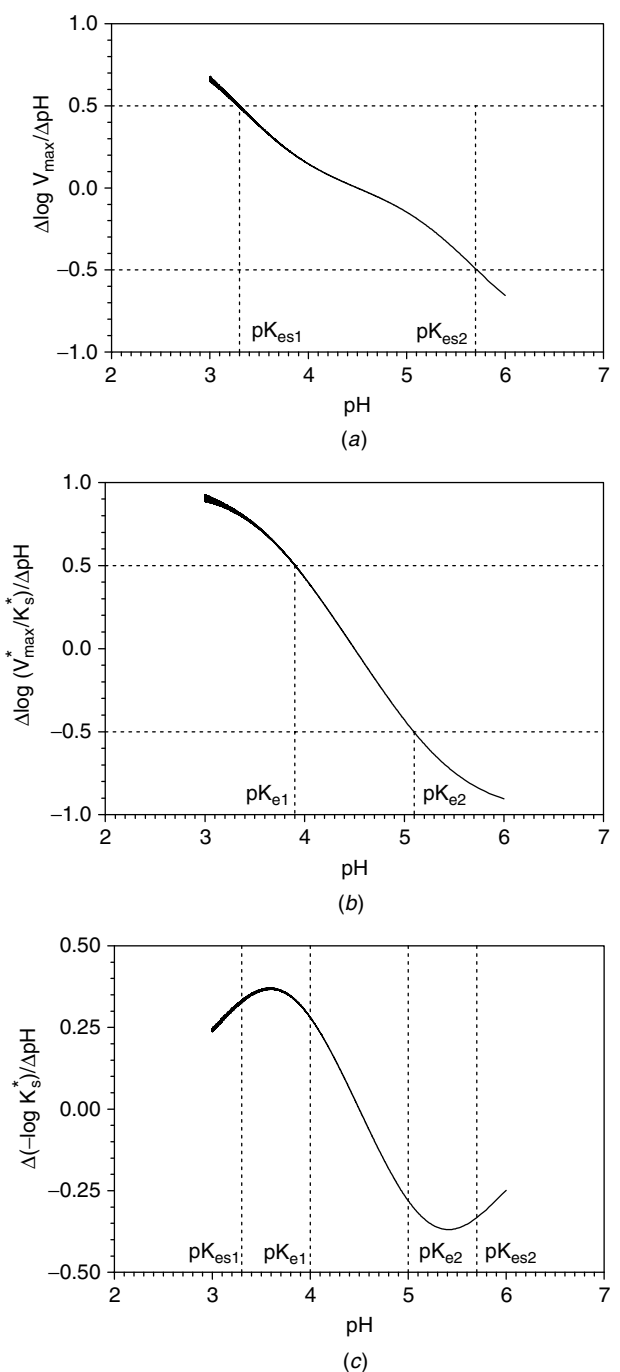
Figure 6.4. Variation in the slope of the (*a*) $\log V_{max}$, (*b*) $\log V_{max}/K_s$ and (*c*) $-\log K_s$ versus pH plots as a function of pH.

Consider the expression for the hydrogen ion dependence of the K_s of an enzyme-catalyzed reaction:

$$K_s^* = K_s \frac{1 + [H^+]/K_{e1} + K_{e2}/[H^+]}{1 + [H^+]/K_{es1} + K_{es2}/[H^+]}$$

$$= K_s \frac{K_{es1}}{K_{e1}} \frac{[H^+]^2 + K_{e1}[H^+] + K_{e1}K_{e2}}{[H^+]^2 + K_{es1}[H^+] + K_{es1}K_{es2}} \tag{6.18}$$
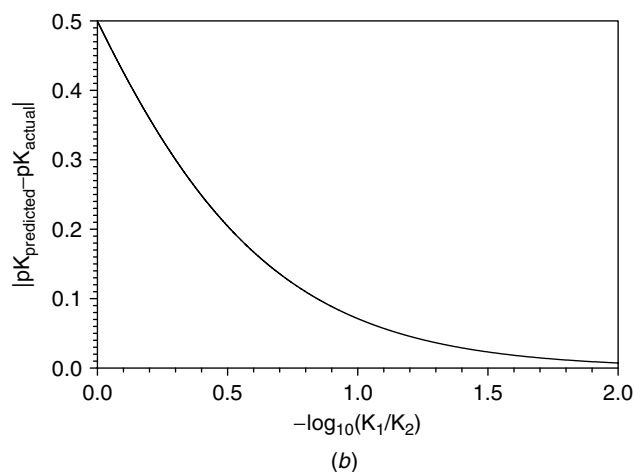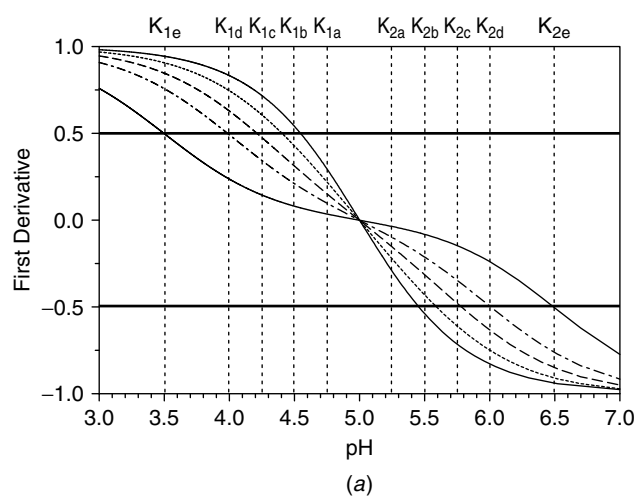
Figure 6.5. (*a*) Simulation of $\log V_{max}/K_s$ or $\log V_{max}$ patterns as a function of the closeness between K_1 and K_2 values in the enzyme. (*b*) Errors between actual and predicted pK values as a function of the difference in pK values of the catalytic groups in the enzyme.
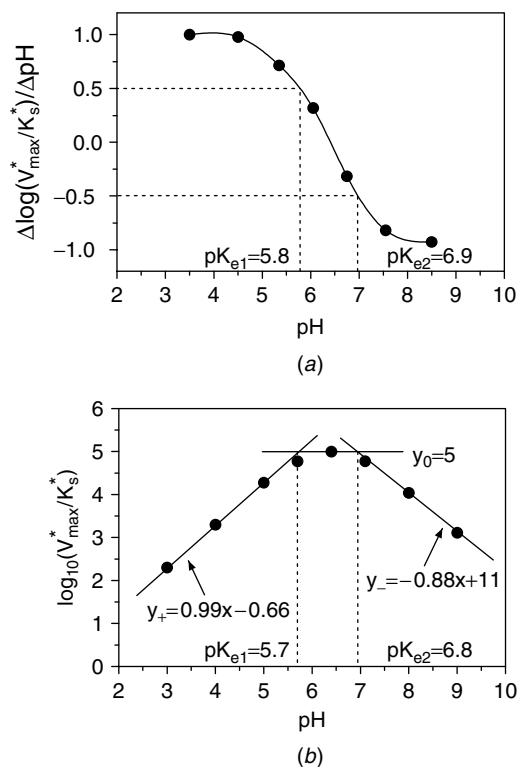
Figure 6.6. (*a*) pH dependence of the slope of a log V_{max}/K_s versus pH data set. (*b*) pH dependence of a log V_{max}/K_s versus pH data set.

A logarithmic transformation of Eq. (5.18), results in the expression

$$-\log K_s^* = -\log \frac{K_s K_{es1}}{K_{e1}} - \log([H^+]^2 + K_{e1}[H^+] + K_{e1}K_{e2})$$
$$+ \log([H^+]^2 + K_{es1}[H^+] + K_{es1}K_{es2}) \tag{6.19}$$

The first derivative of Eq. (6.19) as a function of $-\log[H^+]$ (i.e., pH) is

$$\frac{d(-\log K_s^*)}{d(\text{pH})} = \frac{2[H^+]^2 + K_{e1}[H^+]}{[H^+]^2 + K_{e1}[H^+] + K_{e1}K_{e2}}$$
$$- \frac{2[H^+]^2 + K_{es1}[H^+]}{[H^+]^2 + K_{es1}[H^+] + K_{es1}K_{es2}} \tag{6.20}$$

It is not as easy to calculate a value for this derivative at $[H^+] = K$, since the exact value will depend not only on the relative magnitude of K_{e1}

Figure 6.7. (*a*) Simulation of the pH dependence of the logarithm of the catalytic param-eters V_{max}, V_{max}/K_s, and K_s for a monoprotic enzyme. (*b*) Variation in the slope of the $\log V_{max}$, $\log V_{max}/K_s$, and $-\log K_s$ versus pH plots as a function of pH for a monopro-tic enzyme.

versus K_{e2}, but also of K_{es1} versus K_{es2}. We do not recommend working with this expression, since the results obtained can be ambiguous.

   Caution must be exercised when using this approach to determine the pK values of the catalytic groups since considerable error can be introduced in their determination if they happen to be numerically close. Figure 6.5(*a*) is a simulation of $\log_{10}(V_{max}^*/K_s^*)$ or $\log_{10} V_{max}^*$ versus pH patterns as a function of the closeness between K_1 and K_2 values. Figure 6.5(*b*) shows the error between actual and predicted pK values as a function of the difference between pK values. Our simulation shows

that as long at the difference between p*K* values is greater than 1 pH unit, the error introduced in the determination of p*K* values will be less than 0.1 pH unit.

Figure 6.6(*a*) shows an actual analysis of the pH dependence of V_{max}^*/K_s^* for the hydration of fumarate by the enzyme fumarase. The slope of the line *at the midpoint* between two subsequent pH values was calculated from the data as

$$\text{slope}_{(pH_2 - pH_1)/2} = \frac{\log Y_2^* - \log Y_1^*}{pH_2 - pH_1} \tag{6.21}$$

where Y^* could correspond to V_{max}^*/K_s^* or V_{max}^*. A general trend line through the data points was obtained by interpolation. From this trend line, the pH values at which the slope was $+0.5$ and -0.5 were easily determined. This procedure proved to be rapid, accurate, and reliable.

In our experience, drawing straight lines through the usual small number of data points, as carried out in the Dixon analysis, was not easy, particularly for the slope $= 0$ line. This ambiguity made it difficult to have confidence in the p*K* values determined. The procedure developed in this chapter is more reliable. On the other hand, the p*K* values obtained using the Dixon analysis and the analysis presented in this chapter were found to be similar (Fig. 6.6*b*).

Before leaving this topic, we would like to draw to the attention of the reader that many enzymes may have only one ionizable group among their catalytic groups. For this case, the patterns obtained for the pH dependence of the catalytic parameters will be half that of their two-ionizable-group counterparts (Fig. 6.7). For this case, the determination of pK_e and pK_{es} values is less prone to error since there is no interference from a second ionizable group.

CHAPTER 7

TWO-SUBSTRATE REACTIONS

Up to this point, the kinetic treatment of enzyme-catalyzed reactions has dealt only with single-substrate reactions. Many enzymes of biological importance, however, catalyze reactions between two or more substrates. Using the imaginative nomenclature of Cleland, two-substrate reactions can be classified as ping-pong or sequential. In *ping-pong mechanisms*, one or more products must be released before all substrates can react. In *sequential mechanisms*, all substrates must combine with the enzyme before the reaction can take place. Furthermore, sequential mechanisms can be ordered or Random. In *ordered sequential mechanisms*, substrates react with enzyme, and products are released, in a specific order. In *random sequential mechanisms*, on the other hand, the order of substrate combination and product release is not obligatory. These reactions can be classified even further according to the molecularity of the kinetically important steps in the reaction. Thus, these steps can be uni (unimolecular), bi (bimolecular), ter (termolecular), quad (quadmolecular), pent (pentamolecular), hexa (hexamolecular), and so on. This molecularity applies both to substrates and products. Using Cleland's schematics, examples of ping-pong bi bi, ordered-sequential bi bi, and random-sequential bi bi reactions are, respectively,

$$
\begin{array}{ccccc}
A & P & B & & Q \\
\downarrow & \uparrow & \downarrow & & \uparrow \\
\hline
E & (EA \rightleftharpoons E'P) & E' & (E'B \rightleftharpoons EQ) & E
\end{array}
\tag{7.1}
$$

$$
\begin{array}{ccccccc}
& \text{A} & \text{B} & & \text{P} & \text{Q} & \\
& \downarrow & \downarrow & & \uparrow & \uparrow & \\
\hline
\text{E} & \text{EA} & (\text{EAB} \rightleftharpoons \text{EPQ}) & \text{EQ} & \text{E}
\end{array}
\qquad (7.2)
$$

$$
\text{E} \quad \text{EAB} \rightleftharpoons \text{EPQ} \quad \text{E} \qquad (7.3)
$$
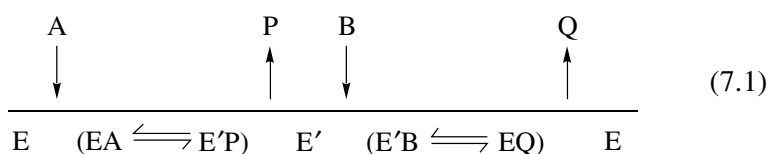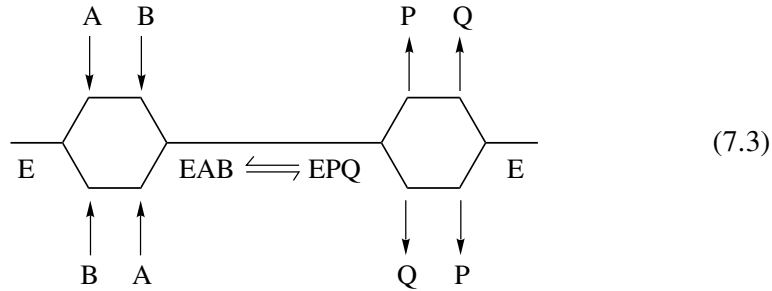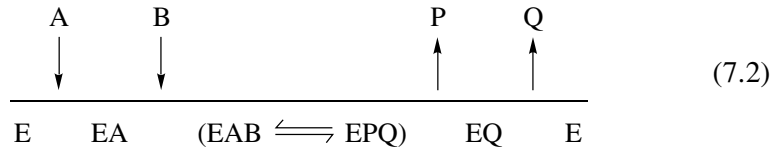
Irrespective of the mechanism, all two-substrate enzyme-catalyzed reactions of the type

$$
\text{A} + \text{B} \rightleftharpoons \text{P} + \text{Q} \qquad (7.4)
$$

obey the equation

$$
\frac{v}{V'_{\max}} = \frac{[\text{S}]}{K' + [\text{S}]} \qquad (7.5)
$$

under conditions where the concentration of one of the two substrates is held constant while the other is varied. For Eq. (7.5), [S] corresponds to the variable substrate's concentration, while K' and $V'_{\max}$ correspond to the apparent Michaelis constant and apparent maximum velocity for the enzymatic reaction, respectively.

Kinetic analysis of multiple substrate reactions could stop at this point. However, if more in-depth knowledge of the mechanism of a particular multisubstrate reaction is required, a more intricate kinetic analysis has to be carried out. There are a number of common reaction pathways through which two-substrate reactions can proceed, and the three major types are discussed in turn.

7.1 RANDOM-SEQUENTIAL Bi Bi MECHANISM

For the random-sequential bi bi mechanism, there is no particular order in the sequential binding of substrates A or B to the enzyme to form the ternary complex EAB. A general scheme for this type of reactions is

$$
\begin{array}{ccc}
\text{E} + \text{A} & \overset{K_s^{\text{A}}}{\rightleftharpoons} & \text{EA} \\
+ & & + \\
\text{B} & & \text{B} \\
\big\Vert\, K_s^{\text{B}} & & \big\Vert\, K^{\text{AB}} \\
\text{EB} + \text{A} & \underset{K^{\text{BA}}}{\rightleftharpoons} & \text{EAB} \overset{k_{\text{cat}}}{\longrightarrow} \text{E} + \text{P} + \text{Q}
\end{array}
\tag{7.6}
$$
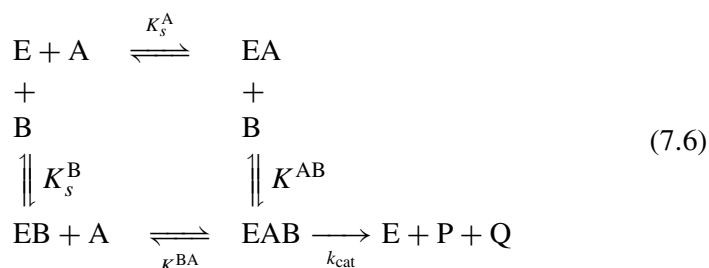
In this model we assume that rapid equilibrium binding of either substrate A or B to the enzyme takes place. For the second stage of the reaction, equilibrium binding of A to EB and B to EA, or a steady state in the concentration of the EAB ternary complex, may be assumed.

The rate equation for the formation of product, the equilibrium dissociation constant for the binary enzyme–substrate complexes EA and EB (K_s^{A} and K_s^{B}), the equilibrium dissociation (K_s) or steady-state Michaelis (K_m) constants for the formation of the ternary enzyme–substrate complexes EAB (K^{AB} and K^{BA}), and the enzyme mass balance are, respectively,

$$
v = k_{\text{cat}}[\text{EAB}]
\tag{7.7}
$$

$$
K_s^{\text{A}} = \frac{[\text{E}][\text{A}]}{[\text{EA}]} \qquad K_s^{\text{B}} = \frac{[\text{E}][\text{B}]}{[\text{EB}]}
$$

$$
K^{\text{BA}} = \frac{[\text{EB}][\text{A}]}{[\text{EBA}]} \qquad K^{\text{AB}} = \frac{[\text{EA}][\text{B}]}{[\text{EAB}]}
\tag{7.8}
$$

$$
[\text{E}_T] = [\text{E}] + [\text{EA}] + [\text{EB}] + [\text{EAB}]
\tag{7.9}
$$

A useful relationship exists among these constants:

$$
\frac{K_s^{\text{A}}}{K_s^{\text{B}}} = \frac{K^{\text{BA}}}{K^{\text{AB}}}
\tag{7.10}
$$

Normalization of the rate equation by total enzyme concentration ($v/[\text{E}_T]$) and rearrangement in light of Eq. (7.10) results in the rate equation for random-order bi bi mechanisms:

$$
\frac{v}{V_{\text{max}}} = \frac{[\text{A}][\text{B}]}{K_s^{\text{A}} K^{\text{AB}} + K^{\text{AB}}[\text{A}] + K^{\text{BA}}[\text{B}] + [\text{A}][\text{B}]}
\tag{7.11}
$$

where $V_{\text{max}} = k_{\text{cat}}[\text{E}_T]$.

7.1.1 Constant [A]

For the case where the concentration of substrate A is held constant, Eq. (7.11) can be expressed as

$$\frac{v}{V'_{\max}} = \frac{[B]}{K' + [B]} \tag{7.12}$$

where

$$V'_{\max} = \frac{V_{\max}[A]}{K^{BA} + [A]} \tag{7.13}$$

and

$$K' = \frac{K_s^A K^{AB} + K^{AB}[A]}{K^{BA} + [A]} = \frac{K^{AB}(K_s^A + [A])}{K^{BA} + [A]} \tag{7.14}$$

From determinations of K' and $V'_{\max}$ at different fixed concentrations of substrate A, it is possible to obtain estimates of $V_{\max}$, K_s^A, K^{AB}, and K^{BA}. $V'_{\max}$ displays a hyperbolic dependence on substrate A concentration (Fig. 7.1a). Thus, by fitting Eq. (7.13) to $V'_{\max}$–[A] experimental data using nonlinear regression, it is possible to obtain estimates of $V_{\max}$ and K^{BA}. K' also displays a hyperbolic dependence on substrate A concentration (Fig. 7.1b). However, this hyperbola does not go through the origin. At [A] = 0 (y-intercept), $K' = K_s^A K^{AB}/K^{BA}$ (or K_s^B), while in the limit where [A] approaches infinity, $K' = K^{AB}$ (Fig. 7.1b). Thus, by fitting Eq. (7.14) to K' − [A] experimental data using nonlinear regression, it is possible to obtain estimates of $K_s^A K^{AB}/K^{BA}$ and K^{AB}. Since the values of K^{AB}, K^{BA}, and K_s^B (y-intercept) are known, it is straightforward to obtain an estimate of K_s^A using Eq. (7.10):

$$K_s^A = \frac{K_s^B K^{BA}}{K^{AB}} \tag{7.15}$$

7.1.2 Constant [B]

For the case where the concentration of substrate A is held constant, Eq. (7.11) can be expressed as

$$\frac{v}{V'_{\max}} = \frac{[A]}{K' + [A]} \tag{7.16}$$

where

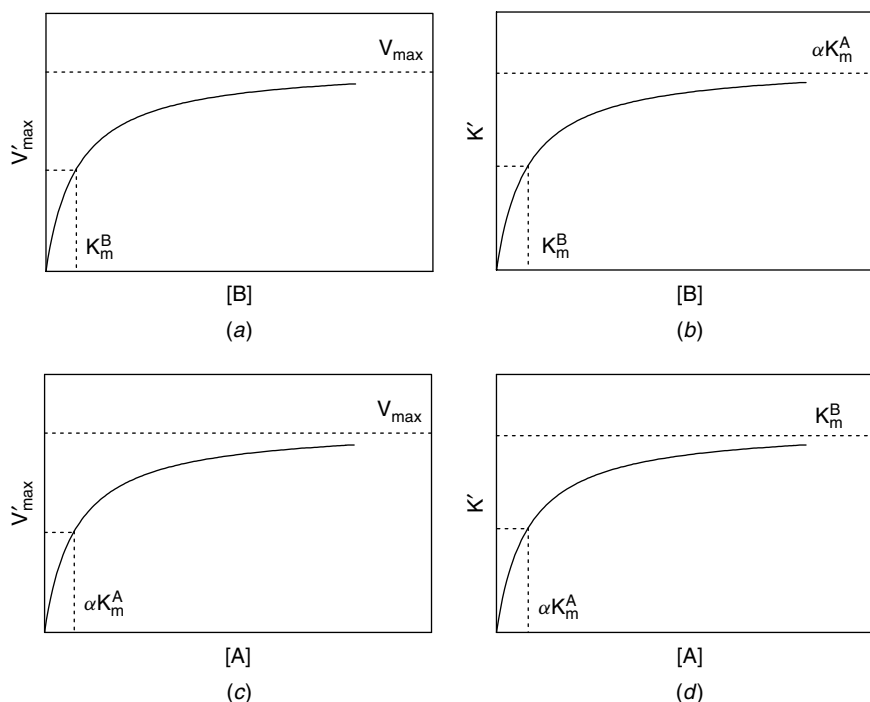$$V'_{\max} = \frac{V_{\max}[B]}{K^{AB} + [B]} \tag{7.17}$$
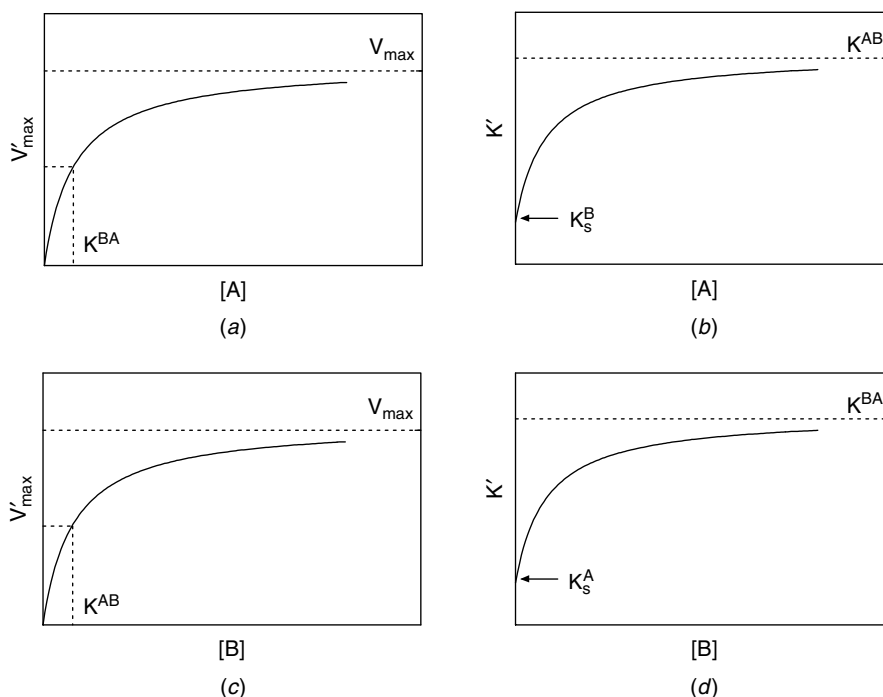
Figure 7.1. Fixed substrate concentration dependence for enzymes displaying random-sequential mechanisms: (*a*) Dependence of V'_{max} on [A]; (*b*) dependence of K' on [A]; (*c*) dependence of V'_{max} on [B]; (*d*) dependence of K' on [B].

and

$$K' = \frac{K_s^A K^{AB} + K^{BA}[B]}{K^{AB} + [B]} = \frac{K_s^B K^{BA} + K^{BA}[B]}{K^{AB} + [B]} = \frac{K^{BA}(K_s^B + [B])}{K^{AB} + [B]}$$
(7.18)

From determinations of K' and V'_{max} at different *fixed* concentrations of substrate B, it is possible to obtain estimates of V_{max}, K_s^B, K^{AB}, and K^{BA}. V'_{max} displays a hyperbolic dependence on substrate B concentration (Fig. 7.1*c*). Thus, by fitting Eq. (7.17) to V'_{max}–[B] experimental data using nonlinear regression, it is possible to obtain estimates of V_{max} and K^{AB}. K' also displays a hyperbolic dependence on substrate B concentration (Fig. 7.1*d*). However, this hyperbola does not go through the origin. At [B] = 0 (*y*-intercept), $K' = K_s^B K^{BA}/K^{AB}$ (or K_s^A), while in the limit where [B] approaches infinity, $K' = K^{BA}$ (Fig. 7.1*d*). Thus, by fitting Eq. (7.18) to K'–[B] experimental data using nonlinear regression, it is possible to obtain estimates of K_s^A and K^{BA}. Since the values of K^{AB},

K^{BA}, and K_s^{A} are known, it is straightforward to obtain an estimate of K_s^{B} using Eq. (7.10):

$$K_s^{\mathrm{B}} = \frac{K_s^{\mathrm{A}} K^{\mathrm{AB}}}{K^{\mathrm{BA}}} \tag{7.19}$$

7.2   ORDERED-SEQUENTIAL Bi Bi MECHANISM

For this mechanism, the enzyme must bind substrate A first, followed by binding of substrate B, to form the ternary complex EAB. A general scheme for this type of reactions is
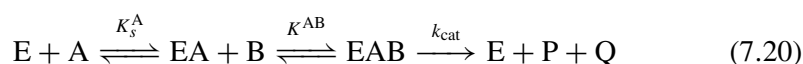
$$\mathrm{E} + \mathrm{A} \underset{}{\overset{K_s^{\mathrm{A}}}{\rightleftharpoons}} \mathrm{EA} + \mathrm{B} \underset{}{\overset{K^{\mathrm{AB}}}{\rightleftharpoons}} \mathrm{EAB} \xrightarrow{k_{\mathrm{cat}}} \mathrm{E} + \mathrm{P} + \mathrm{Q} \tag{7.20}$$

The rate equation for the formation of product, the equilibrium dissociation constant for the binary enzyme–substrate complex EA (K_s^{A}), the equilibrium dissociation (K_s), or steady-state Michaelis (K_m) constant for the formation of the ternary enzyme–substrate complex EAB (K^{AB}), and the enzyme mass balance are, respectively,

$$v = k_{\mathrm{cat}}[\mathrm{EAB}] \tag{7.21}$$

$$K_s^{\mathrm{A}} = \frac{[\mathrm{E}][\mathrm{A}]}{[\mathrm{EA}]} \qquad K^{\mathrm{AB}} = \frac{[\mathrm{EA}][\mathrm{B}]}{[\mathrm{EAB}]} \tag{7.22}$$

$$[\mathrm{E}_T] = [\mathrm{E}] + [\mathrm{EA}] + [\mathrm{EAB}] \tag{7.23}$$

Normalization of the rate equation by total enzyme concentration ($v/[\mathrm{E}_T]$) and rearrangement results in the rate equation for ordered-sequential bi bi mechanisms:

$$\frac{v}{V_{\mathrm{max}}} = \frac{[\mathrm{A}][\mathrm{B}]}{K_s^{\mathrm{A}} K^{\mathrm{AB}} + K^{\mathrm{AB}}[\mathrm{A}] + [\mathrm{A}][\mathrm{B}]} \tag{7.24}$$

where $V_{\mathrm{max}} = k_{\mathrm{cat}}[\mathrm{E}_T]$.

7.2.1   Constant [B]

For the case where the concentration of substrate B is held constant, Eq. (7.24) can be expressed as

$$\frac{v}{V_{\mathrm{max}}'} = \frac{[\mathrm{A}]}{K' + [\mathrm{A}]} \tag{7.25}$$

where

$$V'_{\max} = \frac{V_{\max}[B]}{K^{AB} + [B]} \tag{7.26}$$

and

$$K' = \frac{K_s^A K^{AB}}{K^{AB} + [B]} \tag{7.27}$$

From determinations of K' and $V'_{\max}$ at different *fixed* concentrations of substrate B, it is possible to obtain estimates of $V_{\max}$, K_s^A, and K^{AB}. $V'_{\max}$ displays a hyperbolic dependence on substrate B concentration (Fig. 7.2a). Thus, by fitting Eq. (7.26) to $V'_{\max}$–[B] experimental data using nonlinear regression, it is possible to obtain estimates of $V_{\max}$ and K^{AB}. K' also displays a hyperbolic dependence on substrate B concentration (Fig. 7.2b). However, the y-intercept ([B] $= 0$) of this hyperbola equals K_s^A, while in the limit where [B] approaches infinity, $K' = 0$ (Fig. 7.2b). Thus, by fitting Eq. (7.27) to K'–[B] experimental data using nonlinear regression, it is possible to obtain an estimate of K_s^A.

7.2.2   Constant [A]

For the case where the concentration of substrate A is held constant, Eq. (7.24) can be expressed as

$$\frac{v}{V'_{\max}} = \frac{[B]}{K' + [B]} \tag{7.28}$$

where

$$V'_{\max} = V_{\max} \tag{7.29}$$

and

$$K' = \frac{K_s^A K^{AB}}{[A]} + K^{AB} \tag{7.30}$$

From determinations of K' at different *fixed* concentrations of substrate A, it is possible to obtain estimates of K_s^A and K^{AB}. K' displays a hyperbolic dependence on substrate A concentration (Fig. 7.2c). The slope of this function equals $K_s^A K^{AB}$. In the limit where [A] approaches infinity, $K' = K^{AB}$ (Fig. 7.2c). Thus, by fitting Eq. (7.30) to K'–[A] experimental data using nonlinear regression, it is possible to obtain estimates of K_s^A and K^{AB}.
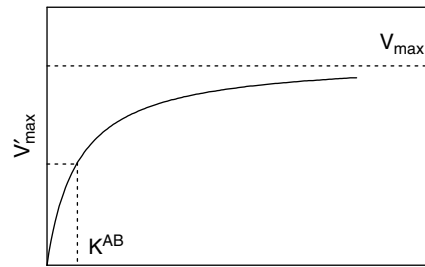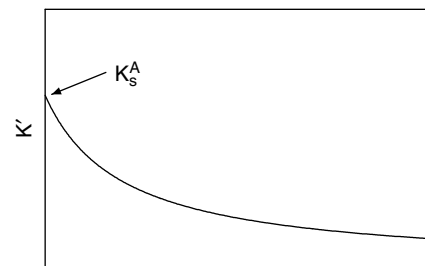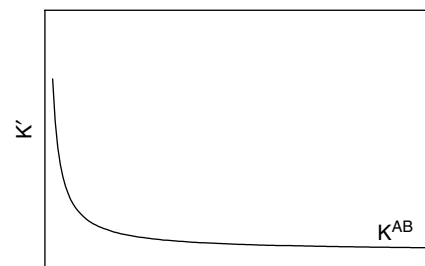
Figure 7.2. Fixed substrate concentration dependence for enzymes displaying ordered sequential mechanisms: (*a*) Dependence of $V'_{\max}$ on [B]; (*b*) dependence of K' on [B]; (*c*) dependence of K' on [A].

7.2.3 Order of Substrate Binding

The dependence of $V'_{\max}$ on the fixed substrate's concentration can be used as an indicator of substrate-binding order. A fixed substrate's concentration dependence of $V'_{\max}$ is associated with the second substrate to bind to the enzyme. A fixed substrate's concentration independence of $V'_{\max}$ is associated with the first substrate to bind to the enzyme.

7.3   PING-PONG Bi Bi MECHANISM

For this mechanism, the enzyme must bind substrate A first, followed by the release of product P and the formation of the enzyme species E′. This is followed by binding of substrate B to E′ and the breakdown of the E′B complex to free enzyme E and the second product Q. Thus, for ping pong mechanisms, no ternary complex is formed. A general steady-state scheme for this type of reactions is

$$
\text{E} + \text{A} \underset{k_{-1}}{\overset{k_1}{\rightleftharpoons}} \overset{K_m^{\text{A}}}{\text{EA}} \xrightarrow{k_2} \text{E}' + \text{B} \underset{k_{-3}}{\overset{k_3}{\rightleftharpoons}} \overset{K_m^{\text{B}}}{\text{E}'\text{B}} \xrightarrow{k_4} \text{E} \tag{7.31}
$$
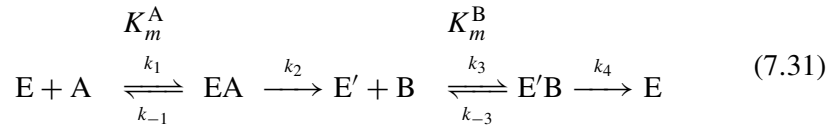
The rate equation, steady-state Michaelis constants, and enzyme mass balance for this mechanism are, respectively,

$$
v = k_4[\text{E}'\text{B}] \tag{7.32}
$$

$$
K_m^{\text{A}} = \frac{k_{-1} + k_2}{k_1} = \frac{[\text{E}][\text{A}]}{[\text{EA}]} \qquad K_m^{\text{B}} = \frac{k_{-3} + k_4}{k_3} = \frac{[\text{E}'][\text{B}]}{[\text{E}'\text{B}]} \tag{7.33}
$$

$$
[\text{E}_T] = [\text{E}] + [\text{EA}] + [\text{E}'] + [\text{E}'\text{B}] \tag{7.34}
$$

A relationship between E and E′ can also be obtained, assuming a steady-state in the concentration of E′:

$$
[\text{E}] = \frac{k_4}{k_2} \frac{K_m^{\text{A}}}{K_m^{\text{B}}} \frac{[\text{E}'][\text{B}]}{[\text{A}]} \tag{7.35}
$$

Normalization of the rate equation by total enzyme concentration ($v/[\text{E}_T]$), substitution, and rearrangement yields the following rate equation for ping-pong bi bi mechanisms:

$$
\frac{v}{V_{\max}} = \frac{[\text{A}][\text{B}]}{(k_4/k_2)K_m^{\text{A}}[\text{B}] + K_m^{\text{B}}[\text{A}] + [\text{A}][\text{B}](1 + k_4/k_2)} \tag{7.36}
$$

where $V_{\max} = k_{\text{cat}}[\text{E}_T]$ and $k_{\text{cat}} = k_4$. For the case where the rate-limiting step of the reaction is the conversion of E′B into EQ (i.e., $k_2 \ggg k_4$), Eq. (7.36) reduces to

$$
\frac{v}{V_{\max}} = \frac{[\text{A}][\text{B}]}{\alpha K_m^{\text{A}}[\text{B}] + K_m^{\text{B}}[\text{A}] + [\text{A}][\text{B}]} \tag{7.37}
$$

where $\alpha = k_4/k_2$.

7.3.1 Constant [B]

For the case where the concentration of substrate B is held constant, Eq. (7.37) can be expressed as

$$\frac{v}{V'_{\max}} = \frac{[A]}{K' + [A]} \tag{7.38}$$

where

$$V'_{\max} = \frac{V_{\max}[B]}{K_m^B + [B]} \tag{7.39}$$

and

$$K' = \frac{\alpha K_m^A [B]}{K_m^B + [B]} \tag{7.40}$$

From determinations of K' and $V'_{\max}$ at different fixed concentrations of substrate B, it is possible to obtain estimates of $V_{\max}$, αK_m^A, and K_m^B. $V'_{\max}$ displays a hyperbolic dependence on substrate B concentration (Fig. 7.3*a*). Thus, by fitting Eq. (7.39) to $V'_{\max}$–[B] experimental data using nonlinear regression, it is possible to obtain estimates of $V_{\max}$ and K_m^B. K' also displays a hyperbolic dependence on substrate B concentration (Fig. 7.3*b*). Thus, by fitting Eq. (7.40) to K'–[B] experimental data using nonlinear regression, it is possible to obtain estimates of αK_m^A and K_m^B.

7.3.2 Constant [A]

For the case where the concentration of substrate A is held constant, Eq. (7.37) can be expressed as

$$\frac{v}{V'_{\max}} = \frac{[A]}{K' + [A]} \tag{7.41}$$

where

$$V'_{\max} = \frac{V_{\max}[A]}{\alpha K_m^A + [A]} \tag{7.42}$$

and

$$K' = \frac{K_m^B [A]}{\alpha K_m^A + [A]} \tag{7.43}$$

From determinations of K' and $V'_{\max}$ at different fixed concentrations of substrate A, it is possible to obtain estimates of $V_{\max}$, αK_m^A, and K_m^B. $V'_{\max}$ displays a hyperbolic dependence on substrate A concentration (Fig. 7.3*c*).

Figure 7.3. Fixed substrate concentration dependence for enzymes displaying ping-pong mechanisms: (*a*) Dependence of $V'_{\max}$ on [B]; (*b*) dependence of K' on [B]; (*c*) dependence of $V'_{\max}$ on [A]; (*d*) dependence of K' on [A].

Thus, by fitting Eq. (7.42) to $V'_{\max}$–[A] experimental data using nonlinear regression, it is possible to obtain estimates of $V_{\max}$ and αK_m^A. K' also displays a hyperbolic dependence on substrate A concentration (Fig. 7.3*d*). Thus, by fitting Eq. (7.43) to K'–[A] experimental data using nonlinear regression, it is possible to obtain estimates of αK_m^A and K_m^B.

7.4   DIFFERENTIATION BETWEEN MECHANISMS

Differentiation between reaction mechanisms can be achieved by careful scrutiny of the K' versus substrate concentration patterns (Fig. 7.4). The adage that a picture tells a thousand words is quite applicable in this instance. It is difficult to determine the mechanism of an enzyme-catalyzed reaction from steady-state kinetic analysis. The determination of the mechanism of an enzymatic reaction is neither a trivial task nor an easy task. The use of dead-end inhibitors and alternative substrates, study of the patterns of product inhibition, and isotope-exchange experiments
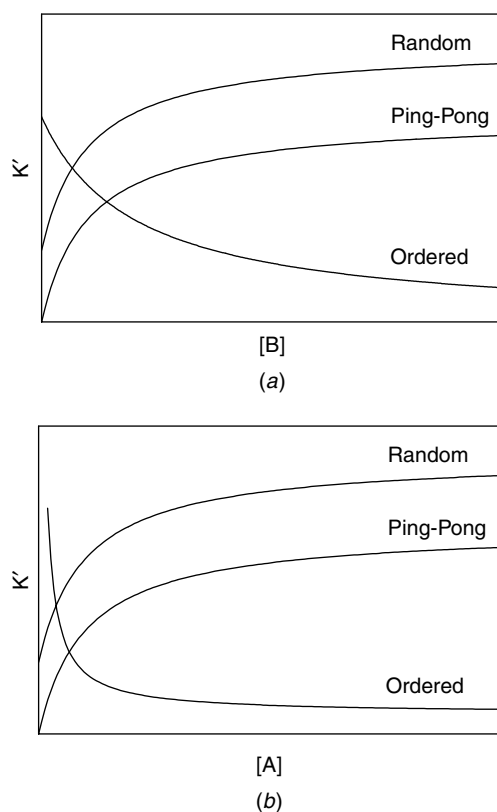
Figure 7.4. Dependence of the apparent Michaelis constant (K') on the concentration of fixed substrate for random-sequential, ordered-sequential, and ping-pong mechanisms.

all shed light on the possible nature of a mechanism. Haldane and Dalziel relationships sometimes help discriminate between possible mechanisms. Once very popular, the use of steady-state kinetic analysis to determine the mechanism of an enzymatic reaction has decreased in favor of pre-steady-state analysis of kinetic data obtained from rapid-reaction techniques.

CHAPTER 8

MULTISITE AND COOPERATIVE ENZYMES

Many enzymes are oligomers composed of distinct subunits. Often, the subunits are identical, each bearing an equivalent catalytic site. If the sites are identical and independent of each other, the presence of substrate at one site will have no effect on substrate binding and catalytic properties at other sites. Therefore, kinetic treatments developed for single-site enzymes will also apply to multisite enzymes. Phenomenologically, the kinetic behavior of n single-site enzymes is indistinguishable from the behavior of one enzyme with n active sites. Thus, the rate equation for an oligomeric enzyme with n independent, noninteracting active sites is

$$\frac{v}{V_{\max}} = \frac{[S]}{k_s + [S]} \tag{8.1}$$

where $V_{\max} = k_{\text{cat}}[E_T]$ and k_s is the microscopic dissociation constant of the ES_n complexes.

In cooperative enzymes, on the other hand, low- and high-affinity substrate binding sites are present, and cooperative binding of substrate to enzyme can take place. The binding of one substrate molecule induces structural and/or electronic changes that result in altered substrate binding affinities in the remaining vacant sites. The enzyme's substrate binding affinity can theoretically either increase (positive cooperativity) or decrease (negative cooperativity). An increase in affinity upon substrate binding is, however, the most common response.

102
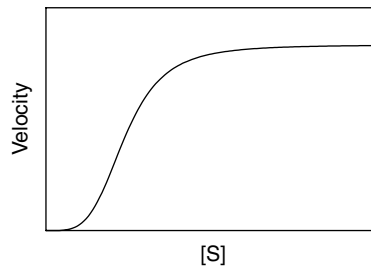
Figure 8.1. Initial velocity versus substrate concentration curve for a cooperative enzyme.

Enzyme activity can also be affected by binding of substrate and non-substrate ligands, which can act as activators or inhibitors, at a site other than the active site. These enzymes are called *allosteric*. These responses can be homotropic or heterotropic. *Homotropic* responses refer to the allosteric modulation of enzyme activity strictly by substrate molecules; *heterotropic* responses refer to the allosteric modulation of enzyme activity by nonsubstrate molecules or combinations of substrate and nonsubstrate molecules. The allosteric modulation can be positive (activation) or negative (inhibition). Many allosteric enzymes also display cooperativity, making a clear differentiation between allosterism and cooperativity somewhat difficult.

Cooperative substrate binding results in sigmoidal v versus [S] curves (Fig. 8.1). The Michaelis–Menten model is therefore not applicable to cooperative enzymes. Two major equilibrium models have evolved to describe the catalytic behavior of cooperative enzymes: the sequential interaction and concerted transition models. The reader should be aware that other models have also been developed, such as equilibrium association–dissociation models, as well as several kinetic models. These are not discussed in this chapter.

8.1 SEQUENTIAL INTERACTION MODEL

8.1.1 Basic Postulates

The basic premise of the sequential interaction (SI) model is that significant changes in enzyme conformation take place upon substrate binding, which result in altered substrate binding affinities in the remaining active sites (Fig. 8.2). For the case of positive cooperativity, each substrate molecule that binds makes it easier for the next substrate molecule to bind. The resulting v versus [S] curve therefore displays a marked slope increase as a function of increasing substrate concentration. Upon saturation of the
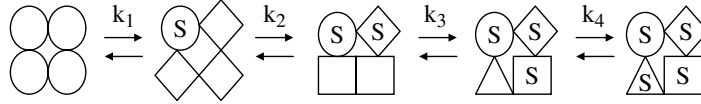
Figure 8.2. Diagrammatic representation of the sequential interaction of substrate with a four-site cooperative enzyme. Binding of one substrate molecule alters the substrate affinity of other sites. The constants k depict microscopic dissociation constants for the first, second, third, and fourth sites, respectively.

active sites, the slope of the curve steadily decreases. This results in a sigmoidal v versus [S] curve (Fig. 8.1). For a hypothetical tetrameric cooperative enzyme with four active sites, the rate equation for the formation of product and enzyme mass balance are

$$v = k_{\text{cat}}[\text{ES}_1] + 2k_{\text{cat}}[\text{ES}_2] + 3k_{\text{cat}}[\text{ES}_3] + 4k_{\text{cat}}[\text{ES}_4] \qquad (8.2)$$

$$[\text{E}_T] = [\text{E}] + [\text{ES}_1] + [\text{ES}_2] + [\text{ES}_3] + [\text{ES}_4] \qquad (8.3)$$

The equilibrium dissociation constants, both macroscopic or global (K_n) and microscopic or intrinsic (k_n), for the various ES_n complexes are

$$K_1 = \frac{1}{4}k_1 = \frac{[\text{E}][\text{S}]}{[\text{ES}_1]} \qquad [\text{ES}_1] = \frac{[\text{E}][\text{S}]}{K_1} = \frac{4[\text{E}][\text{S}]}{k_1}$$

$$K_2 = \frac{2}{3}k_2 = \frac{[\text{ES}_1][\text{S}]}{[\text{ES}_2]} \qquad [\text{ES}_2] = \frac{[\text{E}][\text{S}]^2}{K_1 K_2} = \frac{6[\text{E}][\text{S}]^2}{k_1 k_2}$$

$$K_3 = \frac{3}{2}k_3 = \frac{[\text{ES}_2][\text{S}]}{[\text{ES}_3]} \qquad [\text{ES}_3] = \frac{[\text{E}][\text{S}]^3}{K_1 K_2 K_3} = \frac{4[\text{E}][\text{S}]^3}{k_1 k_2 k_3} \qquad (8.4)$$

$$K_4 = 4k_4 = \frac{[\text{ES}_3][\text{S}]}{[\text{ES}_4]} \qquad [\text{ES}_4] = \frac{[\text{E}][\text{S}]^4}{K_1 K_2 K_3 K_4} = \frac{[\text{E}][\text{S}]^4}{k_1 k_2 k_3 k_4}$$

Upon substrate binding, dissociation constants can decrease for the case of positive cooperativity (increased affinity of enzyme for substrate) or decrease in the case of negative cooperativity (decreased affinity of enzyme for substrate).

Normalization of the rate equation by total enzyme concentration ($v/[\text{E}_T]$), substitution of the different ES_n terms with the appropriate expression containing microscopic dissociation constants, and rearrangement results in the following expression for the velocity of a four-site

cooperative enzyme:

$$\frac{v}{V_{max}} = \frac{[S]/k_1 + 3[S]^2/k_1k_2 + 3[S]^3/k_1k_2k_3 + [S]^4/k_1k_2k_3k_4}{1 + 4[S]/k_1 + 6[S]^2/k_1k_2 + 4[S]^3/k_1k_2k_3 + [S]^4/k_1k_2k_3k_4}$$

(8.5)

where $V_{max} = 4k_{cat}[E_T]$. For the special case where an enzyme has pronounced positive cooperativity, the concentrations of ES, ES_2, and ES_3 are small compared to the concentration of ES_4. Thus, if these terms are omitted from both the rate equation and enzyme mass balance [Eqs. (8.2) and (8.3)], Eq. (8.5) reduces to

$$\frac{v}{V_{max}} \approx \frac{[S]^4/k_1k_2k_3k_4}{1 + [S]^4/k_1k_2k_3k_4} = \frac{[S]^4}{k' + [S]^4}$$

(8.6)

where $k' = k_1k_2k_3k_4$.

8.1.2 Interaction Factors

The concept of interaction factors is frequently used in the treatment of cooperative enzymes. In this treatment, all substrate-binding sites are assumed to have the same intrinsic microscopic dissociation constant, k. The intrinsic dissociation constant of the ES complex was defined previously as k_1, and for this treatment, k_1 becomes k.

Upon substrate binding to the first active site, the intrinsic dissociation constant of the second substrate-binding site (ES_2) will change by a factor α:

$$k_2 = \alpha k$$

(8.7)

Upon binding of a second substrate molecule, the intrinsic dissociation constant of the third substrate-binding site will change further by a factor β:

$$k_3 = \alpha\beta k$$

(8.8)

Upon binding of a third substrate molecule, the intrinsic dissociation constant of the fourth substrate-binding site will change further by a factor γ:

$$k_4 = \alpha\beta\gamma k$$

(8.9)

Thus, for a four-site highly cooperative enzyme, the overall enzyme–substrate intrinsic dissociation constant (k') of the enzyme can be expressed

as the product of the four separate constants, or as the product of three interaction factors and the intrinsic dissociation constant of all sites:

$$k' = k_1 k_2 k_3 k_4 = \alpha^3 \beta^2 \gamma k^4 \tag{8.10}$$

Interaction factors (f) will have values in the range $f < 1$ for positive cooperativity and $f > 1$ for negative cooperativity. It is very difficult to obtain accurate estimates of individual interaction factors, or intrinsic dissociation constants, from steady-state kinetic analysis of enzyme activity.

8.1.3   Microscopic versus Macroscopic Dissociation Constants

It is important to understand the difference between macroscopic and microscopic dissociation constants. The number of different ways that substrate molecules can occupy n active sites within an enzyme, without replacement and without regard to the order of the occupancy (i.e., the number of combinations, C) is given by

$$C = \frac{n!}{(n-s)! \, s!} \tag{8.11}$$

where n represents the number of sites available for substrate binding in the enzyme and s corresponds to the number of substrate molecules bound per enzyme. For example, in the case of a tetramer with four active sites ($n = 4$), where only two sites are filled ($s = 2$), the number of possible ways in which enzyme and substrate can form an ES_2 microscopic species equals 6 (see Fig. 8.3). The concentration of each individual microscopic ES_2 species would then be $[ES_2]/6$. Relationships between macroscopic and microscopic dissociation constants are obtained upon substitution of macroscopic ES_n concentration terms with microscopic ES_n concentration terms. This treatment assumes an equal probability of occurrence for each microscopic species. For example, the macroscopic dissociation constant for the reaction $ES_3 \rightleftharpoons ES_2 + S$ is

$$K_s = \frac{[ES_2][S]}{[ES_3]} \tag{8.12}$$

As discussed above, the number of possible ways in which enzyme and substrate can form an ES_2 microscopic species equals 6. For the ES and ES_3 complexes, four different microscopic species can form, while only one microscopic species exists for the ES_4 complex (Fig. 8.3). Thus, the
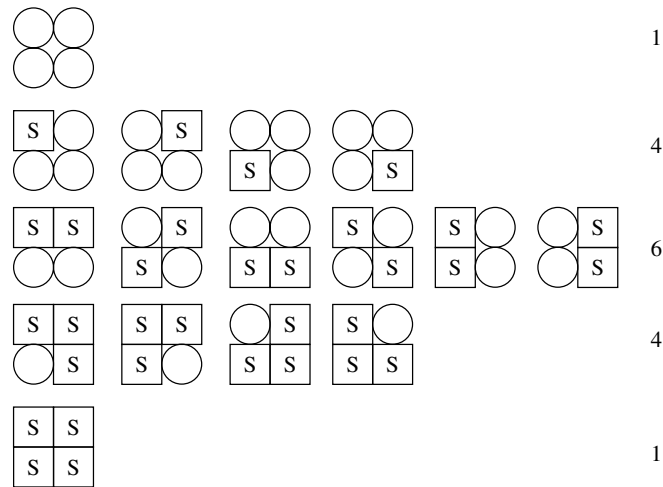
Figure 8.3. Possible ways in which, respectively, one, two, three, and four substrate molecules can randomly occupy binding sites in a four-site cooperative enzyme.

concentration of ES_2 microscopic species is $[ES_2]/6$. The concentration of the ES, ES_3, and ES_4 complexes is, respectively, $[ES]/4$, $[ES_3]/4$, and ES_4. Considering the above, the microscopic dissociation constant for the reaction $ES_3 \rightleftharpoons ES_2 + S$ is

$$k_s = \frac{([ES_2]/6)[S]}{[ES_3]/4} = \frac{2}{3}\frac{[ES_2][S]}{[ES_3]} \tag{8.13}$$

Therefore, the relationship between macroscopic (K_s) and microscopic (k_s) dissociation constants for this reaction is

$$K_s = \frac{3}{2}k_s \tag{8.14}$$

8.1.4 Generalization of the Model

It follows from Eq. (8.6) that for the case of an enzyme with n active sites displaying a high degree of cooperativity,

$$\frac{v}{V_{max}} = \frac{[S]^n}{k' + [S]^n} \tag{8.15}$$

This model has the same form as the well-known Hill equation. For historical reasons, the SI model in the form of Eq. (8.15) will be referred

to as the Hill equation. It is important to realize that Hill equation was not originally derived in the fashion described above. The Hill constant, k', Hill coefficient, n, and V_{max} are parameters used to characterize the catalytic properties of cooperative enzymes. The Hill constant is related to the enzyme–substrate dissociation constants ($k' = \Pi k_n$) and provides an estimate of the affinity of the enzyme for a particular substrate. The relationship between the Hill constant and the substrate concentration at $\frac{1}{2}V_{max}$ [$S_{0.5}$] is

$$k' = [S_{0.5}]^n \qquad (8.16)$$

The Hill constant is an index of the affinity of the enzyme for the substrate, but it is not the enzyme–substrate dissociation constant. It has units of (concentration)^n, which makes comparison between reactions with different n values difficult.

The Hill coefficient is an index of the cooperativity in the substrate binding process—the greater the value of n, the higher the cooperativity. For the case where $n = 1$ (no cooperativity), the Hill equation reduces to the Michaelis–Menten model. If the cooperativity of the sites is low, n will not correspond to the number of substrate-binding sites, but the minimum number of effective substrate-binding sites. Regardless of this limitation, the Hill equation can still be used to characterize the kinetic behavior of a cooperative enzyme. In this case, n becomes merely an index of cooperativity, which can have noninteger values.

Estimates of the parameters k' and n are obtained using standard nonlinear regression procedures available in most modern graphical software packages. By fitting the Hill equation to experimental v versus [S] data, estimates of k', n, and V_{max} can easily be obtained. Simulations of v versus [S] behavior using Eq. (8.15) are shown in Fig. 8.4. As can be appreciated in Fig. 8.4(a), the greater the Hill exponent, the more pronounced the sigmoidicity of the curve. For the case where $n = 1$, the Hill equation reduces to the Michaelis–Menten model. Increases in the value of the Hill constant, k', will decrease the steepness of the v versus [S] curve (Fig. 8.4b). Thus, from a topological perspective, the shape (i.e., sigmoidicity and steepness) of the curve can be adequately described by these two parameters.

The Hill equation is a three-parameter function (k', n, V_{max}), and constitutes the simplest equation that describes the kinetic behavior of cooperative enzymes. From a practical point of view, the next most useful model is the symmetry model. Even though it only accounts for positive cooperativity and is based on somewhat arbitrary assumptions, this model can account for allosteric effects.
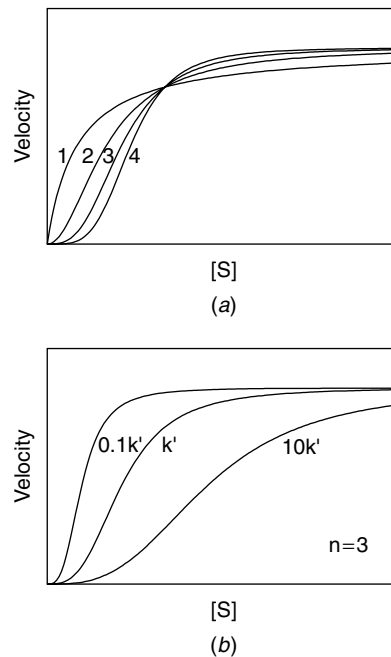
Figure 8.4. (*a*) Simulation of the effects of varying the Hill exponent (*n*) on the shape of the initial velocity versus substrate concentration curve for a cooperative enzyme. (*b*) Simulation of the effects of varying the Hill constant (k') on the shape of the initial velocity versus substrate concentration curve for a cooperative enzyme.

8.2 CONCERTED TRANSITION OR SYMMETRY MODEL

The concerted transition (CT) or symmetry model, a departure from prior models of cooperativity, accounted for allosterism but could not explain anticooperativity. This model is based on the following postulates:

1. Allosteric enzymes are composed of identical protomers that occupy equivalent positions within the enzyme. A protomer is a structural unit that contains a unique binding site for each specific ligand (e.g., substrate and activator). A protomer does not necessarily correspond to one subunit (a single polypeptide chain).

2. Each protomer can only exist in either of two conformational states, R (relaxed, or high substrate binding affinity) or T (taut, or low substrate binding affinity). The dissociation constant for the R-state protomer–substrate complexes, k_R, is lower than that of the T-state protomer–substrate complexes, k_T (Fig. 8.5).

T_o L R_o

$+S \downarrow\uparrow k_T$ $+S \downarrow\uparrow k_R$

TS L RS

$+S \downarrow\uparrow k_T$ $+S \downarrow\uparrow k_R$

TS_2 L RS_2
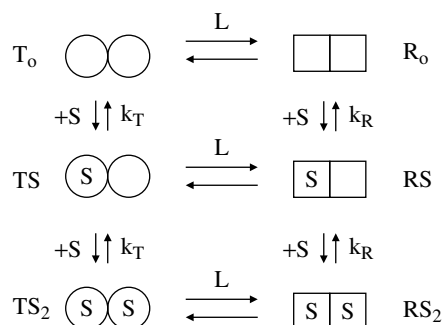
Figure 8.5. Diagrammatic representation of the concerted transition model for a two-site cooperative enzyme.

3. All protomers within the enzyme must be in either the R or T state—mixed conformations are not allowed. The R and T states of the enzyme are in equilibrium with each other. Thus, an equilibrium constant (L) can be written for the R $\rightleftharpoons$ T transition ($L = [T]/[R]$).
4. The binding affinity of a specific ligand depends on the conformation of the enzyme (R or T), and not on neighboring site occupancy.

Based on equilibrium arguments, a general expression for the velocity of a cooperative enzyme-catalyzed reaction can be derived. The equilibrium macroscopic (K_T, K_R) and microscopic (k_T, k_R) dissociation constants for the different enzyme–substrate species present in a two-protomer enzyme are

$$
\begin{aligned}
K_R &= \frac{1}{2}k_R = \frac{[R][S]}{[RS]} & [RS] &= \frac{[R][S]}{K_R} = \frac{2[R][S]}{k_R} \\
K_R &= 2k_R = \frac{[RS][S]}{[RS_2]} & [RS_2] &= \frac{[R][S]^2}{K_R^2} = \frac{[R][S]^2}{k_R^2} \\
K_T &= \frac{1}{2}k_T = \frac{[T][S]}{[TS]} & [TS] &= \frac{[T][S]}{K_T} = \frac{2[T][S]}{k_T} \\
K_T &= 2k_T = \frac{[TS][S]}{[TS_2]} & [TS_2] &= \frac{[T][S]^2}{K_T^2} = \frac{[T][S]^2}{k_T^2}
\end{aligned}
\tag{8.17}
$$

A useful parameter sometimes reported in kinetic studies is the nonexclusive binding coefficient (c). This coefficient is defined as the ratio of the intrinsic enzyme–substrate dissociation constants for the enzyme in the R

and T states:

$$c = \frac{k_R}{k_T} \tag{8.18}$$

A lower value of the nonexclusive binding coefficient is associated with a higher cooperativity, and therefore sigmoidicity, of the velocity curves. A lower value of this coefficient implies a decreased affinity of the T state for substrate relative to the R state. If the enzyme in the T state does not bind substrate ($k_T = \infty$), $c = 0$.

To simplify the mathematical treatment, further assumptions have to be made (see Fig. 8.6):

1. Substrate can only bind to the R state of the protomer; substrate does not bind to the T state of the protomer ($c = 0$).
2. The R state of the protomer is catalytically active and the T state is catalytically inactive.
3. The values of k_R, k_T, and L are the same for all ES_n species.

Thus, the rate equation for the formation of product and the mass balance for the enzyme are given by

$$v = k_{cat}[RS] + 2k_{cat}[RS_2] \tag{8.19}$$

$$[E_T] = [R_0] + [T_0] + [RS] + [RS_2] \tag{8.20}$$

Normalization by total enzyme concentration ($v/[E_T]$), substitution of the different terms containing microscopic dissociation constants, and
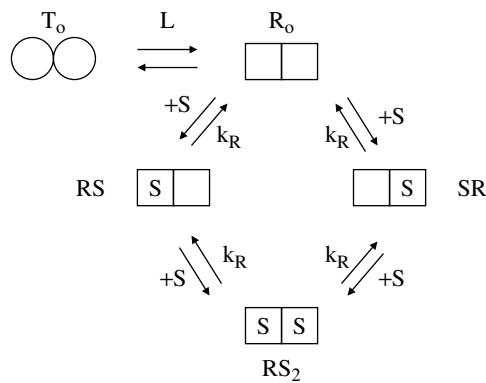
Figure 8.6. Simplified version of the concerted transition model for a two-site cooperative enzyme. In this case the T state of the enzyme is assumed not to bind substrate.

rearrangement results in the following rate equation for a two-protomer allosteric enzyme:

$$\frac{v}{V_{\text{max}}} = \frac{([S]/k_R)(1 + [S]/k_R)}{L + (1 + [S]/k_R)^2} \tag{8.21}$$

where $V_{\text{max}} = 2k_{\text{cat}}[E_T]$. This equation can be generalized for the case of an n-protomer enzyme:

$$\frac{v}{V_{\text{max}}} = \frac{([S]/k_R)(1 + [S]/k_R)^{n-1}}{L + (1 + [S]/k_R)^n} \tag{8.22}$$

where $V_{\text{max}} = nk_{\text{cat}}[E_T]$, n is the number of protomers per enzyme, k_R is the intrinsic enzyme–substrate dissociation constant for the R-state enzyme, and L is the allosteric constant for the $R \rightleftharpoons T$ transition of the native enzyme ($L = [T_0]/[R_0]$).

One could envision how an allosteric effector would alter the balance between the R and T states, thus affecting L. The presence of an activator would lead to a decrease in L, while the presence of an inhibitor would lead to an increase in L. An activator is believed to bind preferentially to, and therefore stabilize, the R state of an enzyme, while an inhibitor is believed to bind preferentially to, and stabilize, the T state of an enzyme. An activator would therefore decrease the sigmoidicity of the v versus [S] curve, while an inhibitor would increase it.

The effect of activators and inhibitors on the value of the conformational equilibrium constant L can be determined from

$$L_{\text{app}} = L \frac{(1 + [I]/k_{TI})^n}{(1 + [A]/k_{RI})^n} \tag{8.23}$$

where L_{app} is the apparent allosteric constant in the presence of both activators and inhibitors, [I] is the concentration of allosteric inhibitor, [A] is the concentration of allosteric activator, k_{TI} is the dissociation constant for the TI complex, k_{RA} is the dissociation constant for the RA complex, and n is the number of protomers per enzyme. For this treatment, it is assumed that activators bind exclusively to the R state of the protomers, while inhibitors bind exclusively to the T state of the protomers. If only activators or inhibitors are present, [I] or [A], correspondingly, would be set to zero. This expression could be included into Eq. (8.23). This

is, however, not recommended, due to the complexity of the resulting equation and its effects on curve-fitting performance.

Simulations of v versus [S] behavior using Eq. (8.22) are shown in Fig. 8.7. Surprisingly, neither n nor L affect the sigmoidicity of the curve. It is only the steepness of the curve that is affected by these parameters. As can be appreciated in Fig. 8.7(a), the curve is very sensitive to the value of n. Small changes in n result in large changes in the observed v versus [S] behavior. As for the Hill model, the greater the value of n, the more pronounced the steepness of the curve. Increases in the value of the allosteric constant L, on the other hand, lead to increases in the steepness of the v versus [S] curve (Fig. 8.7b). Thus, from a topological perspective, the shape of the sigmoidal curve can be described by these two parameters. In the limit where the steepness of the curve is extreme, the sigmoidicity of the curve will not be apparent.
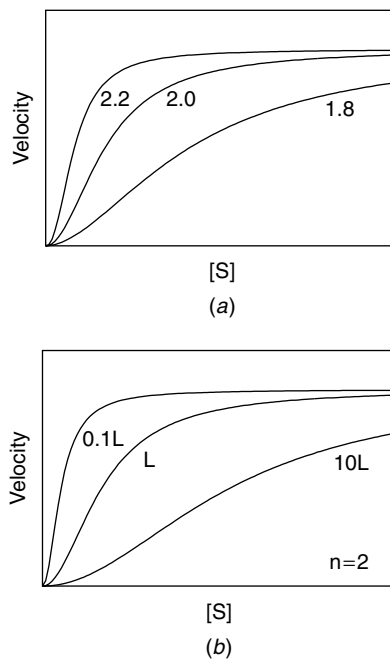
Figure 8.7. (a) Simulation of the effects of varying the effective number of active sites in an enzyme (n) on the shape of the initial velocity versus substrate concentration curve for a cooperative enzyme. (b) Simulation of the effects of varying the allosteric constant (L) on the shape of the initial velocity versus substrate concentration curve for a cooperative enzyme.

8.3   APPLICATION

It is of interest to assess the ability of these two models to describe the v versus [S] behavior of an enzyme. Figure 8.8*a* corresponds to a curve fit using the Hill equation, while Fig. 8.8(*b*) corresponds to a curve fit using the simplified CT model. The absolute sum of squares for the fit of the Hill equation to the data set is 1.38×10^{-17} M^2 min^{-2}, while for the CT model is 1.88×10^{-17} M^2 min^{-2}. In this case, there is no need to carry out an F-test to decide which model fits the data best. Since the Hill equation has fewer parameters and the absolute sum of squares for the fit of the model to the data is lower, one can safely conclude that the Hill equation fits the data statistically better than does the CT model.
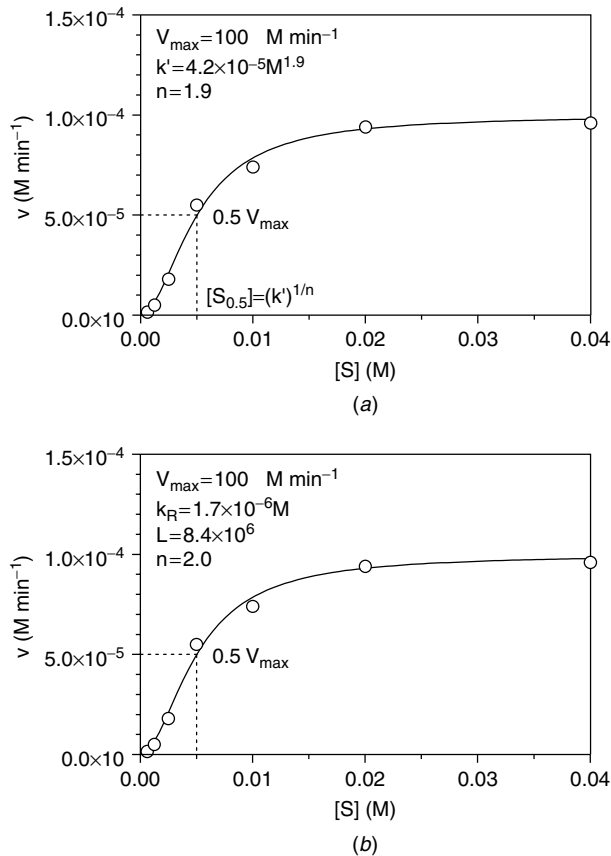
Figure 8.8. Analysis of the initial velocity versus substrate concentration data for a cooperative enzyme using (*a*) the Hill model and (*b*) the MWC model.

An advantage of the CT model, however, is the fact that it is possible to estimate the magnitude of the enzyme–substrate dissociation constant of the enzyme. This is not possible with the Hill equation. As described before, the Hill constant is a complex term that is related but is not equivalent to, the enzyme–substrate dissociation constant. By using the CT model, it is also possible to obtain estimates of the allosteric constant, L. This may prove useful in the study of allosteric modulators of enzyme activity.

8.4   REALITY CHECK

One of the major problems with the use of any of these models, and particularly more complex models of cooperativity and allosterism, is the inability independently to check the accuracy of the estimated catalytic parameters. Even for the simple models discussed above, the experimental determination of these catalytic parameters remains a daunting task. In the absence of independent experimental confirmation, estimates of k', n, k_R, and L are nothing more than parameters obtained from curve fits of an equation to data.

In this simple treatment of cooperativity and allosterism, one should be reluctant to entertain more complex models. It is our belief that an overreductionist approach inevitably leads to the development of extremely complex equations of limited analytical practicality. This is due primarily to both the excessive number of parameters to be estimated simultaneously and the inability ever to be able to check their accuracy independently.

CHAPTER 9

IMMOBILIZED ENZYMES

The catalytic properties of an immobilized enzyme can be characterized using the Michaelis–Menten model. The exact form of the model will depend on the type of enzyme reactor used. In general, whenever non-steady-state conditions prevail, the integrated form of the Michaelis–Menten model is used:

$$K'_m \ln \frac{[S_0]}{[S]} + [S_0 - S] = V_{max}t = k_{cat}[E_T]t \qquad (9.1)$$

where K'_m is the apparent Michaelis constant for the enzyme, $[E_T]$ corresponds to total enzyme concentration, $[S_0]$ and $[S]$ are, respectively, substrate concentration at time zero and time t, k_{cat} is the zero-order rate constant for the enzymatic reaction under conditions of substrate saturation, and t is the reaction time.

The three main types of immobilized enzyme reactors used are batch (Fig. 9.1), plug-flow (Fig. 9.2), and continuous-stirred (Fig. 9.3). In both batch and plug-flow reactors, non-steady-state reaction conditions prevail, while in continuous-stirred reactors, steady-state reaction conditions are prevalent.

9.1 BATCH REACTORS

For the case of a batch reactor, Eq. (9.1) is modified to account explicitly for the volume of the reactor (V_r). To do this, the total
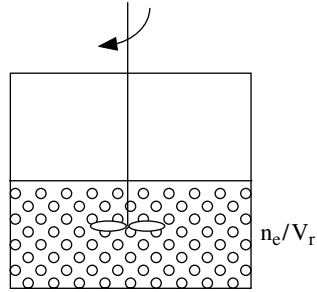
Figure 9.1. Diagrammatic representation of a batch reactor.
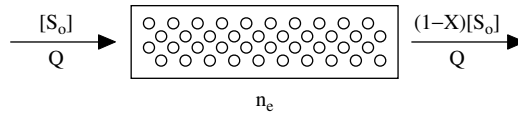
Figure 9.2. Diagrammatic representation of a plug-flow reactor.
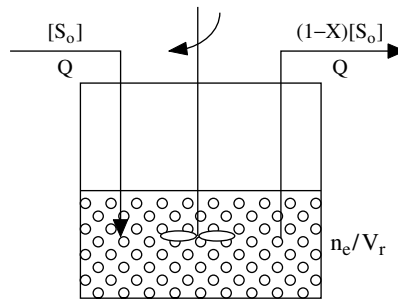
Figure 9.3. Diagrammatic representation of a continuous-stirred reactor.

enzyme concentration term ($[E_T]$) is substituted by n_e/V_r, thus yielding the expression

$$K'_m \ln \frac{[S_0]}{[S]} + [S_0 - S] = \frac{k_{\text{cat}} n_e t}{V_r} \tag{9.2}$$

where n_e corresponds to the moles of enzyme in the reactor ($n_e = [E_T]V_r$). The proportion of substrate that has been converted to product (X) can be defined as

$$X = 1 - \frac{[S]}{[S_0]} \tag{9.3}$$

Thus, considering that $X[S_0] = [S_0 - S]$, Eq. (9.2) can be expressed as

$$X[S_0] - K'_m \ln(1 - X) = \frac{k_{cat} n_e t}{V_r} \tag{9.4}$$

In this model, X is not an explicit function of time. This can represent a problem since most commercially available curve-fitting programs cannot fit implicit functions to experimental data. Thus, to be able to use this implicit function in the determination of k_{cat} and K'_m, it is necessary to modify its form and transform the experimental data accordingly. Dividing both sides by t and K'_m and rearranging results in the expression

$$\frac{\ln(1 - X)}{t} = \frac{X[S_0]}{K'_m t} - \frac{k_{cat} n_e}{K'_m V_r} \tag{9.5}$$

A plot of $\ln(1 - X)/t$ versus X/t yields a straight line with slope $= [S_0]/K'_m$, the x-intercept $= k_{cat} n_e / V_r [S_0]$, and the y-intercept $= -k_{cat} n_e / K'_m V_r$ (Fig. 9.4a). The values of the slope and intercepts can readily be obtained using linear regression. Thus, from a single progress curve (i.e., a single $X-t$ data set) it is possible to obtain estimates of K'_m and k_{cat}.

9.2   PLUG-FLOW REACTORS

For the case of a plug-flow reactor, the quantity V_r/t in Eq. (9.2) can be substituted for by the flow rate (Q) through the packed bed, since $Q = V_r/t$. Equation (9.2) then becomes

$$X[S_0] - K'_m \ln(1 - X) = \frac{k_{cat} n_e}{Q} \tag{9.6}$$

where n_e corresponds to the moles of enzyme in the reactor, $[S_0]$ to substrate concentration in the feed entering the column, and X to the proportion of substrate converted to product in the stream exiting the column.

Dividing both sides by K'_m, multiplying by Q, and rearranging results in the expression

$$Q \ln(1 - X) = \frac{XQ[S_0]}{K'_m} - \frac{k_{cat} n_e}{K'_m} \tag{9.7}$$

A plot of $Q \ln(1 - X)$ versus XQ yields a straight line with slope $= [S_0]/K'_m$, the x-intercept $= k_{cat} n_e / [S_0]$, and the y-intercept $= -k_{cat} n_e / K'_m$
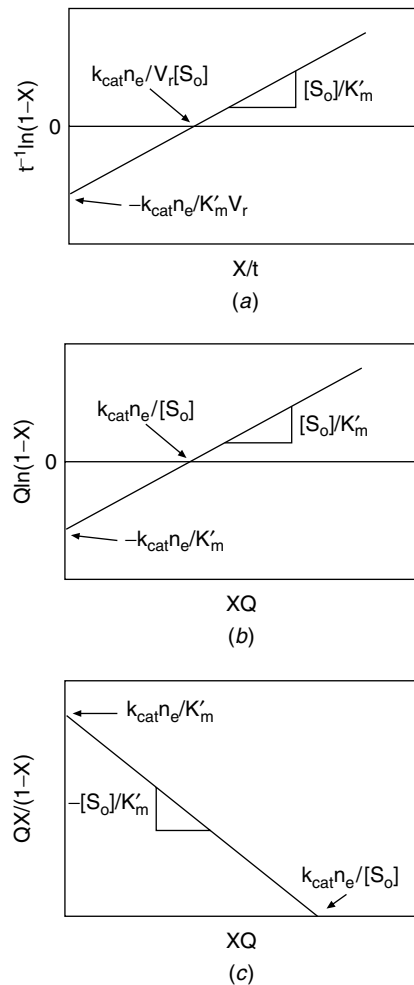
Figure 9.4. Linear plots used in determination of the catalytic parameters of immobilized enzymes for the case of (*a*) batch, (*b*) plug-flow, and (*c*) continuous-stirred reactors.

(Fig. 9.4*b*) Thus, by determining X as a function of different Q, it is possible to obtain estimates of K'_m and k_{cat}.

9.3 CONTINUOUS-STIRRED REACTORS

In a continuous-stirred reactor, steady-state reaction conditions prevail. Therefore, the model used is different from the one used for batch and plug-flow reactors. For the case of a continuous-stirred reactor, the reaction velocity (v) equals the product of the flow rate (Q) through a reactor

of volume V_r times the difference between inflowing and outflowing substrate concentrations, which itself equals the Michaelis–Menten model expression:

$$v = \frac{Q[S_0 - S]}{V_r} = \frac{V_{\max}[S]}{K'_m + [S]}$$ (9.8)

Substitution of $V_{\max}$ with $k_{cat}[E_T]$, $[E_T]$ with n_e/V_r, and rearrangement leads to the expression

$$K'_m \frac{[S_0 - S]}{[S]} + [S_0 - S] = \frac{k_{cat}n_e}{Q}$$ (9.9)

where n_e corresponds to the number of moles of enzyme in the reactor. Dividing numerator and denominator by $[S_0]$ yields

$$K'_m \frac{1 - ([S]/[S_0])}{[S]/[S_0]} + [S_0 - S] = \frac{k_{cat}n_e}{Q}$$ (9.10)

Considering that $X = 1 - [S]/[S_0]$ and $X[S_0] = [S_0 - S]$, Eq. (9.10) can be expressed as

$$X[S_0] + K'_m \frac{X}{1 - X} = \frac{k_{cat}n_e}{Q}$$ (9.11)

Dividing both sides by K'_m, multiplying by Q, and rearranging results in the expression

$$Q\frac{X}{1 - X} = -\frac{XQ[S_0]}{K'_m} + \frac{k_{cat}n_e}{K'_m}$$ (9.12)

A plot of $QX/(1 - X)$ versus XQ yields a straight line with slope $= -[S_0]/K'_m$, the x-intercept $= k_{cat}n_e/[S_0]$, and the y-intercept $= k_{cat}n_e/K'_m$ (Fig. 9.4c). Thus, by determining X as a function of different Q, it is possible to obtain estimates of K'_m and k_{cat}.

CHAPTER 10

INTERFACIAL ENZYMES

Interfacial enzymes act on insoluble substrates. Phospholipases and lipases are two important examples from this group of enzymes. Lipases, for example, hydrolyze the ester bond of triacylglycerols, which are insoluble in aqueous media. During the digestion of lipids, triacylglycerols are emulsified by surfactants such as bile salts, forming large emulsion droplets. Thus, to hydrolyze triacylglycerols, lipases must first bind to the oil droplets. The kinetics of this binding process are described by a rate constant of adsorption and a rate constant of desorption (Fig. 10.1). Upon binding to the interface, the enzyme will usually undergo a structural change and adopt an interfacial conformation (Fig. 10.1). Once bound, the enzyme is effectively sitting on the substrate that it must act on—at the interface between oil and water. The concept of substrate concentration is rather difficult to define in this case. More relevant to the case of interfacial catalysis is the concept of concentration of interfacial area or the amount of interfacial area per unit volume ($[A_s]$). As depicted in Fig. 10.2, for a given amount of substrate, the smaller the substrate droplets, the greater the amount of interfacial area per unit volume. Thus, for a given amount of substrate, an interfacial enzyme would "see" a higher effective substrate concentration in case 1 versus case 2. The use of volumetric substrate concentrations in the treatment of interfacial enzyme kinetics is therefore not recommended. The amount of available interfacial area per unit volume effectively becomes the substrate concentration in this treatment.

In determination of the catalytic parameters of an enzyme-catalyzed interfacial reaction, increasing amounts of substrate are added to a solution
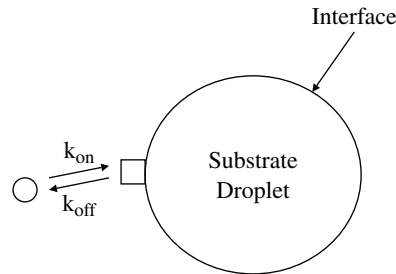
Figure 10.1. Binding of an interfacial enzyme to a substrate interface. Upon binding, the enzyme adopts an interfacial conformation. The kinetics of binding is described by the rate constants of binding (k_{on}) and dissociation (k_{off}).
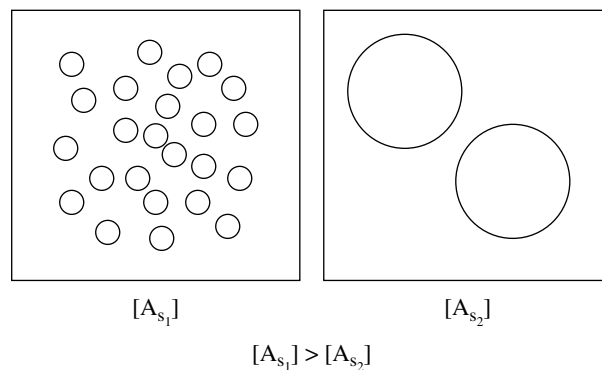
Figure 10.2. Decreases in the amount of interfacial area per unit volume on increases in the size of the globules at a fixed substrate concentration.

containing a fixed amount of enzyme. The velocity of the enzymatic reaction is then determined at each substrate concentration. As before, this velocity versus substrate concentration curve is used in the determination of the apparent catalytic parameters. Increasing substrate concentration refers to the increase in the number of substrate droplets present in the system. This effectively results in an increase in the amount of interfacial area per unit volume, which translates into a higher reaction velocity.

10.1 THE MODEL

10.1.1 Interfacial Binding

In this treatment we consider the binding of an interfacial enzyme to a substrate interface to be accurately described by the Langmuir adsorption

isotherm. Interfacial enzyme coverage is defined as

$$\theta = \frac{(E^*)}{(E^*_{max})} \tag{10.1}$$

where (E^*) represents the amount of interfacial enzyme per unit area (mol m^{-2}), and (E^*_{max}) represents the effective saturation surface concentration of interfacial enzyme (mol m^{-2}).

The change in interfacial enzyme coverage (θ) as a function of time can be expressed as

$$\frac{d\theta}{dt} = k_{on}[E](E^*_{max} - E^*)[A_s] - k_{off}(E^*)[A_s] \tag{10.2}$$

where k_{on} is the rate constant for the adsorption, or binding, of enzyme to the interface, k_{off} is the rate constant for the desorption, or dissociation, of enzyme from the interface, [E] represents the concentration of free enzyme in solution (mol L^{-1}), and [A$_s$] corresponds to the amount of surface area per unit volume in the system (m^2 L^{-1}).

At equilibrium, $d\theta/dt = 0$, and Eq. (10.2) can be rearranged to

$$\theta = \frac{(E^*)}{(E^*_{max})} = \frac{[E]}{K_d^* + [E]} \tag{10.3}$$

where K_d^* is the dissociation constant of the interfacial enzyme:

$$K_d^* = \frac{k_{off}}{k_{on}} = \frac{[E](E^*_{max} - E^*)}{(E^*)} = \frac{[E](1 - \theta)}{\theta} \tag{10.4}$$

10.1.2 Interfacial Catalysis

In this treatment of interfacial catalysis we adopt the following model:

$$E \overset{K_d^*}{\rightleftharpoons} E^* + S \overset{K_s}{\rightleftharpoons} E^* S \overset{k_{cat}}{\rightleftharpoons} E^* + P \tag{10.5}$$
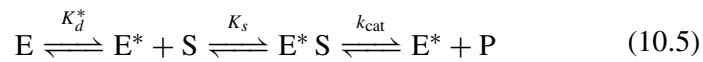
where E corresponds to the free enzyme in solution, E* represents the enzyme bound to the substrate interface, and E*S corresponds to the interfacial enzyme–substrate complex.

In this model it is assumed that the rate-limiting (slow) step in the reaction is still the breakdown of substrate to product. We also treat enzyme interfacial binding as an equilibrium process that can be described by an equilibrium dissociation constant (K_d^*). We also assume that once the

enzyme has partitioned toward the interface, it will rapidly bind substrate. Thus, interfacial binding and substrate binding are grouped as a single step in this treatment. This assumption was made because of difficulties in defining substrate concentration at the interface, since the enzyme is bound to an interface composed of substrate. More appropriate perhaps would be a treatment that considers the extraction of a substrate molecule from the interface to the enzyme's active site. This possibility, however, was not explored further in this treatment. An important consideration in enzyme interfacial catalysis is the loss of activity of the enzyme at the interface. Enzyme inactivation will happen at the interface, both upon initial binding and in time. In this treatment velocity measurements take place in the initial region where time-dependent enzyme inactivation is minimal. For the instantaneous (initial) component of enzyme inactivation, if a constant proportion of enzyme is inactive during measurements of enzyme activity, this will translate into a decrease in the specific activity of the enzyme. This may lead to an underestimation of the values of V_{max} and k_{cat}, without affecting estimates of K_d^*. The effects of this constant amount of inactive enzyme can be factored out by determining (E_{max}^*) properly, as described below.

As discussed previously, the rate equation for the formation of product, the dissociation constants for enzyme–interface and enzyme–substrate complexes, and the enzyme mass balance are, respectively,

$$v = k_{cat}(E^*)[A_s] \tag{10.6}$$

$$K_d^* = \frac{[E](E_{max}^* - E^*)}{E^*} \tag{10.7}$$

$$[E_T] = [E] + (E^*)[A_s] \tag{10.8}$$

Normalization of the rate equation by total enzyme concentration $(v/[E_T])$ and rearrangement results in the following expression for the velocity of a reaction catalyzed by an interfacial enzyme:

$$v = \frac{V_{max}\alpha}{K_d^* + \alpha} \tag{10.9}$$

where $V_{max} = k_{cat}[E_T]$ and

$$\alpha = (E_{max}^*)(1 - \theta)[A_s] \tag{10.10}$$

Thus, a velocity versus "substrate concentration" (α) plot is still a rectangular hyperbola (Fig. 10.3). It is informative to explore the effects of the
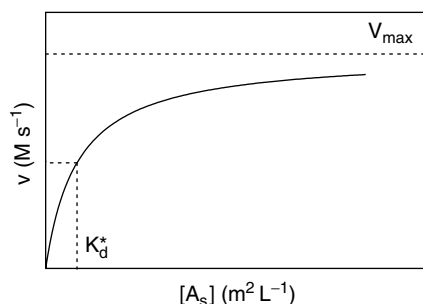
Figure 10.3. Initial velocity versus interfacial area per unit volume plot for an interfacial enzyme.

various parameters in Eq. (10.9) on the velocity of a reaction catalyzed by an interfacial enzyme. As the enzyme–interface dissociation constant increases (i.e., the affinity of the enzyme for the interface decreases) so does the velocity of the reaction (Fig. 10.4a). As the relative amount of interfacial coverage increases, the velocity of the reaction decreases. This is not surprising since if greater amounts of interface are covered by the enzyme, less substrate interface will be available for binding and catalysis (Fig. 10.4b). Finally, as the total number of interfacial binding sites decreases, so does the velocity of the reaction (Fig. 10.4c). Obviously, as the concentration of interface increases, so does the velocity of the reaction. It is important to keep in mind the units of these constants and parameters, shown in Table 10.1.

10.2   DETERMINATION OF INTERFACIAL AREA PER UNIT VOLUME

For kinetic studies of interfacial enzymes, it is necessary to determine the interfacial area of substrate present in the reaction mixture. For this purpose, light-scattering techniques are routinely used in measurement of the radius of emulsion droplets (r_d). Assuming droplet sphericity, it is possible to calculate an equivalent volume from

$$V_d = \tfrac{4}{3}\pi r_d^3 \qquad (10.11)$$

The total number of droplets in the system is obtained by dividing the volume of substrate used in the experiment (V_s) by the volume of an individual droplet:

$$N_p = \frac{V_s}{V_d} \qquad (10.12)$$
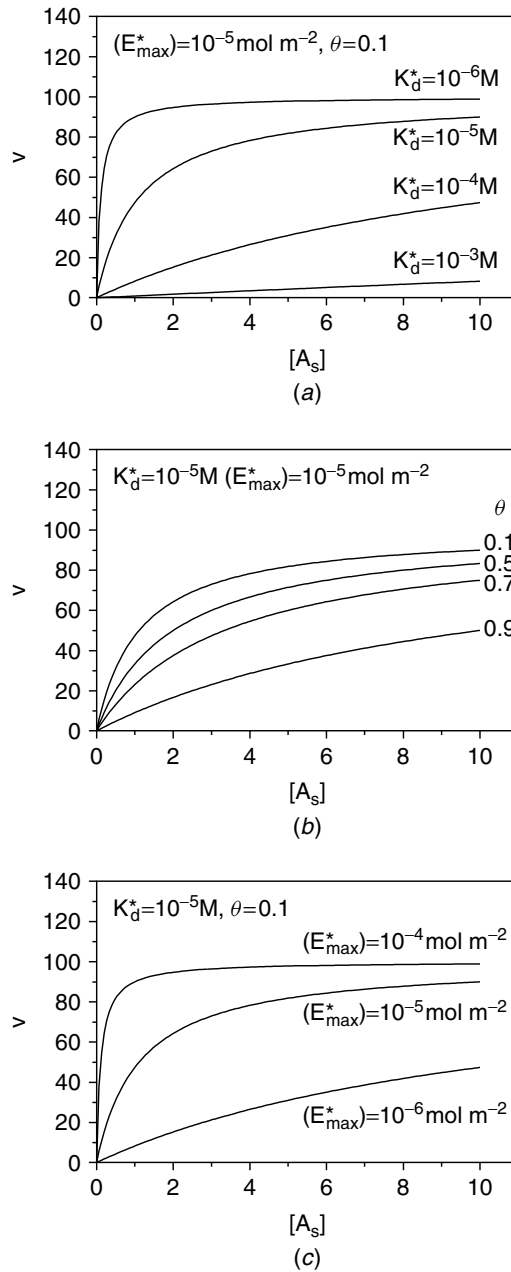
Figure 10.4. Simulations of the effects of changing (*a*) the dissociation constant of the interfacial enzyme (K_d^*), (*b*) interfacial enzyme coverage, and (*c*) effective saturation surface concentration of interfacial enzyme (E_m^*) on initial velocity versus interfacial area per unit volume patterns.

TABLE 10.1   Units for Variables Used in Analysis of the Kinetics of Interfacial Enzymes

Variable	Unit
$[E]$	mol L^{-1}
(E^*)	mol m^{-2}
(E_{max}^*)	mol m^{-2}
$[A_s]$	m^2 L^{-1}
K_d^*	mol L^{-1}
v	mol L^{-1} s^{-1}
V_{max}	mol L^{-1} s^{-1}

The interfacial area of substrate per unit reaction volume ($[A_s]$) can then be determined by dividing the surface area of substrate by the reaction volume (V_r):

$$[A_s] = \frac{4\pi r_d^2 N_p}{V_r} \tag{10.13}$$

10.3   DETERMINATION OF SATURATION INTERFACIAL ENZYME COVERAGE

The amount of enzyme required to saturate the substrate interface can be determined from a velocity versus $[E_T]$ plot at a fixed value of $[A_s]$. As the interface becomes saturated with enzyme, the amount of new enzyme
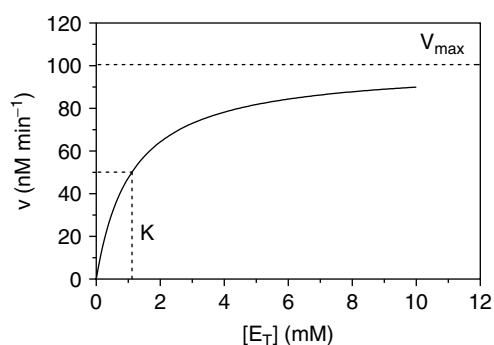
Figure 10.5. Initial velocity versus total enzyme concentration plot used in determination of the effective saturation surface concentration of interfacial enzyme (E_m^*).

able to partition to the interface will progressively decrease relative to the total amount of enzyme present in the system. Since the enzyme catalyzes an interfacial reaction, velocity profiles will follow the same trend (Fig. 10.5). Thus, it is possible to obtain an estimate of $V_{\max}$ by fitting velocity versus $[E_T]$ data to a Langmuir model,

$$\theta = \frac{v}{V_{\max}} = \frac{[E_T]}{K + [E_T]} \qquad (10.14)$$

From the value of $V_{\max}$ (M s^{-1}) obtained and knowledge of the specific activity (μ, mol s^{-1} kg^{-1}) of the enzyme, its molecular weight (MW$_e$, kg mol^{-1}), and the value of $[A_s]$ (m^2 L^{-1}), it is possible to obtain an estimate of $(E^*_{\max})$:

$$(E^*_{\max}) = \frac{V_{\max} \cdot \mathrm{MW}_e}{\mu[A_s]} \qquad (10.15)$$

CHAPTER 11

TRANSIENT PHASES OF ENZYMATIC REACTIONS

Consider a typical mechanism for an enzyme-catalyzed reaction:

$$E + S \underset{k_{-1}}{\overset{k_1}{\rightleftharpoons}} ES \overset{k_2}{\longrightarrow} E + P \tag{11.1}$$

Steady-state kinetic analysis provides estimates of K_m and $V_{\max}$, where

$$K_m = \frac{k_{-1} + k_2}{k_1} \tag{11.2}$$

and

$$V_{\max} = k_2[E_T] \tag{11.3}$$

To determine individual rate constants (i.e., k_1 and k_{-1}) for the mechanism depicted above, it is necessary to monitor the progress of the reaction before establishment of the steady state. This *pre-steady-state* region of an enzymatic reaction is called the *transient phase* of an enzymatic reaction. For this purpose, it is necessary to carry measurements of a single turnover of substrate into product, usually using enzyme concentrations in the range of those of substrate ($[E] \approx [S]$).

Two methods exist for the determination of individual rate constants of an enzymatic reaction: rapid-reaction techniques and relaxation techniques. In *rapid-reaction techniques*, reaction rates are determined after

129

very short times, as low as 2 to 3 ms, before the steady state is established. In *relaxation techniques*, a system at equilibrium is perturbed and the position of equilibrium changes. The movement of the system toward the new equilibrium position is then followed.

11.1   RAPID REACTION TECHNIQUES

Measurement of changes in the concentration of enzyme, substrate, reaction intermediates, and products before the establishment of the steady state can be carried out using continuous-flow and stopped-flow techniques. The experiments are carried out when the observed kinetics are first order. This is usually achieved by making all reactant concentrations, other than the one being monitored, high.

In *continuous-flow techniques*, enzyme and substrate solutions are pumped into a mixing chamber. This mixture flows out of the mixing chamber, into a reaction delay line, and past an observation tube, where the reaction progress is monitored (Fig. 11.1). The time at which measurements are taken is dictated by the volume of the line and the flow rate relative to the position of the observation tube. This method is no longer used since it requires large amounts of enzyme and substrate.

In *stopped-flow techniques*, enzyme and substrate solutions are loaded into syringes. Small amounts of enzyme and substrate ($\sim$40 μL) are
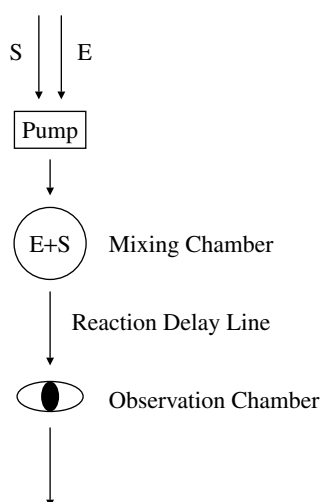
Figure 11.1. Typical continuous-flow setup.

forced from syringes, past a mixing chamber, into an observation chamber, where the reaction is monitored. The enzyme–substrate solution stops at the observation chamber, due to the action of a third syringe. The fluid in this syringe is continuous with the enzyme–substrate solution. The plunger from the third syringe is therefore pushed out as the enzyme–substrate solution is pumped toward the observation chamber. A stopping barrier will halt displacement of the third syringe, thus impeding the flow of the reaction mixture. The system is calibrated in such a fashion that the reaction mixture will stop at the observation chamber. It is important that the mixing and delay times before reaching the observation chamber be very short. The detector, usually a photomultiplier tube connected to a cathode-ray oscilloscope, can measure the intensity of light transmitted through the sample or the intensity of a fluorescence signal from the sample (Fig. 11.2). Sophisticated computer-controlled stepping-motor drives with high-helix-drive screws are used to drive the syringe plungers accurately and precisely to deliver the solutions as quickly as mechanically possible. In the past, compressed air drive systems were used.

In *quick-quench-flow techniques*, enzyme, substrate and quench solutions are loaded into three separate syringes. The reaction is started by pumping enzyme and substrate solutions into a reaction delay line. While traveling down this line, enzyme and substrate react for a defined period of time dictated by the volume of the line and the flow rate. The reaction is then stopped by addition of a quench solution (sodium dodecyl sulfate, acid), pumped from the third syringe. The quenched mixture of enzyme,
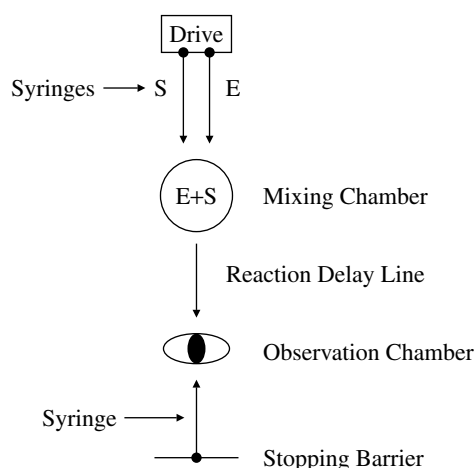
Figure 11.2. Typical stopped-flow setup.
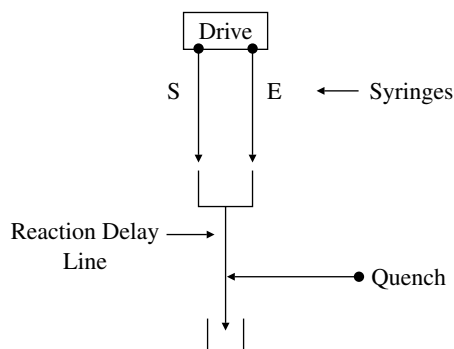
Figure 11.3. Typical quick-quench-flow setup.

substrate, reaction intermediates, and reaction products is then collected and analyzed off-line (Fig. 11.3).

An alternative to the purchase of sophisticated apparatuses for the study of pre-steady-state kinetics of enzymatic reactions is the use of poor substrates, or carrying out the reaction at low temperatures. By using a poor substrate, the pre-steady-state region of the reaction is effectively shifted from a range of milliseconds to one of seconds. Carrying out the enzymatic reaction at low temperatures (e.g., $-50\,^{\circ}\text{C}$) will also slow down the reaction considerably.

From the patterns obtained for changes in enzyme, substrate, enzyme–substrate, and product concentrations in time, it is possible to propose a mechanism by which substrate is converted to product and obtain estimates of the individual rate constants of the reaction. Interest in determining the mechanism by which an enzyme catalyzes the conversion of substrate into product arises from the need for rational design of enzyme inhibitors. Proposing and proving a mechanism is not an easy task. This topic was covered extensively in Chapter 1.

11.2 REACTION MECHANISMS

In this section we consider only the typical enzyme mechanism:

$$\text{E} + \text{S} \underset{k_{-1}}{\overset{k_1}{\rightleftharpoons}} \text{ES} \overset{k_2}{\longrightarrow} \text{E} + \text{P} \tag{11.4}$$

The differential equation and mass balance that describe changes in ES concentration as a function of time are

$$\frac{d[\text{ES}]}{dt} = k_1[\text{E}][\text{S}] - k_{-1}[\text{ES}] - k_2[\text{ES}]$$

$$= k_1[\text{E}][\text{S}] - (k_{-1} + k_2)[\text{ES}] \tag{11.5}$$

$$[\text{E}_T] = [\text{E}] + [\text{ES}] \tag{11.6}$$

Substituting [E] with $[\text{E}_T - \text{ES}]$, and for the condition $[\text{S}_t] \approx [\text{S}_0]$, Eq. (11.5) can be rewritten as

$$\frac{d[\text{ES}]}{dt} = k_1[\text{E}_T - \text{ES}][\text{S}] - (k_{-1} + k_2)[\text{ES}]$$

$$= k_1[\text{E}_T][\text{S}_0] - (k_1[\text{S}_0] + k_{-1} + k_2)[\text{ES}] \tag{11.7}$$

The rate of conversion of ES complex into product is given by

$$v = \frac{d[\text{P}]}{dt} = k_2[\text{ES}] \tag{11.8}$$

Differentiation with respect to time yields

$$\frac{d^2[\text{P}]}{dt^2} = k_2\frac{d[\text{ES}]}{dt} \tag{11.9}$$

Combining the differential Eqs. (11.8) and (11.9) and substituting $d[\text{P}]/dt$ for $k_2[\text{ES}]$ results in the second-order differential equation

$$\frac{d^2[\text{P}]}{dt^2} + \frac{d[\text{P}]}{dt}(k_1[\text{S}_0] + k_{-1} + k_2)k_2[\text{ES}] - k_1k_2[\text{E}_T][\text{S}_0] = 0 \tag{11.10}$$

This differential equation applies to both the pre-steady-state and steady-state stages of the enzymatic reaction. The analytical solution for the case where substrate concentration is essentially unchanged from its initial value $[\text{S}_0]$ is

$$[\text{P}_t] = [\text{P}_0] + \frac{k_2[\text{S}_0][\text{E}_T]t}{[\text{S}_0] + (k_{-1} + k_2)/k_1}$$

$$+ \frac{k_1k_2[\text{S}_0][\text{E}_T]}{(k_1[\text{S}_0] + k_{-1} + k_2)^2}(e^{-(k_1[\text{S}_0]+k_{-1}+k_2)t} - 1) \tag{11.11}$$

where $[\text{P}_0]$ is the initial product concentration. A plot of $([\text{P}_t] - [\text{P}_0])$ versus time is shown in Fig. 11.4. Equation (11.11) has the general form

$$y = y_0 + A \cdot x + B(e^{-C \cdot x} - 1) \tag{11.12}$$
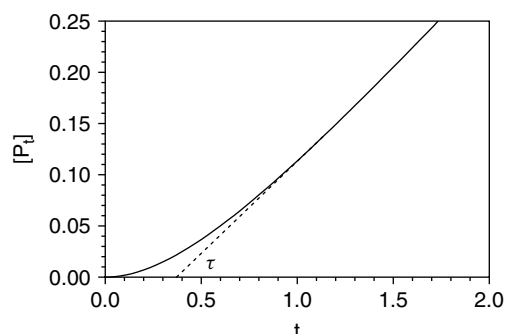
Figure 11.4. Simulation of increases in product concentration as a function of time for a typical enzyme reaction mechanism $E + S \rightleftharpoons ES \rightarrow E + P$. The parameter ϑ is obtained by extrapolating the linearly increasing section of the curve to the time axis.

Thus, this function contains three terms: a constant, a linear term with respect to x, and an exponential term with respect to x. The value of y at $t = 0$ is given by y_0. For small values of x, the exponential term $B(e^{-Cx} - 1)$ predominates, thus leading to a gradual exponential increase in y. For larger values of x, however, the magnitude of linear term Ax becomes greater than that of the exponential term, and the shape of the curve approaches that of a straight line. Valuable information can be gained from analysis of the early and late stages of this reaction.

11.2.1   Early Stages of the Reaction

The exponential term in Eq. [11.11] can be expanded into a series using Taylor's theorem. The contribution from terms beyond the third term in this series is negligible for small values of t and can therefore be neglected. A simplified form of this equation is thus obtained:

$$[P_t] - [P_0] = \frac{\alpha[E_T][S_0]t^2}{2} \tag{11.13}$$

where $\alpha = k_1 k_2$. Nonlinear curve fits of this model to product concentration–time data will yield estimates of α. It is not wise to float individual parameters within α, since estimates of their values will be highly correlated. An estimate of k_2 can be obtained from knowledge of $V_{\max}$ and $[E_T]$, since $k_2 = V_{\max}/[E_T]$. Thus, k_1 can be determined from $k_1 = \alpha/k_2$. The value of k_{-1} can be obtained from knowledge of K_m, k_1, and k_2:

$$k_{-1} = k_1 K_m - k_2 \tag{11.14}$$

11.2.2   Late Stages of the Reaction

As discussed above, the upward curvature during the early stages of the reaction is given by the exponential term in Eq. (11.11). When time is sufficiently long, the exponential term becomes negligibly small, and the curve becomes essentially a straight line. For the case $[S_0] \ggg K_m$, as $t \to \infty$, Eq. (11.11) reduces to:

$$[P_t] - [P_0] = k_2[E_T]t - \frac{k_2[E_T]}{k_1[S_0]} \tag{11.15}$$

A plot of $[P_t - P_0]$ versus time yields a straight line with

$$\text{slope} = k_2[E_T] \tag{11.16}$$

The x-axis intercept of this line, sometimes referred to as the *relaxation time* (τ) (Fig. 11.4), at $[P_t - P_0] = 0$ corresponds to

$$\tau = \frac{1}{k_1[S_0]} \tag{11.17}$$

Thus, from knowledge of the values of the slope, x-intercept, and initial substrate concentration, estimates of k_1 and k_2 and be obtained. An estimate of k_{-1} can be obtained from knowledge of K_m, k_1, and k_2:

$$k_{-1} = k_1 K_m - k_2 \tag{11.18}$$

This exercise is merely one example, among many, of pre-steady-state kinetic analysis of enzyme-catalyzed reactions.

11.3   RELAXATION TECHNIQUES

The time resolution of rapid-flow methods is limited by the rate at which two reactants are mixed, which is restricted to about 1 ms. To measure faster reactions, alternative methods are required. A generally applicable method is the measurement of system adjustment following a relatively small perturbation. A system at equilibrium is perturbed by a sudden temperature or pressure jump, applied as a single rapid change or as a periodic oscillation. Changes in the concentration of reactants and products are subsequently monitored. From the patterns observed, individual rate constants can be obtained.

Consider the opposing reaction:

$$A \underset{k_{-1}}{\overset{k_1}{\rightleftharpoons}} B \qquad (11.19)$$

After a rapid perturbation that causes a small disturbance of the equilibrium state of a reaction, the change in concentration of either species follows a simple exponential pattern. As discussed in Chapter 1, Eq. (1.29) describes changes in the concentration of B:

$$\frac{d[B]}{dt} = k_1[A] - k_{-1}[B] = k_1[A_0 - B] - k_{-1}[B] \qquad (11.20)$$

The deviation of [B] from its equilibrium concentration will be given by $\Delta[B] = [B_{eq}] - [B]$. Changes in the *concentration difference* in species B as it approaches the new equilibrium position, for a small perturbation ($[\Delta B_0] \lll [B]$), is given by

$$-\frac{d[\Delta B]}{dt} = k_1[A_0] - (k_1 + k_{-1})([B_{eq}] - [\Delta B]) \qquad (11.21)$$

At the new equilibrium after the perturbation, $d[B]/dt = 0$, and $k_1([A_0] - [B_{eq}]) = k_{-1}[B_{eq}]$. It follows that

$$\frac{d[\Delta B]}{dt} = -(k_1 + k_{-1})[\Delta B] \qquad (11.22)$$

Integration of this equation using the boundary conditions $[\Delta B] = [\Delta B_0]$ at $t = 0$ yields

$$\ln \frac{[\Delta B]}{[\Delta B_0]} = -(k_1 + k_{-1})t \quad \text{or} \quad [\Delta B] = [\Delta B_0]e^{-(k_1+k_{-1})t} \qquad (11.23)$$

By monitoring the first-order decay of $[\Delta B]$ in time, it is possible to determine $k_1 + k_{-1}$ (Fig. 11.5). From knowledge of K_m and k_2, it is possible to obtain estimates for the individual rate constants. By defining $\alpha = k_1 + k_{-1}$, it is possible to express $k_{-1} = \alpha - k_1$. Substitution of this form of k_{-1} into K_m ($K_m = (k_{-1} + k_2)/k_1$) and rearrangement allows for the calculation of k_1:

$$k_1 = \frac{\alpha + k_2}{1 + K_m} \qquad (11.24)$$

Consider the substrate binding reaction of an enzyme:

$$E + S \underset{k_{-1}}{\overset{k_1}{\rightleftharpoons}} ES \qquad (11.25)$$
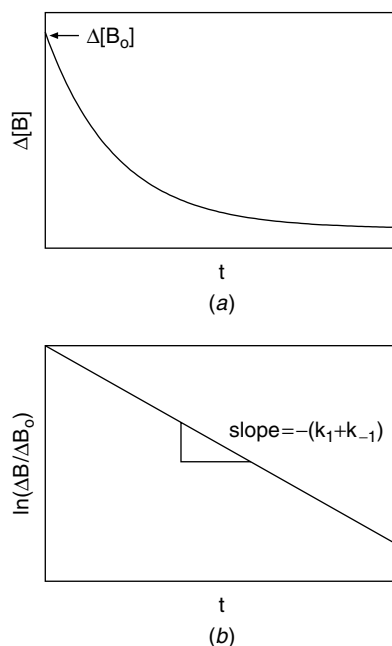
Figure 11.5. (*a*) Decay in the difference between product concentration at time *t* and the equilibrium product concentration ΔB_t, as the system relaxes to a new equilibrium after a small perturbation. (*b*) Semilog arithmic plot used in the determination of individual reaction rate constants for the reaction A $\rightleftharpoons$ B.

The differential equation that describes changes in the concentration of ES in time is

$$\frac{d[\text{ES}]}{dt} = k_1[\text{E}][\text{S}] - k_{-1}[\text{ES}] \tag{11.26}$$

Equations describing the difference in concentration between the initially perturbed and new equilibrium states for enzyme, substrate, and enzyme–substrate complex, respectively, are

$$[\Delta\text{E}] = [\text{E}_{eq}] - [\text{E}] \qquad [\Delta\text{S}] = [\text{S}_{eq}] - [\text{S}]$$
$$[\Delta\text{ES}] = [\text{ES}_{eq}] - [\text{ES}] \tag{11.27}$$

Substituting these expressions into Eq. (11.26) yields

$$\frac{d([\text{ES}_{eq}] - [\Delta\text{ES}])}{dt} = k_1([\text{E}_{eq}] - [\Delta\text{E}])([\text{S}_{eq}] - [\Delta\text{S}])$$
$$- k_{-1}([\text{ES}_{eq}] - [\Delta\text{ES}]) \tag{11.28}$$

At equilibrium, $d[ES]/dt = 0$ and $k_1[E_{eq}][S_{eq}] = k_{-1}[ES_{eq}]$. Substituting $k_{-1}[ES_{eq}]$ for $k_1[E_{eq}][S_{eq}]$ in Eq. (11.28), ignoring the small term $[\Delta E][\Delta S]$, and substituting $-[\Delta ES]$ for both $[\Delta E]$ and $[\Delta S]$, since $[\Delta E] \approx [\Delta S] \approx -[\Delta ES]$, results in the expression

$$\frac{d[\Delta ES]}{dt} = -k_1([E_{eq}] + [S_{eq}])[\Delta ES] - k_{-1}[\Delta ES] \qquad (11.29)$$

Integration of this equation yields

$$\ln \frac{[\Delta ES_0]}{[\Delta ES]} = -(k_1^* + k_{-1})t \quad \text{or} \quad [\Delta B] = [\Delta B_0]e^{-(k_1^* + k_{-1})t} \qquad (11.30)$$

where $k_1^* = k_1([E_{eq}] + [S_{eq}])$.

By monitoring the first-order decay of $[\Delta ES]$ in time, it is possible to determine $k_1^* + k_{-1}$. From knowledge of the equilibrium concentrations of enzyme and substrate and the values for K_m and k_2 from steady-state kinetic analysis, it is possible to obtain estimates of the individual rate constants. By defining $\beta = [E_{eq}] + [S_{eq}]$, and $\alpha = k_1\beta + k_{-1}$, it is possible to express $k_{-1} = \alpha - k_1\beta$. Substitution of this form of k_{-1} into K_m [$(K_m = (k_{-1} + k_2)/k_1$] and rearrangement allows for the calculation of k_1:

$$k_1 = \frac{\alpha + k_2}{\beta + K_m} \qquad (11.31)$$

An estimate of k_{-1} can then be obtained from $k_{-1} = \alpha - k_1\beta$.

TABLE 11.1 Apparent First-Order Rate Constants for the Relaxation of a Thermodynamic System to a New Equilibrium

Reaction	Apparent First-Order Rate Constant (time^{-1})
A $\Longleftrightarrow$ B	$k_1 + k_{-1}$
A + C $\Longleftrightarrow$ B + C	$(k_1 + k_{-1}[C_{eq}])$
2A $\Longleftrightarrow$ A2	$4k_1[A_{eq}] + k_{-1}$
A + B $\Longleftrightarrow$ C	$k_1([A_{eq}] + [B_{eq}]) + k_{-1}$
A + B $\Longleftrightarrow$ C + D	$k_1([A_{eq}] + [B_{eq}]) + k_{-1}([C_{eq}] + [D_{eq}])$
A + B + C $\Longleftrightarrow$ D	$k_1([A_{eq}][B_{eq}] + [A_{eq}][C_{eq}] + [B_{eq}][C_{eq}]) + k_{-1}$

The treatment shown above applies to single-step reactions. The treatment for more complex reaction pathways (e.g., multiple-step reactions) is beyond the scope of this book. Expressions for the apparent rate constants for a number of relaxation reactions are summarized in Table 11.1.

CHAPTER 12

CHARACTERIZATION OF ENZYME STABILITY

In many enzyme-related studies, an index of enzyme stability is required. Enzyme stability can be characterized kinetically or thermodynamically.

12.1 KINETIC TREATMENT

12.1.1 The Model

For the phenomenological kinetic characterization of enzyme stability, the discussion will be restricted to the case where losses in activity, or decreases in concentration of native enzyme, follow a first-order decay pattern in time (Fig. 12.1a). This process can be modeled as

$$N \xrightarrow{k_D} D \tag{12.1}$$

where N represents the native enzyme, D represents the denatured, inactive enzyme, and k_D (time^{-1}) represents the first-order activity decay constant for the enzyme. The first-order ordinary differential equation and enzyme mass balance that characterize this process are

$$\frac{d[N]}{dt} = -k_D[N - N_{min}] \tag{12.2}$$

$$[N_0] = [N] + [N_{min}] \tag{12.3}$$
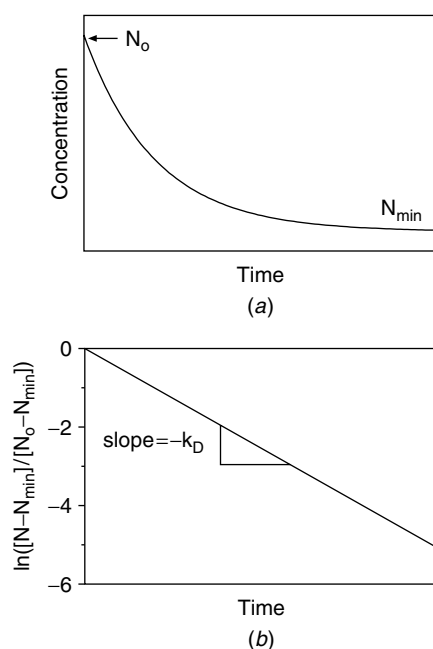
Figure 12.1. (*a*) Decreases in native enzyme concentration, or activity, as a function of time (N → D) from an initial value of N_0 to a minimum value of N_{min}. (*b*) Semilogarithmic plot used in determination of the rate constant of denaturation (k_D).

where [N_{min}] represents the enzyme activity, or native enzyme concentration at $t = \infty$. Integration of this equation for the boundary conditions $N = N_0$ at $t = 0$,

$$\int_{N_0}^{N} \frac{d[N]}{[N - N_{min}]} = -k_D \int_0^t dt \qquad (12.4)$$

results in a first-order exponential decay function which can be expressed in linear or nonlinear forms:

$$\ln \frac{[N - N_{min}]}{[N_0 - N_{min}]} = -k_D\, t \qquad (12.5)$$

or

$$[N] = [N_{min}] + [N_0 - N_{min}]e^{-k_D t} \qquad (12.6)$$

Estimates of the rate constant can be obtained by fitting either of the models above to experimental data using standard linear [Eq. (12.5)] or nonlinear [Eq. (12.6)] regression techniques (Fig. 12.1). A higher rate constant of denaturation would imply a less stable enzyme.

If the amount of denatured enzyme is being monitored as a function of time instead, the first-order ordinary differential equation that characterizes the increase in the concentration of denatured enzyme and enzyme mass balance are

$$\frac{d[D]}{dt} = k_D[N - N_{min}] = k_D[D_{max} - D] \qquad (12.7)$$

$$[N_{min} + D_{max}] = [N + D] = [N_0 + D_0] \qquad (12.8)$$

where D_{max} represents the concentration of denatured enzyme at $t = \infty$. Integration for the boundary conditions $D = D_0$ at $t = 0$,

$$\int_{D_0}^{D} \frac{d[D]}{[D_{max} - D]} = k_D \int_{0}^{t} dt \qquad (12.9)$$

results in a first-order exponential growth function that can be expressed in linear or nonlinear forms:

$$\ln \frac{[D_{max} - D]}{[D_{max} - D_0]} = -k_D t \qquad (12.10)$$

or

$$[D] = [D_{max}] - [D_{max} - D_0]e^{-k_D t} \qquad (12.11)$$

A more familiar form of a first-order exponential growth function can be obtained by subtracting D_0 from both sides of Eq. (12.11), resulting in the expression

$$[D] = [D_0] + [D_{max} - D_0](1 - e^{-k_D t}) \qquad (12.12)$$

Estimates of the rate constant can be obtained by fitting either of the models above to experimental data using standard linear [Eq. (12.10)] or nonlinear [Eq. (12.12)] regression techniques (Fig. 12.2). A higher rate constant of denaturation would imply a less stable enzyme.

12.1.2 Half-Life

A common parameter used in the characterization of enzyme stability is the half-life ($t_{1/2}$). As described in Chapter 1, the reaction half-life for a first-order reaction can be calculated from the rate constant:

$$t_{1/2} = \frac{0.693}{k_D} \qquad (12.13)$$
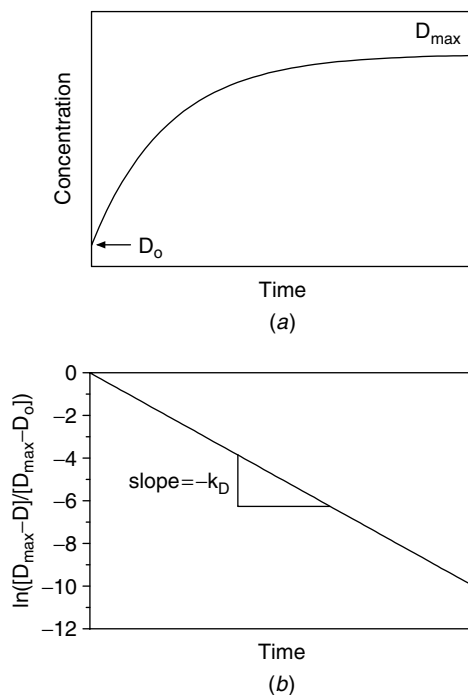
Figure 12.2. (*a*) Increases in denatured enzyme concentration as a function of time $(N \rightarrow D)$ from an initial value of D_0 to a maximum value of D_{max}. (*b*) Semilogarithmic plot used in the determination of the rate constant of denaturation (k_D).

The half-life has units of time and corresponds to the time required for the loss of half of the original enzyme concentration, or activity.

12.1.3 Decimal Reduction Time

A specialized parameter used by certain disciplines in the characterization of enzyme stability is the decimal reduction time, or *D* value. The decimal reduction time of a reaction is the time required for one $\log_{10}$ reduction in the concentration, or activity, of the reacting species (i.e., a 90% reduction in the concentration, or activity, of a reactant). Decimal reduction times can be determined from the slope of $\log_{10}([N_t]/[N_0])$ versus time plots (Fig. 12.3). The modified first-order integrated rate equation has the following form:

$$\log_{10} \frac{[N_t]}{[N_0]} = -\frac{t}{D} \qquad (12.14)$$

or

$$[N_t] = [N_0] \cdot 10^{-t/D} \qquad (12.15)$$
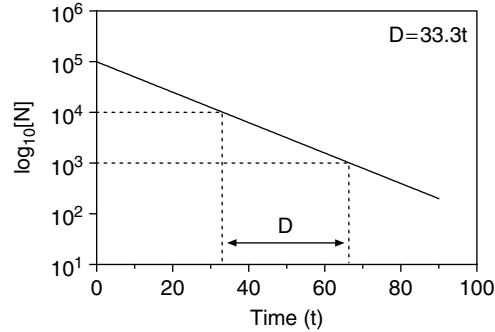
Figure 12.3. Semilogarithmic plot used in the determination of the decimal reduction time (D value) of an enzyme.

The decimal reduction time (D) is related to the first-order rate constant (k_r) in a straightforward fashion:

$$D = \frac{2.303}{k_r} \qquad (12.16)$$

12.1.4   Energy of Activation

If rate constants are obtained at different temperatures, an estimate of the energy of activation for denaturation can also be obtained. This is achieved by fitting the linear or nonlinear forms of the Arrhenius model to experimental data (Fig. 12.4):

$$\ln k_D = \ln A - \frac{E_a}{RT} \qquad (12.17)$$

or

$$k_D = Ae^{-E_a/RT} \qquad (12.18)$$

The frequency factor A (time^{-1}) is a parameter related to the total number of collisions that take place during a chemical reaction, E_a (kJ mol^{-1}) the energy of activation, R (kJ mol^{-1} K^{-1}) the universal gas constant, and T (K) the absolute temperature. From Eq. (12.17) we can deduce that for a constant value of A, a higher E_a translates into a lower k_D. As discussed previously, at a constant A, the higher the value of k_D, the more thermostable the enzyme. Thus, the rate constant of denaturation, k_D, and the energy of activation of denaturation, E_a, are useful parameters in the kinetic characterization of enzyme stability.
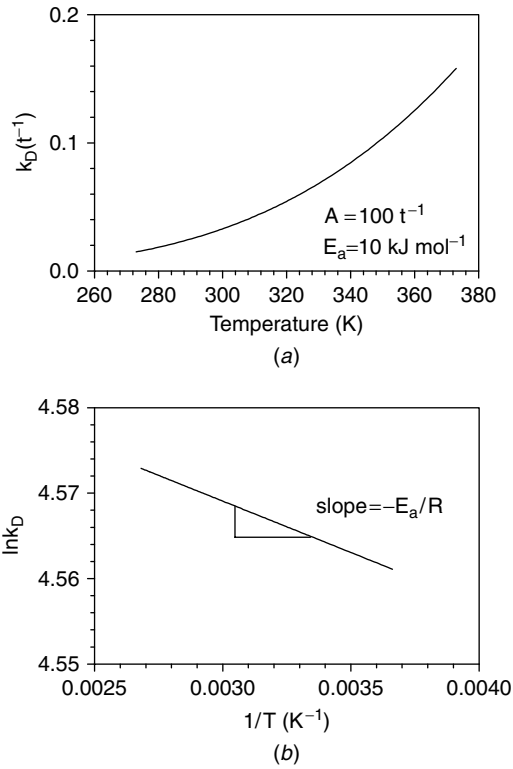
Figure 12.4. (*a*) Simulation of increases in the reaction rate constant of denaturation (k_D) as a function of increasing temperature. (*b*) Arrhenius plot used in the determination of the energy of activation of denaturation (E_a).

12.1.5 *Z* Value

A parameter closely related to the energy of activation is the Z value, the temperature dependence of the decimal reduction time (D). The Z value is the temperature increase required for a one-$\log_{10}$ reduction (90% decrease) in the D value. The Z value can be determined from a plot of $\log_{10} D$ versus temperature (Fig. 12.5). The temperature dependence of the decimal reduction time can be expressed in linear and nonlinear forms:

$$\log_{10} D = \log_{10} C - \frac{T}{Z} \tag{12.19}$$

or

$$D = C \cdot 10^{-T/Z} \tag{12.20}$$
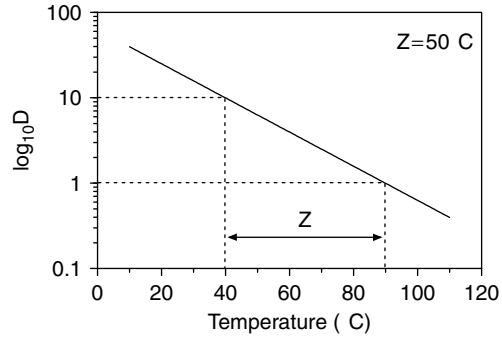
Figure 12.5. Semilogarithmic plot used in determination of the Z value of an enzyme.

where C is a constant related to the frequency factor A in the Arrhenius equation. Alternatively, if D values are known only at two temperatures, the Z value can be determined using the following equation:

$$\log_{10} \frac{D_2}{D_1} = -\frac{T_2 - T_1}{Z} \tag{12.21}$$

It can be shown that the Z value is inversely related to the energy of activation (E_a):

$$Z = \frac{2.303 R T_1 T_2}{E_a} \tag{12.22}$$

where T_1 and T_2 are the two temperatures used in the determination of E_a.

This treatment of enzyme stability is strictly phenomenological in nature and does not necessarily address the true mechanism of denaturation of the enzyme. Any truly mechanistic characterization of a process would be much more complex.

12.2   THERMODYNAMIC TREATMENT

For the thermodynamic characterization of enzyme stability, the denaturation process is also considered a one-step, reversible transition between the native and denatured states:

$$N \underset{}{\overset{K_D}{\rightleftharpoons}} D \tag{12.23}$$

where K_D is the equilibrium constant of denaturation,

$$K_D = \frac{[D]}{[N]} \tag{12.24}$$

For the thermodynamic characterization of enzyme stability, the most critical step is the determination of the equilibrium constant of denaturation. The equilibrium constant can be calculated from knowledge of the relative proportions of native and denatured enzymes at a particular temperature. The equilibrium constant can thus be calculated as

$$K_D = \frac{f_D}{f_N} = \frac{f_D}{1 - f_D} \tag{12.25}$$

where f_D corresponds to the fraction of denatured enzyme and f_N corresponds to the fraction of native enzyme. The calculation of this fractional quantity can be carried out in many ways. For example, consider the case where enzyme activity is being monitored as a function of time at a temperature that leads to activity losses (Fig. 12.6). The fraction of denatured or native enzyme at a particular temperature can be calculated from

$$f_D(T) = \frac{N_0 - N_{min}(T)}{N_0 - N_{lim}} \tag{12.26}$$

$$f_N(T) = \frac{N_{min}(T) - N_{lim}}{N_0 - N_{lim}} \tag{12.27}$$

where N_{lim} corresponds to the limiting, residual enzyme activity after the enzyme has been completely denatured (i.e., the background activity of the preparation). This background activity could be zero. A data set can thus be created for the fraction of denatured enzyme as a function of temperature (Fig. 12.7), from which equilibrium constants can be calculated.

Obviously, the larger the equilibrium constant of denaturation at a particular temperature, the less stable the enzyme. The enthalpy, entropy, and
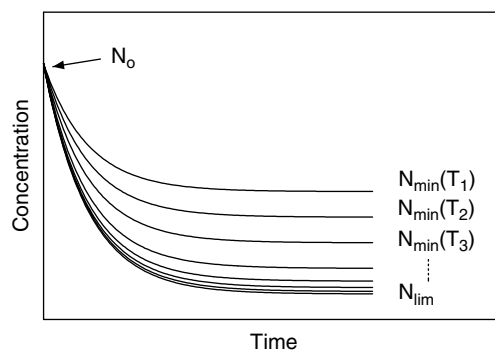
Figure 12.6. Decay in native enzyme concentration, or activity, from an initial value of N_0 to different values of N_{min}. As reaction temperature increases, N_{min} decreases, until reaching a limiting value, N_{lim}.
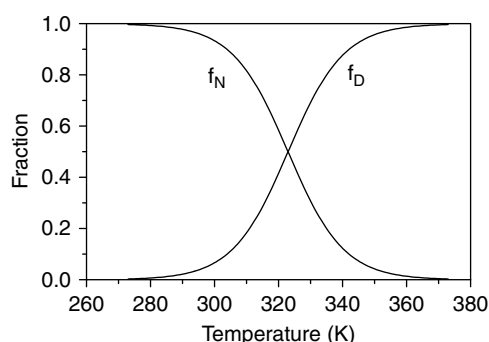
Figure 12.7. Decrease in the fraction of native enzyme (f_N) and increases in the fraction of denatured enzyme (f_D) as a function of increasing temperature.

free energy of denaturation can be calculated directly from the equilibrium constants. A standard-state free energy of denaturation (ΔG_D°) can be calculated from the equilibrium constant (Fig. 12.8):

$$\Delta G_D^\circ = -RT \ln K_D \tag{12.28}$$

The standard-state enthalpy of denaturation (ΔH_D°) can be calculated from the slope of the natural logarithm of the equilibrium constant versus inverse temperature plot (Fig. 12.9*b*) using the van't Hoff equation:

$$\ln K_D = \frac{\Delta S_D^\circ}{R} - \frac{\Delta H_D^\circ}{RT} \tag{12.29}$$
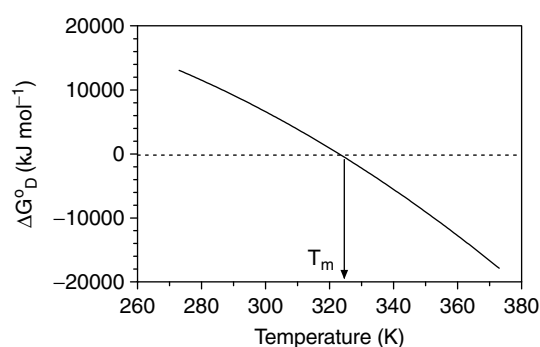
Figure 12.8. Simulation of decreases in the standard state free energy of denaturation (ΔG_D°) as a function of increases in temperature. T_m denotes the denaturation midpoint temperature.
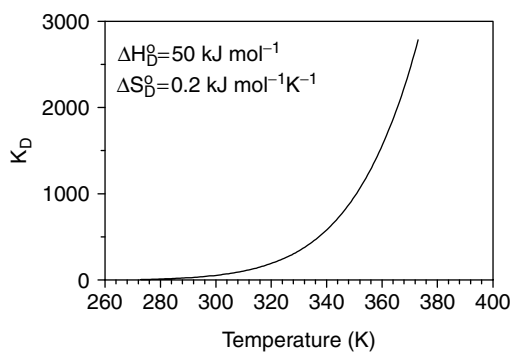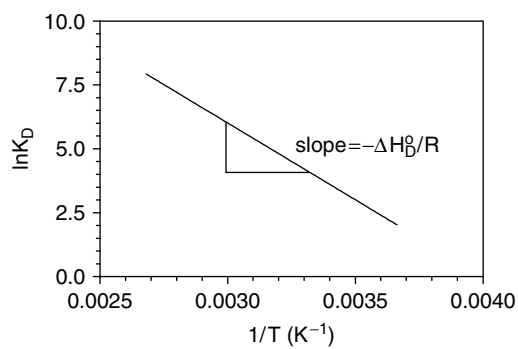
Figure 12.9. (*a*) Simulation of increases in the equilibrium constant of denaturation (k_D) as a function of increases in temperature. (*b*) van't Hoff plot used in the determination of the standard-state enthalpy of denaturation (ΔH_D°).

where ΔS_D° corresponds to the standard-state entropy of denaturation. Inspection of Eq. (12.29) reveals that the standard-state entropy of denaturation can easily be determined from the *y*-intercept of the van't Hoff plot (Fig. 12.9*b*).

The standard-state entropy of denaturation can also be determined easily by realizing that at the transition midpoint temperature (T_m), where $f_D = f_N$, $K_D = 1$, and thus $\ln K_D = 0$, ΔG_D° is equal to zero (Fig. 12.8):

$$\Delta G_D^\circ(T_m) = \Delta H_D^\circ + T_m \, \Delta S_D^\circ = 0 \qquad (12.30)$$

The standard-state entropy of denaturation can therefore be calculated as

$$\Delta S_D^\circ = \frac{\Delta H_D^\circ}{T_m} \qquad (12.31)$$

Alternatively, $\Delta S_{\mathrm{D}}^{\circ}$ could be calculated from knowledge of $\Delta G_{\mathrm{D}}^{\circ}$ at a particular temperature and $\Delta H_{\mathrm{D}}^{\circ}$:

$$\Delta S_{\mathrm{D}}^{\circ} = \frac{\Delta H_{\mathrm{D}}^{\circ} - \Delta G_{\mathrm{D}}^{\circ}(T)}{T} \tag{12.32}$$

The treatment above assumes that there are no differences in heat capacity between native and denatured states of an enzyme and that the heat capacity remains constant throughout the temperature range studied.

The enthalpy of denaturation (J mol^{-1}) is the amount of heat required to denature the enzyme. A large and positive enthalpic term could be associated with a more stable enzyme, since greater amounts of energy are required for the denaturation process to take place. The entropy of denaturation is the amount of energy per degree (J mol^{-1} K^{-1}) involved in the transition from a native to a denatured state. A positive $\Delta S_{\mathrm{D}}^{\circ}$ term is indicative of increases in the disorder, or randomness, of the system (protein–solvent) upon denaturation. A negative $\Delta S_{\mathrm{D}}^{\circ}$ term, on the other hand, is indicative of decreases in the disorder, or randomness, of the system (protein–solvent) upon denaturation. Usually, an increase in the randomness of the system (i.e., a positive $\Delta S_{\mathrm{D}}^{\circ}$ term) is associated with denaturation. Thus, the larger the change in entropy of the system upon denaturation, the less stable the enzyme. The free-energy term, on the other hand, includes the contributions from both enthalpic and entropic terms and is a more reliable indicator of enzyme stability. A smaller, or more negative, standard-state free-energy change is associated with a more spontaneous process. Thus the smaller, or more negative, $\Delta G_{\mathrm{D}}^{\circ}$ term, the more readily the enzyme undergoes denaturation. This could be interpreted as a less stable enzyme.

12.3 EXAMPLE

For the kinetic characterization of enzyme stability, enzyme solutions are incubated at a particular temperature and aliquots removed at the appropriate times. Enzyme activity in these samples is then measured at the enzyme's temperature optimum. This activity is usually determined immediately after the temperature treatment. These data will be used in the kinetic characterization of enzyme activity.

For the thermodynamic characterization of enzyme stability, the minimum enzyme activity has to be determined. Enzyme solutions are incubated at a particular temperature and aliquots removed at the appropriate times. Enzyme activity in these samples is then measured at the enzyme's

EXAMPLE   **151**

temperature optimum. This activity is usually determined immediately after the temperature treatment. Enzyme activity will decrease in time, approaching a minimum value. These minimum activities are then used in the thermodynamic characterization of enzyme stability. An important point to consider is that any thermodynamic treatment implies reversibility. A thermodynamic treatment of enzyme stability inherently implies reversibility of the enzyme inactivation process. That is, enzyme activity must be (fully) recovered in time after exposure to elevated temperatures. This condition must not be met for the case of a kinetic treatment of enzyme stability.

12.3.1   Thermodynamic Characterization of Stability

The activities of two enzymes as a function of temperature are shown in Table 12.1 and Fig. 12.10. In the lower temperature range, increases in temperature lead to increases in the activity of the enzymes, since the rate of a reaction increases with temperature. However, since enzymes are proteins, higher temperatures also lead to protein denaturation. A consequence of these two competing processes is the existence of a temperature optimum. At temperatures below the optimum, an activation of the reaction

TABLE 12.1   Relative Activity of Two Enzymes as a Function of Temperature

Temperature (°C)	Enzyme 1	Enzyme 2
10	25	10
15	37.5	15
20	50	20
25	75	25
30	100	30
35	100	50
40	95	75
45	85	100
50	70	100
55	50	95
60	30	90
65	15	80
70	10	65
75	5	50
80	5	35
90	5	20
100	5	10
105	5	5
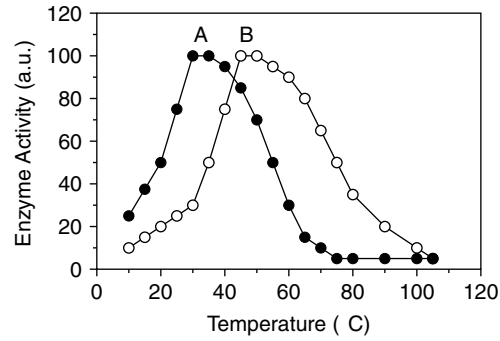
Figure 12.10. Changes in enzyme activity as a function of temperature for two enzymes with differing temperature sensitivities.
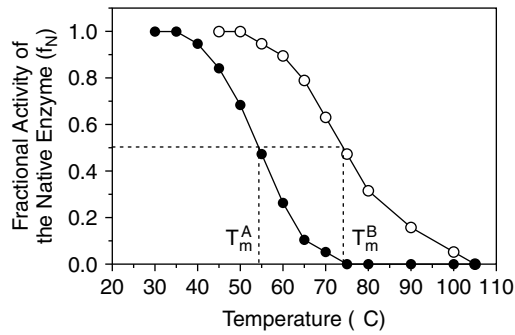
Figure 12.11. Decreases in the fraction of native enzyme as a function of increasing temperature for two enzymes with differing temperature sensitivities.
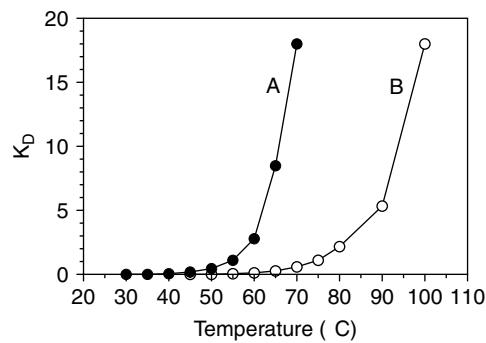
Figure 12.12. Increases in the equilibrium constant of denaturation (k_D) as a function of increases in temperature for two enzymes with differing temperature sensitivities.

EXAMPLE   **153**

takes place, while at temperatures above the optimum, losses in activity due to denaturation are predominant. Thus, a temperature optimum is the point where reaction activation is balanced by the competing process of protein denaturation.

The fractional activity of the native enzymes (f_N) can be calculated from activity data using Eq. (12.27) (Fig. 12.11). The denaturation midpoint temperature (T_m) corresponds to the temperature at which half of the enzyme has lost activity. As can be appreciated in Fig. 12.11, the T_m of enzyme A is lower than that of enzyme B. This could be interpreted as enzyme B being more thermostable than enzyme A.

The equilibrium constant of denaturation (K_D) can easily be calculated from fractional activity data using Eq. (12.25). Changes in K_D as a function of temperature are shown in Fig. 12.12 and the corresponding
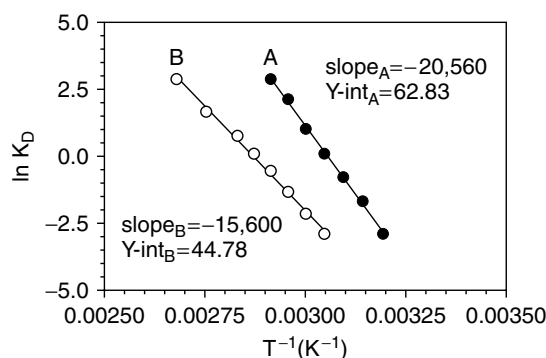
Figure 12.13. van't Hoff plot for two enzymes with differing temperature sensitivities.
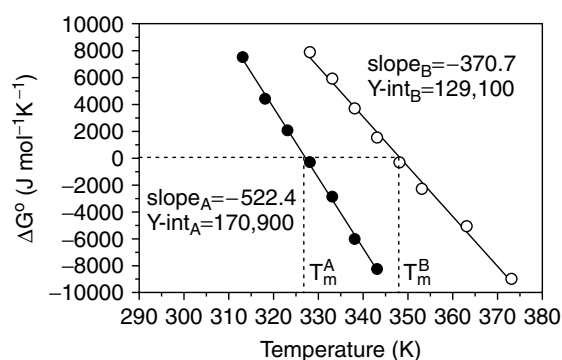
Figure 12.14. Decreases in the standard-state free energy of denaturation (ΔG_D°) as a function of increases in temperature for two enzymes with differing temperature sensitivities.

TABLE 12.2   Changes in the Relative Activity of an Enzyme as a Function of Time at Various Temperatures

Time (min)	Temperature (°C)			
	5	15	25	35
0	1	1	1	1
1	0.88	0.77	0.60	0.36
2	0.77	0.60	0.36	0.13
3	0.68	0.47	0.22	0.05
4	0.60	0.36	0.13	1.80×10^{-2}
5	0.53	0.28	0.08	7.00×10^{-3}
6	0.47	0.22	0.05	2.50×10^{-3}
7	0.41	0.17	3.00×10^{-2}	9.00×10^{-4}
8	0.36	0.13	1.80×10^{-2}	3.30×10^{-4}
9	0.32	0.10	1.10×10^{-2}	1.23×10^{-4}
10	0.28	0.08	7.00×10^{-3}	4.50×10^{-5}
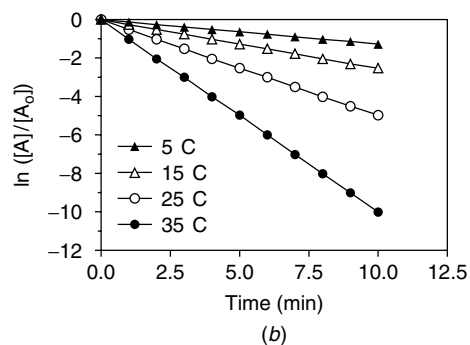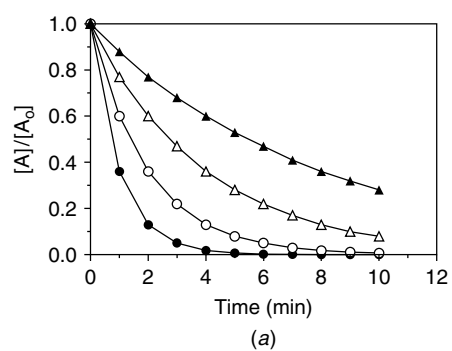
Figure 12.15. (*a*) Decreases in enzyme activity as a function of time at four different temperatures. (*b*) Semilogarithmic plot used in the determination of the rate constant of denaturation of an enzyme at different temperatures.

EXAMPLE **155**
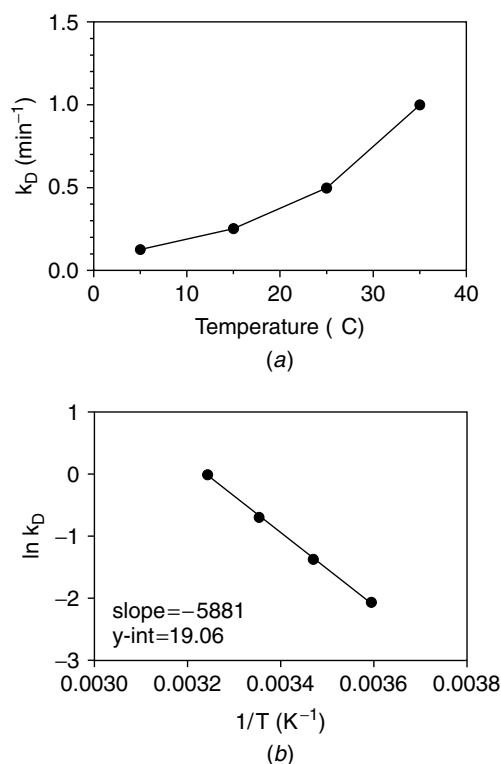
Figure 12.16. (*a*) Increases in the rate constant of denaturation (k_D) of an enzyme as a function of increasing temperature. (*b*) Arrhenius plot used in determination of the energy of activation (E_a) of denaturation for the enzyme.

van't Hoff plot in Fig. 12.13. The slope of the van't Hoff plot corresponds to—$\Delta H_D^\circ/R$, while the *y*-intercept corresponds to $\Delta S_D^\circ/R$. From this plot we can calculate values for the standard state enthalpy and entropy of denaturation: $\Delta H_D^\circ(A) = 171$ kJ mol^{-1}, $\Delta H_D^\circ(B) = 130$ kJ mol^{-1}, ΔS_D° (A) = 522 J mol^{-1} K^{-1}, and $\Delta S_D^\circ(B) = 372$ J mol^{-1} K^{-1}. Interestingly, based solely on enthalpic considerations, one would predict that enzyme A is more thermostable than enzyme B, since higher ΔH_D° values suggest that more energy is required for enzyme denaturation to take place. However, based on entropic considerations, one would predict that enzyme B is more thermostable than enzyme A, since enzyme A has the highest ΔS_D°. The free energy of denaturation (ΔG_D°) includes both enthalpic and entropic contributions and is thus a more accurate and reliable predictor of enzyme stability. Figure 12.14 shows the temperature dependence of ΔG_D° for the two enzymes. At every temperature, the ΔG_D° of enzyme B

is higher than that of enzyme A. As described previously, a higher $\Delta G_{\mathrm{D}}^{\circ}$ value is associated with a more stable enzyme. Thus, based on free-energy considerations, one would predict that enzyme B is more thermostable than enzyme A.

12.3.2 Kinetic Characterization of Stability

Decreases in the activity of an enzyme as a function of time, at different temperatures, are shown in Table 12.2 and Fig. 12.15*a*. Assuming that enzyme inactivation can be modeled as a first-order process, data can be linearized using Eq. (12.5) (Fig. 12.15*b*). The slopes of the lines in Fig. 12.14*b* correspond to the first-order rate constant of denaturation (k_D). As the temperature increases, so does the rate of inactivation, which is mirrored in increases in k_D (Fig. 12.16*a*). The Arrhenius model can then be used to determine the energy of activation (E_a) of denaturation and estimate the value of the frequency factor, $E_a = 48, 9$ kJ mol^{-1} and
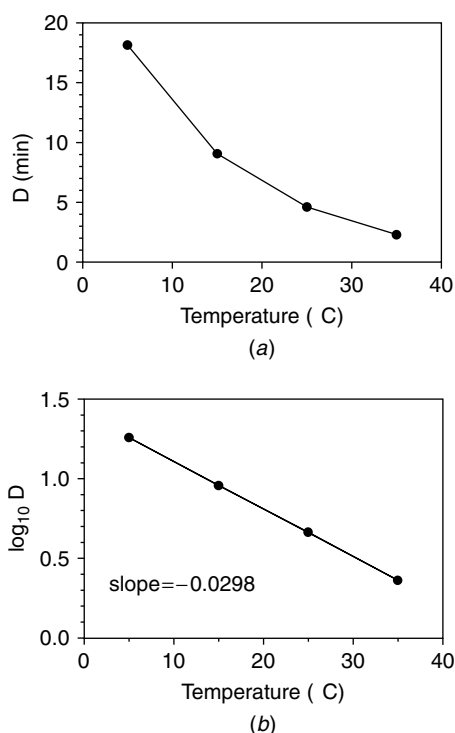
Figure 12.17. (*a*) Decreases in the decimal reduction time (*D* value) as a function of increasing temperature. (*b*) Semilogarithmic plot used in determination of the *Z* value.

EXAMPLE **157**

$A = 1.9 \times 10^8$ min^{-1} (Fig. 12.16*b*). As discussed previously, the decimal reduction time (D) is merely the inverse of the first-order reaction rate constant. From knowledge of the temperature dependence of the D value of an enzyme (Fig. 12.17*a*), the Z value can easily be determined: $Z = 33.5\,^{\circ}$C (Fig. 12.17*b*).

CHAPTER 13

MECHANISM-BASED INHIBITION

LESLIE J. COPP*

In this chapter, mechanism-based inhibition is discussed in its broadest sense, where an inhibitor is converted by the enzyme catalytic mechanism to form an enzyme–inhibitor complex. Other terms used in the literature for mechanism-based inhibitors include *suicide inhibitors, suicide substrate inhibitors, alternate substrates, substrate inhibitors*, and *enzyme inactivators*, as well as *irreversible, catalytic*, or k_{cat} *inhibitors*. The terms *alternate substrate inhibition* and *suicide inhibition* are used here to describe the two major subclasses of mechanism-based inhibition.

Alternate substrates are processed by an enzyme's normal catalytic pathway to form a stable covalent enzyme–inhibitor intermediate, such as an acyl-enzyme in the case of serine proteases, where the complex is essentially trapped in a potential energy well. As such, the inhibition is both time dependent and active-site directed. Theoretically, alternate substrates are reversible inhibitors, since the enzyme is essentially unchanged; rather, it is suspended at a point within the catalytic process. However, in practical terms, the enzyme–inhibitor complex can be of such stability as to render the inhibition virtually irreversible.

Suicide inhibitors are also processed by an enzyme's catalytic mechanism, but in this case, enzyme catalysis of the relatively unreactive inhibitor uncovers a latent reactive moiety. This intermediate then reacts

* Department of Food Science, University of Guelph, Guelph, Ontario, Canada N1G 2W1.

to make a covalent linkage with the enzyme, such as an alkylation of an active site residue, which is not part of normal catalysis. These inhibitors are time dependent, active site specific, and irreversible in their action. It is possible for suicide inhibitors to have an alternate substrate mode of action as well.

The lure of mechanism-based inhibition for pharmaceutical, food and other industries is the prospect of target specificity and long-lasting effects. A simple competitive enzyme inhibitor would have to be maintained at saturating conditions to provide adequate inhibition of a target enzyme. It would need to be replaced as it was metabolized, consumed, or flushed out of the system, be it a human body or an industrial process. In contrast, once a mechanism-based inhibitor interacts with an enzyme, the enzyme is essentially removed from the system. In this case more inhibitor isn't needed until the enzyme is resynthesized or replaced. Given enough time, adequate stability and bioavailability, potent mechanism-based inhibitors should be effective at low concentrations. In practice, of course, time limitations, compound stability, and bioavailability are major hurdles to overcome. In the case of drug development of an enzyme inhibitor, compounds should be orally active, yet not susceptible to general protein binding, and potent enough in the presence of natural (often protein) substrates. Compounds must be stable to metabolism, such as hydrolysis or loss of chirality. A further challenge is providing sufficient selectivity or specificity for an enzyme. Often, whatever mechanism is invoked in suicide or alternate substrate inhibition can work across an entire class of enzymes, such as serine or cysteine proteases. While the inhibitor must act as a substrate, presenting a scissile bond to the active-site residues, many inhibitors featured in the literature show little resemblance to natural substrates. However, known enzyme specificity can be used to enhance inhibitor specificity. For example, different amino acid derivatives of an inhibitor could be synthesized to take advantage of the primary subsite specificity of related enzymes, such as valine and phenylalanine derivatives for the serine proteases human leukocyte elastase and α-chymotrypsin, respectively (Groutas et al., 1998).

13.1 ALTERNATE SUBSTRATE INHIBITION

An alternate substrate inhibitor produces a stable intermediate during the normal course of catalysis, tying up the enzyme in its E−I form. Although there can be many steps during the process, and more than one product may be formed, Scheme 13.1 shows the essential steps of the mechanism of inhibition. To fully characterize alternate substrate inhibition, the

$$E + I \underset{k_{-1}}{\overset{k_1}{\rightleftharpoons}} E - I \xrightarrow{k_2} E + X$$

Scheme 13.1

various kinetic constants should be determined, the reaction products identified, and the nature of the inhibition confirmed. If the inhibition is not competitive in nature, it does not require the catalytic mechanism and cannot be alternate substrate inhibition.

The on rate, k_{on}, is equivalent to k_1, and the off rate, k_{off}, is equivalent to the sum of all pathways of E–I breakdown, in this case, $k_{-1} + k_2$. It is possible that multiple products are formed, and the rates of formation of these should be included in the k_{off} term. A progress curve or continuous assay is the best way to determine the k_{on} and K_i of an alternate substrate. Addition of an alternate substrate inhibitor to an enzyme assay results in an exponential decrease in rate to some final steady-state turnover of substrate (Fig. 13.1). In an individual assay, both the rate of inhibition (k_{obs}) and the final steady-state rate (C) will depend on the concentration of inhibitor. Care must be taken to have a sufficient excess of inhibitor over enzyme concentration present, since the inhibitor is consumed during the process. Where possible, working at assay conditions well below the K_m of the assay substrate simplifies the kinetics, as the substrate will not interfere in the inhibition. If the
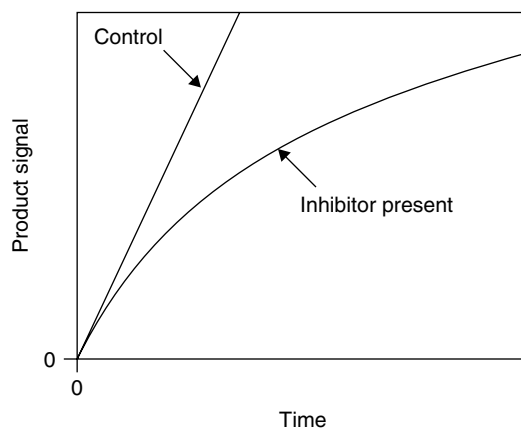
Figure 13.1. Rate of product formation from an enzymatic reaction with substrate in the presence of an alternate substrate inhibitor, showing an exponential decrease in rate to some final steady-state inhibited rate, compared to a control rate in the absence of inhibitor.

rate of inhibition is too fast to be determined in this fashion, saturating or near-saturating concentrations of assay substrate will act as competition for the inhibition reaction and slow the observed rates. The inhibition data are fitted to the following equation for a series of inhibitor concentrations:

$$Y = Ae^{-k_{obs}t} + Ct + B \quad \text{or} \quad Y = A(1 - e^{-k_{obs}t}) + Ct + B \quad (13.1)$$

where Y is the assay product, A and B are constants, C is the final steady-state rate, and k_{obs} is the rate of inhibition.

The second-order rate constant k_{on} is the slope of a plot of k_{obs} versus [I] for inhibitor at nonsaturating concentrations, where $[S] \ll K_m$:

$$k_{obs} = k_{on}[I] \quad (13.2)$$

where k_{obs} is the rate of inhibition. The second-order rate constant k_{on} is equivalent to k_i/K_i when inhibitor is present at saturating concentrations, when the assay substrate is present at concentrations well below its K_m. K_i and the maximum rate of inhibition k_i can also be determined using the equation

$$k_{obs} = \frac{k_i[I]}{K_i + [I]} \quad (13.3)$$

where k_i is the maximum rate of inhibition and K_i is the dissociation constant for inhibition.

If the enzyme assays are run at substrate concentrations near or greater than the K_m, the on rate must be corrected for the effect of substrate:

$$k_{obs} = \frac{k_{on}[I]}{1 + [S]/K_m} \quad (13.4)$$

where k_{obs} is the rate of inhibition and K_m is the dissociation constant for the enzyme and substrate. If a time-point assay is used, with dilution of a mixture of enzyme and alternate substrate inhibitor into the assay mixture at various time points, the k_{obs} for each assay can be determined as the negative slope of a plot of $\ln(v_t/v_0)$ versus time. However, in this type of assay, the off rate can interfere with the calculation, as the enzyme–inhibitor complex will degrade to produce free enzyme in the absence of more inhibitor.

The final steady-state rates C, from Eq. (13.1), are used for calculation of the alternate substrate's K_i via the standard competitive inhibition equation (Chapter 4). The K_i is also equivalent to the ratio of the rates

of breakdown of the enzyme–intermediate complex to the rates of formation of the enzyme–intermediate complex, as seen below. The standard steady-state assumption used in enzyme kinetics,

$$0 = \frac{\partial (\text{EI})}{\partial t} = k_1(\text{E})(\text{I}) - k_{-1}(\text{EI}) - k_2(\text{EI}) \qquad (13.5)$$

can be rearranged to obtain the dissociation constant K_i:

$$K_i = \frac{(\text{E})(\text{I})}{(\text{EI})} = \frac{k_{-1} + k_2}{k_1} = \frac{k_{\text{off}}}{k_{\text{on}}} \qquad (13.6)$$

where K_i is the dissociation constant for inhibition, k_{-1} the rate of dissociation, k_1 the rate of acylation, and k_2 the rate of product formation.

The off rate, k_{off}, of the inhibition can be determined by calculation using Eq. (13.6) or by direct measurement. Enzyme–inhibitor complex can be isolated from excess inhibitor by size exclusion chromatography, preferably with a shift in pH to a range where the enzyme is stable but inactive, to stabilize the complex (Copp et al., 1987). It can then be added back to an activity assay, to measure the return of enzyme activity over time. The recovery of enzyme activity, k_{off}, should be a first-order process, independent of inhibitor, enzyme, or E–I concentrations. The final rate, C, will depend on [E–I] (and any free E that might have been carried through the chromatography).

$$Y = Ae^{-k_{\text{off}} t} + Ct \qquad (13.7)$$

where Y is the assay product, A is a constant, C is the final steady-state rate, and k_{off} is the rate of reactivation. Proof that the inhibition by alternate substrates is active-site directed is provided by a decrease in the rate of enzyme inhibition in the presence of a known competitive inhibitor or substrate.

The process of identifying the products of the interaction between the enzyme and alternate substrate depends a great deal on the inhibitor itself. If the compound contains a chromophore or fluorophore, changes in the absorbance or fluorescence spectra with the addition of enzyme can be monitored and used to identify products (Krantz et al., 1990). For multiple product reactions, single turnover experiments can be used to determine relative product distribution. Stoichiometric quantities of enzyme and inhibitor can be incubated for full inhibition, followed by the addition of a rapid irreversible inhibitor of the enzyme, such as an affinity label. This will act as a trap for enzyme as the enzyme–inhibitor complex breaks down. Analysis of the products will determine relative

rates of k_{-1}, k_2, and rates of formation of any other product (Krantz et al., 1990).

13.2 SUICIDE INHIBITION

A suicide inhibitor is a relatively chemically stable molecule with latent reactivity such that when it undergoes enzyme catalysis, a highly reactive, generally electrophilic species is produced (I^*). As shown in Scheme 13.2, this species then reacts with the enzyme/coenzyme in a second step that is not part of normal catalysis, to form a covalent bond between I^* and E, to give the inactive $E\diamond X$. For a compound to be an ideal suicide inhibitor, it should be very specific for the target enzyme. The inhibitor should be stable under biological conditions and in the presence of various biologically active compounds and proteins. The enzyme-generated species I^* should be sufficiently reactive to be trapped by an amino acid side chain, or coenzyme, at the active site of the enzyme and not be released from the enzyme to solution. These characteristics minimize the "decorating" of various nontarget biological compounds with the reactive I^*. These nontargeted reactions result in a decrease of available inhibitor concentration and can have deleterious effects on other biological reactions and interactions within a system.

To identify a compound as a suicide inhibitor, the inhibition must be established as time dependent, irreversible, active-site directed, requiring catalytic conversion of inhibitor, and have $1:1$ stoichiometry for E and X in the $E\diamond X$ complex. To assess the potency and efficacy of a suicide inhibitor, the kinetics of the inactivation and the partition ratio should be determined. Identification of both X and the amino acid/cofactor labeled in the $E\diamond X$ complex is useful in establishing the actual mechanism of inactivation.

As with alternate substrate inhibitors, a progress curve or continuous enzyme assay is the most useful to begin to characterize the kinetics of inhibition. There can be immediate, or diffusion-limited inhibition of the

$$E + I \underset{k_{-1}}{\overset{k_1}{\rightleftharpoons}} E - I \xrightarrow{k_2} E - I^* \xrightarrow{k_4} E = X$$
$$\downarrow k_3$$
$$E + P$$
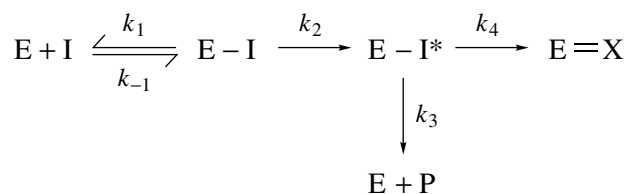
Scheme 13.2

enzyme, before the time-dependent phase of inhibition begins. This may represent inhibition by the noncovalent Michaelis complex, which is then followed by the time-dependent phase of the catalysis of the alternate substrate. The initial rates of inhibition are analyzed as for any competitive substrate (see Chapter 4). In general, addition of a suicide inhibitor to an enzyme assay will result in a time-dependent, exponential decrease to complete inactivation of the enzyme. The reactions do not always follow first-order kinetics. If [I] decreases significantly throughout the progress of the assay, due either to compound instability or enzyme consumption, rates will deviate from first-order behavior and incomplete inhibition may be observed. Also, biphasic kinetics have been observed when two inactivation reactions occur simultaneously, as can happen with racemic mixtures of inhibitors. However, using the more general case, the data can be fit to a simple exponential equation:

$$Y = Ae^{-k_{obs}t} + B \tag{13.8}$$

where Y is the assay product, A and B are constants, and k_{obs} is the rate of inhibition.

Because continuous assays monitor only free enzyme, they do not distinguish between E·I, E—I, or the $E\overset{\wedge}{\underset{\vee}{}}X$ complex. Therefore, k_{obs} represents the apparent inactivation rate, a combination of inhibition and inactivation. As with alternate substrate inhibition, the second-order apparent inactivation rate can be determined from one of the following equations, depending on whether or not saturation kinetics are observed and the concentration of substrate:

$$k_{obs} = k_{inact}^{app}[I] \tag{13.9}$$

where k_{obs} is the rate of inhibition and k_{inact}^{app} is the apparent inactivation rate when no saturation is observed and $[S] \ll K_m$;

$$k_{obs} = \frac{k_{inact}^{app}[I]}{K_{inact}^{app} + [I]} \tag{13.10}$$

where k_{obs} is the rate of inhibition, k_{inact}^{app} is the apparent inactivation rate, and K_{inact}^{app} is the apparent dissociation constant of inactivation when $[S] \ll K_m$; or

$$k_{obs} = \frac{k_{inact}^{app}[I]}{1 + [S]/K_m} \tag{13.11}$$

where k_{obs} is the rate of inhibition, k_{inact}^{app} is the apparent inactivation rate, and K_m is the dissociation constant of the enzyme with substrate.

Incubation/dilution assays or rescue assays can help distinguish between the reversible and irreversible steps in the inactivation. In incubation/dilution assays, enzyme and inhibitor are incubated in the absence of substrate under assay conditions. At various time points, Δt, an aliquot of this incubation is diluted into an assay mixture containing substrate, and the activity monitored. A *rescue assay* is a standard progress assay in which the inhibitor is removed in situ, at various time points, Δt, by the addition of a chemical nucleophile, which consumes free inhibitor (Fig. 13.2). In both cases, either by dilution or by chemical modification, the free inhibitor is effectively removed from the reaction. Any time-dependent recovery of activity should represent k_3, as shown in Fig. 13.2 (although in the rescue assay, the rate of disappearance of the inhibitor will also effect enzyme recovery). Any decrease in the final steady-state rate of activity as compared to the initial enzyme activity is due to inactivated enzyme, $E_{\vee}^{\wedge}X$.

$$\frac{v_f}{v_0} \propto \frac{[E_0] - [EX]}{[E_0]} \tag{13.12}$$

By varying Δt for each inhibitor concentration, k_{obs} for each assay can be determined as the negative slope of $\ln(v_t/v_0)$ versus Δt. Repeating this for a series of [I] and using Eq. (13.2), (13.3), or (13.4), depending on whether or not the system is saturating in inhibitor or substrate, the actual
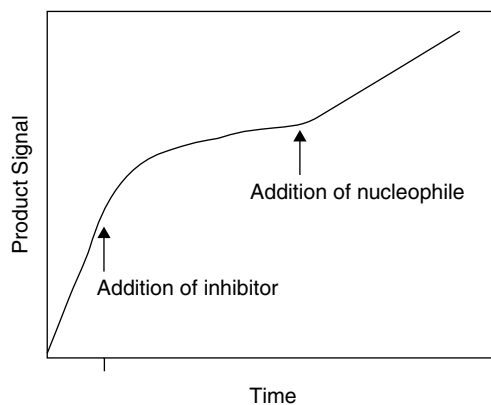
Figure 13.2. Rescue assay. The initial straight line shows product formation by enzyme in the absence of inhibitor. An exponential decrease in rate follows addition of the suicide substrate. Upon addition of the nucleophile at time t, which consumes all excess inhibitor, a partial recovery of enzyme activity is observed. The final enzymatic rate is dependent on [I] and t.

inactivation kinetics can be determined:

$$k_{obs} = k_{inact}[I] \tag{13.13}$$

where k_{obs} is the rate of inhibition and k_{inact} is the inactivation rate;

$$k_{obs} = \frac{k_{inact}[I]}{K_{inact} + [I]} \tag{13.14}$$

where k_{obs} is the rate of inhibition, k_{inact} is the inactivation rate, and K_{inact} is the dissociation constant of inactivation; or

$$k_{obs} = \frac{k_{inact}[I]}{1 + [S]/K_m} \tag{13.15}$$

where k_{obs} is the rate of inhibition, k_{inact} is the inactivation rate, and K_m is the dissociation constant of the enzyme with substrate. If the inactivation kinetics, as described above, are the same as the apparent inactivation kinetics observed from the standard progress curves, it implies that k_2 is the rate-limiting step (i.e., $k_2 \ll k_4$, and k_3 is negligible; therefore, $k_{inact} \sim k_2$.

The partition ratio is an important parameter in assessing the efficacy of a suicide inhibitor. The partition ratio, r, is defined as the ratio of turnover to inactivation events; ideally, r would equal zero. That is, every catalytic event between enzyme and the suicide inhibitor would result in inactivated enzyme, with no release of reactive inhibitor product. The value for the partition ratio can be determined in several ways. If the kinetic constants can be determined individually, r is the ratio of the rate constants for catalysis and inactivation.

$$r = \frac{k_3}{k_4} \tag{13.16}$$

where r is the partition ratio, k_3 is the rate of reactivation, and k_4 is the rate of inactivation.

The partition ratio is also equal to the ratio of final product concentration following complete inactivation to initial enzyme concentration and should be independent of the initial [I].

$$r = \frac{[P_f]}{[E_0]} \tag{13.17}$$

where r is the partition ratio, $[P_f]$ is the final concentration of inhibitor product, and $[E_0]$ is the initial enzyme concentration. The partition ratio
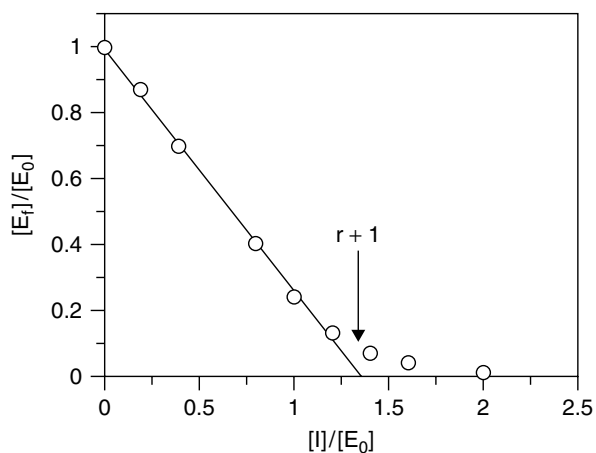
Figure 13.3. Titration curve to calculate the partition ratio r.

can also be determined by direct stoichiometric titration of the enzyme with the suicide inhibitor. The horizontal intercept of a plot of $[E_f]/[E_0]$ versus $[I]/[E_0]$ is equivalent to $r + 1$ (Fig. 13.3).

Irreversibility of inhibition can be established in a number of ways. Basically, excess inhibitor must be removed from the enzyme to isolate the possible reactivation process and enzyme activity monitored with time to test for any reactivation. Methods include exhaustive dialysis of inhibited enzyme with uninhibited enzyme as a control, removing all excess inhibitor and allowing time for reactivation, followed by assay for activity. An incubation of enzyme and inhibitor followed by dilution into assay solution will measure spontaneous recovery. The stability of the enzyme adduct to exogenous nucleophiles can be determined by diluting the incubation mixture into a solution containing an exogenous nucleophile, such as β-mercaptoethanol or hydroxylamine. Gel filtration or fast filtration columns also effectively remove inhibitor, and activity assays of the protein fraction can monitor any reactivation of the enzyme–inhibitor complex.

The enzyme inactivation by suicide inhibitors should be active-site directed. Not only must the inhibitor be processed by the enzyme's catalytic site, but the resulting reactive moiety should react at the active site also and not inactivate the enzyme by covalently binding amino acid residues outside the active site. Protection from inactivation by enzyme substrate or a simple competitive inhibitor is evidence for active-site directedness. Enzyme activity should also be monitored in the presence of exogenous reactive inhibitor, produced noncatalytically, to ensure that

inactivation does not result from modifications outside the active site. Difference spectroscopy, fluorescence, or ultraviolet (UV) spectroscopy can be used to monitor the physical structure of the suicide inhibitor during catalysis to provide evidence for the formation of reactive complex with enzyme (for examples see Copp et al., 1987; Vilain et al., 1991; Eckstein et al., 1994). Product analysis by high-performance liquid chromatography, (HPLC), UV spectroscopy, nuclear magnetic resonance (for examples see Smith et al., 1988; Blankenship et al., 1991; Kerrigan and Shirley, 1996; Groutas et al., 1997), specialized electrodes (for an example see Eckstein et al., 1994) can all help identify the reactive inhibitor moiety and confirm that it is generated by enzyme catalysis.

Ideally, the actual enzyme–inhibitor complex can be identified, showing the inhibitor bound to the active site. X-ray crystallography of the enzyme inhibitor complex is the ultimate method of identifying the mechanism of enzyme inhibition (for examples see Cregge et al., 1998; Swarén et al., 1999; Taylor et al., 1999; Ohmoto et al., 2000). Many other methods have been detailed in the literature. Using known x-ray crystal structures of enzymes, molecular modeling can be used to predict possible enzyme–inhibitor adducts (for examples see Hlasta et al., 1996; Groutas et al., 1998; Macchia et al., 2000; Clemente et al., 2001). Amino acid analysis of both native and inactivated enzyme can identify which amino acid is modified (for examples see Pochet et al., 2000). A radiolabeled suicide inhibitor and autoradiography can also be used to identify the amino acid modified by the inhibitor (for examples see Eckstein et al., 1994).

Certain inferences about the mechanism of inactivation can be made from inactivation kinetics. Structure–activity relationships of a series of compounds can lend support to various mechanisms with knowledge of the active site of the target enzyme (for examples see Lynas and Walker, 1997). The effect of the inhibitor's chirality can also provide information regarding how the suicide inhibitor is reacting with the enzyme.

Full kinetic characterization for mechanism-based inhibition can be a challenge. Not only are there multiple rates to determine, but the mechanism of inhibition is often a combination of several different steps. The dividing line between alternate substrate inhibitors and the more complex suicide inhibitors is often blurred, with some alternate substrates being virtually irreversible and some suicide substrates with high partition ratios and a significant alternate substrate element of inhibition. The following examples describe the characterization of an alternate substrate inhibitor and a suicide inhibitor of the serine protease human leukocyte elastase.

1
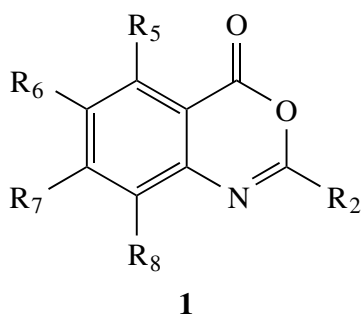
13.3   EXAMPLES

13.3.1   Alternative Substrate Inhibition

$4H$-3,1-Benzoxazin-4-ones (structure **1**) were identified and characterized as inhibitors of serine proteases (Krantz et al., 1990 and references therein) and continue to be pursued as possible pharmaceutical products (Gütschow et al., 1999 and references therein). Krantz et al. (1990) synthesized a large number of substituted benzoxazinones (175), and characterized their inhibition of the enzyme human leukocyte elastase. The method used to determine the rate constant k_{on} and the inhibition constant K_i was the continuous assay or progress curve method using a fluorescent substrate, 7-(methoxysuccinylalanylalanylprolylvalinamido)-4-methylcoumarin. The fluorescent assay was very sensitive, allowing for analysis at $[S] \ll K_m$ (in this case, $[S]/K_m = 0.017$), thereby avoiding perturbation of the inhibition rates due to competition from the substrate. Enzyme and substrate were combined in assay buffer and an initial, uninhibited rate was obtained before addition of an aliquot of inhibitor. The data were fit to Eq. (13.1). Linear regression of the observed k versus [I] gave k_{on} [Eq. (13.2)]. No saturation of these rates was observed in the study. The inhibition constant K_i was calculated from regression of the steady-state rates C versus [I] as described in Chapter 4. The deacylation rate (k_{off}) was either calculated as $k_{on*}K_i$ [Eq. (13.6)] or, in a few cases, determined directly by isolating the acyl-enzyme using a size exclusion column at low pH. Deacylation was monitored by the reappearance of enzyme activity upon dilution (1 in 40) of acyl-enzyme into assay buffer containing fluorogenic substrate.

The products of enzyme catalysis of a number of the inhibitors were also determined. In some cases, products were determined by analysis of the fluorescence spectrum after exhaustive incubation of enzyme with inhibitor and compared with synthesized standards of possible products. Catalytic products of other benzoxazinones were identified and relative

rates of formation estimated by single-turnover experiments using UV absorption spectra and HPLC analysis. Stoichiometric amounts of elastase and inhibitor (12.5 μM of each) were placed in separate compartments of split cuvettes and a baseline difference spectrum was obtained. The sample cuvette was then mixed, and a difference spectrum and an HPLC analysis of the mixture were obtained immediately. Following these determinations immediately and before significant deacylation could occur, 4 equiv. of the protein soybean trypsin inhibitor were added to irreversibly trap the enzyme into approximate single-turnover conditions. Difference spectra and HPLC analyses were obtained after incubation to allow for deacylation of the inhibitor from the enzyme. Catalytic products were identified, and their relative quantities determined, by comparison to the difference spectra and HPLC retention times of known base-hydrolysis and rearrangement products. A third method used for catalytic product identification utilized size exclusion chromatography of fully inhibited enzyme at pH 4, to stabilize the acyl-enzyme but remove any excess inhibitor. The protein fraction was then returned to assay conditions (pH 7.8) to allow deacylation to occur. A UV spectrum and HPLC analysis of the solution allowed identification of the products.

Using the enzyme inhibition kinetics and product identification and model studies of alkaline hydrolysis of the compounds, structure–activity relationships of the enzyme inhibitor interactions could be understood and predicted. With this knowledge the authors were able to design alternate substrate inhibitors with reasonable chemical stability, inhibition constants in the nanomolar range, and very slow deacylation rates (k_{off}), resulting in virtually irreversible inhibition.

13.3.2 Suicide Inhibition

A series of ynenol lactones (structure **2**) were studied as inhibitors of human leukocyte elastase (Tam et al., 1984; Spencer et al., 1986; Copp et al., 1987). Some of the compounds were alternate substrate inhibitors, being hydrolyzed by the enzyme to the reactive I* but then deacylating without an inactivation step. However, with the compound 3-benzyl ynenol butyrolactone (structure **2**, where R = benzyl, R' = H), the acyl-enzyme (E–I*) was stable enough to allow the second alkylation step, resulting in inactivated enzyme. All kinetic constants were determined. Continuous assays gave biphasic kinetics, the second minor phase possibly due to the presence of isozymes or enantiomers of the inhibitor. Immediate diffusion-limited inhibition was observed and gave a competitive K_i value of 4.3 ± 0.7 μM. The first phase of inhibition was saturable, and analysis of the rates gave $k_{inact}^{app} = 0.090 \pm 0.007$ s^{-1}, and

2
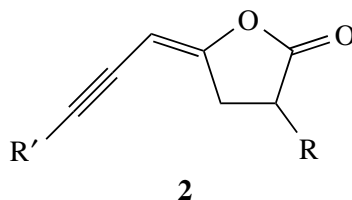
$K_{\text{inact}}^{\text{app}} = 4.1 \pm 0.7\ \mu M$. These rates were also pH dependent, with pK_a = 6.58, in reasonable agreement with the catalytic pK_a value for a serine protease. The actual inactivation rate was determined from rescue experiments. At various times t following addition of suicide substrate inhibitor to enzyme, 10 mM of the nucleophile β-mercaptoethanol was added. This nucleophile reacted rapidly with excess ynenol lactone, allowing any enzyme not inactivated to deacylate to regenerate active enzyme, as shown in Fig. 13.2. The inactivation rates were also saturable, giving k_4 or $k_{\text{inact}} = 0.0037 \pm 0.0001\ \text{s}^{-1}$ and $K_{\text{inact}} = 0.63 \pm 0.08\ \mu M$. Gel filtration of the enzyme–inhibitor mixture before full inactivation could occur, followed by dilution into assay conditions, allowed determination of the deacylation rate, $k_3 = 0.0056\ \text{s}^{-1}$. The pH dependence of this rate was also determined and found to have a pK_a value of 7.36. This value was in excellent agreement with the catalytic pK_a value, providing further evidence for the role of enzyme catalysis in the mechanism of inactivation.

The inhibition of human leukocyte elastase by the ynenol lactone was irreversible in the presence of the nucleophiles β-mercaptoethanol and hydroxylamine and after size exclusion chromatography. The partition ratio r was evaluated in two different ways. Titration of the enzyme by suicide substrate using the plot shown in Fig. 13.3 gave $r = 1.7 \pm 0.5$. The partition ratio was also determined from the ratio of rates: $k_3/k_4 = 1.5$.

That the inactivation was active-site directed was also established in several ways. As mentioned above, the pK_a values of k_2 and k_3, were consistent with the pK_a value of catalytic activity for a serine protease. Difference spectra of enzyme with inhibitor showed the reactive product being formed in the presence of enzyme. Rates of inhibition decreased in the presence of a known competitive inhibitor, elastatinal (Okura et al., 1975). The reactive intermediate was generated by mild alkaline hydrolysis and added to assay buffer at a concentration 25 times higher than the K_i of the ynenol lactone. Enzyme and substrate were added to the mixture, and neither inhibition nor time-dependent inactivation was observed. Therefore, inactivation was unlikely to occur by enzymatic release of the reactive intermediate followed by nonspecific alkylation outside the active site.

REFERENCES

Blankenship, J. N., H. Abu-Soud, W. A. Francisco, and F. M. Raushel, *J. Am. Chem. Soc.* **113**, 8560–8561 (1991).

Clemente, A., A. Domingos, A. P. Grancho, J. Iley, R. Moreira, J. Neres, N. Palma, A. B. Santana, and E. Valente, *Bioorg. Med. Chem. Lett.* **11**, 1065–1068 (2001).

Copp, L. J., A. Krantz, and R. W. Spencer, *Biochemistry* **26**, 169–178 (1987).

Cregge, R. J., S. L. Durham, R. A. Farr, S. L. Gallion, C. M. Hare, R. V. Hoffman, M. J. Janusz, H.-O. Kim, J. R. Koehl, S. Mehdi, W. A. Metz, N. P. Peet, J. T. Pelton, H. A. Schreuder, S. Sunder, and C. Tardif, *J. Med. Chem.* **41**, 2461–2480 (1998).

Eckstein, J. W., P. G. Foster, J. Finer-Moore, Y. Wataya, and D. V. Santi, *Biochemistry* **33**, 15086–15094 (1994).

Groutas, W. C., R. Kuang, R. Venkataraman, J. B. Epp, S. Ruan, and O. Prakash, *Biochemistry* **36**, 4739–4750 (1997).

Groutas, W. C., R. Kuang, S. Ruan, J. B. Epp, R. Venkataraman, and T. M. Truong, *Bioorg. Med. Chem.* **6**, 661–671 (1998).

Gütschow, M., L. Kuerschner, U. Neumann, M. Peitsch, R. Löser, N. Koglin, and K. Eger, *J. Med. Chem.* **42**, 5437–5447 (1999).

Hlasta, D. J., J. J. Court, R. C. Desai, T. G. Talomie, and J. Shen, *Bioorg. Med. Chem. Lett.* **6**, 2941–2946 (1996).

Kerrigan, J. E. and J. J. Shirley, *Bioorg. Med. Chem. Lett.* **6**, 451–456 (1996).

Krantz, A., R. W. Spencer, T. F. Tam, T. J. Liak, L. J. Copp, E. M. Thomas, and S. P. Rafferty, *J. Med. Chem.* **33**, 464–479 (1990).

Lynas, J. and B. Walker, *Biochem. J.* **325**, 609–616 (1997).

Macchia, B., D. Gentili, M. Macchia, F. Mamone, A. Martinelli, E. Orlandini, A. Rossello, G. Cercignani, R. Pierotti, M. Allegretti, C. Asti, and G. Caselli, *Eur. J. Med. Chem.* **35**, 53–67 (2000).

Ohmoto, K., T. Yamamoto, T. Horiuchi, H. Imanishi, Y. Odagaki, K. Kawabata, T. Sekioka, Y. Hirota, S. Matsuoka, H. Nakai, M. Toda, J. C. Cheronis, L. W. Spruce, A. Gyorkos, and M. Wieczorek, *J. Med. Chem.* **43**, 4927–4929 (2000).

Okura, A., H. Morishima, T. Takita, T. Aoyagi, T. Takeuchi, and H. Umezawa, *J. Antibiot.* **28**, 337–339 (1975).

Pochet, L., C. Doucet, G. Dive, J. Wouters, B. Masereel, M. Reboud-Ravaux, and B. Pirotte, *Bioorg. Med. Chem.* **8**, 1489–1501 (2000).

Smith, R. A., L. J. Copp, P. J. Coles, H. W. Pauls, V. J. Robinson, R. W. Spencer, S. B. Heard, and A. Krantz, *J. Am. Chem. Soc.* **110**, 4429–4431 (1988).

Spencer, R. W., T. F. Tam, E. Thomas, V. J. Robinson, and A. Krantz, *J. Am. Chem. Soc.* **108**, 5589–5597 (1986).

Swarén, P., I. Massova, J. R. Bellettini, A. Bulychev, L. Maveyraud, L. P. Kotra, M. J. Miller, S. Mobashery, and J.-P. Samama, *J. Am. Chem. Soc.* **121**, 5353–5359 (1999).

Tam, T. F., R. W. Spencer, E. M. Thomas, L. J. Copp, and A. Krantz, *J. Am. Chem. Soc.* **106**, 6849–6851 (1984).

Taylor, P., V. Anderson, J. Dowden, S. L. Flitsch, N. J. Turner, K. Loughran, and M. D. Walkinshaw, *J. Biol. Chem.* **274**, 24901–24905 (1999).

Vilain, A.-C., V. Okochi, I. Vergely, M. Reboud-Raveax, J.-P. Mazalelyrat, and M. Wakselman, *Biochim. Biophys. Acta* **1076**, 401–405 (1991).

CHAPTER 14

PUTTING KINETIC PRINCIPLES INTO PRACTICE

KIRK L. PARKIN*

The overall goal of efforts to characterize enzymes is to document their molecular and kinetic properties. Regardless of the exact mechanism of an enzyme reaction, a kinetic characterization often makes use of the simple Michaelis–Menten model:

$$E + S \underset{k_{-1}}{\overset{k_1}{\rightleftharpoons}} ES \overset{k_2}{\longrightarrow} E + P \tag{14.1}$$
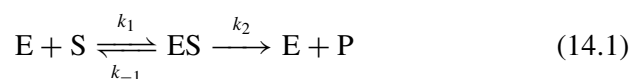
the ultimate objective being to provide estimates of the kinetic constants, K_m and V_{max}, under a defined set of conditions:

$$K_m = \frac{k_{-1} + k_2}{k_1} \tag{14.2}$$

$$V_{max} = k_2[E_T] \tag{14.3}$$

Once these kinetic constants are determined, the specificity constant for various substrates and under defined conditions can be obtained as

$$\frac{V_{max}}{K_m} \propto \frac{k_{cat}}{K_m} \tag{14.4}$$

*Department of Food Science, Babcock Hall, University of Wisconsin, Madison, WI 53706.

Since significant meaning is placed on these measured constants and parameters, it is important that they be determined accurately and unambiguously. It is also important that the reader or practitioner in the field of enzymology be able to assess if the measurement of these parameters is reliable. Furthermore, since enzyme behavior is often modeled as Michaelis–Menten (hyperbolic) kinetics, it seems reasonable that interpretations of observations should be made in the context of the Michaelis–Menten model. In some cases, alternative explanations for enzyme kinetic behavior may be appropriate and one may be inclined to select one interpretation over another (preferably based on a kinetic analysis, although too often this is done on intuition).

The purpose of this chapter is to illustrate some simple approaches to surveying the soundness of newly gathered or published information on enzyme kinetic characterization. This is intended to orient the developing enzymologist working in this field, as well guide those assessing literature reports on enzyme kinetic characterization. Fictitious examples have been constructed for this purpose, although they have been inspired by actual reports in the scientific literature encountered by this author. These specific examples will be used to illustrate putting simple kinetic principles to practice in an effort to draw the appropriate conclusions from enzyme kinetic data (and avoid reliance on one's intuition). Each of the following sections is titled in the form of a question, and these questions represent the most basic types of issues that one should consider upon reviewing enzyme kinetic data, whether it is one's own or has been generated by the studies of others.

14.1   WERE INITIAL VELOCITIES MEASURED?

Perhaps the most elementary consideration that should be satisfied is that the measured rates of enzyme reactions under all conditions represent *initial velocities* (v_0). The indication that *initial rates* or *linear rates* were measured are other ways to convey that this standard of experimentation has been met. One of the original stipulations of the general applicability of the Michaelis–Menten model (as well as many others) is that $d[S_0]/dt \approx 0$ during the time period over which the rate of product formation is measured. Thus, the measured reaction rate is representative of that taking place initially at the $[S_0]$ selected. This condition is especially important at low $[S_0]$ values, where reaction rates are nearly first order with respect to $[S_0]$. In practice, up to 5 to 10% depletion of $[S_0]$ can be tolerated over the time frame used to assay $[P]$ for the purpose of determining reaction rates, because error caused by normal experimental

variance may exceed any systematic error brought about by this degree of consumption of $[S_0]$ during the assay period.

Continuous assay procedures facilitate estimation of initial rates since the opportunity exists to linearize the initial portion of the reaction progress curve (Fig. 14.1). In contrast, the fixed-point assay, where the reaction or assay is quenched at a preselected interval(s) to allow for product measurement, requires greater care and vigilance to ensure that an estimation of initial velocity was obtained ($d[P]/dt$ must be linear during the entire assay period). Using the data in Fig. 14.1 as an example, a fixed-point assay interval of 10+ minutes would not provide for an estimate of initial velocity, whereas intervals of 6 minutes or less would.

Occasionally, fixed-point assays on the order of hours are encountered in published reports, and in these cases the reader should look very carefully and critically for assurances that measured reaction rates were linear. This author has even encountered reports where it was stated to the effect that "... reaction rates were linear and $[S_0]$ depletion was limited to 30% in all cases." Such a statement should be treated with great skepticism, since in this scenario the greatest degree of $[S_0]$ depletion would almost certainly occur at the low $[S_0]$ range tested, where the rates would most quickly deviate from linearity. It would also defy kinetic principles that reaction rates would be linear at $[S_0] \ll K_m$ for the period of time in which 30% depletion of $[S_0]$ occurred.

What could possibly go wrong if the measurement of linear rates was not assured? Well, an example has been provided to illustrate that it could mean the difference between falsely concluding that an enzyme reaction is allosteric (cooperative) and not correctly concluding that it behaves according to the simpler Michaelis–Menten model (Allison and Purich, 1979, Fig. 2). The reader is encouraged to peruse this reference for a
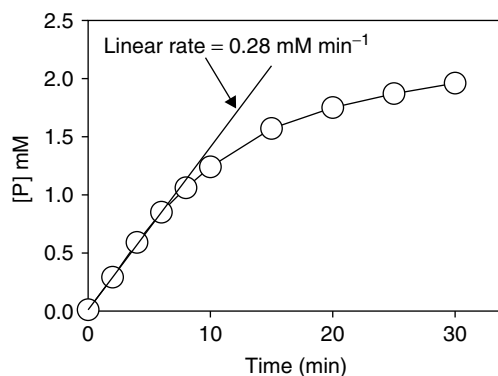
Figure 14.1. Enzyme reaction progress curve and estimation of initial velocity.

refresher on the considerations to be made in measuring *initial velocities*, which in those authors' words "... is of prime importance for achieving a detailed and faithful analysis of any enzyme."

14.2   DOES THE MICHAELIS–MENTEN MODEL FIT?

Perhaps the second most elementary (and very common) consideration regarding the kinetic profiling of an enzyme reaction is to assess whether or not it can be fitted to the Michaelis–Menten model. This assessment is not always taken as seriously as it should. Rather than truly *assess* whether or not the data conform to a Michaelis–Menten model, it is often simply stated (or blindly assumed) that they do, and various linear transformations are conducted to arrive at estimations of the kinetic constants K_m and V_{max}.

Consider the data presented in Fig. 14.2, where an accompanying comment may very well be something like "... the response of enzyme activity to increasing [S_0] was hyperbolic." The inset of Fig. 14.2 also illustrates a common and almost reflexive practice to transform these original data to a linear plot, often with quite "unconventional" methods for linearizing the transformed data. (The curvature to the data points in the inset appears to have been ignored, and although there are proper data weighting procedures for this specific linear plot, they appear seldom to have been evoked.) The double-reciprocal (Lineweaver–Burke) plot is the most often selected linear transform [despite repeated cautions that it is the least trustworthy of the linear plots most often considered (Henderson, 1978; Fukuwaka et al., 1985)].

Although the data in Fig. 14.2 may appear to be visually consistent with a rectangular hyperbola pattern (Michaelis–Menten model), it is a rather simple matter to test the observed data for fit to the Michaelis–Menten
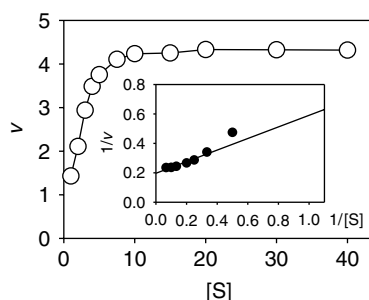
Figure 14.2. Enzyme rate data and transformation to double-reciprocal plot (inset).

model (although this is not done often enough). Taking the same data in Fig. 14.2 and imposing the rectangular hyperbola function on it,

$$y = \frac{ax}{b + x} \tag{14.5}$$

where y is the velocity, x represents $[S_0]$, a represents V_{max}, and b represents K_m, yields the boldface line in Fig. 14.3. It is clear that there is a systematic deviation of the data from the model that is readily apparent at the high- and medium-range $[S_0]$ tested. The significance of this analysis is twofold:

1. The kinetics of the enzyme reaction are more complicated than a Michaelis–Menten model can accommodate (further diagnostic tests, such as the use of the Hill plot, may reveal allosteric behavior or cooperativity as a kinetic characteristic).

2. The estimation and discussion of K_m (the Michaelis constant) may be irrelevant because K_m is a constant defined by (and confined within) use of the Michaelis–Menten model (hyperbolic kinetics) in the first place.

Different kinetic models have different conventions, and in the case of cooperative enzyme kinetic behavior, the term $K_{0.5}$ is used in a sense analogous to K_m for hyperbolic enzymes. In fact, transforming the original data in Fig. 14.2 to a Hill plot,

$$\log \frac{v}{V_{max} - v} = n \log[S] - \log K' \tag{14.6}$$
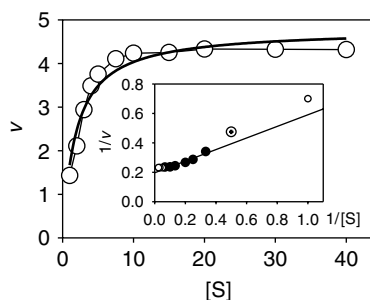
Figure 14.3. Enzyme rate data from Fig. 14.2, with predicted hyperbolic kinetics pattern (bold curve) superimposed. Inset shows data appearing in linear plot in Fig. 14.2 inset (●, ◉), as well as that not appearing in Fig. 14.2 inset (○).
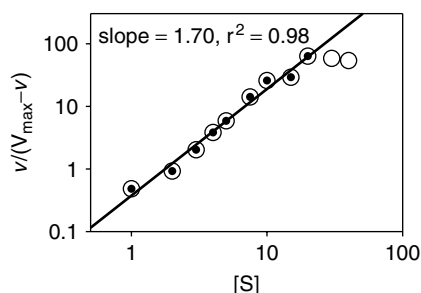
Figure 14.4. Transformation of the enzyme rate data in Fig. 14.2 to a Hill plot. Points appearing as ($\bigcirc$) were not included in the regression analysis.

where K' is a modified intrinsic dissociation constant and n is the apparent number of enzyme subunits (and slope on the Hill plot), yields a linear region (Fig. 14.4) for the most meaningful portion of the curve in Fig. 14.2. This plot is indicative of a cooperative enzyme with two apparent subunits and a K' (or $K_{0.5}$) value of 1.8 mM (the deviation from the linear plot at the high [S] value could be caused by a cofactor becoming limiting in the assay, among other reasons).

For the discerning reader, a closer examination of the Fig. 14.2 inset, and comparison of the axis values (1/[S]) with those ([S]) of the original data set, reveals that only a subset of the original velocity versus [S$_0$] data set is used to construct the linear plot (both high and low [S$_0$] points on the linear plot are omitted). This appears to be a classic case of imposing a model on a data set rather than using the data set to direct selection of the appropriate model for enzyme kinetic behavior. Figure 14.3 (inset) shows all of the original data transformed to the linear plot, and a systematic departure from linearity is clearly evident.

14.3 WHAT DOES THE ORIGINAL [S] VERSUS VELOCITY PLOT LOOK LIKE?

From the preceding discussion it should be evident that perhaps the most important and insightful data set on enzyme kinetic behavior is the original velocity versus [S$_0$] plot. However, it seems more often than not that this relationship is presented as a linear plot and not as original, non-transformed data. This approach may serve to cloud one's vision instead of offering insight into enzyme kinetic behavior [see Klotz (1982) for an example of diagnosing flawed receptor/binding analysis].

As an example, consider the findings reported in Fig. 14.5 regarding the nature of inhibition of an enzyme reaction. At increasing concentrations
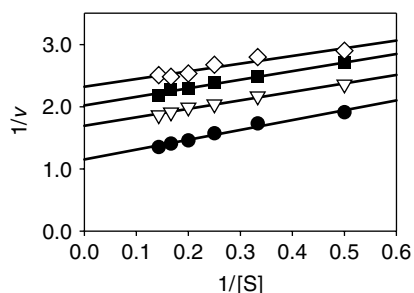
Figure 14.5. Double-reciprocal plot of enzyme rate data for assays done in the absence of inhibitor (●), and at progressively increasing levels of an inhibitor ($\triangledown$, ■, $\lozenge$).

of inhibitor [I], the transformed velocity versus $[S_0]$ plots for noninhibited and inhibited reactions display the classical pattern of uncompetitive inhibition, diagnosed as parallel plots on this linear plot for reactions inhibited by increasing levels of [I]. This data set would be used to estimate both K_m and K_I as a kinetic characterization of the inhibited enzyme reaction.

However, a closer inspection of the linear plot reveals that a very narrow range of $[S_0]$ of only 2 to 7 mM was used for these studies. Reverting the data back to the original coordinates of velocity versus $[S_0]$, it is also evident that the range of $[S_0]$ used was $\geq K_m$, creating a bias in the data set where velocity is becoming independent of $[S_0]$ (Fig. 14.6). If the data points encompassing the "missing" $[S_0]$ range are filled in, predicted by nonlinear regression plots derived from the original data, it is clear that the range of K_m values calculated (0.56 to 1.49 mM) is rather narrow. This limited data set that does little to define or resolve the curvature of these plots, and consequently the study is not reliable or sufficiently conclusive. Finally, and to put this particular data set into a broader context, the conclusion that uncompetitive inhibition occurs should be immediately
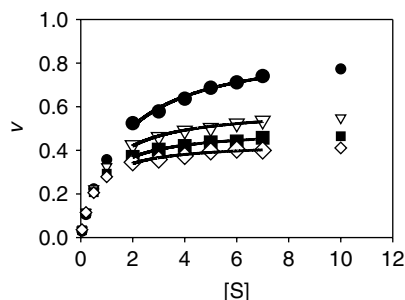
Figure 14.6. Transformation of enzyme rate data in Fig. 14.5 to a conventional velocity versus [S] plot (symbols are the same as in Fig. 14.5).

scrutinized because it is extremely rare (Segel, 1975; Cornish-Bowden, 1986). Certainly, a more compelling and persuasive data set than that in Figs. 14.5 and 14.6 would be required to support the conclusion that a rare kinetic property was discovered for a particular enzyme.

14.4   WAS THE APPROPRIATE [S] RANGE USED?

As an extension of some of the issues raised in Section 14.3, it is universally accepted that when using traditional approaches to kinetic analysis, a range of $[S_0]$ must be used to obtain reliable estimates of K_m and V_{max} (Segel, 1975; Whitaker, 1994). A range of $[S_0]$ of 0.3 to $3K_m$ (or better yet, 0.1 to $10K_m$, solubility permitting) for the purpose of estimating K_m and V_{max} encompasses the transition of $[S_0]$ going from being most limiting to being nonlimiting to the reaction. At $[S_0]$ exclusively $<K_m$ or $>K_m$, there is bias in the data set (Fig. 14.7) toward either of the two linear portions of this plot, with few measurements corresponding to the zone of curvature in (Fig. 14.7 inset).

Obtaining accurate measurements of K_m is important because K_m provides a quantitative measure of enzyme–substrate complementarity in binding (when $K_m \approx K_s$), and such values can be used to compare relative affinities of competing substrates. Second, the combined determination of V_{max} ($\propto k_{cat}$) and K_m for competing substrates provides for a quantitative comparison of specificity (selectivity) of the enzyme among substrates through the use of the specificity constant, or V_{max}/K_m [Eq. (14.4)] (Fersht, 1985).
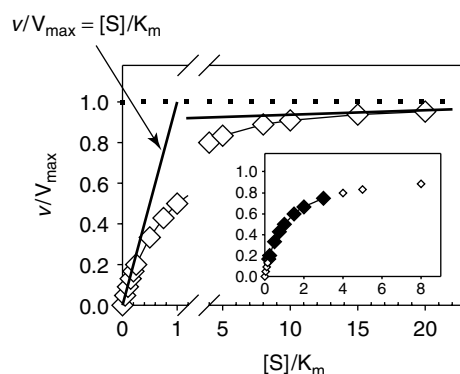
Figure 14.7. Conventional velocity (as a fraction of V_{max}) versus [S] (as a multiple of K_m) plot showing the two linear portions of a hyperbolic curve. Inset shows range of $[S]/K_m$ (◆) conducive to providing reliable estimates of V_{max} and K_m.

Studies that seek to compare specificity constants among different substrates under a defined set of conditions are often focused on the nature of enzyme–substrate interaction or structure–function relationships that confer reaction selectivity. In other cases, the determination of specificity constants for a single substrate under a variety of conditions is often an attempt to infer something about factors that govern or modulate reaction selectivity. In both cases, obtaining reliable data and estimates of kinetic constants are of paramount importance. The collection of observations in Table 14.1 provides an example of such a study, where different substrates were assayed over different ranges of [S] at a known [E] to yield estimates of k_{cat} and K_m.

The conclusions to be drawn for this type of study are likely to focus on the relationship between systematic changes in structural features of the substrates and the attendant changes in reaction selectivity (relative k_{cat}/K_m values). This may allow certain inferences to be drawn about the chemical nature of enzyme–substrate interactions that lead to productive binding and/or transition-state stabilization.

For example, a possible conclusion to be reached from the data in Table 14.1 is: "Reaction selectivity with substrate 7 was two orders of magnitude greater than for substrates 5 or 6". Based on structural differences between substrate 7, and 5 and 6, conclusions may be further delineated to suggest that specific functional groups of the substrate (and enzyme) may participate in catalysis by facilitating substrate binding or substrate transformation. Such conclusions would be valid or at least firmly supported if measurements of k_{cat} and K_m are accurate and reliable (Table 14.1).

It is a rather simple task to judge the reliability of this data set by calculating the K_m value (from the fourth and fifth columns in Table 14.1) and comparing it to the range of [S] values used (the second column in

TABLE 14.1 Selectivity Constants Determined for a Series of Substrates

Substrate (S)	Range of [S] Tested (mM)	Number of [S] Tested	k_{cat} (s^{-1})	k_{cat}/K_m (s^{-1} M^{-1})
1	0.50–2.5	6	0.897	296
2	1.0–6.0	8	0.184	36.0
3	0.50–8.0	6	2.97	1830
4	0.50–2.5	7	0.407	152
5	2.5–12.0	10	0.183	23.8
6	0.50–2.5	5	0.138	29.1
7	1.5–5.0	7	1.68	2260

TABLE 14.2 Assessment of Bias in [S] Range Used for Determining Selectivity Constants

Substrate (S)	Range of [S] Tested (mM)	Calculated K_m (mM)	Any Bias in [S]/K_m?
1	0.50–2.5	3.0	[S] $< K_m$
2	1.0–6.0	5.1	[S] $\leq K_m$
3	0.50–8.0	1.6	None
4	0.50–2.5	2.7	[S] $\leq K_m$
5	2.5–12.0	7.7	None
6	0.50–2.5	4.7	[S] $< K_m$
7	1.5–5.0	0.74	[S] $> K_m$

Table 14.1) for each substrate evaluated. This analysis is quite revealing in that the data set is biased for five of the seven substrates examined, such that estimates of both K_m and k_{cat} ($\propto V_{max}$) may be quite erroneous (Table 14.2).

The scenario described above pertains to the design of experiments and collection of observations for the purpose of estimating V_{max}/K_m using conventional linear or nonlinear transformations. It should be pointed out that there is another approach to the measurement of V_{max}/K_m, based on the principle that at low [S], the reaction velocity is proportional to V_{max}/K_m (Fig. 14.7). V_{max}/K_m approximates an apparent second-order rate constant (k_{cat}/K_m) describing the behavior of the free enzyme, but this relationship also holds at any [S] (Fersht, 1985). The utility of this relationship is founded on the fact that the relative velocities (v) of reactions between competing substrates is described as

$$\frac{v_A}{v_B} = \frac{(V_{max}/K_m)_A[S]_A}{(V_{max}/K_m)_B[S]_B} \tag{14.7}$$

From a practical point, each of several competing substrates may be incorporated into a reaction mixture at a single [S$_0$] value (they can be the same or different [S$_0$] values), and reactions may be allowed to proceed beyond the period where linear rates exist. Linear (log-log) transformations (Deleuze et al., 1987) are based on Eq. (14.7) and the relationships of

$$\frac{v_A}{v_B} = \alpha \frac{[S]_A}{[S]_B} \qquad \text{where} \qquad \alpha = \frac{(V_{max}/K_m)_A}{(V_{max}/K_m)_B} \tag{14.8}$$
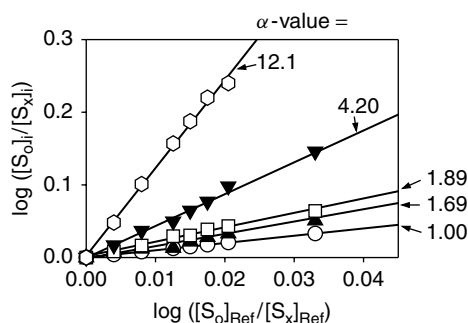
Figure 14.8. Log-log plots of enzyme reaction progress curves to provide estimates of relative V_{max}/K_m values (specificity constants). Different symbols are different substrates.

and

$$\log \frac{([S_0]_i)}{([S_x]_i)} = \alpha \log \frac{([S_0]_{ref})}{([S_x]_{ref})} \qquad (14.9)$$

where $[S_0]$ and $[S_x]$ are the concentrations of substrate initially and at any time (respectively) during the reaction for any substrate (i) relative to a reference (ref) substrate. The log-log plots (Fig. 14.8) represent the fractional conversion of each substrate relative to $[S]_{ref}$ at all time intervals assayed. The ratios of the slopes of the linear plots are equivalent to the α values for the multiple comparisons that can be made.

Data used to construct these plots are useful to the point where there is a departure from linearity (usually, a downward deflection). The most likely causes for this departure from linearity include product inhibition, approaching reaction equilibrium, and enzyme inactivation during the course of reaction. These α values are *relative* quantities. However, if the actual V_{max} (or k_{cat}) and K_m values are determined accurately for one substrate (probably the reference), reasonable quantitative estimates of selectivity constants (V_{max}/K_m) may be calculated for all the substrates in the series evaluated.

14.5 IS THERE CONSISTENCY WORKING WITHIN THE CONTEXT OF A KINETIC MODEL?

In this final section we examine a set of observations that may be interpreted in alternative ways: the point being that interpretation should be made within the context of any model that is evoked to represent enzyme kinetic behavior. The simplest and most commonly applied model, the

Michaelis–Menten or hyperbolic kinetics model, is used here to illustrate how a model can be employed to guide interpretations and conclusions.

Substrate inhibition in studies on enzyme kinetics is a property observed more often than perhaps one would anticipate. An example of an enzyme reaction subject to substrate inhibition is illustrated in Fig. 14.9. A conclusion that may be reached upon the presentation of such data is "... the enzyme reaction was subject to substrate inhibition at [S] of greater than 2 mM." This would be a naïve comment; a more a precise comment would be that "... the enzyme reaction was subject to substrate inhibition *and reaction rates started to decline* at [S] of greater than 2 mM." The difference between these statements lies much deeper than simply semantics.

To make an appropriate assessment of the pattern of inhibition, one need only compare the pattern of reaction velocity versus [S] observed relative to the pattern predicted from an application of the hyperbolic kinetics model. This requires making an estimate of V_{max} and K_m from the data available. Transforming the original data to a Lineweaver–Burke plot *(despite the aforementioned limitations)* indicates that only four data points (at low [S]) can be used to estimate V_{max} and K_m (as 3.58 units and 0.48 mM, respectively, Fig. 14.10). The predicted (uninhibited) behavior of the enzyme activity can now be calculated by applying the rectangular hyperbola [Eq. (14.5)] (yielding the upper curve in Fig. 14.11), and it becomes clear that inhibition was obvious at [S] ≤ 1 mM. The degree of inhibition is expressed appropriately as the difference between observed and predicted activity at any [S] value, if one makes interpretations within the context of the Michaelis–Menten model.

Because of the leveling off of enzyme activity at 3 to 5 mM [S] (Fig. 14.9), another conclusion that may be reached through intuition is that "... this pattern of activity can be explained by the presence of two
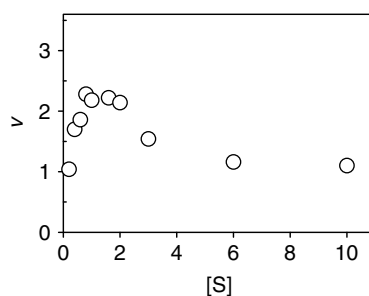
Figure 14.9. Rate data for an enzyme subject to substrate inhibition.
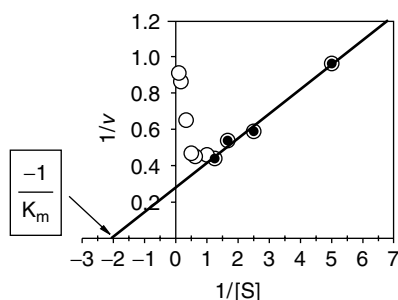
Figure 14.10. Data from Fig. 14.9 transformed to a double-reciprocal plot. Only some data (⊙) were used to construct the linear plot and allow estimates of V_{max} and K_m.
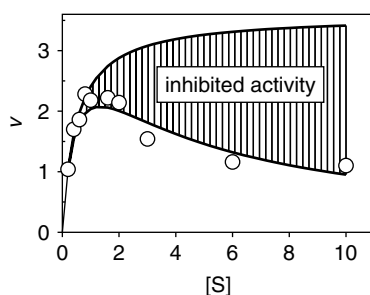
Figure 14.11. Example rate data in Fig. 14.9 (○) contrasted with the predicted behavior (upper curve) of an uninhibited enzyme with the V_{max} and K_m values derived from Fig. 14.10.

enzymes that act on this substrate, one enzyme subject to substrate inhibition, and the other enzyme not subject to substrate inhibition." To assess this statement, one must attempt to account mechanistically for the nature of enzyme inhibition by substrate. One can envision the nature of substrate inhibition using a modified form of the model in Eq. (14.1):

$$
\begin{array}{c}
\mathrm{E + S} \underset{k_{-1}}{\overset{k_1}{\rightleftharpoons}} \mathrm{ES} \overset{k_2}{\longrightarrow} \mathrm{E + P} \\
\mathrm{+2\,S} \\
\Big\| \, \kappa_I \\
\mathrm{ESS}
\end{array}
\qquad (14.10)
$$
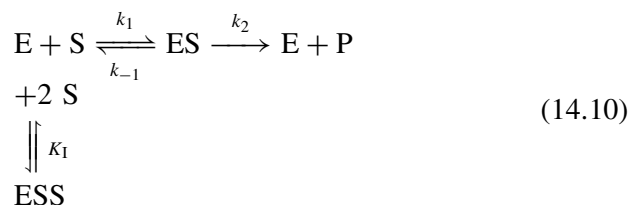
where the added feature is the process whereby two molecules of S bind at the active site to form a deadend (nonproductive) complex, characterized

by a dissociation constant (K_I) for the inhibited enzyme species (ESS):

$$K_I = \frac{[E][S]^2}{[ESS]} \qquad (14.11)$$

Conceptually, this mode of inhibition can be visualized as each of two substrate molecules binding to different subsites of the enzyme active site, resulting in nonalignment of reactive groups (designated as "∗") on E and S (Fig. 14.12). Using the conventional approach of deriving the reaction velocity expressions yields

$$v = \frac{V_{max}[S]}{K_m + [S] + (K_m[S]^2)/K_I} \qquad (14.12)$$

This relationship takes the form of the original rectangular hyperbola [Eq. (14.5)] modified by the incorporation of the substrate inhibition step:

$$y = \frac{ax}{b + x + bx^2/c} \qquad (14.13)$$

Since a and b were determined earlier (Fig. 14.10), the equation only needs to be solved for c (K_I). There are at least two ways to solve for
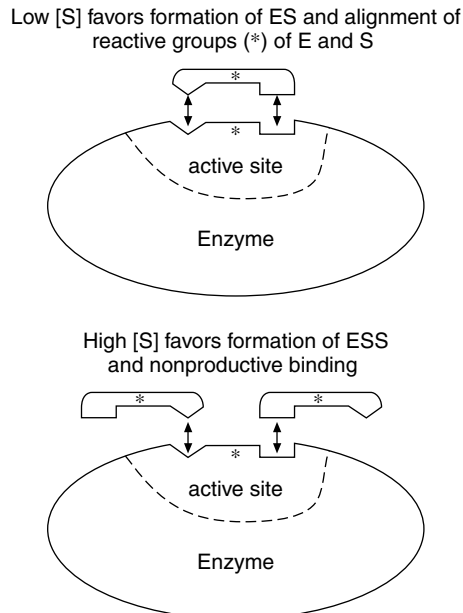
Figure 14.12. Visualization of model derived for substrate inhibition of enzyme in Eq. (14.10).

K_I, one of which is through nonlinear regression fitting of the actual data using the relationship just described [Eq. (14.13)], and this yields a value for K_I of 1.85 mM ($r^2 = 0.98$). A second and nonconventional way is to use Fig. 14.10 and consider the points corresponding to the four greatest [S] as observations in the presence of competitive inhibitor (Fig. 14.13). This provides four estimates of K_I if the plot is interpreted as behaving by classical competitive inhibition kinetics (the exception being that the [S]^2 and not [I] parameter [based on scheme (14.10)] is used in the term corresponding to the x-intercept). The mean of these four estimates of K_I is 1.78 mM (with a narrow range of 1.2 to 2.2 mM), very close to the 1.85 mM value determined by nonlinear regression.

Based on the two analyses just described, a K_I value of 1.8 mM was used and the pattern of enzyme activity predicted using the model [Eqs. (14.10) through (14.13)] is shown as the lower curve in Fig. 14.11. It is apparent that although there is some systematic deviation of the actual data from the curve modeling substrate inhibition, the approximation to the data observed is nonetheless reasonable.

To further evaluate the alternative views of the presence of one versus two enzymes, one could proceed with evaluating how well the data fit a two-enzyme model. In this scenario one is forced to make certain assumptions about the relative kinetic properties and contribution of each enzyme to the behavior observed in Fig. 14.9. For the sake of this analysis, the
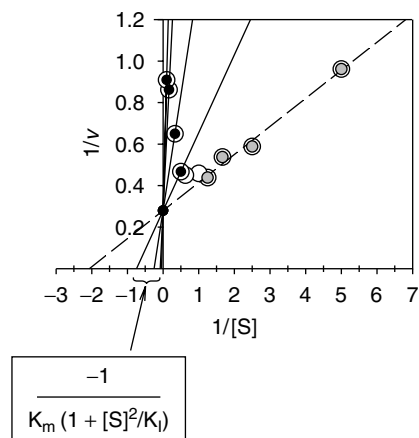
Figure 14.13. Same plot as Fig. 14.10 except for the addition of four plots at high [S] value (◉) modeled as competitive inhibition by substrate. Intersects at $1/V_{max}$ were constructed to arrive at four separate estimates of inhibition constant (K_I) based on the model in Eqs. (14.10) and (14.11). Original estimates of K_m and V_{max} were based on the data used to construct the broken line plot, as in Fig. 14.10.

assumptions made here are that:

1. The K_m values for the two enzymes are the same (primarily because without any further information, it would be difficult to assume a priori that one enzyme has a greater or lesser K_m value than the other).
2. The relative contribution of activity of each enzyme at [S] = 10 mM is equal.

Based on these assumptions, the contribution of the second, noninhibited enzyme to the data observed (Fig. 14.9) can be calculated. The data observed can now be partitioned into the individual contributions of the two enzymes (Fig. 14.14a). The lower curve represents the uninhibited enzyme and the upper curve represents the inhibited enzyme, which is
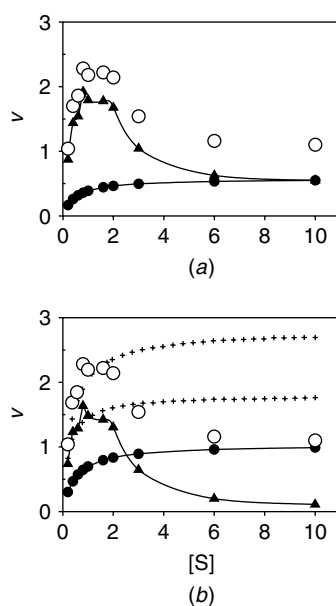
Figure 14.14. Modeling of a two-enzyme system, with one enzyme subject to substrate inhibition (▲) and the other not inhibited by substrate (●) using the data in Fig. 14.9 (○). (*a*) Both enzymes are assumed to have the same K_m and make equal contributions to activity observed at 10 mM [S]. (*b*) Both enzymes are assumed to have the same K_m and the uninhibited enzyme contributes 90% of the activity observed at 10 mM [S]. Additional plots (+ + +) in (*b*) predict the behavior of an enzyme subject to substrate inhibition by binding only one molecule to S to form an inactive E′S complex with a K_I value of 1.8 mM (upper curve) or 0.5 mM (lower curve).

calculated as the difference between the data observed (open symbols) and the contribution of the uninhibited enzyme.

One now needs to evaluate how well the inhibition constant (K_I) can afford a fit to the pattern predicted for the inhibited enzyme (upper curve in Fig. 14.14*a*) of the two-enzyme model. One approach would be to apply a nonlinear regression (which in this case did not allow for convergence or a good fit). An alternative approach is a more pencil-and-paper type of exercise to test the inhibited enzyme (of the two-enzyme model) for fit by rearranging Eq. (14.12) to solve for K_I by calculating K_I for the inhibited enzyme component for each datum point or observation made:

$$K_I = \frac{K_m/[S]}{(V_{max}/v) - (K_m/[S]) - 1} \qquad (14.14)$$

This was done first for the original data (Fig. 14.9) after estimating K_m and V_{max} (Fig. 14.10) and omitting the first four observations at [S] ≤ 4 mM because some "nonsense" or negative numbers were obtained (the extent of inhibition at low [S] is negligible and may be difficult to decipher). The single-enzyme system subject to substrate inhibition and modeled by the lower curve in Fig. 14.11 had a calculated [using Eq. (14.14)] mean K_I value of 2.2 mM (range 1.3 to 3.2 mM, again very close to the 1.8 mM value derived from the two other approaches employed). When these same data are modeled as a two-enzyme system, the inhibited enzyme was characterized by a calculated [using Eq. (14.14)] K_I value of 1.5 mM (range 0.79 to 2.6 mM). This analysis and the calculation of mean (and range of) K_I provide little as a basis to differentiate conclusively between the ability of one model to fit the observations better than the other, and in this case, the most conservative approach would be to conclude that the simpler (one-enzyme) model is valid.

Furthermore, if one modifies the assumptions to have the noninhibited enzyme in the two-enzyme model constitute a greater proportion (e.g., about 90%) of the activity observed at the greatest [S] (10 mM) (Fig. 14.14*b*), the calculation of K_I [using Eq. (14.14)] is subject to less precision (mean of 1.0 mM and range of 0.22 to 2.2 mM), and there is a systematic decline in K_I as one progresses toward greater [S]. Thus, the more the two-enzyme system model is emphasized in the analysis, the less it fits the observed data, whereas a single-enzyme system (Fig. 14.11) appears to explain the observations sufficiently well.

Finally, a model for substrate inhibition alternative to Eqs. (14.10) and (14.11) was evaluated by testing if a nonproductive E–S complex could involve only one (and not two) molecules of bound substrate (E′S as the inhibited species as opposed to ESS). This was done using the

kinetic constants ($V_{\max}$ and K_m) derived earlier from Fig. 14.10 and K_I values of 1.8 and 0.5 mM. The resulting plot predicted by this alternative model are the two curves indicated by plus signs (+) for these respective K_I values in Fig. 14.14(b). It is obvious that simple enzyme inhibition by a single molecule of bound substrate does not predict the cooperative inhibitory effect of high [S] (2 to 10 mM in Fig. 14.9) as well as does the model depicted in Eq. (14.10).

14.6 CONCLUSIONS

The purpose of this chapter is to illustrate how the application of simple kinetic principles and relationships are critical to analyzing and reaching appropriate conclusions for experimental observations on enzyme kinetic properties. Many misrepresentations or errors in interpretation of experimental data can be avoided by working within (or verifying the applicability of) a kinetic model and not relying on intuition. Resisting the immediate temptation to linearize the original data and analyze the transformed data without careful consideration would also help!

REFERENCES

Allison, R. D. and D. L. Purich, 1979. Practical considerations in the design of initial velocity enzyme rate assays, in *Methods in Enzymology*, Vol. 63, *Enzyme Kinetics and Mechanism, Part A, Initial Rate and Inhibitor Methods* (D. A. Purich, Ed.), pp. 3–22, Academic Press, San Diego, CA.

Cornish-Bowden, A., 1986. Why is uncompetitive inhibition so rare? A possible explanation, with implications for the design of drugs and pesticides. *FEBS Lett.* **203**: 3–6.

Deleuze, H., G. Langrand, H. Millet, J. Baratti, G. Buono, and C. Triantaphylides, 1987. Lipase-catalyzed reactions in organic media: competition and applications. *Biochim. Biophys. Acta* **911**: 117–120.

Fersht, A., *Enzyme Structure and Mechanism*, 2nd edition, W.H. Freeman, New York, 1985.

Fukagawa, Y., M. Sakamoto, and T. Ihsikura, 1985. Micro-computer analysis of enzyme-catalyzed reactions by the Michaelis–Menten equation. *Agric. Biol. Chem.* **49**: 835–837.

Henderson, P. J. F., 1978. Statistical analysis of enzyme kinetic data, in *Techniques in Protein and Enzyme Biochemistry, Part II*, Vol. B1/II (H. L. Kornberg, J. C. Metcalfe, D. H. Northcote, C. I. Pigson, and K. F. Tipton, Eds.), pp. 1–43, Elsevier/North-Holland Biomedical Press, Amsterdam, The Netherlands.

Klotz, I. M., 1982. Numbers of receptor sites from Scatchard plots: facts and fantasies. *Science* **217**: 1247–1249.

Segel, I. H., *Enzyme Kinetics: Behavior and Analysis of Rapid Equilibrium and Steady-State Enzyme Systems*, John Wiley & Sons, New York, 1975.

Whitaker, J. R., *Principles of Enzymology for the Food Sciences*, 2nd edition, Marcel Dekker, New York, 1994.

CHAPTER 15

USE OF ENZYME KINETIC DATA IN THE STUDY OF STRUCTURE–FUNCTION RELATIONSHIPS OF PROTEINS

TAKUJI TANAKA* and RICKEY Y. YADA*

The ability to change specific residues or regions of proteins through the use of techniques in molecular biology (e.g., site-directed mutagenesis) has allowed for rapid and sizable advances in an understanding of the structure–function relationships in proteins. Integral to these studies is the analysis of enzyme kinetic data. In this chapter we examine how enzyme kinetic data, by posing various questions, can be used in protein structure–function studies based on molecular biological techniques. The questions relate to our work with aspartic proteinases.

15.1   ARE PROTEINS EXPRESSED USING VARIOUS MICROBIAL SYSTEMS SIMILAR TO THE NATIVE PROTEINS?

In protein structure–function studies in which molecular biological techniques are used, the protein in question is expressed in either a procaryotic system (e.g., bacteria such as *Escherichia. coli*) or a eucaryotic system (e.g., yeast such as *Pichia pastoris*). Using such expression systems allows for rapid production of a protein or enzyme that has been cloned from its original source [e.g., porcine pepsin(ogen) expressed in *E. coli*]. These systems are, however, not without their problems. In addition, when using

* Department of Food Science, University of Guelph, Guelph, Ontario, Canada N1G 2W1.

such systems, the question arises: Is the cloned protein similar to the native or noncloned protein?

Except for the case of human immunodeficiency virus protease (Seelmeier et al., 1988; Danley et al., 1989; Darke et al., 1989; McKeever et al., 1989; Meek et al., 1989), most efforts have failed to express soluble protein (Nishimori et al., 1982, 1984; Lin et al., 1989; Chen et al., 1992). Researchers have therefore been forced to express recombinant aspartic proteases as inclusion bodies. Proteins formed as inclusion bodies must be unfolded and then refolded to obtain a "properly" folded protein. Many research groups have reported that the folding step is protein dependent and that a successful method for one protein does not always apply to other proteins (Creighton, 1978; Kane and Hartley, 1988; Georgiou and De Bernardez-Clark, 1991). Such results suggest that slight differences between experiments may result in different forms of the protein (i.e., refolded and unfolded protein). In addition, refolding does not ensure that the entire protein molecule is folded in the correct configuration.

Expression as a fusion protein (e.g., thioredoxin), has often been used to obtain soluble proteins (Nilsson et al., 1985; LaVallie et al., 1993). In this light, we were able to fuse porcine pepsinogen successfully to the thioredoxin gene and express this fusion protein in *E. coli* (Tanaka and Yada, 1996). We were able to generate r-pepsin from both r-pepsinogen and the fused protein (i.e., thioredoxin + pepsinogen). Amino terminal analyses confirmed that the *E. coli* expression system was able to produce soluble pepsin and pepsinogen molecules. Porcine pepsin A (c-pepsin, commercial pepsin) was purified from its zymogen (c-pepsinogen) using the same method as was used for recombinant pepsin (r-pepsin) and served as a reference for our studies. Recombinant (r-) and c-pepsins showed similar milk clotting and proteolytic activities. Kinetic analyses of r- and c-pepsins are shown in Table 15.1. Michaelis and rate constants for both pepsins were similar, as was pH dependency. From this study we concluded that the fusion pepsinogen expression system could successfully produce recombinant porcine pepsinogen as a soluble protein, which could be activated into active pepsin.

Despite the benefits of fusion protein systems, there are limitations. The biggest limitation is the requirement for enzymatic digestion to obtain the zymogen. In addition, *E. coli* does not possess a posttranslational modification system. Recently, the methylotrophic yeast *P. pastoris* has become a dominant tool in molecular biology for the production of recombinant proteins. As a eucaryote, it is capable of posttranslational modifications during expression, such as proteolytic processing, folding, disulfide bond formation, and glycosylation (Cregg et al., 2000). A further advantage of the *Pichia* expression system is that it uses a signal peptide fused to target

TABLE 15.1 Kinetic Analysis of Recombinant and Commercial Pepsin[a]

Enzyme[b]	Milk Clotting (units/mg)	Proteolysis (units/mg)	K_m (mM)	k_{cat} (s^{-1})
r-pepsin*	27.9 ± 1.5	19.8 ± 0.3	0.033 ± 0.005	65.4 ± 3.1
r-pepsin[†]	27.7 ± 1.6	ND	ND	ND
c-pepsin	28.3 ± 0.8	21.1 ± 0.5	0.026 ± 0.004	79.5 ± 3.8

[a] See Section 15.7 for abbreviations. ND, no data.
[b], * and [†] represent pepsin purified from r-pepsinogen and Trx-PG, respectively. One unit of milk clotting activity was defined as the amount of protein that gave a 0.4 unit change in absorbance over 1 s. One unit of proteolytic activity was defined as the amount of protein that gave a change of 1 absorbance unit (due to soluble peptides) at 280 nm in 1 min. Each value represents the mean of three determinations $\pm$ standard deviation.

TABLE 15.2 Kinetic Analysis of *Pichia* Expressed and Commercial Pepsin[a]

Enzyme	pH	K_m (mM)	k_{cat} (s^{-1})	k_{cat}/K_m (s^{-1} mM^{-1})
r-pepsin	1.0	0.091 ± 0.010	217.1 ± 10.1	2390 ± 174
	2.0	0.062 ± 0.003	162.1 ± 5.9	2600 ± 47
	3.0	0.048 ± 0.007	183.8 ± 8.6	3820 ± 397
c-pepsin	1.0	0.062 ± 0.010	115.8 ± 9.2	1900 ± 177
	2.0	0.054 ± 0.010	105.7 ± 10.4	2010 ± 268
	3.0	0.040 ± 0.010	105.6 ± 1.1	2640 ± 46

[a] See Section 15.7 for abbreviations. Kinetic constants represent a minimum of three determinations $\pm$ standard deviation. No significant difference was found between r- and c-pepsin at the various pH values using a Student's *t*-test at the 0.05 level of significance.

the protein gene that is digested off during secretion. This secretion has an advantage over intracellular expression systems since most of the protein in the culture medium will be the desired protein, thus making purification easier. We have developed a protein expression for pepsin(ogen) using *P. pastoris* (Yoshimasu et al., 2002). The K_m and k_{cat} values for commercial and recombinant pepsins were not significantly different ($p > 0.05$) (Table 15.2). In addition, there were no differences in pH dependency of the activity. In conclusion, two different expression systems can be employed, depending on the objectives of the research.

15.2 WHAT IS THE MECHANISM OF CONVERSION OF A ZYMOGEN TO AN ACTIVE ENZYME?

The mechanism by which the zymogen of the enzyme is converted to the active form of the enzyme has been the focus of a number of researchers.

For pepsin, activation from pepsinogen can occur via two different mechanisms. One is a bimolecular reaction (an intermolecular reaction), in which a pepsin molecule converts pepsinogen into pepsin; the other is an unimolecular reaction (self-activation; an intramolecular reaction), in which a pepsinogen molecule cleaves itself to yield a pepsin molecule (Herriott, 1939; Bustin and Conway-Jacobs, 1971; Al-Janabi et al., 1972; McPhie, 1974).

In our *E. coli* expression system, fusion pepsinogen (Trx-PG) can be activated (1) directly without generating pepsinogen, or (2) through pepsinogen via pepsin (Tanaka and Yada, 1997). Analysis of the activation kinetics of these two possibilities revealed an interesting observation. Activation kinetics of r-pepsinogen (r-PG) were plotted in Fig. 15.1(*a*). r-PG exhibited an initial lag phase (closed triangles, Fig. 15.1*a*), after which the rate of activation accelerated. This observation would indicate that the pepsin molecule, which is initially activated from r-PG by a unimolecular reaction, began to hydrolyze other r-PG molecules (bimolecular activation) and that bimolecular activation, rather than self-activation, became the dominant reaction (due to increasing amounts of pepsin being released). When both bimolecular and unimolecular activation occur, first- and second-order rate constants should be determined in order to obtain the activation rate constants (Al-Janabi et al., 1972). The equation used to fit the data is

$$\frac{-\Delta[\text{r-PG}]}{\Delta t} = k_1[\text{r-PG}] + k_2[\text{r-PG}][\text{r-pepsin}] \qquad (15.1)$$

Equation 15.1 describes a sigmoidal activation curve as long as k_1 and k_2 exist. However, no sigmoidal curve was observed at any of the pH values examined for the Trx-PG's. In addition, the fusion protein exhibited no difference (within error) in activation in the absence or presence of a 1 : 1 molar ratio of pepsin molecules (Fig. 15.1*b*), whereas r-PG activation was accelerated in the presence of exogenous pepsin (Fig. 15.1*a*). Again, if activation of Trx-PG by pepsin is much faster than self-activation, as was observed in r-PG, faster activation would be expected with exogenous pepsin, but no such effect was observed. These results do not discount the existence of bimolecular activation of Trx-PG, but would suggest that bimolecular activation was extremely slow in comparison to unimolecular activation. Based on the results above, the activation of Trx-PG followed

$$\frac{-\Delta[\text{Trx-PG}]}{\Delta t} \approx k[\text{Trx-PG}] \qquad (15.2)$$

and can be analyzed by a conventional Guggenheim plot (Guggenheim, 1926) to calculate the rate constant for unimolecular activation for Trx-PG.
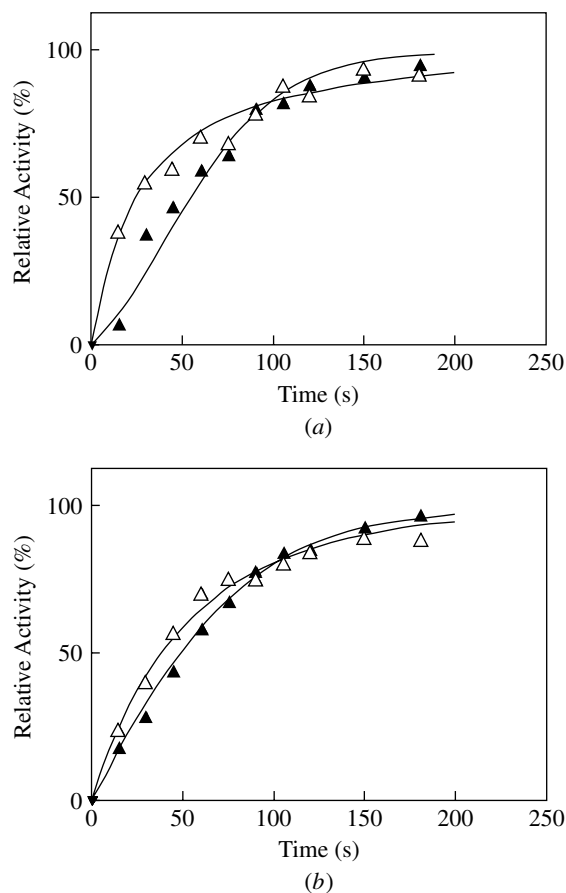
Figure 15.1. Example of the activation time course of (*a*) recombinant pepsinogen (r-PG), and (*b*) fusion pepsinogen (Trx-PG) at pH 2.0. The ratio of activated zymogens was calculated from the activity measurements. Nonactivated samples are defined as 0% and the plateau of the activation curves is defined as 100%. Open symbols represent pepsinogen activated in the presence of exogenous pepsin, closed symbols represent pepsinogen in the absence of exogenous pepsin. Each data point represents the mean of a minimum of three determinations.

The rate constants for Trx-PG were 0.0276 ± 0.0004, 0.0120 ± 0.0010, and 0.0099 ± 0.0001 s^{-1} at pH 1.1, 2.0, and 3.0, respectively. The results showed that the unimolecular activation of the fusion protein was dominant and different from that of r-PG. The difference in the activation mechanism was definitely caused by thioredoxin. The presence of thioredoxin itself, however, did not alter r-PG activation mechanism since the sigmoidal curve of r-PG activation indicated that the unimolecular activation was extremely slow even in the presence of thioredoxin molecules,

which existed in r-PG solution as the cleaved *prosegment*. Only when thioredoxin was covalently bonded to pepsinogen was unimolecular activation dominant. The thioredoxin portion is approximately one-fourth of the entire fusion molecule (Fig. 15.2*a*). The bulky prosegment of the fusion protein would stabilize the catalytic intermediate of unimolecular activation and could also retard bimolecular activation. The bulkiness of the prosegment of the fusion protein could prevent pepsin molecules from approaching the cleavage site, Leu44p-Ile1 (Fig. 15.2*b*).

15.3   WHAT ROLE DOES THE PROSEGMENT PLAY IN THE ACTIVATION AND STRUCTURE–FUNCTION OF THE ACTIVE ENZYME?

Some proteinases are synthesized as zymogens (inactive forms), which allows them to exist in a stable form until the active form of the enzyme is required. Under physiological conditions, porcine pepsin is secreted in the stomach as a zymogen, pepsinogen. In pepsinogen, a 44-residue peptide, referred to as a prosegment, blocks the entrance to the active site. During the conversion from pepsinogen to pepsin, the prosegment is removed. The prosegment in pepsinogen covers the active site, although the actual cleavage site between the enzyme body and the prosegment is not in the active site. The removal of the prosegment must occur in conjunction with a conformational change in order to bring the digested position into an active site (Richter et al., 1998).

In pepsinogen, Lys36p forms salt bridges with the catalytic aspartic acid residues. These salt bridges seem to be a key factor governing the stability of the prosegment. Therefore, it is possible that replacing Lys36p with Glu, Arg, and Met will increase the rate of conformational change required for activation by affecting the dissociation of the prosegment (Richter et al., 1999). Therefore, three mutants were constructed in our lab: Lys36pGlu, Lys36pMet, and Lys36pArg. Arg and Met mutations did affect the pH range in which activation occurred, while the two mutations did not alter the pH optimum for activation. In addition, relative to wild-type Trx-PG, which exhibited no conversion to pepsin at pH ≥ 4, Lys36pArg and Lys36pMet were capable of activation up to pH 5.0 and pH 5.5, respectively. In the case of Lys36pGlu, the pH dependence of the potential pepsin activity could not be determined accurately since Lys36pGlu Trx-PG was not stable at neutral pH which was used to quench the activation reaction.

The activation curves for wild-type, Lys36pArg, and Lys36pMet Trx-PG at pH 1.1, 2.0, and 3.0 are shown in Fig. 15.3. Under these conditions,
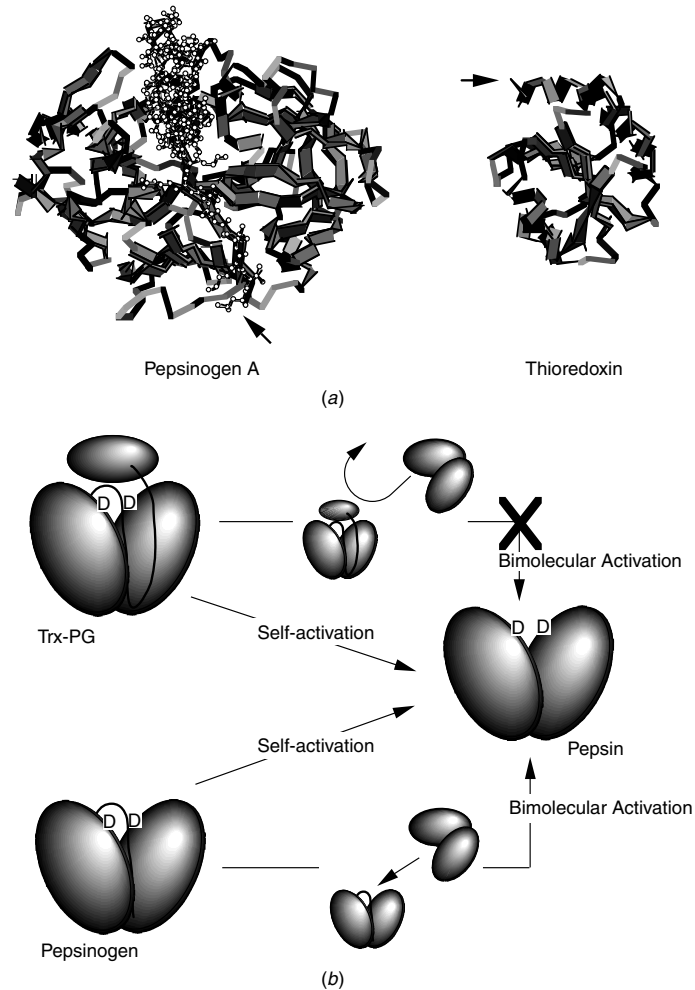
Figure 15.2. Three-dimensional structure of pepsinogen and thioredoxin, and schematic scheme of activation of Trx-PG. (*a*) Three-dimensional structures of pepsinogen and thioredoxin (Protein Data Bank 3PSG and 2TRX, respectively) are shown in the same scale. The prosegment of pepsinogen is shown in ball-and-stick models. The N-terminal of pepsinogen and C-terminal of thioredoxin are indicated with arrows. Thioredoxin consists of 108 amino acid residues, and pepsinogen is 371 amino acid residues long. In Trx-PG, both proteins are connected by a 20-amino acid residue linker. (*b*) Proposed scheme of how thioredoxin prevents pepsin from cleaving the fusion protein. In both the fusion protein (Trx-PG) and pepsinogen, two aspartic active sites (two D's in the figure) are covered with a prosegment (the thick lines in the figure). Pepsinogen can be activated into pepsin through either self-activation or bimolecular activation. Trx-PG has a large independent domain (i.e., thioredoxin portion) at the amino terminal of the prosegment. This large domain would prevent pepsin from approaching the susceptible site on the prosegment, and therefore the bimolecular reaction could not occur.
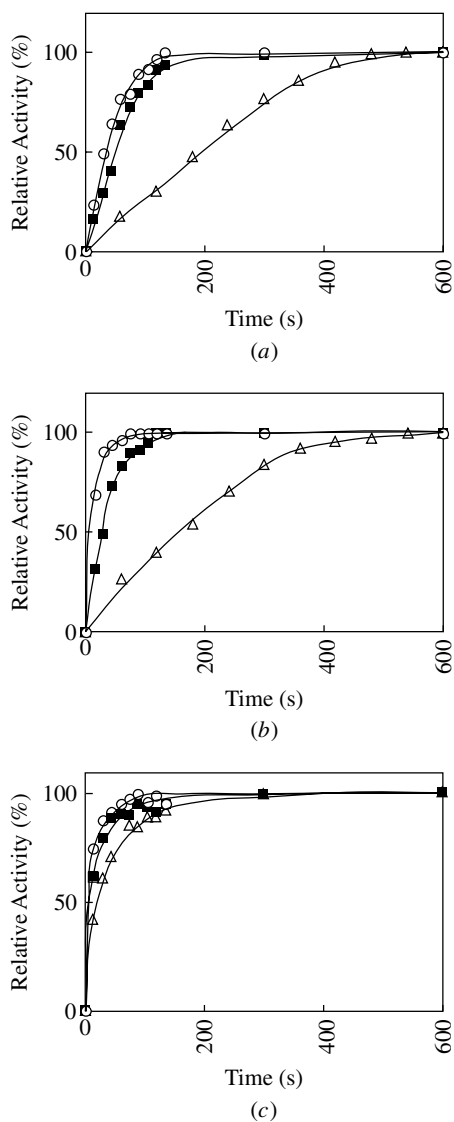
Figure 15.3. Time course of activation of (*a*) wild-type, (*b*) Lys36pArg, and (*c*) Lys36p-Met Trx-PG (0.067 mg/mL) at 14°C. Each activation curve was measured at pH 1.1, 2.0, and 3.0 by a synthetic substrate assay. Activation curves at pH 1.1, open circles; activation curves at pH 2.0, closed squares; activation curves at pH 3.0, open triangles.

the activation curves were exponential in shape, suggesting that the rate-limiting step in the conversion of pepsinogen to pepsin occurs by a first-order reaction. First-order activation kinetics were confirmed by (1) linear semilogarithmic plots of pepsinogen concentration versus time, and (2) by

showing that the first-order rate constant calculated from a first-order rate equation was similar to that obtained from a mixed first- and second-order equation. These findings indicate that a negligible amount of pepsinogen was converted to pepsin by a second-order pepsin-catalyzed reaction (k_2 values were less than 1% of k_1 values). Therefore, the rate-limiting step, in the activation of wild-type, Lys36pArg, and Lys36pMet Trx-PGs, proceeds predominantly by a first-order reaction and thus an intramolecular mechanism at pH $\leq$ 3 (Tanaka and Yada, 1997).

The first-order activation rate constants (k_1) for wild-type, Lys36pMet, and Lys36pArg Trx-PGs shown in Table 15.3 indicated that the rate of intramolecular activation of Lys36pArg was 5.3-, 2.4-, and 1.7-fold higher than that of the wild-type at pH 1.1, 2.0, and 3.0, respectively. In addition, Western blots of the activation process showed that Lys36pArg Trx-PG disappeared more rapidly than did wild-type Trx-PG at pH 1.1 and 2.0 (data not shown). The activation of Lys36pMet Trx-PG showed higher k_1 values than those of Lys36pArg. Activation of Lys36pMet at pH 1.1 and 2.0 was 9.4- and 12.6-fold faster than WT, respectively. At pH 3.0, Lys36pMet had a k_1 value 6.2 times higher than that of the wild-type enzyme. This activation rate was even faster than WT at pH 2.0. Western blots of the activation reaction at pH 1.1 and 2.0 clearly show more rapid disappearance of Lys36pMet pepsinogen relative to the disappearance of wild-type Trx-PG (data not shown). Therefore, mutating Lys36p to Arg and Met appears to have increased the rate of the rate-limiting step in the intramolecular activation of Trx-PG.

The kinetic constants for the pepsins derived from the acidification of the wild-type and the three mutant Trx-PGs are shown in Table 15.4. Although the Lys36p mutation had little or no effect on K_m, the mutations resulted in decreases in k_{cat}. Although Lys36pGlu also had lower k_{cat} values, it was difficult to determine the catalytic rate of this mutant,

TABLE 15.3 First-Order Rate Constants (k_1) for the Activation of Wild-Type, Lys36pArg, and Lys36pMet Trx-PG at 14°C determined with the Synthetic Peptide Substrate Lysine–Proline–Alanine–Glutamic Acid–Phenylalanine–Phenylalanine (NO$_2$)–Alanine–Leucine[a]

| | First-Order Rate Constant (min^{-1}) $\pm$ SD | | |
pH	1.1	2.0	3.0
Wild-type	1.10 ± 0.10	0.519 ± 0.058	0.109 ± 0.011
Lys36pArg	5.80 ± 0.51	1.25 ± 0.13	0.185 ± 0.025
Lys36pMet	10.3 ± 1.2	6.56 ± 0.64	0.675 ± 0.012

[a] See Section 15.7 for abbreviations. Rate constants represent the mean of three determinations $\pm$ standard deviation.

TABLE 15.4   Kinetic Parameters for Pepsins Obtained from Activation of Wild-Type Trx-PG and Lys36pArg and Lys36pMet Trx-PG[a]

	Substrate			
	ss 1[b]		ss 2[c]	
Pepsin	K_m (mM)	k_{cat} (s^{-1})	K_m (mM)	k_{cat} (s^{-1})
Wild-type	0.084 ± 0.019	88.8 ± 10.4	0.023 ± 0.004	49.1 ± 3.8
Lys36pArg	0.050 ± 0.011	24.7 ± 2.4	0.023 ± 0.004	18.3 ± 1.4
Lys36pMet	0.077 ± 0.010	30.6 ± 2.0	0.014 ± 0.002	19.6 ± 0.9

[a]See Section 15.7 for abbreviations. Each value represents the mean of three determinations $\pm$ standard deviation.
[b]ss1, substrate consisting of the peptide lysine–proline–alanine–glutamic acid–phenylalanine–phenylalanine (NO_2)–alanine–leucine.
[c]ss2, substrate consisting of the peptide leucine–serine–phenylalanine (NO_2)–norleucine–leucine–methyl ester.

due to its instability; therefore, the results could not be confirmed. The minimal effect of the mutations on K_m suggests that overall conformation of the substrate-binding cleft was not altered by the mutations, while the reductions in k_{cat} suggest that the mutations produced local changes in residues involved in the catalytic mechanism. One possibility is that the mutations altered the orientation of the catalytically essential aspartates, Asp32 and Asp215, which form ion pairs with the ε-amino group of Lys36p. Changes in the position of these two Asp residues relative to each other or relative to a water molecule, believed to be the nucleophile in the catalytic mechanism, could compromise the ability of the active site to hydrolyze substrate.

From the studies above, it was concluded that electrostatic interactions between K36p and catalytic center residues were critical in stabilizing the prosegment as well as contributing to the higher activity of activated pepsin.

15.4   WHAT ROLE DO SPECIFIC STRUCTURES AND/OR RESIDUES PLAY IN THE STRUCTURE–FUNCTION OF ENZYMES?

Loops are a class of secondary structure that reverse the direction of a polypeptide chain and are usually situated at the protein surface. Unlike α-helices and β-sheets, loop structures have no regular patterns of dihedral angles and hydrogen bonds (Leszczynski and Rose, 1986; Fetrow, 1995).

Loop residues that are involved in catalysis may be more highly conserved than amino acids in surface loops, whose role is purely structural. This sequence conservation can involve amino acids that interact directly with a substrate as well as amino acids that help stabilize various conformations that the loop may adopt during catalysis (Rose et al., 1985).

The crystal structures of pepsin in free and inhibited forms indicate that three flap residues, tyrosine 75, glycine 76, and threonine 77, contribute directly to a particular subsite specificity by hydrogen bonding to substrate residues (Chen et al., 1992; Hartsuck et al., 1992). We therefore undertook various mutations of the aforementioned residues to determine their role(s) in the structure–function relationship of pepsin(ogen). Below is a description of our study involving the mutation of glycine 76. The reader is referred to Tanaka et al. (1998) and Okoniewska et al. (1999) regarding our mutations to residues Tyr75 and Thr77, respectively.

In our glycine 76 study (Okoniewska et al., 2000), this position was substituted with alanine, valine, and serine. These amino acids differ in their van der Waals volumes, accessible surface areas, polarities, and allowable energy levels on Ramachandran plots for individual amino acids. Rate constants for the activation process were calculated for the mutants and the wild-type enzymes at pH 1.1, 2.0, and 3.0. Samples were taken at different activation times, quenched, and the amount of pepsin formed was determined with synthetic substrate I. Activation rate constants presented in Table 15.5 corresponded to first-order reaction constants. All the mutants activated at rates slower than those for the wild-type, regardless of amino acid size and polarity. At all pH conditions, the activation reactions were slowest for valine and serine mutants, which had comparable reaction rates. The alanine mutant activated more slowly than did the wild-type but was faster than the other two mutants.

TABLE 15.5   First-Order Rate Constants for Activation of Thioredoxin–Pepsinogen Fusion Proteins[a]

Enzyme	k_{act} (min^{-1})		
	pH 1.1	pH 2.0	pH 3.0
Wild-type	4.449 ± 0.262	2.819 ± 0.152	1.043 ± 0.089
Gly76Ala	0.311 ± 0.076	0.332 ± 0.0014	0.104 ± 0.029
Gly76Val	0.132 ± 0.001	0.152 ± 0.013	0.054 ± 0.001
Gly76Ser	0.130 ± 0.014	0.166 ± 0.014	0.059 ± 0.003

[a]See Section 15.7 for abbreviations. Rate constants represent the mean of a minimum of two determinations ± standard deviation.

TABLE 15.6   Kinetic Parameters for the Wild-Type Pepsin and G76 Mutants[a]

Substrate	Enzyme	K_m (mM)	k_{cat} (s^{-1})	k_{cat}/K_m (mM^{-1} s^{-1})
ss1[b]	Wild-type	0.043 ± 0.005	180.5 ± 10.3	4198 ± 544
	Gly76Ala	0.098 ± 0.008	47.0 ± 9.9	395 ± 96
	Gly76Val	0.071 ± 0.011	11.1 ± 1.1	160 ± 30
	Gly76Ser	0.085 ± 0.005	2.5 ± 0.6	29 ± 7
ss2[c]	Wild-type	0.011 ± 0.002	88.7 ± 4.6	8064 ± 1525
	Gly76Ala	0.040 ± 0.009	43.4 ± 3.6	1085 ± 260
	Gly76Val	0.044 ± 0.005	1.2 ± 0.1	28 ± 3
	Gly76Ser	0.041 ± 0.008	2.9 ± 0.3	70 ± 16

[a]See Section 15.7 for abbreviations. Each value represents the mean of a minimum of two determinations $\pm$ standard deviation.
[b]ss1, substrate consisting of the peptide lysine–proline–alanine–glutamic acid–phenylalanine–phenylalanine (NO$_2$)–alanine–leucine.
[c]ss2, substrate consisting of the peptide leucine–serine–phenylalanine (NO$_2$)–norleucine–leucine–methyl ester.

   Kinetic properties of wild-type and mutant enzymes were determined with two synthetic substrates, and the kinetic constants K_m and k_{cat} were calculated using a nonlinear least-squares method (Sakoda and Hiromi, 1976). Different synthetic substrates and pH values are used in kinetic analyses to differentiate between differences in substrate binding and catalytic environment The kinetic parameters are presented in Table 15.6.

   All the mutants, regardless of amino acid size and polarity, had lower substrate affinity and turnover numbers than those for the wild-type. The differences in the catalytic parameters were similar for the two synthetic substrates, indicating that the changes were not substrate specific and the results could therefore be attributed to differences in the catalytic environments of the mutants. The kinetic experiments were performed at two different pH values, pH 2.1 for synthetic substrate I and pH 3.95 for synthetic substrate II. The kinetic constants showed the same tendencies at the two different pH conditions. Therefore, it was concluded that the mutations did not change pH dependencies of mature enzymes.

   The results above indicated that the mutations had a minimal effect on substrate binding and influenced primarily the properties of enzyme-bound species in the reaction pathway. Additionally, stereochemical analysis of peptide bond hydrolysis (James and Sielecki, 1985) and pepsin crystal structure (Sielecki et al., 1990) indicated that glycine 76 is in a position most favorable for interactions with reaction intermediates. A possible involvement of glycine 76 in stabilizing the transition state was suggested as a hypothetical catalytic mechanism for pepsin (Pearl, 1987). As indicated above, all the mutants had altered kinetic constants compared to

the wild-type; however, the degree of a change was different for individual enzymes. The alanine mutant was affected less than either valine and serine mutants, which had comparable catalytic constants. Compared to valine and serine, alanine has the smallest van der Waals volume and accessible surface area. Therefore, it introduces a relatively smaller restriction to a polypeptide conformational flexibility and has relatively fewer contacts with surrounding atoms. Valine and serine mutants have larger volumes, and their presence in a polypeptide chain results in greater conformational restrictions, due to an atom-crowding effect. Consequently, the results suggested that all the mutations reduced polypeptide conformational freedom in the flap region. This is in agreement with molecular dynamics calculations and structural analyses of the mutants, where the greatest local perturbations were observed for Gly76Val mutant. Alanine, which has the smallest side chain of the three substituted amino acids, had the smallest effect on enzyme catalysis and local conformation. Introduction of bulkier amino acids, serine and valine, resulted in greater decreases in catalytic parameters and activation rate constants. Our results, combined with observations made in other loop structures, demonstrate that glycine 76 in pepsin contributes to flap flexibility and that this flexibility is essential for efficient catalysis.

15.5   CAN MUTATIONS BE MADE TO STABILIZE THE STRUCTURE OF AN ENZYME TO ENVIRONMENTAL CONDITIONS?

Most proteins are synthesized in a neutral-pH environment; thus their natural conformation state and functionality are adapted to this environment. However, most aspartic proteinases are stable under acidic conditions and become irreversibly denatured at neutral pH conditions (Bohak, 1969; Fruton, 1971). In the case of pepsin, its zymogen, pepsinogen, is stable under neutral-pH conditions. Since pepsin and pepsinogen are almost identical in structure, minor differences may be responsible for pepsin's instability at neutral pHs. Why is pepsin so unstable, despite being similar in conformation to pepsinogen? In a recent study, we undertook various mutations in attempts to stabilize the structure of pepsin.

15.5.1   Charge Distribution

The most obvious differences between pepsin and pepsinogen are found in the prosegment portion. Not only does the prosegment cover the active-site cleft, but it contains a large number of positively charged residues [i.e.,

13 (nine lysine, two arginine, two histidine) out of the 44 residues in the prosegment of pepsinogen are positively charged] (James and Sielecki, 1986; Lin et al., 1989). Pepsin, on the other hand, contains only four positive residues (two arginine, one lysine, one histidine). Therefore, the number and distribution of these positively charged residues contribute to the difference in pH stability between pepsin and pepsinogen. In contrast, unlike most aspartic proteinases, chicken pepsin is relatively stable at neutral pHs (Bohak, 1969). A homology search between porcine and chicken pepsin shows a 74% similarity. Major differences between chicken and porcine pepsins are in charge distribution and in the N-terminal amino acid sequences. In chicken pepsin, there are 21 aspartic acid, 13 glutamic acid, 9 lysine, 5 arginine, and 4 histidine charged residues, whereas in porcine pepsin, 28, 13, 1, 2, and 1 are charged, respectively. For both porcine and chicken pepsin, most of these charged residues are distributed on the surface. In the resultant chicken-like mutant, $N + C$, 7 positive residues were added and 3 negative residues were removed. Kinetic measurements of this mutant were determined at pH 2.1 and 3.95 and shown to have comparable kinetic constants to the wild-type. Therefore, mutations on the surface had little effect on kinetic parameters (Table 15.7). Although the $N + C$ mutant had activity similar to that of the wild-type, the stability at neutral pH changed (Table 15.8 and Fig. 15.4). The mutant was inactivated at about half the rate of the wild-type. The inactivation rates of the mutants that had mutations on only the N- or C-terminal domains (N-DOM and C-DOM,

TABLE 15.7   Kinetic Constants of Mutant and Wild-Type Pepsins[a]

Enzyme	ss1[b]		ss2[c]	
	K_m (mM)	k_{cat} (s^{-1})	K_m (mM)	k_{cat} (s^{-1})
Wild-type	0.034 ± 0.005	65.4 ± 3.1	0.019 ± 0.006	190.5 ± 18.9
$N + C$	0.057 ± 0.005	77.5 ± 2.9	0.031 ± 0.013	50.7 ± 9.4
Del	0.070 ± 0.006	60.9 ± 2.6	0.015 ± 0.002	25.7 ± 1.0
N-frag	0.083 ± 0.015	68.9 ± 6.6	0.028 ± 0.007	80.7 ± 10.2
N-frag (A)	0.075 ± 0.008	186.0 ± 9.8	0.028 ± 0.007	122.0 ± 15.6
N-frag (B)	0.065 ± 0.009	187.1 ± 12.8	0.041 ± 0.005	315.3 ± 16.8
Gly2Cys/Leu167Cys	0.080 ± 0.007	41.6 ± 2.0	0.018 ± 0.001	13.0 ± 0.22

[a] See Sections 15.7 for abbreviations. Each value represents the mean of a minimum of two determinations $\pm$ standard deviation.
[b] ss1, substrate consisting of the peptide lysine–proline–alanine–glutamic acid–phenylalanine–phenylalanine (NO_2)–alanine–leucine.
[c] ss2, substrate consisting of the peptide leucine–serine–phenylalanine (NO_2)–norleucine–leucine–methyl ester.

TABLE 15.8   Rate Constants of Inactivation for Mutant Pepsins at pH 7.0[a]

Enzyme	$k_d(\mathrm{min}^{-1})$[b]
N-frag	0.0169 ± 0.0014
N-frag (glycerol, sucrose)	0.00229 ± 0.00031
N-frag (pH 7.5)	0.268 ± 0.008
N-frag (A)	0.0680 ± 0.0038
N-frag (B)	0.0646 ± 0.0015
Gly2Cys/Leu167Cys	0.0536 ± 0.0051
N + C	0.0421 ± 0.0071
N-DOM	0.0905 ± 0.0173
C-DOM	0.0852 ± 0.0237
Wild-type	0.0991 ± 0.0075
Wild-type (glycerol)	0.0365 ± 0.0026
Wild-type (sucrose)	0.0203 ± 0.0009
Wild-type (glycerol, sucrose)	0.00743 ± 0.00216
Wild-type (pH 7.5)	ND

[a]See Section 15.7 for abbreviations.
[b]K_d values represent the mean of three determinations $\pm$ standard deviation. ND, not determined, inactivation was too rapid (completed within 5 min) under the experimental conditions to determine the inactivation rate.
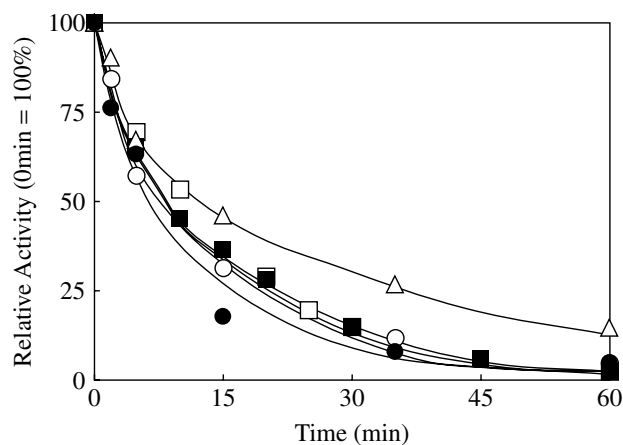
Figure 15.4. Inactivation of wild-type and mutant pepsin. Pepsin was inactivated under the conditions described in the text, and residual activities were plotted; ●, wild-type; △, N + C; ○, Del; □, N-frag(A); ■, N-frag(B). Each data point represents the mean of three determinations.

respectively) were comparable to that of the wild-type. Since Lin et al. (1993) had shown that the initial denaturation occurred in the N-terminal domain, the mutations on the N-terminal domain were expected to have a dominant effect. The negatively charged residues on the N-terminal domain themselves, however, only had a minor effect on the stability. Thus, these results demonstrated that the distribution of negatively charged residues on the surface of the porcine pepsin helped stabilize the enzyme; however, the degree of stabilization was not substantial.

15.5.2   N-Frag Mutant

Another difference between pepsin and pepsinogen is the location of the N-terminal fragment. In the zymogenic form and during activation, the N-terminal fragment is in the active-site cleft. After activation, this N-terminal fragment is placed in the β-sheet at the bottom of the protein. This relocation results in about a 40-Å movement (James and Sielecki, 1986). Since this portion relocates from one side of the protein to the other side, it is suggested that this fragment could readily be moved from its position and could be important for the stabilization of pepsin under neutral-pH conditions. Therefore, it is suggested that stabilizing this fragment in its original position, which was a strand of a β-sheet at the bottom of pepsin molecule, will prevent denaturation in the event of neutralization. To examine this possibility, mutations were introduced into the N-terminal portion to keep it in the fixed position at the bottom of the pepsin molecule. The comparison of the amino acid sequence of the pepsins from porcine and chicken (chicken pepsin is relatively stable at neutral conditions) revealed major differences in the N-terminal portion. We chose five amino acid residues to be replaced. The mutation of the N-terminal portion was done with two sets of mutations, N-frag(A) and N-frag(B). These two mutants and a third mutant which combined both mutations (N-frag) exhibited similar kinetic constants to the wild-type and had comparable catalytic activities for both synthetic substrates (Table 15.7). Stability tests of the N-frag mutant showed that it was 5.8 times more stable than the wild-type (Table 15.8 and Fig. 15.5a). Whereas the wild-type was inactivated in 60 minutes, this mutant retained 30% of its activity after 60 minutes. Even after 4 hours, 18% of the original activity was observed with this mutant. When the pH was raised to 7.5 (Fig. 15.5b), the wild-type showed no activity after 5 minutes. Even the addition of glycerol and sucrose, which have been shown to stabilize the enzyme, had no effect. When the N-frag mutant was exposed to pH 7.5, it retained 5% activity after 15 minutes. The rate constant of inactivation for N-frag at pH 7.5 was 0.268 per minute. Moreover, in the presence of both
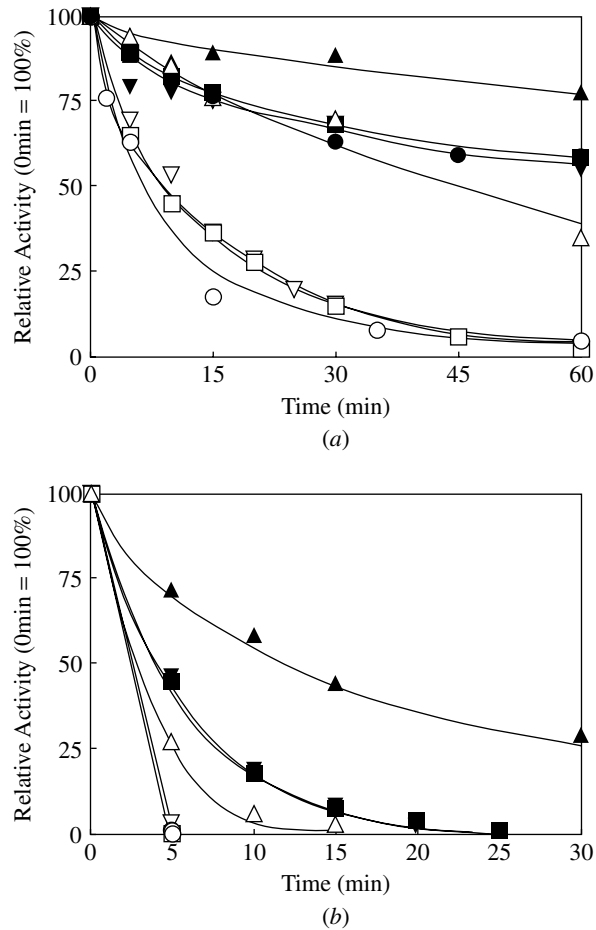
Figure 15.5. Inactivation of amino terminal fragment mutant. Inactivation test of N-fragment, N-frag(A), and N-frag(B) mutants showed that individual mutations in N-fragment mutant were not critical for the stabilization of pepsin. Both N-frag (A) and (B) mutants showed slight stabilization effects (*b*) and were similar in stability (*a*) to the wild-type, while N-frag mutant showed drastic stabilization. (*a*) The inactivation reactions were carried out at pH 7.0; (*b*) the inactivation reactions were carried out at pH 7.5. Symbols are wild-type (○), N-frag(A) (▽), N-frag(B) (□), N-fragment (△), wild-type with glycerol and sucrose (●), N-frag(A) with glycerol and sucrose (▼), N-frag(B) with glycerol and sucrose (■), and N-fragment with glycerol and sucrose (▲) Each data point represents the mean of three determinations.

glycerol and sucrose at pH 7.5, the enzyme retained 25% activity after 30 minutes. Since the N-frag mutant had five amino acid replacements, some of the mutations could be more critical than others. The N-frag(A) and N-frag(B) mutants, however, were less stable than the N-frag mutant

(Fig. 15.5). Both mutants showed an inactivation rate about 1.5 times slower than that of the wild-type, while the N-frag mutant was 5.8 times slower. Also, at pH 7.5, the activities of both N-frag(A) and N-frag(B) mutants were quenched more slowly than the wild-type, but faster than the N-frag mutant. After 5 minutes, N-frag(A), N-frag(B), N-frag, and wild-type had 0, 3, 27, and 0% of the original activity in the absence of glycerol and sucrose, while 45, 46, 0 and 72% of the original activities remained in the presence of glycerol and sucrose, respectively. Molecular minimization using molecular modeling showed that these mutations did not contribute to the internal interactions (Fig. 15.6). The only major difference between the wild-type and N-frag mutant was the addition of a hydrogen bond between serine 2-glycine oxygen and leucine-167 nitrogen in the glycine 2 serine mutation. The kinetics of the N-frag(A) mutant, however, showed that this addition was insufficient to stabilize the protein entirely. It was thus concluded that each of the five replacements by themselves were not critical, but helped to stabilize the enzyme synergistically. Since each of the mutations above in itself was not critical to stabilization, the mechanism of stability was still in question. We, therefore, suggested two possibilities of how the mutations stabilized pepsin: (1) the release of N-terminus portion is prevented with these mutations, or (2) these mutation sites are responsible for the stability of the N-terminal portion released. The crystal structure of inactive cathepsin D at pH 7.5 showed that the N-terminal portion is relocated into the active-site cleft and is stabilized by an interaction to the catalytic site (Lee et al., 1998). From this crystal structure data, we suspect the second possibility to be more likely.

15.5.3   Disulfide Linkages

Disulpfide links are known to connect distal regions of the polypeptide chain and therefore have often been associated with increased stability against denaturation. If the mobility of the N-terminal portion initiates denaturation, it would be logical to think that fixing this portion to the enzyme body would prevent denaturation. To fix the N-terminus portion to the enzyme body, a potential disulpfide bond was introduced. This mutant, Gly2Cys/Leu167Cys, had a cysteine residue at the second residue of the N-terminal portion and another cysteine on the opposite side of the enzyme body (Fig. 15.7). Kinetic studies of this mutant showed a lower, albeit a substantial amount of activity compared to the wild-type enzyme (Table 15.7). The rate constant of inactivation of Gly2Cys/Leu167Cys at pH 7.0 was about half that of the wild-type but was not as low as that for the N-frag mutant. However, inactivation slowed down after 30 minutes, and had lower but noticeable activity
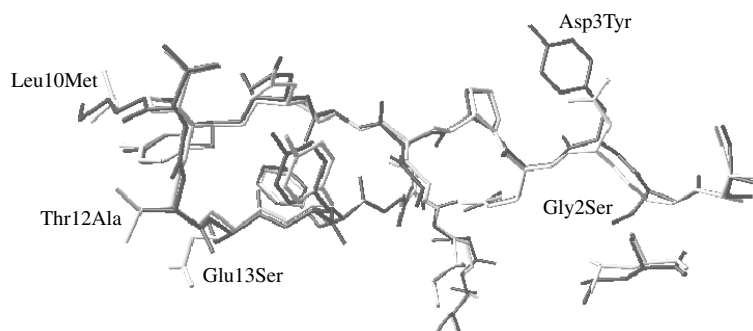
Figure 15.6. Molecular model comparison of wild-type and amino terminal fragment mutant pepsin. Superposition of the bottom β-sheet and N-terminal fragment of wild-type and N-frag mutant models. There were no major differences. Root-mean-square deviation between backbone atoms of wild-type and N-frag was 0.28 Å. The numbers show the mutation sites in N-frag.
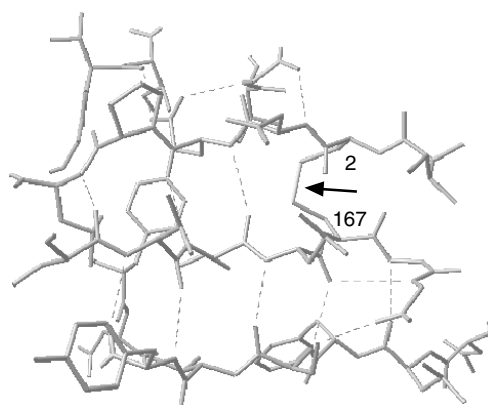
Figure 15.7. Molecular model of the introduced disulfide bond in Gly2Cys/Leu167Cys mutant pepsin. A molecular model around the mutation site of Gly2Cys/Leu167Cys. The introduced disulfide bond, shown by the arrow, is well accommodated in this position.

(3.2%) over 24 hours, whereas the N-frag, N-frag(A), and N-frag(B) mutants were completely inactive after 24 hours. These results would imply that formation of the disulpfide bond prevented denaturation by preventing movement of the N-terminal portion. However, the slower disulfide bond formation seemed to compete with the faster inactivation since substantial activity was lost before reaching the plateau. To increase the rate of disulfide bond formation, oxidizing reagents were used [i.e., $FeCl_3$, $K_3Fe(CN)_6$, o-iodothobenzoate, dithionitrobenzoate, and 3,3′-dithiopyridine]. These reagents had comparable effects. After 24 hours of oxidization with 2 mM $FeCl_3$, the oxidized Gly2Cys/Leu167Cys was
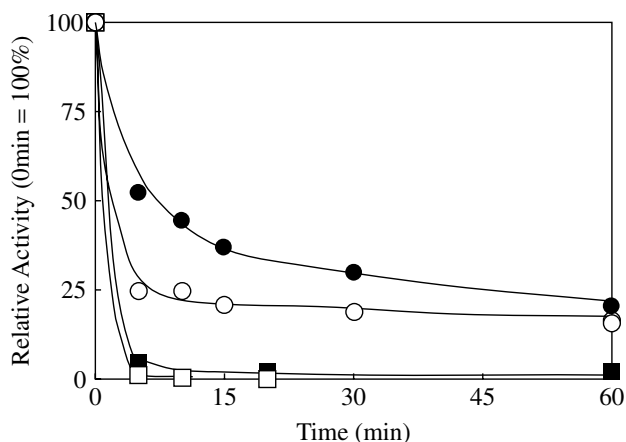
Figure 15.8. Inactivation of Gly2Cys/Leu167Cys mutant pepsin. Inactivation of Gly2Cys/Leu167Cys mutant and the effect of the oxidizing reagent. At pH 7.5, the oxidization did not stabilize the wild-type (□ without oxidization and ■ with oxidization), while oxidization of Gly2Cys/Leu167Cys stabilized the enzyme (○ without oxidization and ● with oxidization). Each data point represents the mean of three determinations.

tested for stability at pH 7.5 (Fig. 15.8). Gly2Cys/Leu167Cys, without oxidizers, showed slower inactivation than did wild-type; however, most of the activity was lost after 480 minutes. In the presence of $FeCl_3$, inactivation slowed down and reached a plateau at 20% of its initial activity. Further inactivation studies showed that activities were retained: 11% at 24 hours and 5% at 74 hours. These results indicated that disulfide bond formation kept the N-terminal fragment close to its native position, thereby stabilizing the enzyme. Formation of disulfide bonds was faster at pH 7.5 than at pH 7.0; thus greater stabilizing effects were observed at the higher pH. From these studies, we concluded that the instability of pepsin at neutral pHs resulted from relocation of the prosegment.

15.6   CONCLUSIONS

Critical to the elucidation of structure–function relationships of enzymes is the determination and analysis of kinetic data used in conjunction with structural information. The more supportive these two data sets (i.e., kinetic and structural information) become, the better will be our ability not only to understand enzyme catalytic mechanisms at a molecular level but also to design enzymes knowledgeably for specific end uses.

15.7   ABBREVIATIONS USED FOR THE MUTATION RESEARCH

Asp 32   Aspartic acid (Asp) at position 32 of the amino acid sequence of pepsin; one of the catalytic active-site residues.

Asp 215   Aspartic acid (Asp) at position 215 of the amino acid sequence of pepsin; one of the catalytic active-site residues.

C-DOM   Mutations that occurred in the carboxyl (C) terminal domain (DOM) of pepsin: serine at position 196 of pepsin mutated to arginine, aspartic acid at position 200 mutated to glycine, and glutamic acid at position 202 mutated to lysine.

c-pepsin   Commercial pepsin.

Del   Mutation involving the deletion of amino acid residues 240 to 246 from the amino acid sequence of pepsin and replacement of this sequence with glycine and aspartic acid to remove the putative mobile portion in the carboxyl-terminal domain.

Gly 76   Glycine (Gly) at position 76 of the amino acid sequence of pepsin.

Gly76Ala   Glycine (Gly) at position 76 in pepsin mutated to alamine (Ala).

Gly76Ser   Glycine (Gly) at position 76 in pepsin mutated to sermine (Ser).

Gly76Val   Glycine (Gly) at position 76 in pepsin mutated to valine (Val).

Gly2Cys/Leu167Cys   Mutations intended to cause the formation of a disulpfide linkage in pepsin; glycine (Gly) at position 2 mutated to cysteine (Cys), leucine (Leu) at position 167 mutated to cysteine.

Leu44p–Ile1   Bond between leucine (Leu) at residue 44 of the sequence of the prosegment of pepsinogen and the first residue of the amino acid sequence of pepsin, isoleucine (Ile).

Lys36p   Lysine (Lys) residue at position 36 of the prosegment (p) of pepsinogen.

Lys36pArg   Lysine residue at position 36 of the prosegment (p) of pepsinogen mutated to arginine (Arg).

Lys36pGlu   Lysine (Lys) residue at position 36 of the prosegment (p) of pepsinogen mutated to glutamic acid (Glu).

Lys36pMet	Lysine residue at position 36 of the prosegment (p) of pepsinogen mutated to methionine (Met).
N + C	Mutations made in both the amino terminal (N) and carboxyl terminal (C) domains of pepsin; a combination of the C- and N-DOM mutations.
N-DOM	Mutations that occurred in the amino terminal (N) domain (DOM) of pepsin: serine at position 46 to lysine, aspartic acid at position 52 to asparagine, asparagine at position 54 to lysine, and glutamine at position 55 to arginine and aspartic acid of pepsin to lysine.
N-frag	Mutations in the amino terminal (N) domain or fragment (frag) of pepsin; a combination of the N-frag (A) and N-frag (B) mutations.
N-frag (A)	Mutations in the amino terminal (N) domain or fragment (frag) of pepsin involving the following: glycine at position 2 mutated to serine and aspartic acid at position 3 mutated to tyrosine.
N-frag (B)	Mutations in the amino terminal (N) domain or fragment (frag) of pepsin that involved the following: leucine at position 10 mutated to methionine, threonine at position 12 mutated to alanine, and glutamic acid at position 13 mutated to serine.
r-pepsin	Recombinant pepsin.
r-PG	Recombinant pepsinogen.
Thr 77	Threonine (Thr) at position 77 of the amino acid sequence of pepsin.
Trx-PG	Fusion pepsinogen (thioredoxin protein plus pepsinogen).
Tyr 75	Tyrosine (Tyr) at position 75 of the amino acid sequence of pepsin.

REFERENCES

Al-Janabi, J., J. A. Hartsuck, and J. Tang (1972). *J. Biol. Chem.* **247**, 4628–4632.

Bohak, Z. (1969). *J. Biol. Chem.* **244**, 4638–4648.

Bustin, M., and A. Conway-Jacobs (1971). *J. Biol. Chem.* **246**, 615–620.

Chen, L., J. W. Erickson, T. J. Rydel, C. H. Park, D. Neidhart, J. Luly, and C. Abad-Zapatero (1992). *Acta Crystallogr. B***48**, 476–488.

Cregg, J. M., J. L. Cereghino, J. Shi, and D. R. Higgins (2000). *Mol. Biotechnol.* **16**, 23–52.

Creighton, T. E. (1978). *Prog. Biophys. Mol. Biol.* **33**, 231–298.

Danley, D. E., K. F. Geoghgan, K. G. Scheld, S. E. Lee, J. R. Merson, S. J. Hawrylik, G. A. Rickett, M. J. Ammirati, and P. M. Hobart (1989). *Biochem. Biophys. Res. Commun.* **165**, 1043–1050.

Darke, P. L., C.-T. Leu, L. J. Davis, J. C. Heimbach, R. E. Diehl, W. S. Hill, R. A. F. Dixon, and I. S. Sigal (1989). *J. Biol. Chem.* **264**, 2307–2312.

Fetrow, J. S. (1995). *FASEB J.* **9**, 708–717.

Fruton, J. S. (1976). *Adv. Enzymol.* **44**, 401–443.

Georgiou, G., and E. De Bernardez-Clark (1991). In *ACS Symposium Series*, American Chemical Society, Washington, DC.

Guggenheim, E. A. (1926). *Philos. Mag.* **2**, 538–543.

Hartsuck, J. A., G. Koelsch, and J. S. Remington (1992). *Proteins* **13**, 1–25.

Herriott, R. M. (1939). *J. Gen. Physiol.* **22**, 65–78.

James, M. N. G., and A. R. Sielecki (1985). *Biochemistry* **24**, 3701–3713.

James, M. N. G., and A. R. Sielecki (1986). *Nature* **319**, 33–38.

Kane, J. F., and D. L. Hartley (1988). *Trends Biotechnol.*, **6.95**(101), 95–101.

LaVallie, E. R., E. A. DiBlasio, S. Kovacic, K. L. Grant, P. F. Schendel, and J. M. McCoy (1993). *Bio/Technology* **11**, 187–193.

Lee, A. Y., V. G. Sergei, and J. W. Erickson (1998). *Nature Struct. Biol.* **5**, 866–871.

Leszczynski, J. F., and G. D. Rose (1986). *Science* **234**, 849–855.

Lin, X.-l., R. N. S. Wong, and J. Tang (1989). *J. Biol. Chem.* **264**, 4482–4489.

Lin, X.-l., R. N. S. Wong, and J. Tang (1993). *Protein Sci.* **2**, 1383–1390.

McKeever, B. M., M. A. Navia, P. M. Fitzgerald, J. P. Springer, C.-T. Leu, J. C. Heimbach, W. K. Herber, I. S. Sigal, and P. L. Darke (1989). *J. Biol. Chem.* **264**, 1919–1921.

McPhie, P. (1974). *Biochem. Biophys. Res. Commun.* **56**, 789–792.

Meek, T. D., B. D. Dayton, B. W. Metcalf, G. B. Dreyer, J. E. Strickler, J. G. Gorniak, M. Rosenberg, M. L. Moore, V. W. Magaard, and C. Debouck (1989). *Proc. Natl. Acad. Sci. USA* **86**, 1841–1845.

Nilsson, B., L. Abrahmsen, and M. Uhlžn (1985). *EMBO J.* **4**, 1075–1080.

Nishimori, K., Y. Kawaguchi, M. Hidaka, T. Uozumi, and T. Beppu (1982). *Gene* **19**, 337–344.

Nishimori, K., Y. Kawaguchi, M. Hidaka, T. Uozumi, and T. Beppu (1984). *Gene* **29**, 41–49.

Okoniewska, M., T. Tanaka, and R. Y. Yada (1999). *Protein Eng.* **12**, 55–61.

Okoniewska, M., T. Tanaka, and R. Y. Yada (2000). *Biochem. J.* **349**, 169–177.

Pearl, L. H. (1987). *FEBS Lett.* **214**, 8–12.

Richter, C., T. Tanaka, and R. Y. Yada (1998). *Biochem. J.* **335**, 481–490.

Richter, C., T. Tanaka, and T. Y. Yada (1999). *Eur. J. Biochem.* **261**, 746–752.

Rose, G. D., L. M. Gierasch, and J. A. Smith (1985). *Adv. Protein Chem.* **37**, 1–109.

Sakoda, M., and K. Hiromi (1976). *J. Biochem. (Tokyo)* **80**, 547–555.

Seelmeier, S., H. Schmidt, V. Turk, and K. von der Helm (1988). *Proc. Natl. Acad. Sci. USA* **85**, 6612–6616.

Sielecki, A. R., A. A. Fedorov, A. Boodhoo, N. S. Andreeva, and M. N. G. James (1990). *J. Mol. Biol.* **214**, 143–170.

Tanaka, T., K. S. L. Teo, K. M. Lamb, L. J. Harris, and R. Y. Yada (1998). *Protein Peptide Lett.* **5**, 19–26.

Tanaka, T., and R. Y. Yada (1996). *Biochem. J.* **315**, 443–446.

Tanaka, T., and R. Y. Yada (1997). *Arch. Biochem. Biophys.* **340**, 355–358.

Tanaka, T., and R. Y. Yada (2001). *Protein. Eng.* **14**, 669–674.

Yoshimasu, M. A., J.-K. Ahn, T. Tanaka, and R. Y. Yada (2002). *Protein Expression and Purification*, in press.

BIBLIOGRAPHY

Books

Copeland, R. A., *Enzymes: A Practical Introduction to Structure, Mechanism, and Data Analysis*, 2nd edition, Wiley-VCH, New York, 1999.

Cook, P. F., *Steady-State Enzyme Kinetics*, Oxford University Press, New York, 1997.

Cornish-Bowden, A., *Principles of Enzyme Kinetics*, Butterworth, London, 1979.

Cornish-Bowden, A., *Analysis of Enzyme Kinetic Data*, Oxford University Press, Oxford, 1995.

Cornish-Bowden, A., *Fundamentals of Enzyme Kinetics*, Portland Press, London, 1995.

Cornish-Bowden, A., and C. W. Wharton, *Enzyme Kinetics*, IRL Press, Oxford, 1988.

Dixon, M. C., and E. C. Webb, *Enzymes*, 3rd edition, Academic Press, San Diego, CA, 1979.

Fersht, A., *Enzyme Structure and Mechanism*, W. H. Freeman, New York, 1977.

Fersht, A., *Enzyme Structure and Mechanism*, 2nd edition, W. H. Freeman, New York, 1985.

Fersht, A., *Structure and Mechanism in Protein Science: A Guide to Enzyme Catalysis and Protein Folding*, W.H. Freeman, New York,1999.

Fromm, H., *Initial Rate Enzyme Kinetics*, Springer-Verlag, New York, 1975.

Gutfreund, H., *Enzymes: Physical Principles*, Wiley-Interscience, London, 1972.

Jencks, W. P., *Catalysis in Chemistry and Enzymology*, Dover Publications, New York, 1987.

Piszkiewicz, D., *Kinetics of Chemical and Enzyme-Catalyzed Reactions*, Oxford University Press, New York, 1977.

Plowman, K. M., *Enzyme Kinetics*, McGraw-Hill, New York, 1972.

Purich, D. L., Ed., *Enzyme Kinetics and Mechanism Part D, Developments in Enzyme Dynamics*, *Methods in Enzymology, Vol. 249*, Academic Press, San Diego, CA, 1995.

Purich, D. L., and R. D. Allison, *Handbook of Biochemical Kinetics*, Academic Press, San Diego CA, 1999.

Schulz, A. R., *Enzyme Kinetics*, Cambridge University Press, Cambridge, 1994.

Segel, I. H., *Enzyme Kinetics: Behavior and Analysis of Rapid Equilibrium and Steady-State Enzyme Systems*, John Wiley and Sons, New York, 1975.

Segel, I. H., *Biochemical Calculations: How to Solve Mathematical Problems in General Biochemistry*, 2nd edition, John Wiley and Sons, New York, 1976.

Silverman, R. B., *Mechanism-Based Enzyme Inactivation: Chemistry and Enzymology*, Vol I and II, CRC Press, Boca Raton, FL, 1988.

Walsh, C. T., *Enzymatic Reaction Mechanisms*, W.H. Freeman, New York, 1979.

Selection of Classic Papers

Cleland, W. W., 1963, The kinetics of enzyme-catalyzed reactions with two or more substrates or products. I. Nomenclature and rate equations. II. Inhibition: nomenclature and theory. III. Prediction of initial velocity and inhibition by inspection, *Biochem. Biophys. Acta* **67**: 104–137, 173–187, 188–196.

Cleland, W. W., 1977, Determining the chemical mechanisms of enzyme-catalyzed reactions by kinetic studies, *Adv. Enzymol.* **45**: 273–387.

Cleland, W. W., 1979, Statistical analysis of enzyme kinetic data, *Methods Enzymol.* **63**: 103–138.

Cleland, W. W., 1987, The use of isotope effects in the detailed analysis of catalytic mechanisms of enzymes, *Bioorg. Chem.* **15**: 283–302.

Duggleby, R. G., 1994. Analysis of progress curves for enzyme-catalyzed reactions: application to unstable enzymes, coupled reactions and transient-state kinetics, *Biochim. Biophys. Acta* **1205**: 268–274.

Fromm, H. J., 1979. Use of competitive inhibitors to study substrate binding order, *Methods. Enzymol.* **63**: 467–486.

Gerlt, J. A., and J. W. Kozarich, 1991, Electrophilic catalysis can explain the unexpected acidity of carbon acids in enzyme catalyzed reactions, *J. Amer. Chem. Soc.* **113**: 9667–9669.

Hill, A. V., 1913. The combinations of haemoglobin with oxygen and with carbon dioxide, *Biochem. J.* **7**: 471–480.

Knowles, J. R., and J. Albery, 1977, Perfection in enzyme catalysis: the energetics of triosephosphate isomerase, *Acc. Chem. Res.* **10**: 105–111.

Koshland, D. E., Jr. and K. E.Neet, 1968, The catalytic and regulatory properties of enzymes, *Annu. Rev. Biochem.* **37**: 359–410.

Koshland, D. E., Jr., G. Nemethy, and D. Filmer, 1966, Comparison of experimental binding data and theoretical models in proteins containing subunits, *Biochemistry* **5**: 365–385.

Kraut, J., 1988, How do enzymes work? *Science* **242**: 533–540.

Mesecar, A. D., and D. E. Koshland, 2000, A new model for protein stereospecificity, *Nature* **403**: 614–615.

Mesecar, A. D., B. L. Stoddard and D. E. Koshland, 1997, Orbital steering in the catalytic power of enzymes: small structural changes with large catalytic consequences, *Science* **277**: 202–206.

Michaelis, L., and M. L. Menten. 1913, Die Kinetik der Invertinwirkung, *Biochem. Z.* **49**: 333–369.

Monod, J., J. P. Changeux and F. Jacob, 1963, Allosteric proteins and cellular control systems, *J. Mol. Biol.* **6**: 306–329.

Monod, J., J. Wyman, and J. P. Changeux, 1965, On the nature of allosteric transitions: a plausible model. *J. Mol. Biol.* **12**: 88–118.

Morrison, J. F., and C. T. Walsh, 1988, The behavior and significance of slow binding enzyme inhibitors, *Adv. Enzymol.* **61**: 201–301.

Page, M. I., and W. P. Jencks, 1971, Entropic contributions to rate enhancement, *Proc. Natl. Acad. Sci. USA* **68**: 1678.

Radzicka, A., and R. Wolfenden, 1995, A proficient enzyme, *Science* **267**: 90–93.

Rudolph, F. B., 1979, Product inhibition and abortive complex formation, *Methods Enzymol.* **63**: 411–436.

Schramm, V. L., 1998, Enzymatic transition states and transition state analog design, *Annu. Rev. Biochem.* **67**: 693–720.

INDEX

221